

Ecole Polytechnique Fédérale de Lausanne
School of Architecture, Civil and Environmental Engineering



Master project in Civil Engineering

**Evaluation and retrofit of the
St. Lawrence Parish House in Petrinja
that was damaged during the 2020
earthquakes in Croatia**

Aline Florence Bönzli

Under the supervision of:

Prof. Dr. Katrin Beyer

Dr. Igor Tomić

In the laboratory of EESD

External expert:

Prof. Dr. Mario Uros

In the Faculty of Civil Engineering,

University of Zagreb

Lausanne, EPFL 2024

Abstract

Efforts to reduce carbon dioxide emissions globally are compelling the construction industry to prioritize sustainability. A key strategy is the prolonged use of existing building stock to minimize additional emissions from concrete production. Many European buildings, however, are constructed with unreinforced masonry (URM), which are known to be less resilient against seismic forces. Assessing the seismic behaviour and reinforcing vulnerable structures, particularly after earthquake damage, becomes crucial.

This thesis focuses on analyzing the seismic response of the St. Lawrence Parish House in Petrinja, Croatia, damaged during the December 29, 2020 earthquake. Employing an equivalent frame model (EFM), a dynamic response history analysis (RHA) using the open-source software OpenSees aims to characterize the structure's seismic behaviour in its initial state. RHA results, compared against Eurocode 1998-1-1 and 1998-3 standards, confirm the building's overall compliance with safety requirements.

However, a detailed study of out-of-plane (OOP) mechanisms reveals potential vulnerabilities not captured by global assessments. Utilizing the N2 method from EN 1998-1-1, it becomes evident that while the structure meets global safety limits, local OOP failure modes form a specific risk which prevents the structure from meeting Eurocode requirements.

To address these concerns, reinforcement is deemed necessary. Specifically, the vaulted structures that support the first-floor slab are a source of vulnerability. An in-depth examination of introducing steel ties above the vaults is thus conducted. Global and local (OOP) analyses on the retrofitted structure assess the efficacy of these measures in securing the building. Additionally, two proposed reparation methods aim to restore the walls' initial stiffness and strength, ensuring the safe future use of the Parish House.

In summary, this study underscores the importance of seismic assessment and targeted reinforcement in preserving and repurposing vulnerable historic structures.

Acknowledgements

I'd like to thank my two supervisors, Professor Katrin Beyer and Dr Igor Tomic from EPFL's EESD lab, for their steadfast support, advice, and vital insights throughout the study process. Their advice and support were important in influencing the course of this thesis. A special appreciation also goes to the EESD laboratory for providing the opportunity to visit Petrinja and learn about the Parish House. I am also grateful for all of the helpful discussions with lab members that helped me discover solutions to the numerous issues I experienced while working on my thesis.

A particular thanks to Caroline Heitmann, my office companion who worked on her thesis over the same period. Our friendship and collaboration made the academic path joyful and enriching. The combined efforts on common subjects and shared discussions considerably contributed to the overall quality of this work.

I am also deeply thankful to Alen Kadić, who enabled the visits of the damaged buildings in Croatia, showed us around and gave us insight into life after the earthquake.

I extend my appreciation to all those who contributed to this thesis, directly or indirectly. Your support has been instrumental in making this academic endeavour a reality.

Glossary

ADRS acceleration-displacement response spectrum. 33, 34, 69

DL damage-limitation. 16, 21, 36, 37, 39, 41–43, 54, 57, 61, 69–72, 74

DOF degree of freedom. 49–51, 73

EFM equivalent frame model. 2, 5, 16, 44, 74

FEM finite element model. 47

MDOF multi-degree-of-freedom. 16, 33

NC near-collapse. 16, 21, 36, 37, 39, 41–43, 54, 57, 58, 61, 69–72, 74

OOP out-of-plane. 2, 5, 10, 12–14, 16, 17, 25–28, 35, 37, 38, 41, 43–47, 52, 56, 61, 63, 64, 66–68, 73–75

RC reinforced concrete. 6, 9, 40, 43, 63

RHA response history analysis. 2, 16, 21, 44, 57, 74

SDOF single-degree-of-freedom. 16, 33, 34

URM unreinforced masonry. 2, 5, 74

Contents

1 Introduction	5
1.1 Motivation	5
2 Presentation of the building	6
2.1 History	6
2.2 Geometry of the building	6
2.2.1 Facades	6
2.2.2 Ground floor	7
2.2.3 First floor	9
2.3 Earthquake damages	10
2.3.1 Façade cracks	10
2.3.2 Interior cracks	11
2.4 Observed out-of-plane-mechanisms	12
2.4.1 West facade	13
2.4.2 East facade	14
3 Methodology	15
3.1 Eurocodes	15
3.2 Software	15
3.3 Analysis procedure	16
3.3.1 Global analysis	16
3.3.2 Out-of-plane analysis	16
3.3.3 Partial factors	16
4 Characteristics of the structure	18
4.1 Material properties	18
4.1.1 Masonry properties	18
4.1.2 Timber properties	20
4.1.3 Concrete properties	20
4.2 Loads and loadcases	21
4.2.1 Seismic load	21
4.2.2 Self-weight	23
4.2.3 Live load	24
4.2.4 Other loads and forces	24
5 Analysis of out-of-plane mechanisms	25
5.1 Unobserved possible out-of-plane mechanisms	25
5.1.1 G-Mechanism	26
5.2 Overview and assumptions	27
5.3 Vault forces	29
5.4 Equilibrium formulation	29
5.4.1 F-Mechanism	29
5.4.2 G-Mechanism	31
5.5 Equivalent single degree of freedom system	33
5.6 N2 method	34
5.7 Results	35

5.7.1	F-Mechanism west facade	35
5.7.2	F-mechanism east facade	37
5.7.3	G-mechanism west facade	39
5.7.4	G-mechanism east facade	41
5.8	Conclusion and discussion	43
5.8.1	Relevant findings for the retrofitting	43
6	Modelling with OpenSees	44
6.1	Macroelements for piers and spandrels	44
6.1.1	Mesh	44
6.2	Slabs and vaults	46
6.2.1	Vaults	46
6.2.2	Staircase vaults	48
6.2.3	FERT Slabs	49
6.3	Reinforced concrete ring beam	50
6.4	Supports	50
6.4.1	Real supports	50
6.4.2	Fictitious nodes	50
6.5	Connections	50
6.6	Masses and loads	51
7	Analysis of the global behaviour: Initial state	52
7.1	Pushover analysis	52
7.1.1	Methodology	52
7.1.2	Results	53
7.1.3	Design limits	54
7.2	Dynamic analysis	55
7.2.1	Modal analysis	55
7.2.2	Response history analysis	57
7.3	Verification and discussion	61
7.3.1	Damage limitation	61
7.3.2	Near collapse	61
8	Proposed retrofitting and behaviour in reinforced state	62
8.1	Methodology	62
8.2	Anamnesis	63
8.3	Diagnosis	63
8.4	Therapy	64
8.4.1	Repointing	64
8.4.2	"Scuci-cuci"	65
8.4.3	Steel ties against vault thrust	66
8.5	Behaviour in the retrofitted state	68
8.5.1	Analysis of the out-of-plane mechanisms	68
8.5.2	Analysis of the global behaviour	71
8.6	Monitoring	72
9	Further investigations	73
10	Conclusion	74
11	Use of AI and data availability	75

A Parish documentation	79
B Earthquake documentation USGS	81
C Plans	82
D Crack inventory	90
E Meeting with the project engineers	132
F Reference peak ground acceleration Petrinja	134
G Geological map Sisak region, Croatia	135
H Calculations, codes and excel files	136
I Modelling	137
J Global results in the initial state	156

1. Introduction

This thesis focuses on the case of the Parish House of the St. Lawrence church in Petrinja, Croatia, that has been heavily damaged during the earthquakes of December 2020. The goal is to verify the resistance of the structure against seismic action and to qualitatively compare the modelled behaviour of the structure to the observed one. The approach consists in modelling the building as an equivalent frame model (EFM) using the macro elements proposed by Vanin et. al. [1] and performing dynamic analyses using the OpenSees software [2]. This analysis will be completed by a set of manual verifications of specific out-of-plane (OOP) mechanisms that are analysed using specially developed Jupyter Notebooks [3]. After the analysis of the structure in its initial state, the models are further used to evaluate the proposed set of solutions to enhance the seismic performance of the structure.

1.1 Motivation

The global effort to reduce carbon dioxide emissions to fight against climate change forces all industries to find solutions to minimize their carbon footprint. The construction sector, being one of the leading emitters of carbon dioxide [4], is not spared either. Especially the production and utilization of cement in concrete constructions is one of the main reasons for the high amount of carbon dioxide emissions [5]. Therefore, it is crucial to reduce the volume of concrete used to build housing and infrastructures to a minimum. One of the most efficient ways to do so is to reuse the existing building stock for as long as possible and reinforce the buildings if necessary to be able to exploit them even longer.

But what happens if buildings are affected by catastrophic events such as earthquakes? A considerable amount of the current European building stock consists of unreinforced masonry (URM) buildings that were not specifically designed to withstand earthquakes and are thus especially vulnerable. But that does not necessarily mean that after a seismic event, those buildings cease to be safely exploitable. The engineers must evaluate those historically valuable structures beforehand to ensure the safety of those buildings during earthquakes. The procedures to evaluate URM buildings however remain limited and bear a lot of uncertainties. It is therefore especially interesting to analyse masonry buildings that have suffered earthquake damage and compare the reality to the modelled results in order to gain more experience on what modelling assumptions to choose. Furthermore, it is interesting to see what simple yet efficient reinforcing techniques can be applied to damaged (or undamaged) structures to enhance their behaviour during a seismic event.

2. Presentation of the building

2.1 History

The Parish House of the St. Lawrence church (Crkva Sv. Lovre) in Petrinja dates from 1783. During the war in 1990, the church, to which the Parish House belongs was destroyed and entirely rebuilt, replicating the previous structure as precisely as possible [6]. Not only the church but also the Parish House suffered under the war: the roof of the Parish House had been entirely destroyed, leaving only the two chimneys [7] (see also Appendix A). The left image of Figure 2.1 [7] displays the restoration and reconstruction in 1996-1997. The main measures were to rebuild the roof structure using a lightweight solution of timber beams and add a FERT slab [8] above the first storey including also a reinforced concrete (RC) ring beam around the perimeter of the facades (see Appendix A [7] and Appendix E [9]). Apart from that, no significant changes can be perceived from the pictures. It can be shown (see Figure 2.1) that the building was built with old, massive brick masonry, but it is difficult to determine the condition of the masonry substance.



(a) Documentation of the reconstruction of the roof [7]



(b) Evidence of sampling (Source: Zvonko Sigmund)

Figure 2.1: Historical documentation

After the reconstruction, the Parish House served for over 20 years until it was hit by the next catastrophic event. On December 29, 2020, a devastating 6.4 magnitude earthquake struck Croatia's Sisak-Moslavina County. The earthquake occurred at a depth of 10 km along the Popusko-Petrinja strike-slip fault within the Eurasian plate, having an epicentre at 45.422°N 16.255°E , three kilometres west-southwest of Petrinja [6]. The statistical documentation can be found in Appendix B [10].

2.2 Geometry of the building

2.2.1 Facades

Looking at the Parish House from the outside, a bisymmetric facade geometry can be perceived: The east and west facades are almost identical and symmetric. Several small differences can however be perceived: the presence of a main entrance door on the west facade and windows of about half the typical size on the right side of the west facade. Because of the main entrance, the central windows on the west facade are slightly further apart compared to the east facade (see Figure 2.2). Since the terrain around the building is sloping, the east facade is slightly elevated (from the ground) compared

to the west facade and can therefore accommodate three cellar windows on the brown edge at the bottom.



Figure 2.2: The west and east facades of the Parish House

The only distinctions between the south and north facades are an extra cellar window on the north and a door instead of the bottom left window on the south (see Figure 2.3).



Figure 2.3: The south and north facades of the Parish House

A full set of plans can be found in Appendix C. In summary, the facades are about 6.1 meters high (without the bottom edge), and the edge adds up to one meter of height to the facade. The east and west facades are 17.7 meters wide and the north and south facades have a width of 11.9 meters. The ground-floor windows are 1.4 meters high, whereas the windows on the first floor are 1.7 meters high. The small windows on the south side of the west facade are only 70 centimetres high. However, all the windows have the same width of 1.1 meters.

2.2.2 Ground floor

The inside of the building is divided into a ground floor, a first floor, a second floor within the roof structure and a cellar, which will not be studied in this thesis. The ground floor is covered by a vaulted system that supports the slab of the first floor. Figure 2.4 depicts the vaults' spanning directions, with red arrows pointing in the direction of the primary curvature and light-blue arrows pointing in the direction of the secondary curvature. In the rooms where the vaults span perpendicular to a window or door opening, a local vault, marked by a turquoise arrow, allows to access the openings. Most of the vaults are barrel vaults (unidirectional) with a few crossed vaults (bi-directional) in the zone of the staircase. Figure 2.5 shows two examples of typical vaults within the building: a big barrel vault in the east room spanning from east to west and a smaller crossed vault in the west part of the building with the main curvature in the east-west direction. Vaults with a bigger span are rounder, starting lower on the sides whereas vaults with a smaller span are flatter, starting higher with a smaller difference between their initial and central heights.

The plan in Figure 2.4 shows that the three rooms in the east of the building are all covered by one vault spanning from the staircase to the east facade. A similar geometry can be perceived in the west where a common vault spans between the stairs and the west facade. Here, the vault is interrupted by the vault in the north-west room whose span is perpendicular to it. Furthermore, the vaults continue above the staircase where they are sloping perpendicular to their primary curvature.

The volume between the outside of the vault, the slab and the walls is filled with gravel material that then acts as the support for the slab. According to the main engineer working on the current retrofitting, this gravel material has a mass of 1.4 tons per m^3 [9] (see also Appendix E).

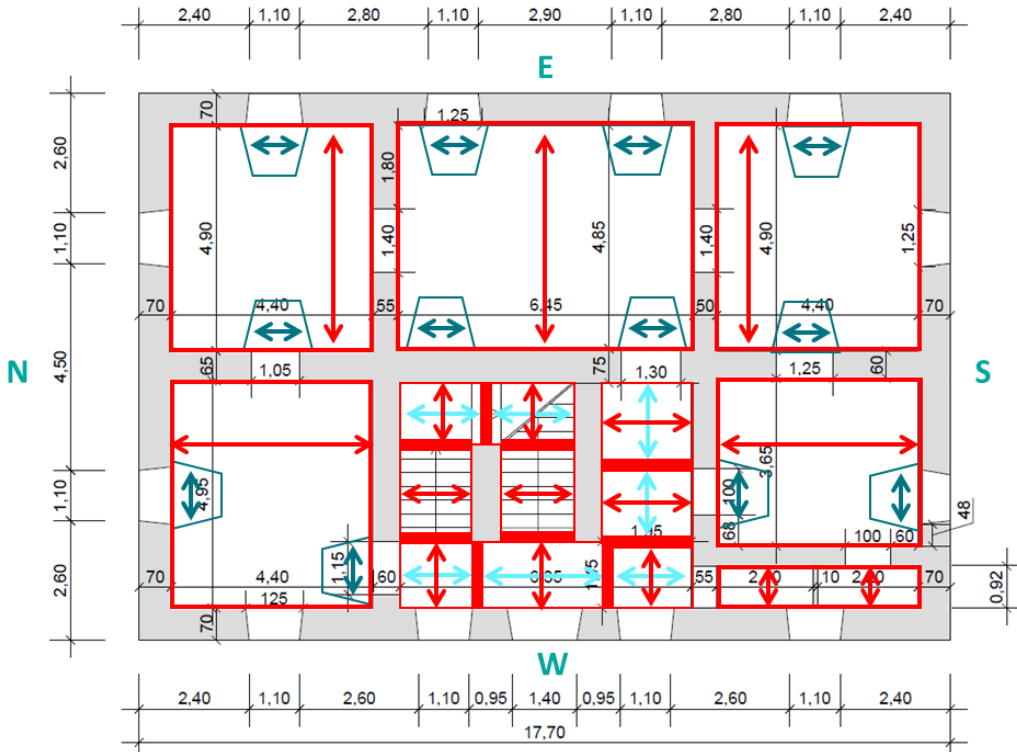


Figure 2.4: Vaulted system in ground floor



Figure 2.5: Vaults examples: east and west

2.2.3 First floor

The floor plan of the first floor strongly resembles the one on the ground floor. The measurements indicate however, that the walls on the first floor are slightly thinner than the walls on the ground floor, which is most likely due to the reduced vertical loads and the lack of horizontal thrust from the vaults in comparison to the ground floor. Furthermore, there are two additional bathrooms on the northeast side between the two rooms, which cannot be found in the plan of the ground floor. At this point, the walls are not supported directly by walls beneath them, but by the vaulted system over the ground floor transmitting the load to the ground floor walls. A detailed plan can be found in Appendix C. These walls seem however to have been built in a later episode and were most likely not part of the original construction meaning that they are not structural elements and do not need to be modelled as such.

During the interview the leading engineer of the retrofitting project currently being executed [9] revealed that the slab above the first floor had been constructed with the FERT [8] methodology after the damage of the war in the 20th century. A FERT slab is composed of reinforced concrete beams with hollow masonry elements spanning between the beams. The whole composition is covered by a concrete layer to connect the elements to each other (see also Figure 2.6)[9]. Furthermore, an reinforced concrete (RC) ring beam going around the perimeter of the top of the walls at the level of the second floor was introduced during the remodelling in 1997 to connect the walls better and give the building a more box-like behaviour. Later in the interview, the engineer [9] also gave up the information that the new roof structure is supported on the facades of the building, as well as on two columns on the second floor, leading the load down to the walls of the first floor (see also Figure E.2 in Appendix E).

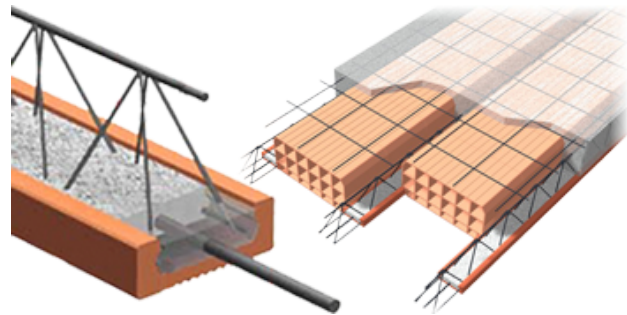


Figure 2.6: FERT slab construction method [11]

2.3 Earthquake damages

During the site visit in April 2023, all the visible damages and cracks on the walls and vaults were documented, numbered and analyzed. The complete inventory can be found in Appendix D. In this chapter, only the main observations are summarized.

2.3.1 Facade cracks

The most interesting and conclusive observations are made by looking at the crack patterns of the facades: the diagonal cracks reveal where the wall failed in shear, whereas the horizontal cracks flexural failure or even failure throughout-of-plane (OOP) mechanisms. In Figures 2.7 and 2.8 the arrows represent the direction of the seismic force corresponding to the cracks of the same colour.

North and south facades

The cracks on the north facade correspond mainly to shear failures in the spandrels as well as in the central pier of the facade (see Figure 2.7). As expected, the diagonal cracks are steeper on the lower part of the facade, corresponding to a failure in shear, and flatter towards the roof, coming from a failure in flexure. Several horizontal cracks at the edges of the facade cannot exactly be identified as a flexural failure but might come from a stress concentration or a global OOP mechanism of the west facade (see more in Chapter 2.4).

On the south facade, the crack pattern is very similar to the one on the north facade. A difference can be noted in the cracks in the piers at the outer edges of the facade, where big shear cracks can be found that are not present on the north facade.

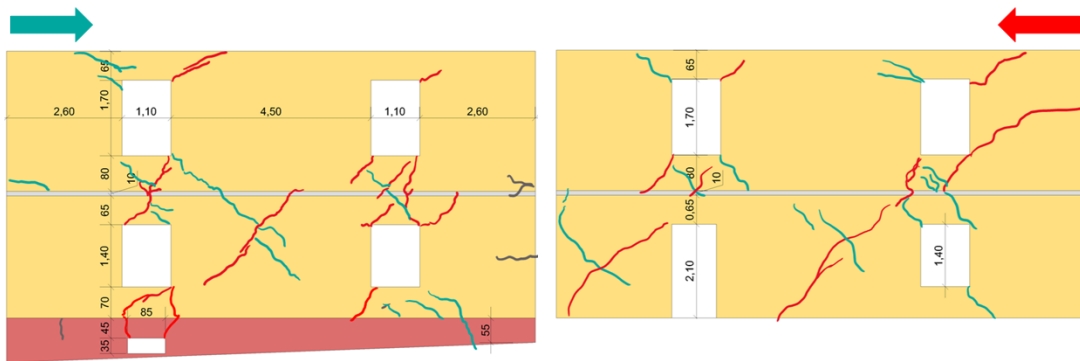


Figure 2.7: Cracks with corresponding direction of acceleration, north and south facade

East and west facades

The east facade shows fewer cracks than the north or south facades. This was to be expected since the seismic load is taken by a bigger wall with an overall bigger area to resist the stress (see Figure 2.8). The shear cracks observed on this facade are almost exclusively in the spandrels and no shear cracking can be observed in the piers. The flat cracks in the top south and north corners could also come from a detaching of the roof as a rigid block, lifting off and rocking on the building during the earthquake motion. The cracks in grey on the south side and the centre of the facade, however, can be associated with an OOP failure of the east facade described more in detail in chapter 2.4. On the west facade, there are even fewer shear cracks than on the east facade. However, the most noticeable damage consists of long horizontal cracks above the windows on the ground floor and the windows on the first floor. These are associated with the OOP mechanism of the west facade due to the combination of seismic force and horizontal thrust of the vault (see chapter 2.4).

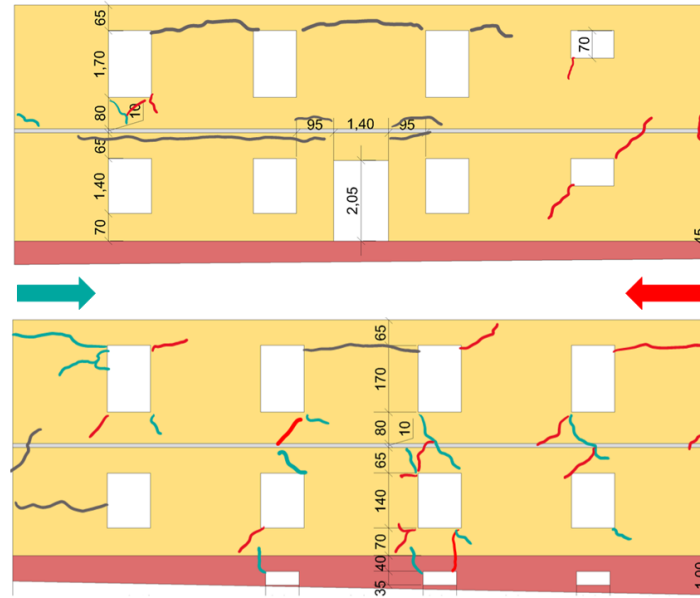


Figure 2.8: Cracking with corresponding direction of acceleration, west and east facade

2.3.2 Interior cracks

The cracks visible from the inside of the building have been documented in a similar way as the ones on the facades. Note that they have been documented on a plan view of the building and in addition, photos have been added to the documentation to see the vertical geometry of the cracks (see also Appendix D). An example of the documentation can be seen in Figure 2.9 below showing the cracks of the ground floor. The cracks that are found on the ceiling can mostly be linked to partial failures of the vaults (for example cracks 5, 6, 12, 14, 15, 17, 22), whereas others are linked to shear deformation such as cracks 7, 8, 10, 11, 20.

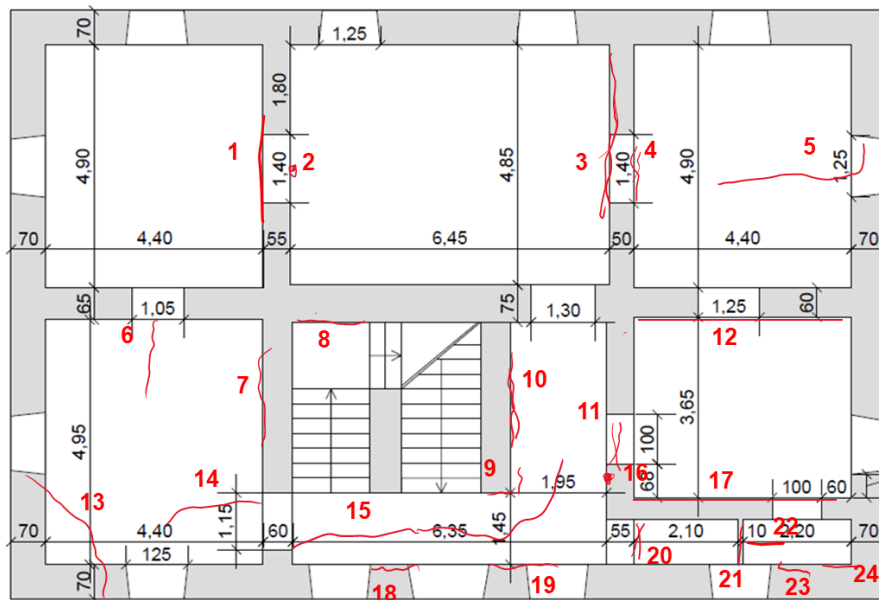


Figure 2.9: Cracking on ground floor

2.4 Observed out-of-plane-mechanisms

When looking at the cracking pattern discussed in chapter 2.3 and documented in Appendix D, two main global mechanisms can be observed. Compared to what D'Ayala and Speranza propose, this would correspond to a variant of the F mechanism [12]. The first one concerns the west facade, which is more pronounced, whereas the second one concerns the east facade and is less visible. The overall behaviour, however, is the same for both and can be described as follows:

The mechanism consists of five elements moving with respect to each other (see Figure 2.10). In a first episode, the seismic action moves the facade slightly out of its plane. The horizontal thrust that the vault exerts on the facade then helps push the latter out even further. For the facade to be pushed out of its plane, it needs to form three hinges, one on the top where it is restrained by a rigid slab and a ring beam, a second one at its foundation and a third one where it breaks in the middle, assumed to be where the thrust from the vault is applied. The inside structure needs to form hinges to be compatible with this global mechanism. Therefore, the vault cracks at mid-span as well as at the supports on the inside wall and the facade.

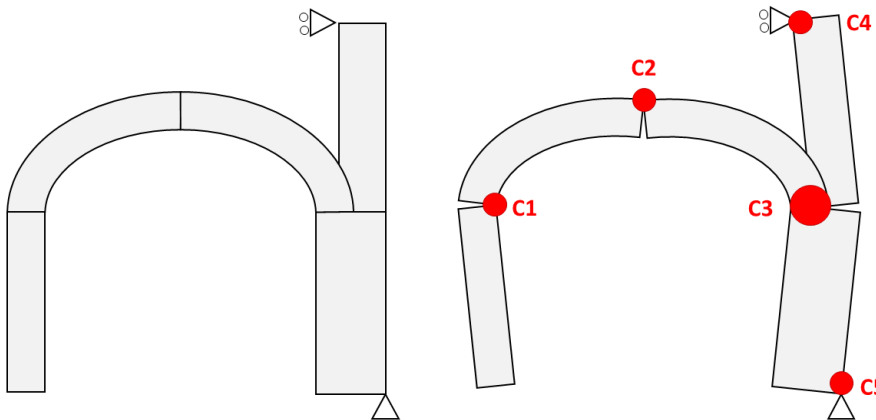


Figure 2.10: Schematic OOP mechanism

2.4.1 West facade

First, the west side of the structure is observed. The concerned area of this mechanism can be seen in Figure 2.11. Several cracks on the facade of the building (see Figure 2.12) can be noticed that indicate the presence of the hinges C3 and C4: Hinge C3 is not very visible but can be assumed to correspond to cracks 3 and 4 of the west facade. Cracks 8, 9 and 10 on the other hand, indicate the presence of hinge C4. Figure 2.9 shows cracks number 9 and 17 on the ground floor that indicate the presence of hinge C1, whereas cracks 14, 15 and 22 correspond to hinge C2.

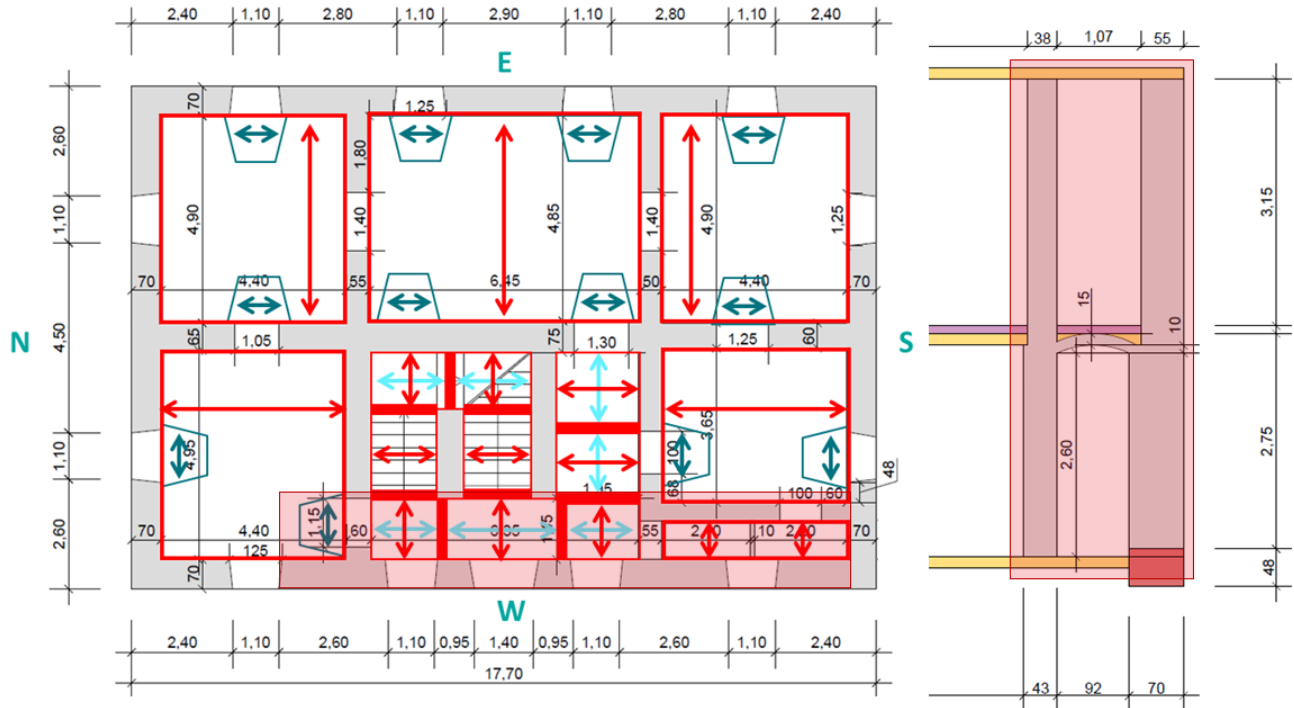


Figure 2.11: OOP mechanism west facade: Plan view and cross-section of the concerned zone

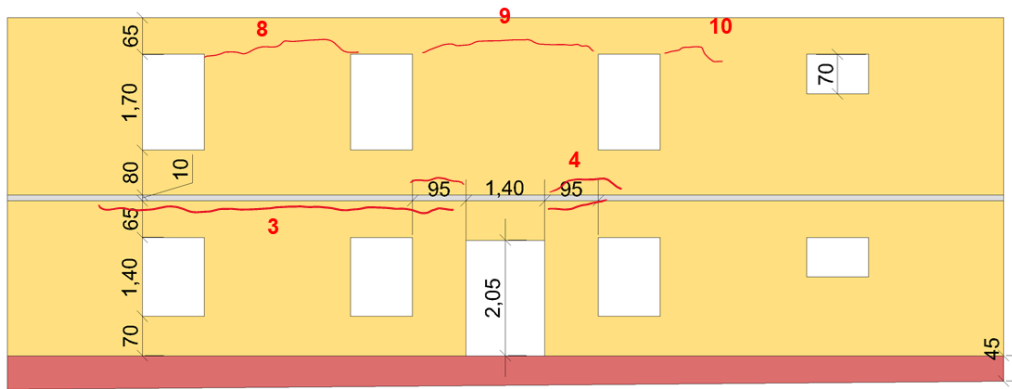


Figure 2.12: OOP mechanism west facade: Relevant cracks that indicate the mechanism, west facade

2.4.2 East facade

The second mechanism, on the east facade, is less obvious, and some of the cracks may be too small to see with the naked eye. Nevertheless, some cracks indicate the presence of an F-mechanism. The concerned part of the building for the east mechanism can be seen in Figure 2.13. First, crack 12 of the ground floor can be the representation of the first hinge (C1) (see Figure 2.9). Although crack 5 does not extend across the entire vault, cracks 2 and 4 indicate that the walls beneath the vault are being torn apart, which could be an indication of the C2 hinge. The C3 hinge is visible in crack 7 of the east facade (Figure 2.14), whereas cracks 1-5 on the east facade indicate the presence of hinge C4. It can be noticed that the mechanism is more pronounced on the south side of the wall (crack 5 ground floor and crack 7 east facade). This could be due to the minimal eccentricity of the stabilizing staircase that is slightly more in the north than the south part of the building, creating a rotational force of the building around its vertical axis. This also makes the south side of the building more flexible, allowing for more deformation and cracking on that side.

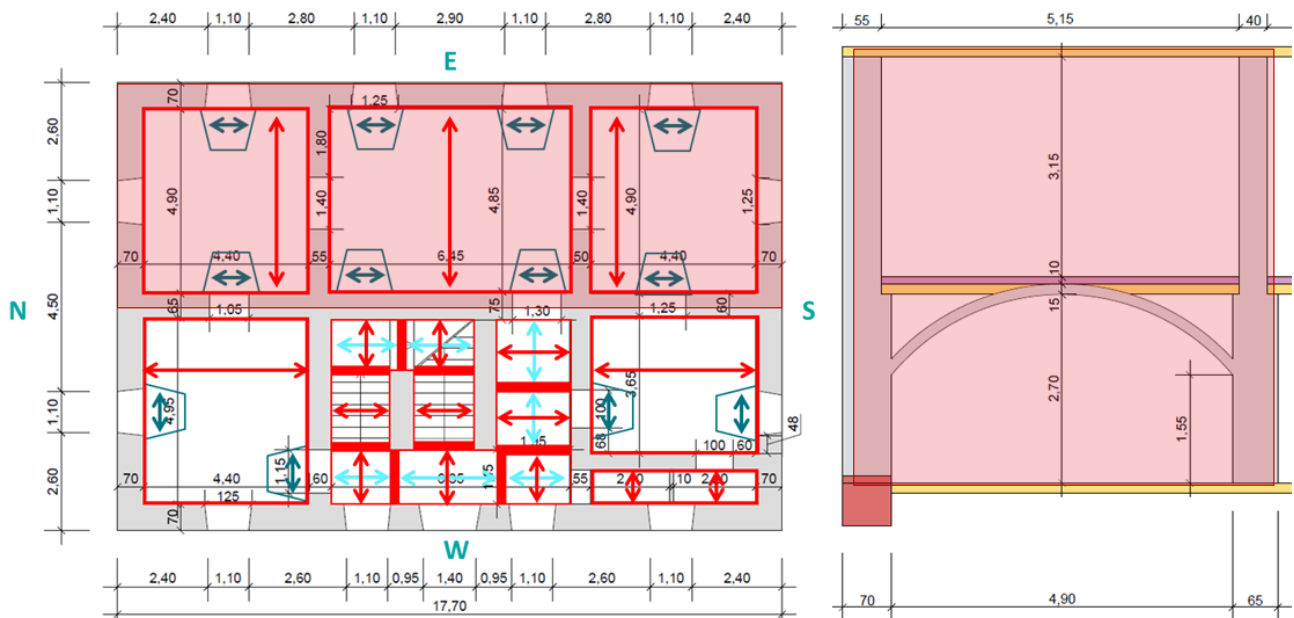


Figure 2.13: OOP mechanism east facade

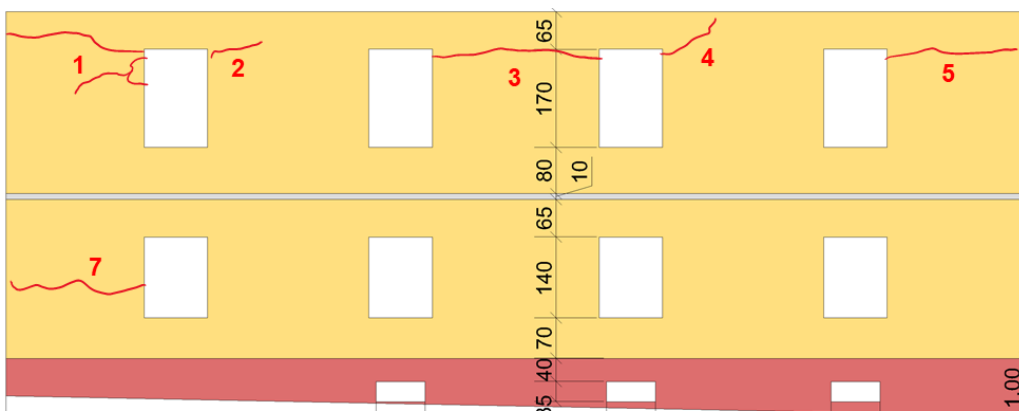


Figure 2.14: OOP mechanism east facade: Relevant cracks that indicate the mechanism, east facade

3. Methodology

This chapter aims to highlight the design and verification bases as well as the methodology of the analyses to be performed on the Parish House of Petrinja. It has been decided to apply the newest version of the Eurocodes and to follow the methodology proposed by Eurocodes 1998-1-1 and 1998-3 as much as possible.

3.1 Eurocodes

The codes and regulations used for the analysis of the Parish House are listed below. The relevant code used is the Eurocode. At the moment the current version (first generation) is under revision. However, due to the implication of my supervisor and mentor Prof. K. Beyer in the editorial of the new generation of Eurocode 6 and 8, the drafted version of the second generation of EC 1996 as well as 1998 parts 1-1 and 3 will be used in this thesis. The relevant codes are the following:

- **EN 1990** Structural safety, serviceability and durability (Version 2002) [13]
- **EN 1991-1-1** Actions on structures, Part 1-1 Densities, self-weight, imposed loads for buildings (Version 2009) [14]
- **EN 1992-1-1** Design of concrete structures - Part 1-1: General rules and rules for buildings (Version 2011) [15]
- **EN 1993-1-1** Design of steel structures - Part 1-1: General rules and rules for buildings (Version 2009) [16]
- **prEN 1996-1-1** Design of masonry structures, Part 1-1 General rules for reinforced and unreinforced masonry structures (Draft 2021) [17]
- **prEN 1998-1-1** Design of structures for earthquake resistance, Part 1-1: General rules and seismic action (Draft 2022) [18]
- **prEN 1998-3** Design of structures for earthquake resistance, Part 3 Assessment and retrofitting of buildings and bridges (Draft 2023) [19]

3.2 Software

The software used in the elaboration of this thesis is the following:

- **AutoCAD 2023/2024**: For the production of the plans and the mesh drawings [20].
- **Jupyter Notebooks**: For the elaboration of pushover curves for different wall geometries in Chapter 5. In addition to the specific scripts in Appendix H, a set of universal notebooks has been created in collaboration with Caroline Heitmann [3].
- **Microsoft Excel**: For the calculation of model properties and pushover curves in the in-plane analysis [21].
- **MATLAB**: To develop scripts for pre- and postprocessing of the analysis data and to run the OpenSees model [22]. Parts of previously written scripts by Dr. Igor Tomić were taken as a base and adapted to the project.
- **OpenSees**: The software used for the dynamic analysis of the equivalent frame model [2].

3.3 Analysis procedure

Since the Parish House is an existing structure, the rules of EN 1998-3 "Assessment and retrofitting of buildings and bridges" will be applied for the analysis of the resistance of the building. In masonry buildings, one of the most common reasons for the failure is the low resistance of the walls against forces in the direction perpendicular to their plane, i.e. out-of-plane (OOP). Therefore, it is not only important to analyse and verify the global behaviour of the structure but also to evaluate localized failure mechanisms, herein called OOP mechanisms. To verify the structure, two limit states referred to as near-collapse (NC) limit state and damage-limitation (DL) limit state are used. The DL limit state is used to verify the serviceability, whereas the NC limit state is determinant to ensure the structural safety.

3.3.1 Global analysis

For the global analysis of the Parish House, the choice is to model the structure with an equivalent frame model (EFM) and to perform a dynamic response history analysis (RHA) as proposed in paragraph "§11.5.1.6 Verification through non-linear response-history analysis" EN 1998-3. Although Eurocode 1998-1-1 requires to use a minimum of seven different ground motions (§6.6 Response-history analysis), it is decided to only use one to remain within a reasonable scope for this thesis. The used ground motion is described in Chapter 4.2.1. The response of the building, i.e. the "design value of action effects", due to the action of the ground acceleration corresponds to the maximum displacement of the top nodes of the model. This effect will be amplified by a factor of $\gamma_{Sd} = 1.15$ according to statement (5) of "§4.2.2 Verification rules" EN 1998-3. To verify the structure, the design value of the action effects should not exceed the resistance limit. In the case of non-linear response history analysis, the resistance corresponds to the displacement of the top node at which the limit state of one element of the structure is reached in a non-linear pushover curve (see EN 1998-3 §11.5.1.6). To obtain the pushover curve, EN 1998-1-1 §6.5 is used. Since the model in OpenSees, used for the dynamic RHA would need a lot of calibration to achieve accurate non-linear static analysis results, this part will be done using a simplified method proposed in Lestuzzi and Badoux [23]. The detailed methodology can be found in Chapter 7.1.

3.3.2 Out-of-plane analysis

For the evaluation of the stability of specific walls against local or global OOP mechanisms, chapter §6.5 EN 1998-1-1 will be applied. The method described in §6.5.4, also known as the N2-method is exploited to evaluate the OOP resistance of the walls using a pushover curve of a multi-degree-of-freedom (MDOF) system that is then transformed into a pushover curve for an equivalent single-degree-of-freedom (SDOF) system. When applying a non-linear kinematic analysis as described in "§11.3.3.2 Non-linear kinematic analysis (displacement capacity of the mechanism)" of EN 1998-3, the displacement capacity according to the statement (2) d) is $d_u = 40\% \cdot d_0$ and $d_{u2} = 60\% \cdot d_0$. The d_0 marks the displacement where the seismic multiplier α reaches zero, meaning there is no lateral resistance. For the verification d_u serves as the limit for the DL limit state and d_{u2} is the limit for the NC limit state.

3.3.3 Partial factors

To account for uncertainties in the modelling, the material and the load parameters of the verification it is of importance to consider safety factors on the characteristic values.

Model based uncertainty

Eurocode 1998-3 proposes a specific approach to this based on the "Knowledge levels" explained in "§5 Information for structural assessment". Since the knowledge of the structure about geometry, construction details, as well as material properties is fairly small and no further investigations are made within this project, the knowledge level is set at 1 for all the categories. Knowing this, the safety factor on deformation capacities is determined according to Table 11.7 EN 1998-3 and can be assumed to be $\gamma_{Rd} = 1.85$.

For the shear resistance of the members, the partial factor depends on the mode of resistance. For the resistance in flexure, the partial factor can be taken as $\gamma_{Rd} = 2.15$ (of Table 11.4 EN 1998-3 [19]). For the resistance of the member against shear sliding the partial factor is set as $\gamma_{Rd} = 1.65$ (Table 11.5 EN 1998-3 [19]). Note that those are the values for piers, the ones for spandrels are slightly different. However, since those resistances only play a role in the elaboration of the pushover curve in Chapter 7.1, where only the resistance of the masonry piers is considered, the partial factors for spandrels are not of importance.

For the verification of the OOP resistance only partial factors are applied on the deformation capacity as described in Chapter 3.3.2

Material uncertainties

For the modelling of the initial state, only the material properties of the masonry are of relevance for the verification of the structure. The partial factor is determined as in Table 4.1 1996-1 [17] and is $\gamma_M = 2.5$. For the modelling of the steel ties for the retrofitted state, the partial factor for steel is determined based on EN 1993-1-1 and is of $\gamma_{M0} = 1.0$ [16].

Load uncertainties

Load and mass uncertainties are accounted for as prescribed in Eurocode 1990 [13]. More explanation can be found in Chapter 4.2.

4. Characteristics of the structure

4.1 Material properties

During the site visit in April 2023, a lot of information about the building could be retrieved such as general dimensions and some construction history about the Parish House (see also chapter 2.1). Nevertheless, there are still a lot of insecurities about other parameters such as the material characteristics of the masonry and the mortar or the concrete of the FERT slab [8]. Therefore, it is important to make realistic assumptions about the material to model the structure as close to reality as possible and receive reasonable results. By clause (1) "§5.5 Representative values of material properties", EN1998-3 the following rule applies:

"For existing materials, design values of material properties X_d for calculating resistances to be used in local verifications, should be taken as the mean. Mean values should be obtained from testing and additional sources of information, and different mean values may be considered in different areas of the structure, as appropriate, based on test results"

Since no testing is possible, the mean value of reference values from the literature can be taken. The resistance values of the masonry will need to be divided by the partial factor γ_M for material properties (as per EN 1996-1 Table 4.1)

4.1.1 Masonry properties

From photos from drone recordings provided by Zvonko Sigmund, in the zones of sampling, the bricks seem to be a reddish to brown colour (see Figure 2.1). Otherwise, there is unfortunately not more information. It makes thus sense to use mean values from the range of what the Italian code [24] suggests:

Table 1. Reference values of the mechanical parameters and average specific weights for selected types of masonry (extract from Table C8A.2.2. of Circ. NTC08, 2009).

Masonry typology	f_m (N/mm ²)	τ_o (N/mm ²)	E (N/mm ²)	G (N/mm ²)	W (kN/m ³)
	min-max	min-max	min-max	min-max	
Irregular stone masonry (pebbles, erratic, irregular stone)	1.0 1.8	0.020 0.032	690 1050	230 350	19
Uncut stone masonry with facing walls of limited thickness and infill core	2.0 3.0	0.035 0.051	1020 1440	340 480	20
Cut stone with good bonding	2.6 3.8	0.056 0.074	1500 1980	500 660	21
Soft stone masonry (tuff, limestone, etc.)	1.4 2.4	0.028 0.042	900 1260	300 420	16
Dressed rectangular (ashlar) stone masonry	6.0 8.0	0.090 0.120	2400 3200	780 940	22
Solid brick masonry with lime mortar	2.4 4.0	0.060 0.090	1200 1800	400 600	18

Figure 4.1: Masonry properties as suggested by the Italian code [24][25]

The following characteristics of solid brick masonry with lime mortar will be the properties that are assumed throughout the entire analysis process:

- Compressive strength of the masonry: $f_M = 3.2 \text{ N/mm}^2$
- Young's modulus: $E = 1500 \text{ N/mm}^2$
- Shear modulus: $G = 500 \text{ N/mm}^2$

The friction coefficient, as well as the Poisson's ratio, can be taken as suggested by Lourenço et. al. [26]: The cohesion is estimated to be $c = 0.18 \text{ MPa}$ and the coefficient of friction is estimated at $\mu = 0.65$. The volumetric load is defined based on the Annex of the SIA 261 (Swiss code) [27] and is taken as $\gamma_{masonry} = 18 \text{ kN/m}^3$ ("Maçonnerie montée sans crépi, briques de terre cuite pleines"). Applying the partial factor $\gamma_M = 2.5$ on the resistance values, the following properties are retained:

- Compressive strength of the masonry: $f_{M,d} = f_M/\gamma_m = 3.2/2.5 = 1.28 \text{ N/mm}^2$
- Young's modulus: $E = 1500 \text{ N/mm}^2$
- Shear modulus: $G = 500 \text{ N/mm}^2$
- Cohesion: $c_d = c/\gamma_M = 0.18/2.5 = 0.072 \text{ N/mm}^2$
- Coefficient of friction: $\mu = 0.65$
- Volumetric load: $\gamma_{masonry} = 18 \text{ kN/m}^3$

The initial shear strength of the masonry can be determined using table 5.4 of EN 1996-1-1: since the compressive strength of the mortar is assumed to be about $f_m = 1.28 \text{ N/mm}^2$, the initial shear strength is about $f_{vk0} = 0.1 \text{ N/mm}^2$. The mean value can be derived using Appendix K 3.2.2 of EN 1996-1-1. $f_{vm0} = 1.3 * f_{vk0} = 0.13 \text{ N/mm}^2$. These values will be of interest in the calculation of the push-over curve in Chapter 7.1.

Drift model

The model used with OpenSees [2] requires the introduction of a drift model to describe the in-plane behaviour of the masonry piers and spandrels. Therefore, the model proposed by Eurocode 1998-3 "§11 Specific rules for masonry buildings" is used. Figure 4.2 shows the general shape of the force-drift curve.

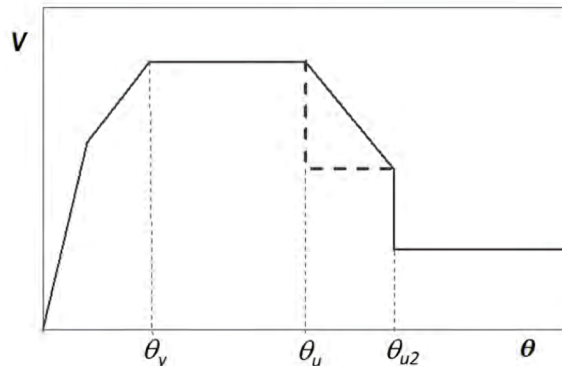


Figure 4.2: Force-drift relationship for masonry members [19]

The curve is characterized by the following values:

- θ_y is the drift at the moment the masonry member starts yielding
- θ_u is the ultimate member drift starting from which the shear resistance starts to drop.
- θ_{u2} is the member drift at which the shear resistance has dropped by 20%.
- V_d is the maximum shear resistance of the member.

These values depend on the mode of failure of the member. If the member fails in flexure the values are:

- $\theta_{f,ud} = \theta_{f,u}/\gamma_{Rd} = 0.012/1.85 = 0.0065$
- $\theta_{f,u2d} = \theta_{f,ud} * 4/3 = 0.0086$

For shear sliding failure the values are:

- $\theta_{s,ud} = \theta_{s,u}/\gamma_{Rd} = 0.008/1.85 = 0.0043$
- $\theta_{s,u2d} = \theta_{s,ud} * 4/3 = 0.0058$

And for diagonal shear failure, the values are:

- $\theta_{d,ud} = \theta_{d,u}/\gamma_{Rd} = 0.006/1.85 = 0.0032$
- $\theta_{d,u2d} = \theta_{d,ud} * 4/3 = 0.0043$

The drift at collapse, i.e. the drift at which the resistance of the wall drops by 50 %, is called θ_c and can be derived based on the approach suggested by Vanin et al. [28]:

$$\theta_c = 1.15 \cdot \theta_{u2} \quad (4.1)$$

4.1.2 Timber properties

The new roof, built in the late 20th century is assumed to be made out of coniferous wood, a light wood with a weight of $\gamma_{timber,mod.} = 5 \text{ kN/m}^3$. The other material characteristics of the roof structure are not of importance because the roof is considered to behave as a rigid block due to the FERT slab that was added during the reconstruction in the late 20th century (see also chapter 2.1). The planks constituting the surface of the first-floor slab (above the vault) are assumed to be made out of local timber essences. According to Lourenço et. al. [26] the weight of the material can be assumed to be $\gamma_{timber,hist.} = 8.1 \text{ kN/m}^3$. The other material properties of timber are not of importance since the timber elements are not analysed as structural members in this study.

4.1.3 Concrete properties

During the renovation and reconstruction works in 1996-1997 the roof, as well as the slab above the first floor, were rebuilt (see chapter 2.1). The reconstruction measures also contained the addition of a FERT slab above the first floor to replace the existing one, as well as an RC ring beam (see Appendix E [9]). Other than that, no information about the construction materials of the roof is available. Therefore, the material properties are roughly estimated using the given values in EC 1992-1-1 :

- Young's modulus for concrete: $E = 30 \text{ GPa}$
- Poisson's ratio: $\nu = 0.2$
- Shear modulus: $G = E/(2(1 + \nu)) = 12.5 \text{ GPa}$

4.2 Loads and loadcases

The load case corresponding to a seismic case should correspond to the one provided in EN 1990 [14] and EN 1991 [13]. According to EN 1990, the general format of the effects of actions should be:

$$E_d = E \{G_{k,j}; P; A_{Ed}; \psi_{2,i} Q_{k,i}\} \quad j \geq 1; i \geq 1$$

Where:

- $G_{k,j}$: Characteristic value of permanent action j , i.e. the self-weight
- P : Relevant representative value of a prestressing action (not present in this case).
- A_{Ed} : Design value of seismic action
- $Q_{k,i}$: Characteristic value of the accompanying variable action i , such as live loads in the building or snow.
- $\psi_{2,i}$: Factor for quasi-permanent value of a variable action i

The actions that are considered to act on the structure during the earthquake are:

- Self-weight (dead load)
- Live load (from people living in the building)
- Load on the roof for maintenance
- Snow load
- Wind action

Keep in mind, that only the seismic load case will be analyzed in this thesis, the ultimate limit state for non-seismic load cases and the serviceability are admitted to be verified.

4.2.1 Seismic load

To verify the structure against the combined action of the gravity loads as well as the actions of a seismic event, a dynamic analysis will be performed using the software OpenSees. This requires entering a representative ground acceleration to perform the RHA. Since there were no measurement stations nearby Petrinja, that had recorded the earthquake in December 2020, a different approach had to be chosen:

The first step is to extract the reference peak ground acceleration (PGA) of Petrinja. The Department of Geophysics at the University of Zagreb offers a website, where the PGA corresponding to different return periods can be looked up [29] (see screenshot of the website in Appendix F). For a return period of 95 years (damage-limitation case), an acceleration of $a_{gR} = 0.074 g$ and for a return period of 475 years (near-collapse case) an acceleration $a_{gR} = 0.152 g$ are given. The next step is to determine the soil class of Petrinja: The geological map of the region Sisak, to which Petrinja belongs, shows that the village lies within the region of category "a1" [30] (see map in Appendix G). This corresponds to a "Sedimentiterasa: siltovi, pijesci, sijunci" (Croatian) which means it is a soil made of silt and clay that indicates a soil category E according to Eurocode 1998-1-1.

Finally, the spectra for the NC limit state and DL limit state as mentioned in Eurocode 1998-3 can be calculated. If they are plotted against the record of the Montenegro earthquake in 1979, measured at the Albatros station in the south of Montenegro (Latitude: 41.919° and Longitude: 19.221°) [31], factorized by 1.0 and 0.5 respectively, it can be seen that the resemblance between the measured ground motion spectra and the design spectra is high.

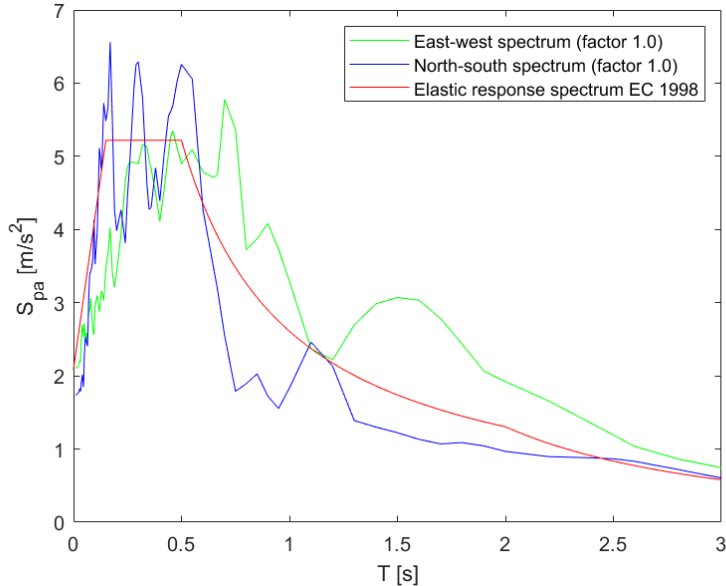


Figure 4.3: Near-Collapse acceleration spectrum against spectra of the Montenegro 1997 earthquake

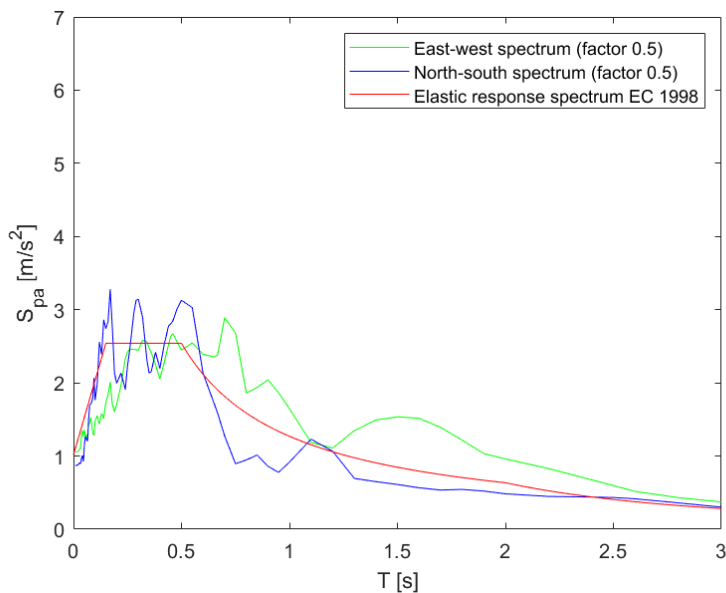


Figure 4.4: Damage Limitation acceleration spectrum against spectra of the Montenegro 1997 earthquake multiplied by a factor of 0.5

The Montenegro earthquake was one of the most damaging ones of the 20th century with its moment magnitude of 6.9 measured during the main shock on 15th of April 1979. The ground acceleration record can be seen in Figure 4.5 for the east-west, as well as for the north-south excitation of the earthquake. The resemblance of the spectrum to the Eurocode spectrum, visible in Figures 4.3 and 4.4, makes it perfectly fitting to use as the ground motion for the response history analysis. In this scenario, the ground acceleration has been scaled as closely as feasible to the design spectrum across the whole period range. However, because the building's periods are quite low, it may have been considered that the spectrum should have been adjusted to better match the spectral acceleration of the lower periods. However, the author has decided to match the ground acceleration employed to the entire design spectrum rather than simply the lower periods.

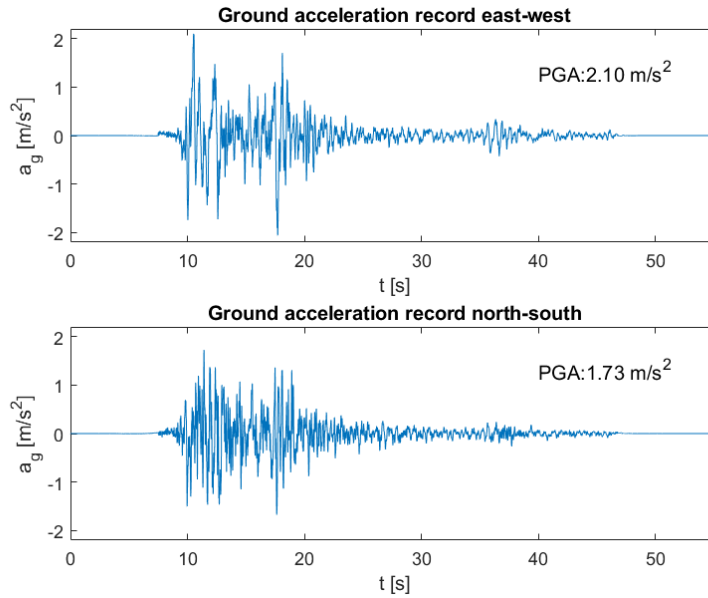


Figure 4.5: Ground acceleration records of the Montenegro earthquake 1979, Albatros station [31]

4.2.2 Self-weight

The self-weight comes from the construction materials, as well as the non-structural parts of the building such as roofing, tiles etc. The materials considered for all further calculations are the following:

- Masonry for construction: $\gamma_{masonry} = 18 \text{ kN/m}^3$ [27]
- Modern timber for construction: $\gamma_{timber,mod.} = 5 \text{ kN/m}^3$ [27]
- Historical timber for construction: $\gamma_{timber,hist.} = 8.1 \text{ kN/m}^3$ [26]
- Timber as covering material of the floors: $\gamma_{timber,covering} = 8 \text{ kN/m}^3$ [32]
- Plasterboards: $\gamma_{plaster} = 12 \text{ kN/m}^3$ [27]
- Concrete: $\gamma_{concrete} = 25 \text{ kN/m}^3$ [27]

The following surface loads or densities can be considered:

- Roof:
 - Roof tiles and lath (proposed by the Swiss code SIA 261 Annex A [27])
 $g_k = 0.75 \text{ kN/m}^2$
 - Roof isolation (since it is a new roof, see for example Swisspor [33])
 $g_k = 0.25 \text{ kN/m}^3 \times 0.2 \text{ m} = 0.05 \text{ kN/m}^2$
 - Timber members of the roof structure (a mean thickness of 0.2 m is admitted)
 $g_k = 5 \text{ kN/m}^3 \times 0.2 = 1 \text{ kN/m}^2$
 - Plasterboards for finishing the roof (bottom visible in rooms, proposed by the Swiss code SIA 261 Annex A [27])
 $g_k = 0.01 \text{ m} \times 12 \text{ kN/m}^3 = 0.12 \text{ kN/m}^2$
- Floor layers of the floor above the first level:
 - Parquet flooring (a mean thickness of 0.015 m is admitted)
 $g_k = 0.8 \text{ kN/m}^3 \times 15 \text{ mm} = 0.1 \text{ kN/m}^2$

- Fert slab (can be assumed to be equivalent to a concrete slab with a thickness of 0.10 m [9] in Appendix E)

$$g_k = 25 \text{ kN/m}^3 \times 0.15 \text{ m}$$

- Floor layers of the floor above the ground floor:

- Parquet flooring (a mean thickness of 0.015 m is admitted)

$$g_k = 8.1 \text{ kN/m}^3 \times 0.015 \text{ m} = 0.1 \text{ kN/m}^2$$
- Timber planks (a mean thickness of 0.03 m is admitted, see [9] in Appendix E)

$$g_k = 8.1 \text{ kN/m}^3 \times 0.1 = 0.8 \text{ kN/m}^2$$
- Filling material above vault (14 tons per m³, see [9] in Appendix E)

$$g_k = 14'000 \text{ kg/m}^3 = 1.4 \text{ kN/m}^3$$
 (volume directly calculated in Excel file)
- Masonry from vaults (see masonry of the walls, thickness of vaults is admitted to 0.15 m)

$$g_k = 18 \text{ kN/m}^3 \times 0.15 \text{ m} = 2.7 \text{ kN/m}^2$$

- Masonry of the walls $g_{k,10} = 18 \text{ kN/m}^3$ (proposed by the swiss code SIA 261 Annex A [27])

4.2.3 Live load

The Parish House's live load is brought about by its use as a residential building. According to EN 1991-1-1 this corresponds to a load category A which implies a characteristic surface load of $q_k = 2.00 \text{ kN/m}^2$ (same for floors or stairs). As mentioned above, this load will need to be multiplied by a factor ψ_2 to consider only the quasi-static part of the load. For category A this corresponds to a factor of $\psi_2 = 0.3$ (see Table A1.1 EN 1990 [14]).

4.2.4 Other loads and forces

A load applied on the roof for maintenance is considered of category H (EN 1991-1-1) but according to EN 1990, its factor for the seismic load case is equal to $\psi_2 = 0.0$ (see Table A1.1 EN 1990). Therefore, this load can be neglected. The same applies to the snow and wind action: although their effect is non-negligible, the load factor for the seismic load case is $\psi_2 = 0.0$ for both of them and those loads can therefore be disregarded.

5. Analysis of out-of-plane mechanisms

In addition to the two observed OOP F-mechanisms, described in Chapter 2.4, this chapter describes which other failure mechanisms were prone to happen. Furthermore, the observed as well as two hypothetical OOP mechanisms will be investigated. To do so, an approach based on the moment equilibrium of the wall or an energy-based approach is used.

Within the scope of this Master's Thesis and in collaboration with Caroline Heitmann, a set of Jupyter Notebooks accompanied by a joint report was elaborated. Those files form an interactive interface for users to discover the OOP resistance of walls for several simple mechanisms that can be personalized to their needs. A full description of those mechanisms can be found in the mentioned co-written report [3]. The specific Jupyter Notebooks, which have been adapted specifically for the mechanisms analyzed in this chapter, can be found in Appendix H. The other Jupyter Notebooks of the collaboration are referenced under [3] and can be downloaded from the respective GitHub repository.

5.1 Unobserved possible out-of-plane mechanisms

Looking at the possible mechanisms presented in the paper "An Integrated Procedure for the Assessment of Seismic Vulnerability of Historic Buildings" by D'Ayala and Speranza [34] (see Figure 5.1), there are several mechanisms that were imaginable but were not observed in the case of the Parish House. It is nevertheless interesting to discuss them from a qualitative perspective and to analyse some of them in a quantitative way to evaluate why they did not appear and what seismic action would have been necessary to trigger the mechanism.

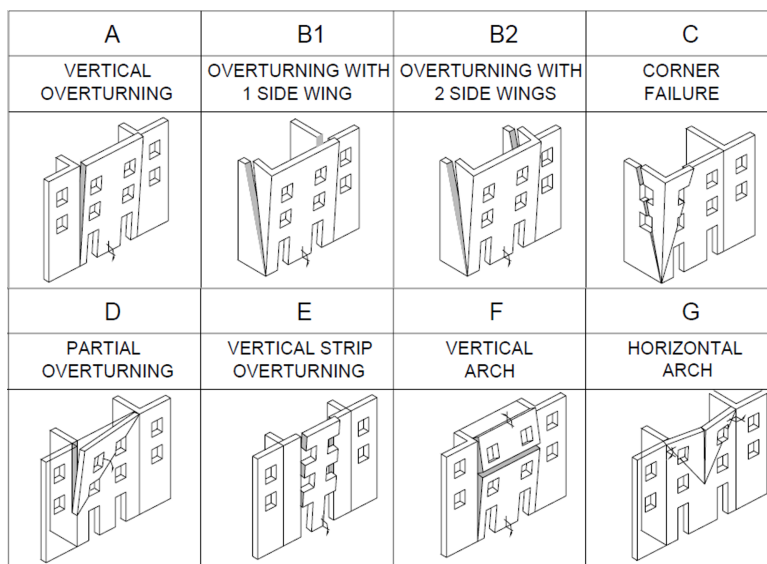


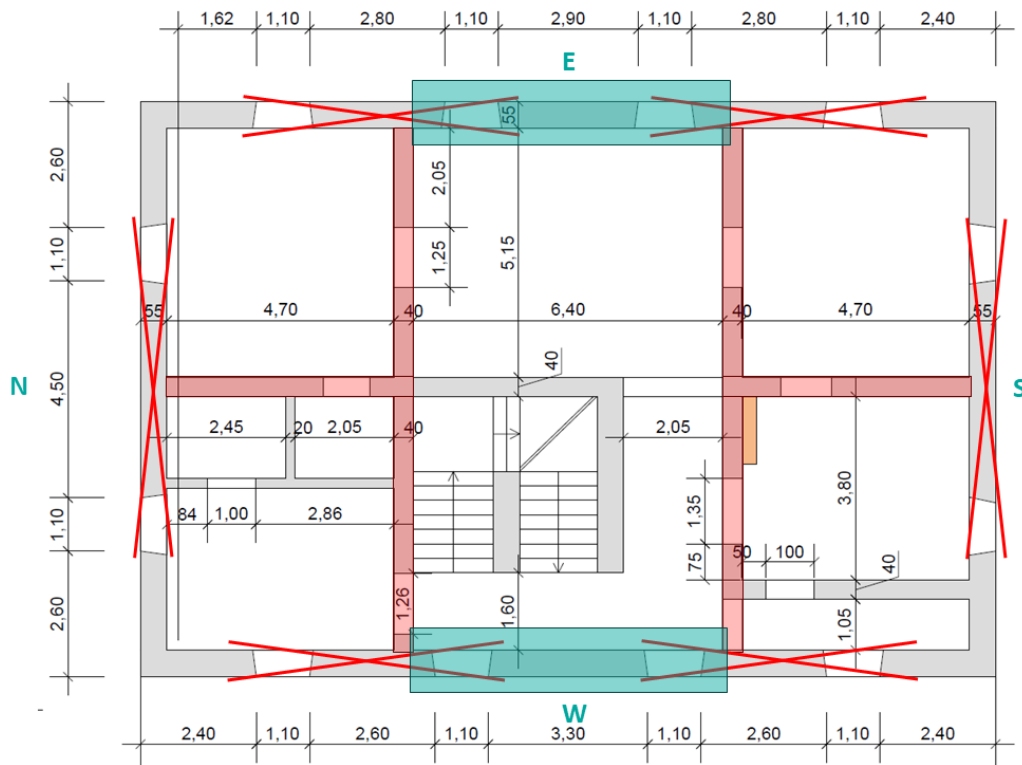
Figure 5.1: Possible mechanisms [34]

Since no vertical cracks at the edges of the facades have been observed (see also Chapter 2.3 and Appendix D), it can be assumed that there is a good interlocking of the bricks in the edges of the facades and the perpendicular walls are in general well connected. Therefore, mechanisms with vertical cracks along the edges of the facade or vertical cracks at the section of connection to a perpendicular wall behind the facade, like mechanisms A, B1, D and E are unlikely to happen and can thus be excluded. Mechanisms B2 and C would be possible especially when the walls are already cracked diagonally from the in-plane action of the earthquake. However, since the top slab is a FERT

slab [8] (see Chapter 2), with the addition of a ring beam around the top perimeter of the facades, the required uplifting of the top slab is almost entirely restricted. Furthermore, the slab restraining the wall at mid-height increases the resistance to those failure mechanisms even further. This makes the mechanisms improbable and is a good reason to exclude them from the quantitative analysis. Therefore, only mechanism G remains and will be analyzed through the means of a quantitative analysis.

5.1.1 G-Mechanism

The G-mechanism, as described by D'Ayala and Speranza [12][34], consists of a wall "horizontally arching" out-of-plane. This means that the fractures are mainly vertical (or diagonal) and the separated wall blocks not only turn around a horizontal axis of rotation but also about a vertical or a diagonal axis. This overturning movement is especially critical for masonry walls that already present vertical/diagonal cracking from previous or the same earthquake action and will eventually start to move out of the plane. If the facade is connected to walls perpendicular to their plane, the interlocking of the well-executed wall-to-wall connection is assumed to restrain this mechanism.



that are excluded for the mechanism marked with a red cross and the zones that are possible locations for the G-mechanism marked in turquoise.

The next step consists of finding the geometry of the blocks moving during the mechanism. By drawing the original mechanism schema proposed by D'Ayala and Speranza [12][34] onto the east and west facades it can be seen that this classical shape, with two triangular blocks, is not compatible with the placing of the slab: The slab is assumed to retain the wall for any OOP movement. Therefore, the diagonal cracks will be interrupted at the slab level. Furthermore, the now remaining trapezoidal shapes would need to turn on their support surface on the bottom to fall out, requiring a lot of energy to overcome the friction on the support surface. As a result, an adapted variant with a rectangular middle block is far more likely (see Figure 5.3). These mechanisms will thus be examined in the following subchapter.

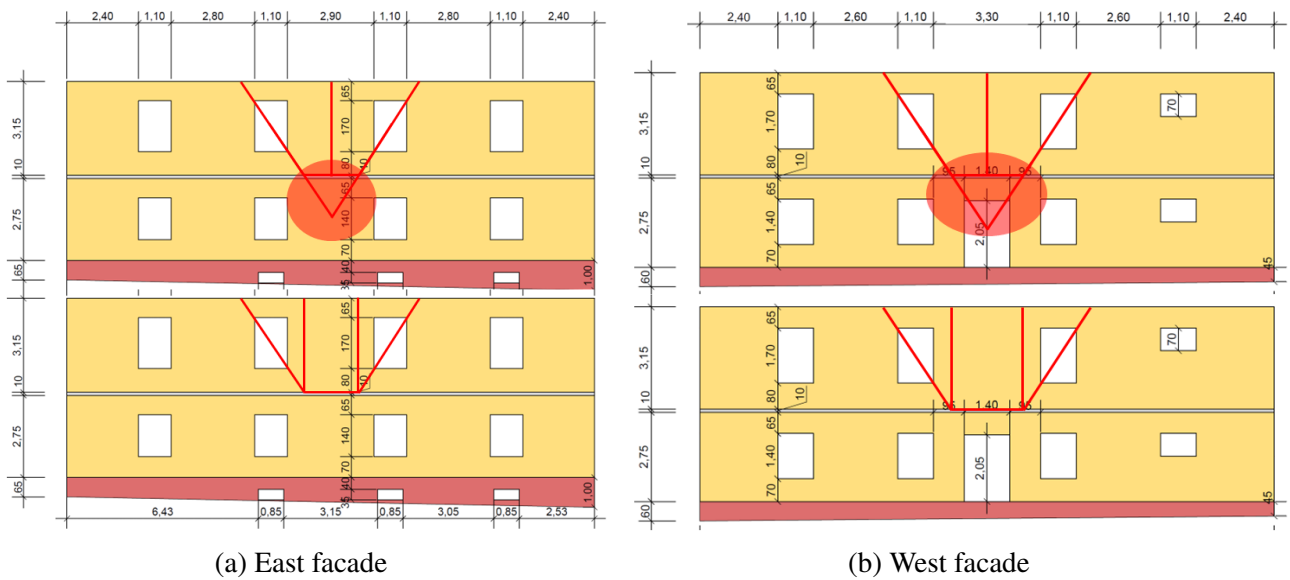


Figure 5.3: Compatible G-mechanisms, top images: incompatible version, bottom: compatible version

5.2 Overview and assumptions

In the next phase the before-described mechanisms, observed or potential, are analysed for their stability and resistance against horizontal acceleration in their respective OOP direction. To recapitulate, four mechanisms are analysed in more detail:

1. A global F-mechanism of the west facade, considering the thrust of the vaulted system on the inside of the building
2. A similar F-mechanism in the east facade
3. A G-mechanism in the upper west facade
4. A G-mechanism in the upper east facade

The F-mechanism proposed by [34] is further treated by Griffith et. al. [35], there the authors model the mechanism as a wall separated into two blocks that move out of their plane by rotating around the top and the base crack while staying connected at the mid crack. By calculating the moment equilibrium about the base point and the mid-point of the wall, the remaining lateral resistance to seismic action for a given deformation can be obtained and a pushover curve can be specified. The G-mechanism on the other hand needs to be analysed by a virtual work / energy-based approach,

considering the displacement and rotation of each block. More details can be found in D'Ayala et al. (2003)[12].

For the analysis, the following assumptions are made:

- Rigid diaphragms at the top and bottom of the F-mechanism, meaning there is no global overturning of the wall.
- Friction between the slab and the wall for the G-mechanism only acts up to a limit displacement $\delta_{max} = t/2$ (t is the thickness of the wall), after that, the friction drops to zero because the connection is lost.
- Only small displacements are considered, i.e. a linearization of the displacements and lever-arms of the forces is done (see also the report co-written with Caroline Heitmann [3] for more background).
- The blocks of the wall remain rigid, meaning that there is no elastic deformation within the moving blocks.
- The added stiffness to the F-mechanisms from the wall perpendicular to the OOP mechanism is neglected.
- The seismic acceleration on the wall is assumed to be constant over the height of the wall, i.e. there is a constant load distribution.
- It is assumed that the slab of the first floor is directly supported by the vault and does not sit on the walls. Therefore, no friction force of the slab on the wall is considered, hence no restraining force.
- The horizontal thrust of the vault increases with the displacement δ because it is proportional to the height, which is, in turn, in relation to the shape of the vault (see also Chapter 5.3).
- The thrust of the vault is lost, once the vault yields, i.e. if its highest point (at mid-span) is lower than its supports. Then the loads coming from the vault turn 0 since it is assumed to have failed.
- The connection between the top and bottom wall is considered to be broken once the displacement (δ) exceeds the thickness of the lower wall. At this point, the loads coming from the upper block are taken directly at the top of the lower block (in reality the wall is considered to be broken at this point).

5.3 Vault forces

As explained in Chapter 2.4, the particular type of F-mechanism analyzed for the Parish House strongly depends on the thrust of the vault on the inside of the building. To model the thrust in the algorithm calculating the pushover curve, the following general model is assumed to estimate the horizontal thrust of the vault:

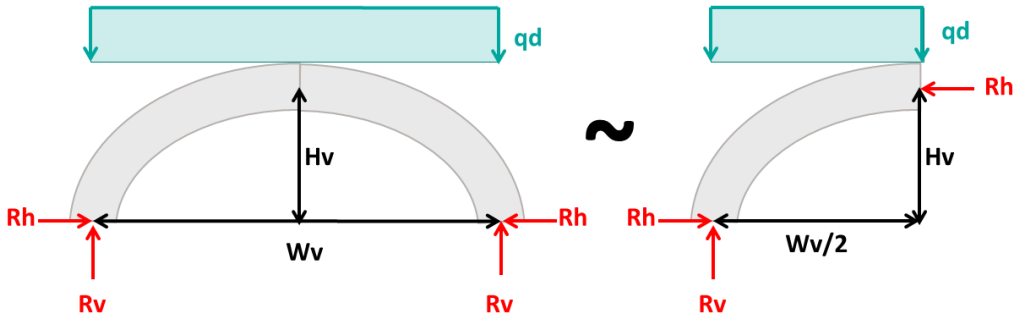


Figure 5.4: Vault model for calculation of thrust

It is assumed that the masonry vault is already cracked at midspan. Then the moment equilibrium of the half-vault (see right side of Figure 5.4) can be calculated as:

$$\sum M_O = R_h \cdot H_v - q_d \cdot W_v/2 * W_v/4 = 0 \quad (5.1)$$

Thus, the reaction forces of the vault can be calculated as follows:

$$R_v = q_d \cdot W_v/2 \quad (5.2)$$

$$R_h = \frac{q_d \cdot W_v^2}{8 \cdot H_v} \quad (5.3)$$

As seen in the equation the horizontal thrust is proportional to the span of the vault squared and inversely proportional to the height of the vault. When considering that the width of the vault increases with the displacement of the wall, meaning that $W_{v,\delta} = W_v + \delta$, and that the vault pieces behave as a rigid block, meaning that $\sqrt{(W_v/2)^2 + H_v^2} = \sqrt{(W_{v,\delta}/2)^2 + H_{v,\delta}^2}$ must remain constant, the horizontal and vertical thrust can be calculated as a function of δ :

$$R_v(\delta) = q_d \cdot (W_v + \delta)/2 \quad (5.4)$$

$$R_h(\delta) = \frac{q_d \cdot W_{v,\delta}^2}{8 \cdot H_{v,\delta}} = \frac{q_d \cdot (W_v + \delta)^2}{8 \cdot \sqrt{(W_v/2)^2 + H_v^2 - (\frac{W_v+\delta}{2})^2}} \quad (5.5)$$

5.4 Equilibrium formulation

5.4.1 F-Mechanism

As mentioned before, the pushover behaviour during the F-mechanism can be described using a moment equilibrium about the base point of rotation in addition to an equilibrium formulation about the upper point of rotation [35]. Two cases have to be considered: The first case applies to the mechanism of the west facade, where the crack line of the C3 hinge is clearly above the window opening. The second case applies to the east facade, where the crack of the wall goes through the window opening. The Figures 5.5 and 5.6 show the geometry of the two variants of the mechanism.

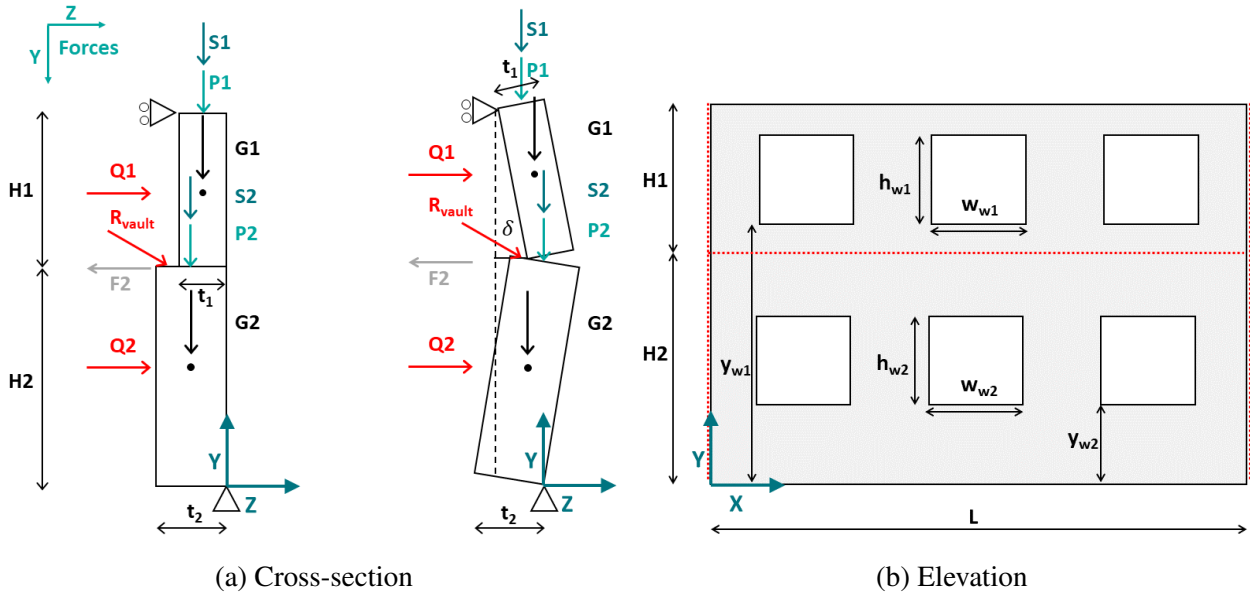


Figure 5.5: F-mechanism west side

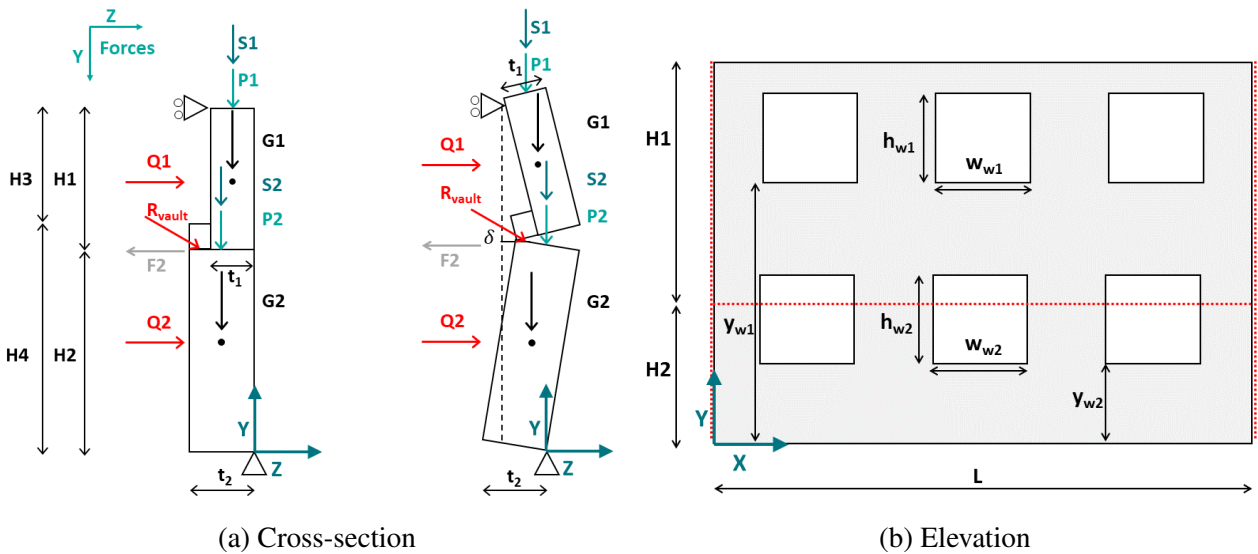


Figure 5.6: F-mechanism east side

Whatever the exact mechanism, the structure can be separated into two moving wall blocks, and the equilibrium formulation can be written as follows:

Global equilibrium about the bottom support:

$$\sum M_{bottom} = \bar{V} \cdot \bar{z}_{la} + \bar{H} \cdot \bar{y}_{la} = \begin{bmatrix} G_1 \\ S_1 \\ P_1 \\ G_2 \\ S_2 \\ P_2 \\ R_v \end{bmatrix} \cdot \begin{bmatrix} \delta_{G1} - t_1/2 \\ t_1/2 \\ t_1/2 \\ \delta - t_2/2 \\ \delta - t_2/2 \\ \delta - t_2/2 \\ \delta - t_2/2 \end{bmatrix} + \begin{bmatrix} Q_1 \\ Q_2 \\ F_1 \\ F_2 \\ R_h \end{bmatrix} \cdot \begin{bmatrix} y_{G1} \\ y_{G2} \\ H_1 + H_2 \\ H_2 \\ H_2 \end{bmatrix} = 0 \quad (5.6)$$

Equilibrium of the top block about its lower rotation axis:

$$\sum M_{top} = \bar{V}_{UB} \cdot \bar{z}_{la,UB} + \bar{H}_{UB} \cdot \bar{y}_{la,UB} = \begin{bmatrix} G_1 \\ S_1 \\ P_1 \end{bmatrix} \cdot \begin{bmatrix} \delta_{G1} + t_1/2 - \delta \\ t_1/2 - \delta \\ t_1/2 - \delta \end{bmatrix} + \begin{bmatrix} Q_1 \\ F_1 \end{bmatrix} \cdot \begin{bmatrix} y_{G1} - H_2 \\ H_1 \end{bmatrix} = 0 \quad (5.7)$$

Where:

- \bar{V} and \bar{H} are the vertical and horizontal forces acting on the wall and \bar{z}_{la} and \bar{y}_{la} their respective lever arms.
- \bar{V}_{UB} and \bar{H}_{UB} are the vertical and horizontal forces acting on the upper block of the wall and $\bar{z}_{la,UB}$ and $\bar{y}_{la,UB}$ their respective lever arms.
- G_1 and G_2 are the self-weight loads of each block
- Q_1 and Q_2 are the seismic forces on each block applied to the centre of gravity of each block respectively, corresponding to the self-weight load times the acceleration factor for each block (y_{G1} and y_{G2} , measured from the bottom)
- S_1 and S_2 are the slab loads on each block (creating friction)
- P_1 and P_2 are other different vertical loads applied to the top centre of each block
- F_1 and F_2 are the horizontal restraining forces on each block, F_2 depends on S_2 but F_1 is in this case unknown until the equations are solved.
- R_h and R_v are the horizontal and the vertical force coming from the vault (see Chapter 5.3)
- δ is the displacement at the separation of the two blocks and δ_{G1} and δ_{G2} are the displacements at the centres of gravity of each block

5.4.2 G-Mechanism

To derive the G-mechanism's push-over curve, an energy-based approach is used similar to the one proposed by D'Ayala [12]. The wall is separated into three blocks, two of which are triangular and the third centre block of a rectangular shape. The crack line diagonally crosses the windows, separating them into two parts diagonally. The geometry can be seen in Figure 5.7 below.

For the energy-based approach, the equilibrium is formulated by looking at a deformed state and adding to it an incremental deformation. The energy of each force/load is then calculated and the sum of the external energy is set equal to the sum of the internal work.

Equilibrium equation:

$$\begin{bmatrix} 2G_1 \\ 2S_1 \\ 2P_1 \\ G_2 \\ S_2 \\ P_2 \end{bmatrix} \cdot \begin{bmatrix} \cos(\beta) (x'_{G1}/x'_\delta * \delta - t/2)/x'_\delta \\ \cos(\beta) (x'_{top,triang}/x'_\delta * \delta - t/2)/x'_\delta \\ \cos(\beta) (x'_{top,triang}/x'_\delta * \delta - t/2)/x'_\delta \\ (\delta/2 - t/2)/H \\ (\delta - t/2)/H \\ (\delta - t/2)/H \end{bmatrix} + \begin{bmatrix} Q_1 \\ Q_2 \\ F_1 \\ F_2 \end{bmatrix} \cdot \begin{bmatrix} x'_{G1}/x'_\delta \\ 1/2 \\ x'_{top,triang}/x'_\delta \\ 1 \end{bmatrix} = 0 \quad (5.8)$$

- G_1 and G_2 are the self-weight loads of each block
- Q_1 and Q_2 are the seismic forces on each block applied to the centre of gravity of each block respectively, corresponding to the self-weight load times the acceleration factor for each block
- S_1 and S_2 are the slab loads on each block (creating friction)
- P_1 and P_2 are other different vertical loads applied to the top centre of each block
- F_1 and F_2 are the horizontal restraining forces on each block due to friction with the slab
- x'_δ is the distance between the top corner of the triangular element (where the displacement is δ) and the diagonal rotation axis, x'_{G1} is the distance between the centre of gravity and the diagonal

rotation axis and $x'_{top,triang}$ is the distance between the centre of the top of the triangular block and the diagonal rotation axis.

- H is the height of the mechanism and t is the wall thickness

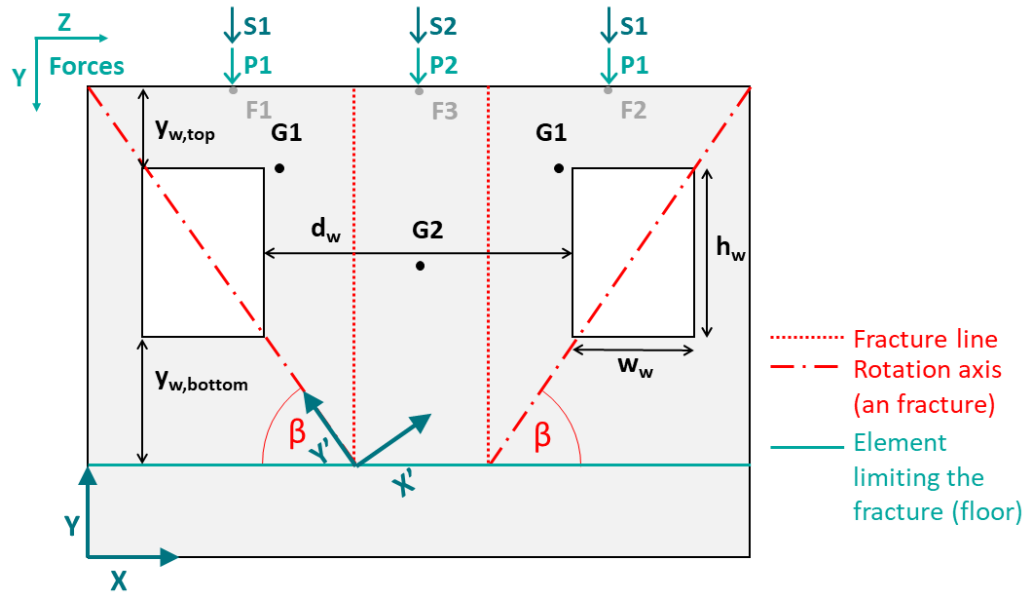


Figure 5.7: G-mechanism elevation

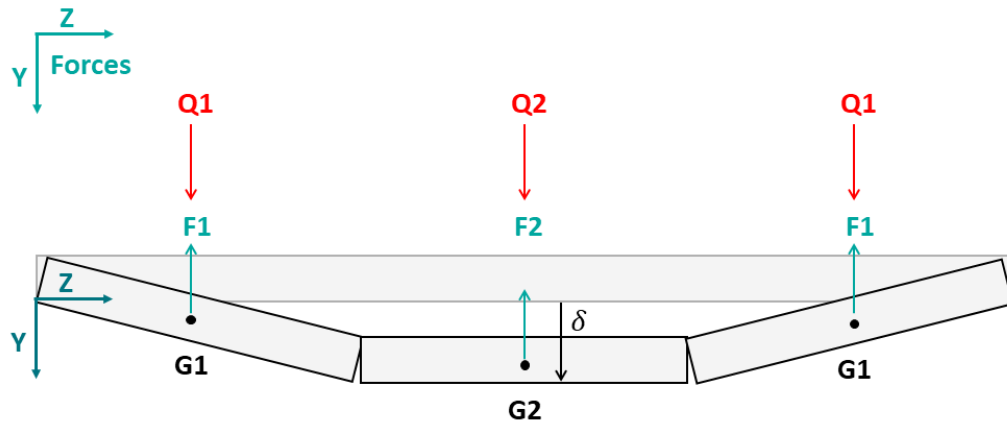


Figure 5.8: G-mechanism plan view

5.5 Equivalent single degree of freedom system

After the pushover curves have been established, the results of these multi-degree-of-freedom (MDOF) systems need to be transformed into equivalent single-degree-of-freedom (SDOF) systems to be able to execute the N2 method. Following the methodology of Eurocode 1998-1-1 [18] §6.5.3 (1) the general procedure is described here:

1. Define the mass vector of the mechanism:

$$m = [V_1 \ V_2 \ \dots \ V_n] * \rho_{masonry} \quad (5.9)$$

$$m = [V_1 \ V_2 \ \dots \ V_n] * \rho_{masonry}$$

Where V_n is the volume of one of the block n moving in the mechanism. For the F-mechanism, this would correspond to two blocks, for the G-mechanism there are three blocks involved.

2. Define the modal shape vector of the mechanism:

$$\phi = [\phi_1 \ \phi_2 \ \dots \ \phi_n] \quad (5.10)$$

Where ϕ_n is the shape coefficient of block n at its centre of gravity. This vector is normalized to one of the blocks of the mechanism, i.e. one of the ϕ values is equal to 1.

3. Calculate the equivalent mass as:

$$m^* = \sum m_i \phi_i \quad (5.11)$$

This is the mass of the equivalent SDOF system representing the mechanism.

4. Calculate the transformation factor as:

$$\Gamma = \frac{m^*}{\sum m_i \phi_i^2} \quad (5.12)$$

5. Transform the forces of the pushover curve into equivalent forces:

$$F^* = \frac{F_b}{\Gamma} \quad (5.13)$$

F_b corresponds to the total force acting on the whole system (all blocks).

6. Use the displacement at the centre of gravity of one block to calculate the equivalent displacement:

$$d^* = \frac{d_n}{\Gamma \phi_n} \quad (5.14)$$

d_n corresponds to the displacement at node (centre of gravity of block n) and ϕ_n corresponds to the corresponding value of the modal vector.

7. The equivalent acceleration of the system can then be calculated as

$$a^* = \frac{F^*}{m^*} \quad (5.15)$$

This will then be used to plot the capacity curve on the same plot as the acceleration-displacement response spectrum (ADRS).

5.6 N2 method

After having determined the values of the equivalent SDOF system, the pushover curve of the equivalent SDOF system is simplified into a tri-linear approximation as proposed by Griffith et al. [35]. And finally, the tri-linear equivalent pushover curve of the SDOF system is plotted against the ADRS curve as explained in EN 1998-1-1 §6.5. In this combined plot, the initial linear part of the pushover curve is continued until reaching an intersection with the ADRS. The process is shown in Figure 5.9 below.

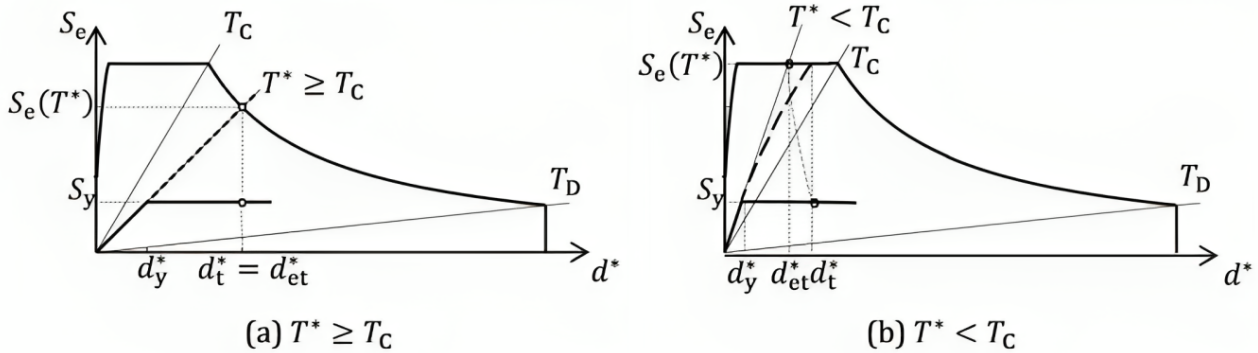


Figure 5.9: Determination of the target displacement for the equivalent SDOF system (hardening neglected)[18]

For cases where $T^* > T_C$ the target displacement can be determined by reading the displacement at the point of intersection of the continued linear part and the ADRS curve. This target displacement can then be compared to the limit displacement as explained in Chapter 3.3.2.

For cases where $T^* < T_C$ the target displacement needs to be calculated as follows:

As can be seen in Figure 5.9 the performance point now lies in the zone of the plateau, and the target displacement needs to be amplified. This is done using the following formulas:

$$d_t^* = \frac{1}{u} \cdot \left[1 + (u - 1) \frac{T_c}{T^*} \right] \cdot d_{et}^* \quad (5.16)$$

With: $u = \frac{S_e(T^*)}{S_y}$

Where d_{et}^* is the point of intersection of the linear prolongation of the pushover curve and the ADRS curve. Since T^* is not known, T_b is taken as a safe approximation.

5.7 Results

5.7.1 F-Mechanism west facade

The first case analysed numerically is the F-mechanism of the west facade shown in Chapter 2.4. The calculations are provided in the Jupyter Notebook for the OOP calculations (see Appendix H). The following geometric properties are obtained from the plans (Appendix C) and the loads are calculated in the modelling Excel file (see Appendix H) and then introduced into the code:

Wall geometry [m]	H_1	H_2	L	t_1	t_2
3.25	2.75	14.2	0.55	0.70	
Window geometry, upper wall [m]	h_{w1}	w_{w1}	y_{w1}	n_{w1}	
1.70	1.10	3.65	4		
Window geometry, lower wall [m]	h_{w2}	w_{w2}	y_{w2}	n_{w2}	
1.40	1.10	0.7	4		
Vault geometry [m]	h_v	w_v	t_v		
0.1	1.75*	0.15			
Deformation limitation [m]	δ_{max}				
	$t_2/2$				

Table 5.1: Geometric characteristics F-mechanism west facade

*For the width of the vault a part of the wall thickness is added.

Loads on the upper body [N]	Roof load (P_1)	Slab load (S_1)
71326	67209	
Loads on the lower body [N]	Load (P_2)**	Slab load (S_2)***
26825	0	
Load on the vault [N/m]	q_{vault}	
37769		

Table 5.2: Loads F-mechanism west facade

** This corresponds to the filling material above the vault.

*** The assumption is made that the slab of the first floor is uniquely supported by the vaults and does not connect directly to the wall. The vertical load on the lower block therefore only comes from the vault. This means the friction between the slab of the first floor and the wall is neglected.

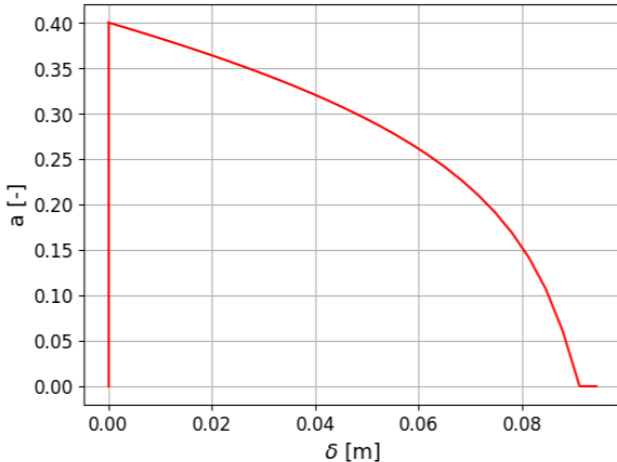
After introducing the characteristics of the mechanism and the loads into the Jupyter Notebook the following output is obtained (see also Figure 5.10):

Start of rocking	δ [m]	α [-]	Q_1 [kN]	Q_2 [kN]
Loss of lateral resistance	0	0.401	153.4	163.0
	0.091	0	0	0

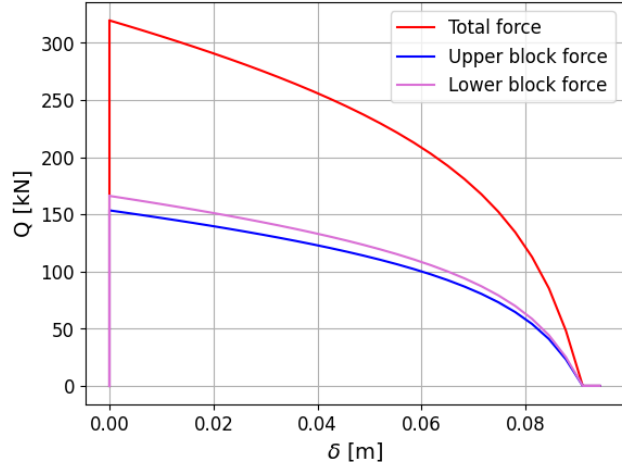
Table 5.3: Characteristic values of the pushover curve of the west facade, F-mechanism

Two points can be noticed in Figure 5.10:

1. The wall starts rocking at an α -value of 0.401
2. At a displacement of only around nine centimetres the wall loses its resistance entirely because the horizontal thrust of the vault becomes too large.



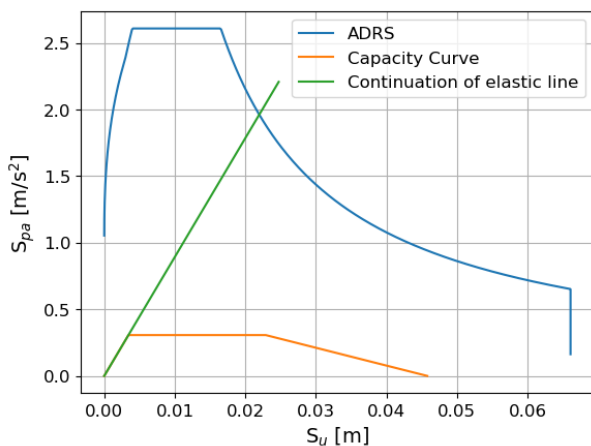
(a) α -Factor describing the seismic load



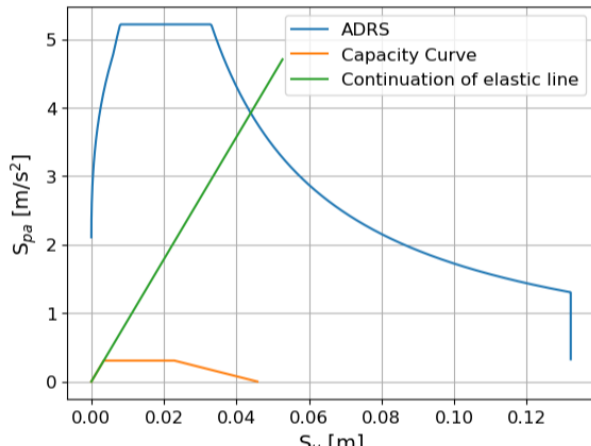
(b) Force-Displacement curve

Figure 5.10: F-mechanism west side results

It is interesting to note that the required acceleration to start the wall rocking is rather low at $a = 3.93 \text{ m/s}^2$. When that limit is reached, the displacement capacity however is quite high at about nine centimetres. Although the vault in this case is rather shallow and would exercise a bigger thrust than a higher vault, the load on it is rather low, which is the main reason for the thrust to stay low. This does however not mean that the mechanism did not produce. On the contrary, the acceleration to trigger the mechanism is relatively low which means that the mechanism was possibly triggered but did not reach failure due to the somewhat big displacement capacity.



(a) Verification DL limit state



(b) Verification NC limit state

Figure 5.11: Verification of the resistance against the F-mechanism west facade with the N2 method

Looking at the results for the N2 verification method it is noticeable that neither the NC limit state nor the DL limit state is verified. The limit value for the NC limit state lies at $d_{u2} = 0.027 \text{ m}$ whereas the target displacement derived from the ADRS Graph lies at $d_{NC} = 0.044 \text{ m}$. Since $d_{u2} < d_{NC}$ this

limit state is not verified. Similarly, the limit value for the DL limit state is $d_u = 0.018\text{ m}$ whereas the target displacement is of $d_{DL} = 0.022\text{ m}$. In the same way, $d_u < d_{DL}$ shows that the limit state is not verified. The details of the calculation can be found in Appendix H.

Even though the analysis seeks to describe the stability of the OOP mechanism as exactly as possible, several factors could not have been taken into account. The negligence of the perpendicular walls supporting the vault, as well as the friction between masonry bricks at the edges of the mechanism, are elements that would increase the resistance and displacement capacity of the system. However, these elements are complex to model and therefore it has been decided to not consider them and aim for the safer side. Although there is only a small non-conformance in the NC and DL states it is necessary to reinforce the building against this mechanism. This mechanism forms a point of risk and weakness, even more so now that the structure already has residual deformation from the earthquake, and it is essential to reinforce the vault (with steel ties) to counter the push and keep the building intact during the next earthquake.

5.7.2 F-mechanism east facade

The same analysis has been done for the second F-mechanism, located on the east side of the building. This mechanism varies slightly because the wall does not break at the interface of the storeys but at the level of the support of the vault (as shown in Figure 5.6). Therefore, the code was slightly adapted to take the different geometry into account (see Jupyter Notebook in Appendix H). The geometric input data is summarized in the table below:

Wall geometry [m]	H_1	H_2	H_3	H_4	L	t_1	t_2
4.55	1.55	2.7	3.4	17	0.55	0.7	
Window geometry, upper wall [m]	h_{w1}	w_{w1}	y_{w1}	n_{w1}			
1.7	1.1	3.65	4				
Window geometry, lower wall [m]	h_{w2}	w_{w2}	y_{w2}	n_{w2}			
1.4	1.1	0.7	4				
Vault geometry [m]	h_v	w_v	t_v				
1.25	5.6	0.15					
Deformation limitation [m]	δ_{max}						
	$t_2/2$						

Table 5.4: Geometric characteristics F-mechanism east facade

The loads calculated to act on top of the wall as well as on the vault are the following:

Loads on the upper body [N]	Roof load (P_1)	Slab load (S_1)
78288	155075	
Loads on the lower body [N]	Load(P_2)	Slab load(S_2)***
248250	0	
Load on the vault [N/m]	q_{vault}	
63000		

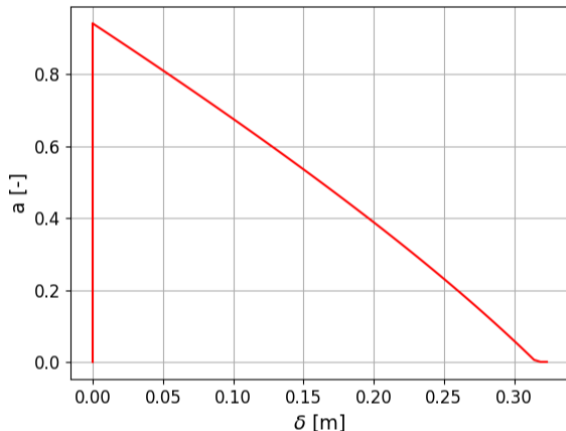
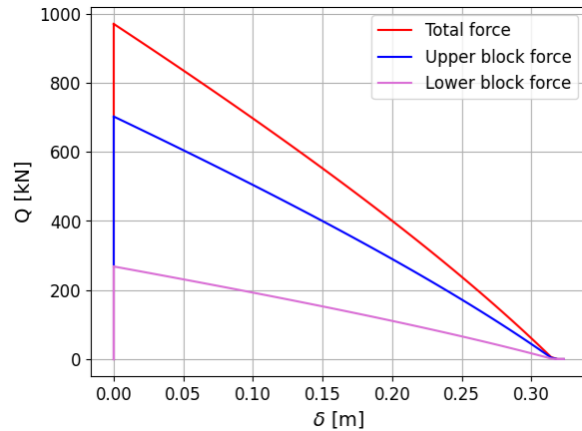
Table 5.5: Loads F-mechanism east facade

After introducing the characteristics of the mechanism and the loads into the Jupyter Notebook the following output is obtained, corresponding to the pushover curve in Figure 5.12:

Start of rocking
Loss of lateral resistance

δ [m]	α [-]	Q_1 [kN]	Q_2 [kN]
0	0.941	702.1	268.1
0.319	0	0	0

Table 5.6: Characteristic values of the pushover curve of the east facade, F-mechanism

(a) α -Factor describing the seismic load

(b) Force-Displacement curve

Figure 5.12: F-mechanism east side results

The same key points as for the east mechanism can also be seen in Figure 5.12. The difference here is that the phase before the vault breaks is remarkably longer and the pushover curve is therefore less curved. The larger size (width and height) of the vault entails two things: the supports of the vault need to be moved further away, i.e. a larger OOP movement is required, before the vault breaks and due to the bigger height, the horizontal thrust of the vault is smaller in comparison to the vault of the west facade.

Comparing those results to the ones from the mechanism observed on the West facade it can be noticed that the acceleration to start the rocking of the facade of the east side is roughly twice as large. It is also worth noting that the displacement capacity is roughly four times that of the west facade. It makes, therefore, sense that fewer cracks corresponding to this OOP mechanism could be observed within the building than for the west mechanism. This mechanism is also less prone to happen due to its larger acceleration to start the rocking in comparison to the west mechanism. In general, this indicates that the larger vaults, where the horizontal component of the support load is smaller due to the higher inclination of the vaults at their supports, are more stable than the small vaults around the main entrance and the stairs.

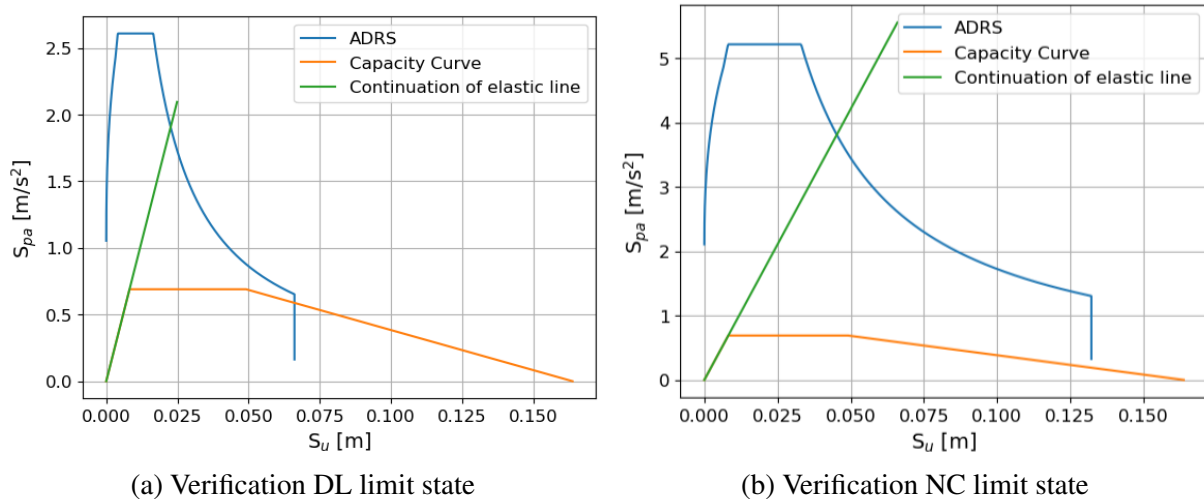


Figure 5.13: Verification of the resistance against the F-mechanism east facade with the N2 method

Looking at the N2 verification the following can be adopted:

The limit value for the NC limit state lies at $d_{u2} = 0.098\text{ m}$ whereas the target displacement derived from the ADRS Graph lies at $d_{NC} = 0.045\text{ m}$. Since $d_{u2} > d_{NC}$ this limit state is verified. Similarly, the limit value for the DL limit state is $d_u = 0.065\text{ m}$ whereas the target displacement is of $d_{DL} = 0.023\text{m}$. In the same way, $d_u > d_{DL}$ shows that the limit state is verified. The details of the calculation can be found in Appendix H. This side of the building therefore does not require reinforcing of the vaults to lessen the thrust.

5.7.3 G-mechanism west facade

After having looked at the mechanism that was observed after the earthquake of 2020 we can now consider two alternative mechanisms that did not occur: The two G-mechanisms on the west and the east facades. The characteristic dimensions assumed for the analysis are measured in the plans (see Appendix C) and can be found in Table 5.7. The loads on the body are calculated in the same way as for the F-mechanism and can be found in Table 5.8 and a friction coefficient between the top slab and the masonry of $\mu = 0.6$ was admitted. Using a second type of Jupyter Notebook (see Appendix H), the results can be seen in Table 5.9 as well as in Figure 5.14.

Wall geometry	$y_{w,top}$	$y_{w,bottom}$	d_w	h_w	w_w	t
[m]	0.65	0.90	3.30	1.70	1.10	0.55
Deformation limitation	δ_{max}					
[m]		$t/2$				

Table 5.7: Geometric characteristics G-mechanism west facade

Loads on the triangular body	Roof load (P_1)	Slab load (S_1)
[N]	11305	10700
Loads on the rectangular body	Roof load(P_2)	Slab load(S_2)
[N]	11479	10865

Table 5.8: Loads G-mechanism west facade

	δ [m]	α [-]	Q_1 [kN]	Q_2 [kN]
Start of rocking	0	0.981	7.5	67.4
Loss of lateral resistance	0.579	0	0	0

Table 5.9: Characteristic values of the pushover curve of the west facade, G-mechanism

By looking at the characteristic values of the pushover curve summarized in the table above, it can be noticed that the acceleration to start the rocking of the two blocks is about the same as the acceleration needed for the F-mechanism on the east side. The initial acceleration to start the mechanism, however, is dependent on the friction coefficient between the wall and the slab above. If we assume that the slab is a FERT slab with an RC ring beam surrounding it, this connection might even be more resistant which would make the mechanism even unlikelier. In addition to that, the displacement capacity of the G-mechanism of the west facade is roughly six times the capacity of the F-mechanism on the west facade. This is mainly because the F-mechanism is enhanced by the thrust of the vaults and thus makes the wall less stable. The ring beam holding the wall of the G-mechanism back further increases the resistance.

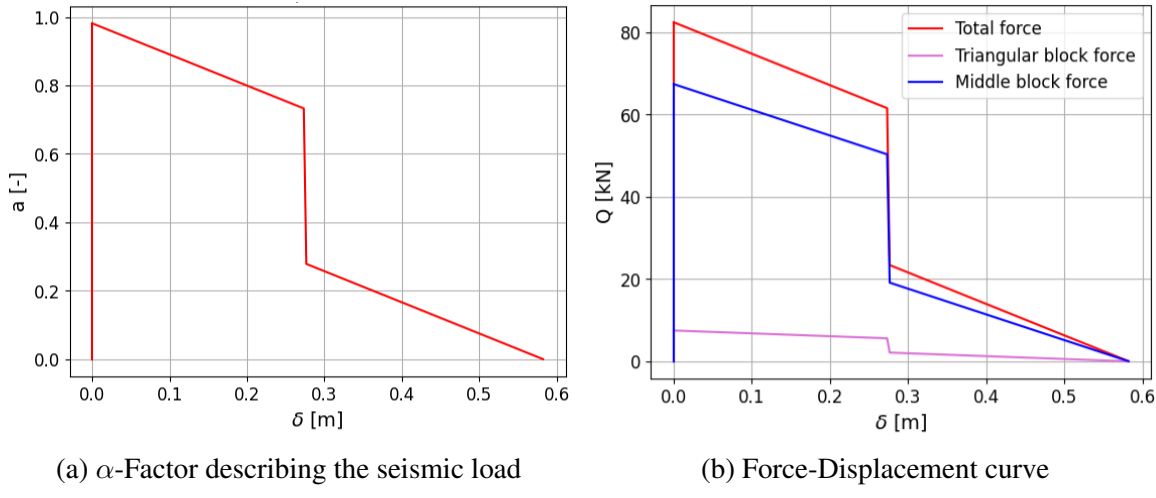


Figure 5.14: G-mechanism west side results

When looking at the pushover curve, one of the main differences from the F-mechanism to be noticed is the shape: The curve follows a linear line with a sudden drop at δ_{max} where the slab loses connection to the wall and does not restrain it any longer. Therefore, it can be seen that the friction restraining the block from falling out, only influences the initial acceleration to start the mechanism, but not the displacement capacity.

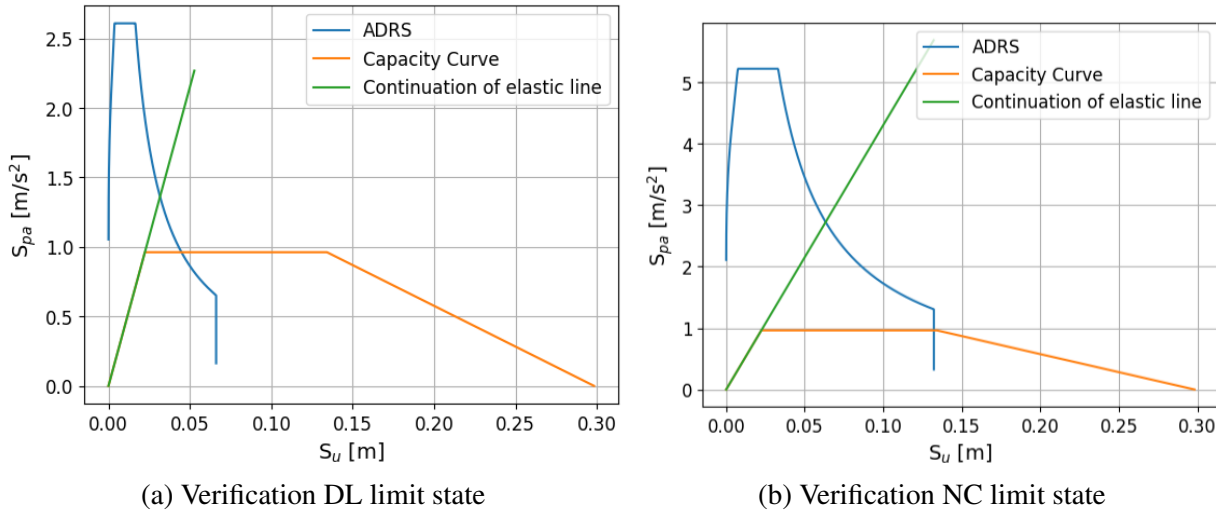


Figure 5.15: Verification of the resistance against the G-mechanism west facade with the N2 method

The verification is performed as follows: The target displacement for the DL limit state is $d_{DL} = 0.032\text{ m}$ which is smaller than the limit displacement $d_{u1} = 0.119\text{ m}$. Therefore, the DL limit state is verified. In the same way, the target displacement for the NC limit state is $d_{NC} = 0.063\text{ m}$ which is smaller than the limit displacement $d_{u2} = 0.179\text{ m}$. Therefore, the NC limit state is verified.

5.7.4 G-mechanism east facade

Looking at the east side, the mechanism analysed is the same as the one on the west side. The main differences consist of a more compact geometry, i.e. the windows are closer together, and there are heavier loads on top of the blocks due to the bigger span of the slab. The details can be seen in Tables 5.10 and 5.11.

Wall geometry	$y_{w,top}$	$y_{w,bottom}$	d_w	h_w	w_w	t
[m]	0.65	0.90	2.90	1.70	1.10	0.55
Deformation limitation	δ_{max}					
[m]		$t/2$				

Table 5.10: Geometric characteristics G-mechanism east facade

Loads on the triangular body	Roof load (P_1)	Slab load (S_1)
[N]	11305	19000
Loads on the rectangular body	Roof load(P_2)	Slab load(S_2)
[N]	9329	15678

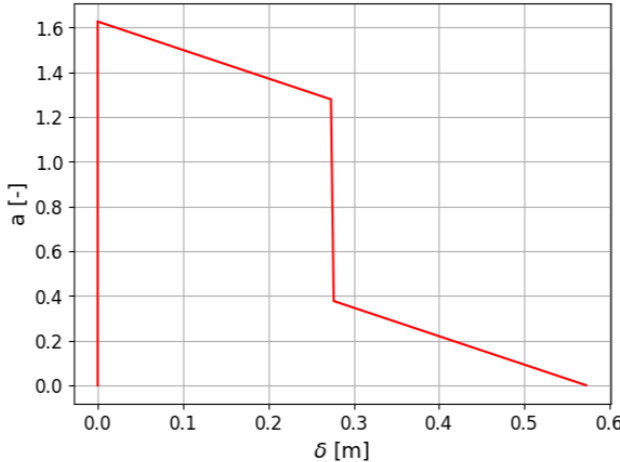
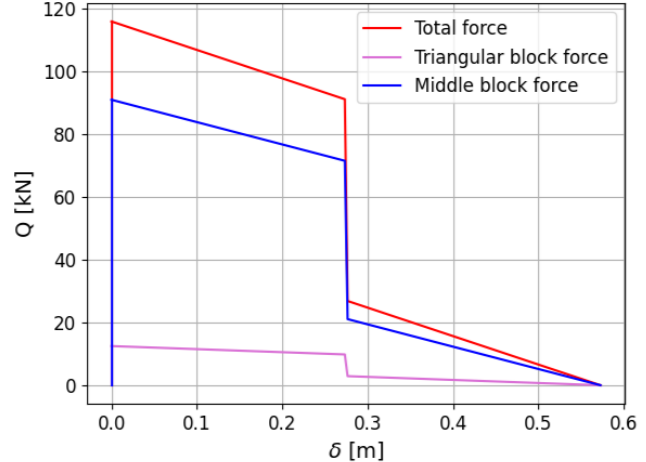
Table 5.11: Loads G-mechanism east facade

The main results of the G-mechanism can be perceived in Table 5.12 below: The acceleration needed to trigger the mechanism is even higher than for the west G-mechanism. This is mainly due to the higher load of the slab and the smaller block size, making it more resistant to OOP action. The displacement capacity however is approximately the same as for the previous mechanism. As already mentioned earlier, the friction on top of the wall only has an influence on the acceleration needed to trigger the rocking but not on the displacement capacity. Since the geometry of this second G-mechanism is fairly similar to the one on the west side, it only makes sense to also have approximately the same displacement capacity.

Start of rocking
Loss of lateral resistance

δ [m]	α [-]	Q_1 [kN]	Q_2 [kN]
0	0.981	7.5	67.4
0.579	0	0	0

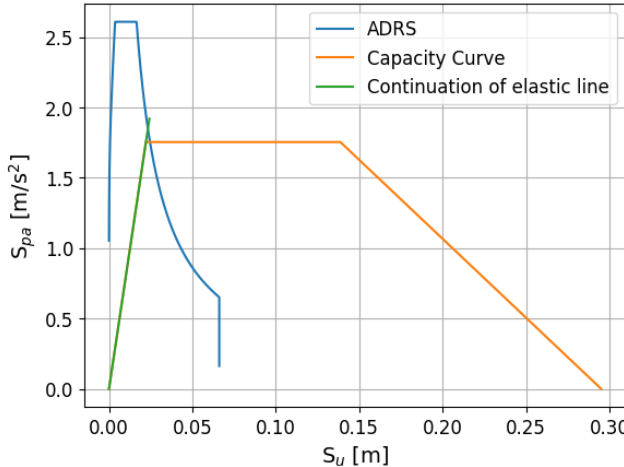
Table 5.12: Characteristic values of the pushover curve of the east facade, G-mechanism

(a) α -Factor describing the seismic load

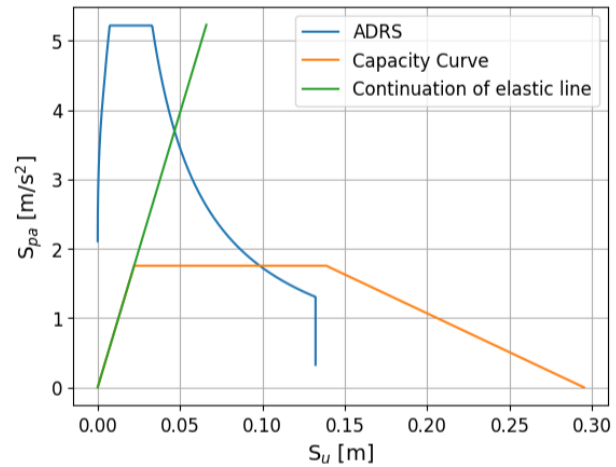
(b) Force-Displacement curve

Figure 5.16: G-mechanism east side results

Looking at the pushover curve of this second mechanism that was not observed and its characteristic values, we can see why this mechanism is even unlikelier to occur than the first G-mechanism on the west facade.



(a) Verification DL limit state



(b) Verification NC limit state

Figure 5.17: Verification of the resistance against the G-mechanism east facade with the N2 method

The verification procedure is the same as for the other three mechanisms: The target displacement for the DL limit state is $d_{DL} = 0.023 \text{ m}$ which is smaller than the limit displacement $d_{u1} = 0.118 \text{ m}$. Therefore, the DL limit state is verified. In the same way, the target displacement for the NC limit state is $d_{NC} = 0.047 \text{ m}$ which is smaller than the limit displacement $d_{u2} = 0.177 \text{ m}$. Therefore, the NC limit state is verified.

5.8 Conclusion and discussion

In conclusion, there is a significant difference in the stability of the facades of the Parish House to different mechanisms. Although the vaults can have a good influence in stiffening the structure, their effect on the OOP resistance of adjacent walls is critical. They even enhance the mechanism if their curvature is low. This makes them more critical for the mechanism on the west facade than on the south facade. The analysis of the G-mechanisms shows a significant difference between the acceleration needed to trigger a G-mechanism compared to an F-mechanism. The G-mechanisms are much less prone to happen due to the good connection of the top of the wall to the RC ringbeam, which tends to hold them in their plane. Therefore, the accelerations to trigger the G-mechanisms need to be significantly higher than the ones to trigger the F-mechanisms. Furthermore, since all the connections at the corners of the building, i.e. the interlocking were well executed, the risk of all other global mechanisms with a whole facade falling out was low to none. Likewise, the connections between the vaults and the walls or the slabs and the walls seem to be well executed. The ring beam could even add to that quality of interlocking which makes the other more local mechanisms unlikely to happen.

5.8.1 Relevant findings for the retrofitting

The table below summarizes the results of the verifications of the stability against the OOP failure in one of the previously described mechanisms. It can be noticed that the target displacement of the three mechanisms is significantly lower than the limit displacement of the corresponding limit state. Only the F-mechanism on the west facade does not meet the necessary resistance and deformation capacity to verify the NC and the DL limit states. Therefore, it is required to reinforce the structure against this mechanism. One of the possible solutions is steel ties above the vaults, spanning between the two walls supporting the vault, to counter the thrust of the vault. The exact solution will be discussed in Chapter 8.

Mechanism	Target displacement		Limit displacement		Verification
	DL [m]	NC [m]	DL [m]	NC [m]	
F west	0.022	0.044	0.018	0.027	Not verified
F east	0.023	0.045	0.065	0.098	OK
G west	0.032	0.063	0.119	0.179	OK
G east	0.023	0.047	0.118	0.177	OK

Table 5.13: Summary of the verification against OOP failure

For the retrofitting of the structure, the main learnings can be summarized as follows:

The most vulnerable item of the construction is the vaults. To prevent OOP mechanisms from happening in the next earthquake they must be strengthened (west facade) or at least repaired and restored to their original state (east OOP). Another important step will be the regular maintenance of all wall-to-wall and all slab/vault-to-wall connections to ensure good interlocking in the future. It can however be concluded that only one out of four OOP scenarios is truly prone to happen, whereas the other three remain rather improbable considering their target displacements that are significantly smaller than the respective limits.

6. Modelling with OpenSees

The modelling approach chosen to analyse the structure is an equivalent frame model (EFM) using macro-elements as proposed by Vanin et al.[1] and performing a non-linear dynamic response history analysis (RHA) using the software OpenSees [2]. Due to the research activity currently happening at the EESD laboratory of EPFL, a lot of resources are available on their GitHub repository, helping in the process of modelling [36]. Especially resources, i.e. code parts as well as model templates, made by Dr. Igor Tomić were used in the process of modelling the Parish House [37]. The model, as well as the Matlab [22] scripts to run the model, can be found on the GitHub repository of this thesis (see Chapter 11 for more information).

6.1 Macroelements for piers and spandrels

To model the walls of the structure, the first step is to divide the walls into piers, spandrels and nodes. The elements are distinguished by their different locations: Piers are the blocks of masonry next to or horizontally in between windows, spandrels are the masonry blocks above or vertically in between windows, and nodes connect the piers and spandrels. Finally, shell elements modelling the slabs will be introduced as proposed in the next chapter.

The spandrels and piers are modelled as three-node, three-dimensional macroelements as proposed by Vanin et. al. [1]. Those elements introduce several differences from previous approaches, making this approach more accurate. Firstly, it extends the methodology of the previously developed macroelement designed to uniquely simulate the in-plane response of masonry panels. In contrast to the previously used macroelements by Lagomarsino et. al. [38], the updated version integrates both the in-plane and out-of-plane (OOP) behaviour of masonry walls. In addition, it incorporates second-order geometric effects through a P- Δ formulation, providing a more realistic representation of the structural behaviour, especially for the nonlinear behaviour of structures. It couples shear behaviour with axial load and flexural behaviour without the need for iterations, ensuring the accurate application of equilibrium conditions at the three flexural interfaces. Moreover, the proposed macroelement accommodates the use of complex material models, allowing for more flexibility in capturing the nonlinear behaviour displayed by masonry panels. [1]

The macroelement is defined as a one-dimensional element in three-dimensional space with two nodes at the element ends and one node in the middle. It is made up of a set of two panels that are separated by three nonlinear sections that account for axial strain deformations and are subjected to the same average shear deformation. The Figure 6.1 shows the three deformation modes the macroelement can model: [1]

1. In-plane flexure
2. In-plane flexure and shear
3. Out-of-plane (OOP) response (particularly important for masonry)

6.1.1 Mesh

Since the structure is mostly regular, with only a few irregularities on the west and the south facade and on the inside walls, the meshing approach described by Bracchi et al. with a minimum clear height is considered [39]. This approach is in this particular case preferred over the average opening

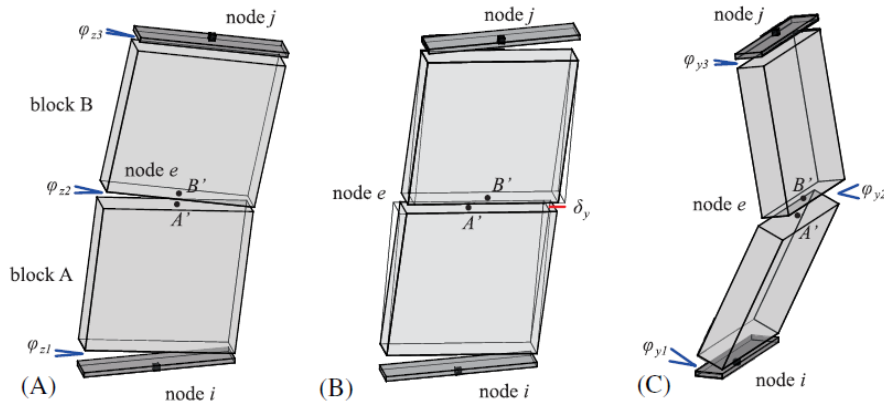


Figure 6.1: Deformation modes of the macroelement: (A) in-plane flexure only, (B) in-plane flexure and shear and (C) OOP response [1])

height or even the 30° rule because of its simple application [40]. As an example, the division of the west facade into elements is shown in Figure 6.3.

To model the inside walls, the openings that are not exactly aligning or that do not have the exact same width have been interpolated to get a regular mesh with openings of the same size that are aligned. The simplifications mostly concern the two smaller windows on the west facade, the two doors of wall 8 and some of the door openings of walls 5-7. Figure 6.2 shows the plan view of the walls with their respective numbers and the axes of the reference system. The longitudinal direction is set to be the X direction whereas the transversal direction is the Y direction and the Z direction is therefore the vertical direction. The structure is first modelled in Tremuri formulation and then transformed into an equivalent OpenSees model. The entire set of plans showing the OpenSees model can be found in Appendix I.

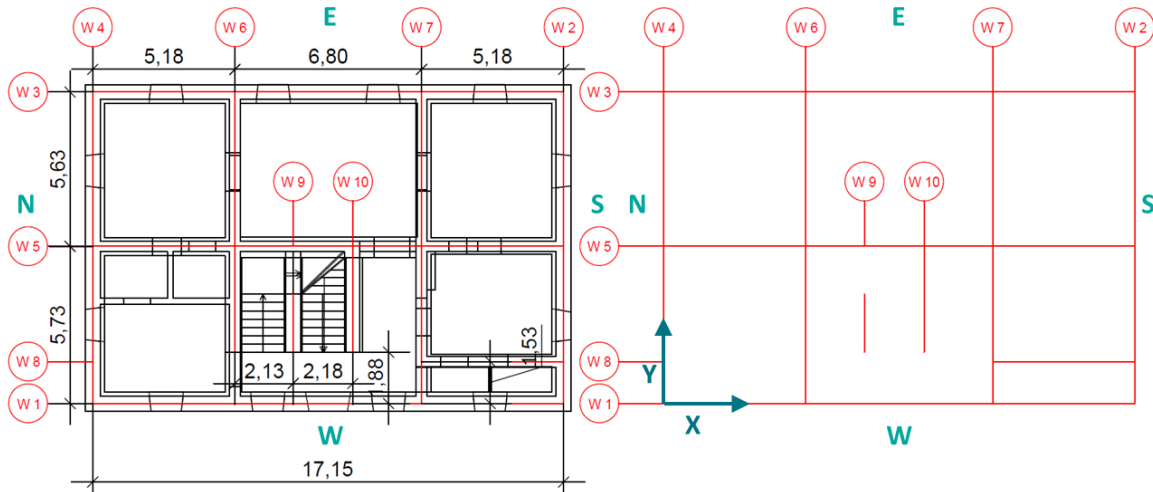


Figure 6.2: Plan view of the walls and reference system

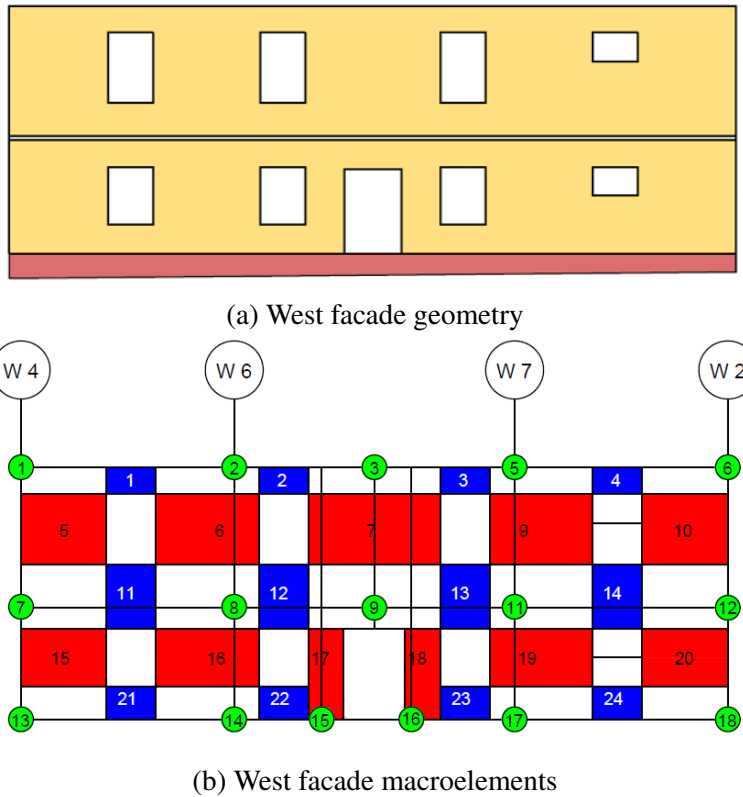


Figure 6.3: Division into macro elements of the west facade

6.2 Slabs and vaults

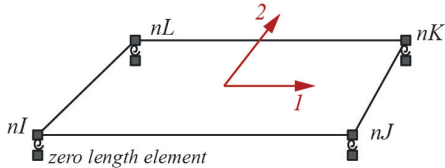


Figure 6.4: Orthotropic membrane element in OpenSees [36]

The slabs and walls of the structure are modelled as elastic orthotropic membranes as suggested on the OpenSees wiki of EESD EPFL [36]. Those elements resist loads in the direction of their plane but have no resistance in bending, i.e. no resistance against loads in their OOP direction. The elements are defined by four nodes, two main axes, material properties for each axis and a common thickness that is the same for both directions of solicitation. For this model, the two axes of the slabs are parallel to the two main axes of the model, i.e. X and Y axis.

The slabs are introduced inside the building connecting the nodes of the walls that support them and adding fictitious nodes only if no real node is already in place to form the geometry of the slab. For the elements of the ground floor slab, the separation has been chosen as close as possible to the real vault elements, i.e. separating sections with different vault geometries from each other. An overview of the slab elements introduced in the model can be found in Appendix I.

6.2.1 Vaults

As established in Chapter 2.2.2, the slab above the ground floor is supported by a complex system of vaults spanning in both directions. The bigger vaults as seen in Figure 2.4 are barrel vaults, meaning that they have one main curvature and one spanning direction, whereas the smaller vaults are cross vaults that span in both directions but have a main curvature. Since the model can only account for

2D elements, the vaults are transformed into equivalent shell elements using orthotropic membrane sections employing the method proposed by Cattari et. al. [41] in their paper "Modelling of vaults as equivalent diaphragms in 3D seismic analysis of masonry buildings". Their work consisted of developing analytical expressions to determine the Young's and the shear modulus of an equivalent slab having the same behaviour as the vault. To validate their hypothesis they compared the results to results of reference vaults modelled using finite element models (FEM). While this is a very simple and efficient way to model the vaults, a major drawback lies within the negligence of the thrust exercised on the support walls. Thus, it is only valid to model the vaults in this way if the effect of the vault on the walls is modelled through the separate OOP mechanisms as done in Chapter 5.

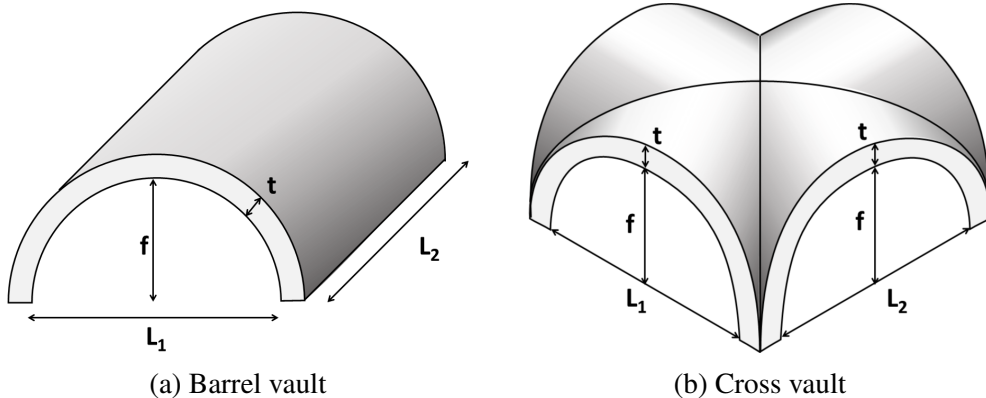


Figure 6.5: General dimensions of barrel and cross vaults

Barrel vaults

To determine the equivalent stiffness of a slab to represent a barrel vault, the vault needs to be looked at in two directions: the direction of the main span (parallel to the curvature) and the longitudinal direction (where the cross-section is arched). Figure 6.5 illustrates a barrel vault and its characteristic dimensions. The vaults are defined using the internal width and height. Assuming material parameters of E (Young's modulus) and G (shear modulus) the stiffness of the vault in the spanning direction can be described using the formulas proposed by Cattari [41].

$$\frac{E_{v,1}}{E} = \left(a_1 \frac{t}{L_1} + a_2 \right) \left(\frac{f}{L_1} \right)^{a_3 \frac{t}{L_1} + a_4} \quad (6.1)$$

$$\frac{G_{v,1}}{G} = \left(b_1 \frac{t}{L} + b_2 \right) \left(\frac{f}{L} \right) + b_3 \frac{t}{L} + b_4 \quad (6.2)$$

Where:

- E is the Young's modulus corresponding to the material
- E_v is the Young's modulus of the slab representing the vault
- t is the thickness of the vault and f is the height of the arch
- L_1 is the span of the vault and L_2 is its length
- a_1, a_2, a_3 and a_4 are factors that were determined during the research of Cattari [41] and are the following:
 $a_1 = 0.05, a_2 = -0.0011, a_3 = 3.1767$ and $a_4 = 0$, for fixed support conditions of the vault.
 $a_1 = 0.05, a_2 = -0.0011, a_3 = 3.1767$ and $a_4 = 0$, for fixed support conditions of the vault.
- In the same way b_1, b_2, b_3 and b_4 are factors that were calibrated and are the following:
 $b_1 = 1.6433, b_2 = -1.8191, b_3 = 0.1133$ and $b_4 = 1.1189$

In the opposite direction, the stiffness must also be changed to an analogous one corresponding to an ordinary slab. The methodology used for this is the following:

$$\frac{E_{v,2}}{E} = \frac{A_v}{A_s} \quad (6.3)$$

Where:

- A_v is the cross-sectional area of the vault, which can be calculated as the area of an ellipse minus the area of a smaller ellipse.

$$A_v = ((L_1/2 + t)(f + t) - L_1/2 \cdot f) \pi$$

- A_s is the area of the cross-section of the equivalent slab.

$$A_s = L_1 \cdot t$$

Cross vaults

The equivalent stiffness of a cross vault is determined in the same way that the equivalent stiffness of a barrel vault is calculated. The fundamental distinction is that the vault has two curvatures in each of the two major directions. As a result, the stiffness and shear modulus are estimated in both directions using calculations similar to those used for the barrel vault. The formulas for one direction are as shown below. To calculate the equivalent values for the other direction only the length L_1 needs to be replaced by L_2 .

$$\frac{E_{v,1}}{E} = \left(a_5 \frac{t}{L_1} + a_6 \right) \ln \left(\frac{f}{L_1} \right) + a_7 \frac{t}{L_1} + a_8 \quad (6.4)$$

$$\frac{G_{v,1}}{G} = \left(b_5 \frac{t}{L} + b_6 \right) \left(\frac{f}{L} \right)^2 + \left(b_1 \frac{t}{L} + b_2 \right) \left(\frac{f}{L} \right) + b_3 \frac{t}{L} + b_4 \quad (6.5)$$

The main dimensions from the formula are indicated in Figure 6.5. The a and b factors are the following:

- a_5, a_6, a_7 and a_8 are the calibrated factors of Cattari [41] and are the following:

$$a_5 = -0.91, a_6 = -0.1567, a_7 = 1.9133 \text{ and } a_8 = 0.0721$$

- In the same way b_1, b_2, b_3, b_4, b_5 and b_6 are factors that were calibrated and are the following:

$$b_1 = -1.12, b_2 = -4.1766, b_3 = 8.9033, b_4 = 0.7273, b_5 = -34.323 \text{ and } b_6 = 5.6202$$

6.2.2 Staircase vaults

As seen in Figure 2.4 of Chapter 2 the staircase leading to the first and second floor is situated in the centre of the building. It has also been mentioned that the stairs going from the ground floor to the first floor are covered by a system of vaults that act at the same time as support for the stairs to the second floor. They consist of inclined barrel vaults at the entrance and exit of the stairs and inclined cross-vaults where the stairs take a turn. Since they are situated on an intermediate level and are furthermore inclined, it is decided not to model them in a detailed way but to opt for a simplified approach. Figure 6.6 below shows the simplification procedure: On the first image, the concerned walls are shown. It is to be noted that only the relevant parts for the staircase of walls 5 and 6 are shown (the plan view of all the walls with their numbers can be found in Appendix I). A qualitative depiction of the vaults is supplied in the centre image. It has been decided to represent them with equivalent slabs, using the previously described method (see the Chapter 6.2.1), with half of them situated at the first-floor level and the other half located on the second-floor level. This modelling strategy is visible in the right-hand drawing of Figure 6.6.

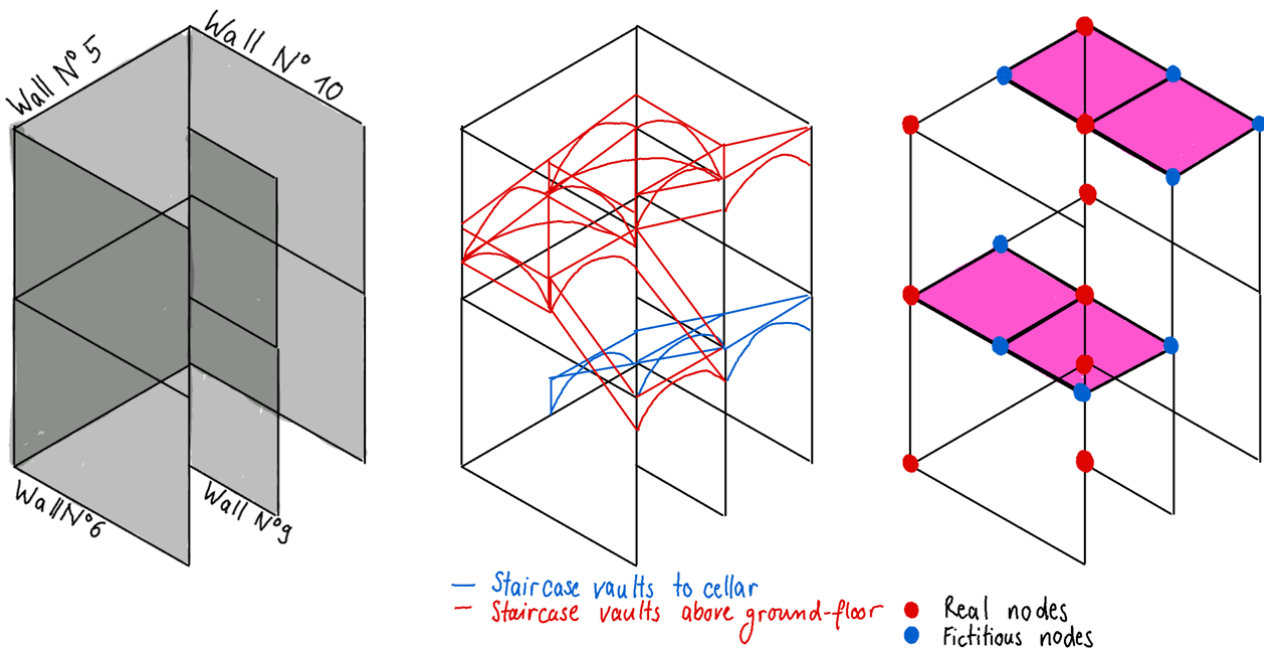


Figure 6.6: Modelling procedure of staircase vaults

After modelling the staircase vaults as equivalent slabs it is important to fix the orthotropic membrane sections with all degree of freedoms (DOFs) fixed to the relevant floor nodes and likewise fix all the DOFs of the floor nodes to the equivalent wall nodes (also the torsional DOFs). Especially the ones connecting the torsional DOF of the staircase walls to the slabs were important to omit the torsion of the walls.

6.2.3 FERT Slabs

The slabs on the first floor were built using the FERT method. This means that the main elements are reinforced concrete beams holding up the secondary elements which are perforated clay bricks (see also Appendix E). The whole system is then connected with a layer of concrete covering the whole surface. In the interview with the construction engineer currently working on the project, they revealed that the usual way to model such slabs is to model them as a concrete slab with a thickness of 10 centimetres [9]. In contrast to conventional concrete slabs, a major static span remains, transferring the loads only to the two supporting walls. Since this slab was added to the structure in the late 20th century, the construction methods were not the same as during the original constructions. This indicates that the spanning directions of the slabs above the first floor do not necessarily correspond to the vaults' spanning directions. Because the concrete pieces are most likely prefabricated, the spans were probably chosen to be the same for each slab. For the Parish House, this would mean that on the east side of the building, the slabs span in an east-west direction (as does the vault), but it is more likely that on the west side of the building, the spanning direction is the same rather than in the north-south direction as the vaults. Therefore, the FERT slabs are introduced as orthotropic membranes made out of concrete with a thickness of 10 cm and material characteristics as defined in Chapter 4.1.3.

6.3 Reinforced concrete ring beam

As discovered in the discussion with the engineer working on the project [9], the addition of a ring beam made out of reinforced concrete, during the remodelling in 1997, added a remarkable amount of overall stiffness to the building and thus increased the box behaviour of the latter. Therefore, this ring beam must be modelled in OpenSees. The beam is assumed to have a rectangular cross-section with the following properties:

- Height $h = 0.3 \text{ m}$ and width $b = 0.5 \text{ m}$
- Cross-section area $A = h \cdot b = 0.15 \text{ m}^2$
- Sectional moment of inertia around vertical axis $I_y = \frac{h \cdot b^3}{12} = 0.003125 \text{ m}^4$
- Sectional moment of inertia around horizontal axis $I_z = \frac{b \cdot h^3}{12} = 0.001125 \text{ m}^4$
- Torsional moment of inertia $J = \frac{b \cdot h \cdot (b^2 + h^2)}{12} = 0.00425 \text{ m}^4$

The same material properties defined in chapter 4.1.3 are also applied to the ring beam. The ring beam is designed in such a way that it connects all of the top nodes of the facades. It is expected that the masonry-concrete connection is well-established and in good shape.

6.4 Supports

6.4.1 Real supports

The structure is supported by the walls that connect to a foundation that is not modelled in this approach. The support nodes are all the nodes at the bottom of each wall with coordinate Z equal to zero. Since the building connects to the cellar in a monolithic way, all the degrees of freedom (DOFs) are fixed, meaning that all translation as well as rotation of the node is restrained by the support.

6.4.2 Fictitious nodes

To model the slabs and vaults described in Chapter 6.2 fictitious nodes need to be included to connect slabs where no real wall nodes are present. Those fictitious nodes are connected to real nodes where possible but they need vertical support where they can not be connected to real nodes. This support is simply required for the model to be statically valid; however, because the slabs are modelled without mass, they do not receive any vertical load. Therefore, the fictitious nodes that are not directly connected to real nodes, by a rigid link for example, receive a support that fixes only the vertical DOF, as well as the rotational DOFs while leaving the other translational DOFs free.

6.5 Connections

Connections are important elements to connect the separate walls. In reality, these connections between walls are highly complex and follow a frictional law of behaviour. In the specific structure of the Parish House, however, it has been determined that the interlocking at wall level is well executed (see also Chapter 5 for more info) which means that the probability of failure at the connections is relatively low in comparison to other failure modes. Therefore, the connections between the walls are modelled with the "equalDOF" function in OpenSees [2]. This means that certain chosen DOFs are connected. The chosen DOFs are the horizontal translational DOFs and for the top nodes also the vertical DOF.

The connections between the walls and slabs are modelled as monolithic connections: In different historical buildings with timber slabs, these connections can be modelled using a frictional law. Yet, in the case of the Parish House, the connections are known to be continuous between the vaults and the walls, i.e. the vault merges seamlessly with the wall, and the introduction of the FERT slabs at the moment of reconstruction implies a good connection between the walls and the slab. Therefore, it has been decided to use the same nodes used for the walls to introduce the slabs and create a monolithic connection. Since the slabs are all modelled using the orthotropic membrane elements, this means that the slab and the walls are connected through the translational DOFs and some through the torsional DOF (moment around the vertical axis) but none of the other rotational DOFs is connected (due to the negligence of bending resistance of the slabs).

6.6 Masses and loads

In OpenSees, the masses relevant for seismic load, and the vertical loads are defined separately. The masses of the piers, spandrels and nodes are modelled automatically, whereas the masses of the slabs and the roof, as well as the live loads, need to be introduced separately. Therefore, the mass of each slab is evenly distributed between the four support nodes. The distribution can be found in Appendix I. However, since the vertical loads need to be led to the foundation through the walls, which is not possible from the fictitious nodes, a different distribution is applied. Thus, the loads are only introduced to the real nodes. The distribution can also be found in Appendix I. (Note: the different colours in the graphics of Appendix I have no special meaning but act as an assistance to better distinguish the different slabs or influence surfaces.)

7. Analysis of the global behaviour: Initial state

7.1 Pushover analysis

7.1.1 Methodology

The elaboration of the pushover curve tightly follows the procedure proposed by Lestuzzi and Badoux described in the book "Evaluation parasismique des constructions existantes" [23] based on the method of SIA 2018 "Vérification de la sécurité parasismique des bâtiments existants" [42]. The only important difference is the negligence of eccentricity due to the symmetry of the building, and the hypothesis, that the drift is constant over the entire height of the pier. The first step is to identify the walls, i.e. the piers, that provide resistance against horizontal forces. For this calculation, the OOP resistance of the walls is neglected. The piers resisting are the ones defined in Chapter 6 including the nodal panels combining the two vertically superposed piers into one single pier with the full height of the building. The resistance of the spandrels is neglected in this approach, they influence however the coupling of the walls. This is reflected in the choice of height between the base of the wall and the point of zero-moment H_0 . For no coupling at all, this height corresponds to the total height of the wall for full frame effect this will correspond to half the height of the piers. In this case, the height to the point of inflection is taken as 1/2 of the height of the pier due to the good coupling of the piers due to the FERT slabs and the vaults.

Next, it is necessary to determine the normal load acting on each of the piers. This is done by calculating the slab load, as well as the load from the roof and the self-weight of the walls and applying them to the walls. The calculation can be found in the Excel file in Appendix H. The shear resistance of each pier can then be determined using the formulas proposed in [23] that are based on the Eurocode 1998-3 §11.4.1.1. Members failing in flexure have a resistance of:

$$V_{f,d} = \frac{V_{f,k}}{\gamma_{Rd}} = \frac{D N}{2 H_0 \gamma_{Rd}} \left(1 - \frac{N}{D t f_{M,m} 0.85}\right) \quad (7.1)$$

Similarly, members failing in shear have a resistance of*:

$$V_{sd} = \frac{V_{sk}}{\gamma_{Rd}} = \frac{D' t}{\gamma_{Rd}} \left(f_{v0} + \frac{\mu N}{D' t}\right) \quad (7.2)$$

*It is expected that shear sliding failure is dominant over shear by diagonal cracking failure.

To determine D' the following formulas are used:

$$D' = 3 D \cdot \left(\frac{1}{2} - \frac{M_u}{N D}\right); \quad M_u = \frac{\sigma_0 D^2 t}{2} \cdot \left(1 - \frac{\sigma_0}{0.85 f_{M,d}}\right); \quad \sigma_0 = \frac{N}{D t}$$

Where:

- D is the in-plane horizontal dimension of the wall (length of the piers).
- t is the thickness of the wall.
- D' is the depth of the compressed area at the end section of the pier.
- H_0 is the distance between the section where the flexural resistance is attained and the contra flexure point.
- N is the axial load at the base section of the pier.

- $f_{M,m}$ is the mean compressive strength of the masonry, i.e. the value of the compressive strength elaborated in Chapter 4.1.1 before applying the partial factor.
- μ is the masonry friction coefficient, which may be assumed equal to 0.5.
- f_{v0} is the shear strength in the absence of vertical load and equal to $f_{vm0} = 0.13 \text{ N/mm}^2$ as calculated in Chapter 4.1.1.
- γ_{Rd} is the partial factor applied to the shear resistance as defined in Chapter 3.3.3. In the case of shear resistance in flexure $\gamma_{Rd} = 2.15$.

Finally, the yield drift can be calculated for each pier using formula (5.8) in [23]:

$$\delta_y = V_{Rd} \left(\frac{H \cdot (3 H_0 - H)}{6 \cdot EI_{eff}} + \frac{6/5}{GA_{eff}} \right) \quad (7.3)$$

Considering also the ultimate drift limits defined in Chapter 4.1.1 the pushover curve for each pier can be established by adding up the pushover curves piers in the analysed direction and then combining all the piers gives the global pushover curve.

7.1.2 Results

North-south direction

Applying the described procedure to the piers of the walls resisting in the north-south direction of the building, i.e. the longitudinal direction, the pushover curve shown on the left side of Figure 7.1 can be established. The following characteristic values for the global pushover behaviour of the wall can be determined from the calculation of the global pushover curve:

- The total shear resistance in the north-south direction is $V_{Rd,NS} = 1279.6 \text{ kN}$.
- The elastic displacement when reaching the maximum shear resistance is $d_{y,NS} = 2.2 \text{ mm}$.
- The maximum displacement before the resistance starts to degrade is $d_{u,NS} = 26.1 \text{ mm}$.

East-west direction

Similar results can be obtained when applying the procedure to the piers in the east-west direction, i.e. the transversal direction. The pushover curve can be found on the right side of Figure 7.1. The following characteristic values for the global pushover behaviour of the wall can be determined from the calculation of the global pushover curve:

- The total shear resistance in north-south direction is $V_{Rd,EW} = 763.0 \text{ kN}$.
- The elastic displacement when reaching the maximum shear resistance is $d_{y,EW} = 1.9 \text{ mm}$.
- The maximum displacement before the resistance starts to degrade is $d_{u,EW} = 26.1 \text{ mm}$.

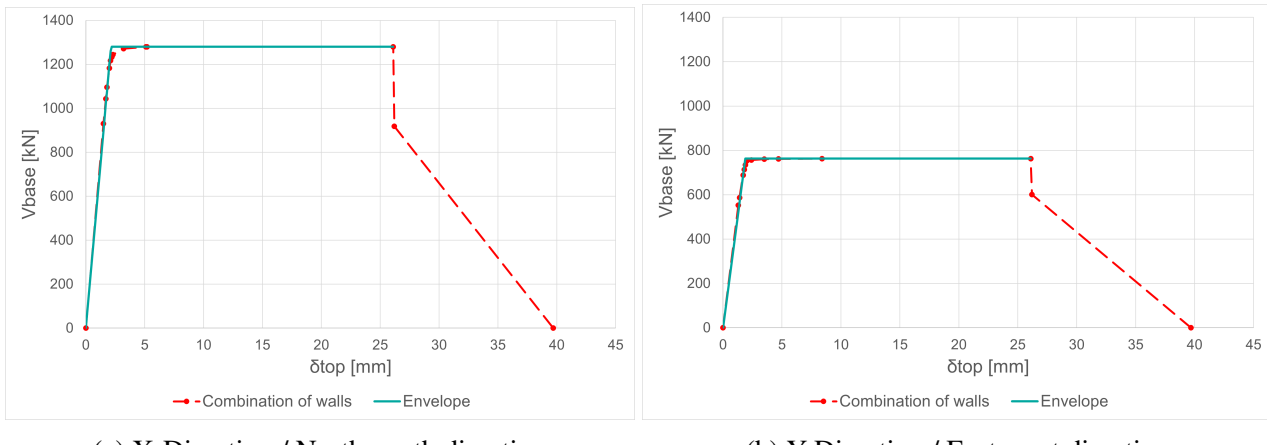


Figure 7.1: Global pushover curve, total base shear versus top displacement

7.1.3 Design limits

Having established the pushover curves in each direction of the building, the limit displacements for the DL limit state can be calculated using formula 11.38 of EN 1998-3:

$$d_{Rd, DL} = d_y / \gamma_{Rd} \quad (7.4)$$

Where: $\gamma_{Rd} = 2.0$ as suggested by Table 11.9 EN 1998-3 [19].

For the verification of the NC limit state the limit deformation is calculated using formula 11.37 EN 1998-3:

$$d_{Rd, NC} = d_u / \gamma_{Rd} \quad (7.5)$$

Where: $\gamma_{Rd} = 1.9$ as suggested by Table 11.8 EN 1998-3 [19]. This results in the following limit values for each direction of solicitation and limit state:

Limit state / Direction	North-south	East-west
Damage limitation (Damage-limitations (DLs))	$d_{Rd, DL NS} = 1.1 \text{ mm}$	$d_{Rd, DL EW} = 1.0 \text{ mm}$
Near collapse (Near-collapses (NCs))	$d_{Rd, NC NS} = 13.7 \text{ mm}$	$d_{Rd, NC EW} = 13.7 \text{ mm}$

Table 7.1: Limit displacements of the roof nodes

7.2 Dynamic analysis

To model the dynamic behaviour of the building in the current state the previously described model (see Chapter 6) is used to perform two types of analyses:

1. A modal analysis, giving as output the periods of the eigenmodes of vibration of the structure and the corresponding deformed shape.
2. A dynamic analysis using the ground motion of the 1979 Montenegro earthquake as an input motion, using the specified factor for each limit state that needs to be verified (see Chapter 4.2.1).

7.2.1 Modal analysis

In the modal analysis, the OpenSees model is used to produce the eigenperiods of the first ten modes of vibration as well as the shape of vibration of the structure corresponding to each mode. All ten modal shapes are given in Appendix J, in this chapter, only the most important modes are discussed. The eigen period as well as the eigenfrequency of each mode are shown in Table 7.2 below:

Mode	1	2	3	4	5	6	7	8	9	10
Period [s]	0.114	0.092	0.091	0.089	0.079	0.074	0.070	0.069	0.062	0.056
Frequency [Hz]	8.74	10.88	11.01	11.19	12.69	13.50	14.20	14.53	16.18	17.92

Table 7.2: Period and frequency of eigenmodes of vibration of the structure

It is interesting to note that the first ten modes of vibration all have a period of about 0.05 to 0.11 seconds which is rather low for a building. This is explained by the thick walls that are evenly dispersed throughout the structure with only a few holes. These walls stiffen and strengthen the structure. Figure 7.2 shows the modal shape of mode 1. The deformation corresponding to this mode

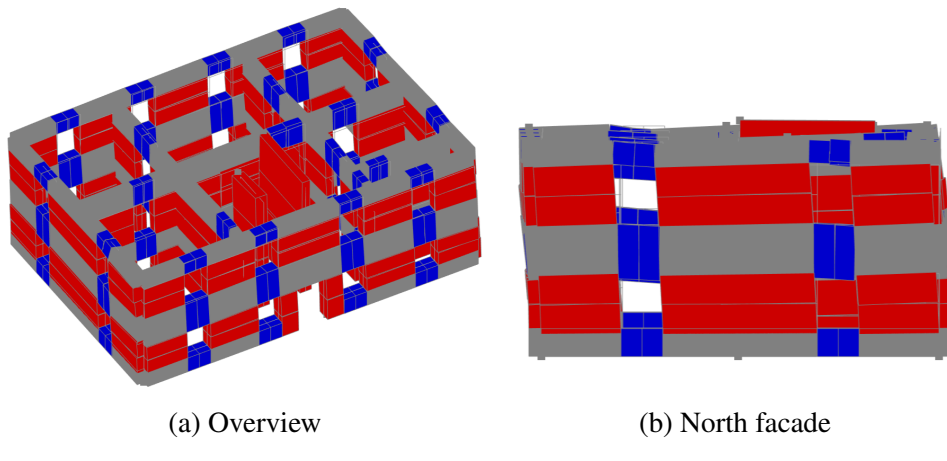


Figure 7.2: Modal shape of mode 1

is mostly composed of an in-plane deformation of the walls that span in the east-west direction of the building. Therefore it is also interesting to look at the elevation of the north facade, to see the piers and spandrels deforming in shear. This is coherent with the cracks of the facades shown in Chapter 2.3.1: The north and south facades experienced a lot of shear cracking due to in-plane deformation of the walls. The next thing to notice is that eigenmodes 2 to 6, as well as modes 8 and 10, mainly concern the building's inside walls. Especially the two walls spanning in the east-west direction are frequently subject to the modal deformation shape. Two examples can be seen in Figure 7.3. This behaviour

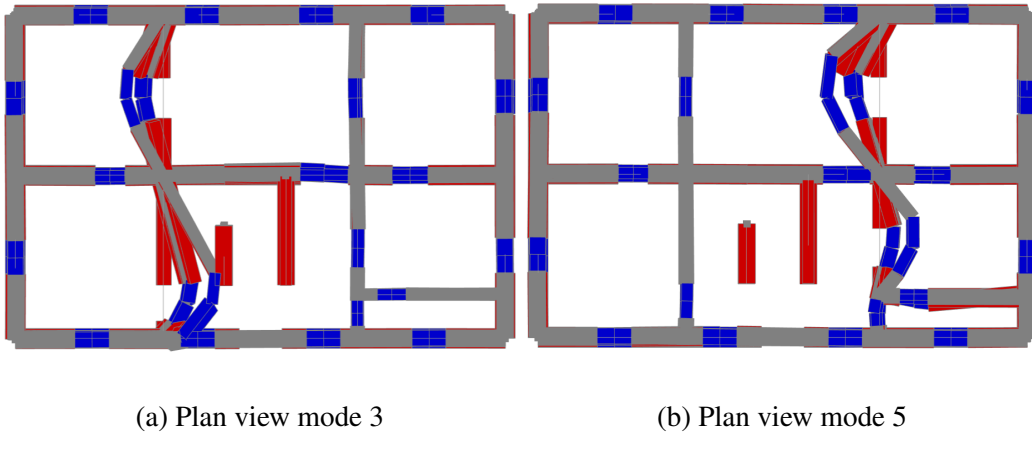


Figure 7.3: Modal shapes of mode 3 and 5

is explained by the modelling procedure of the FERT slabs and the ring beam: First, the ring beam is assumed to only connect the facades to each other and therefore only adds stiffness against OOP movement at the top of those walls, whereas the inside walls of the building remain unrestrained in their OOP direction at their top node. The choice of modelling the slabs using orthotropic membranes does not help to add stability in the OOP direction at those top nodes. Indeed, since the membranes only connect the nodes of the wall and not the macroelements themselves, the rigidifying effect of the slab added to those walls is neglected. The support walls of the FERT slabs should get some OOP restraining from the slabs because this support is linear in reality and not limited to a few local spots. The same is true for the walls that support the vaults. Hence, it would be more realistic to use a type of element that connects the slab linearly to the walls, instead of only at the nodes. Finally when

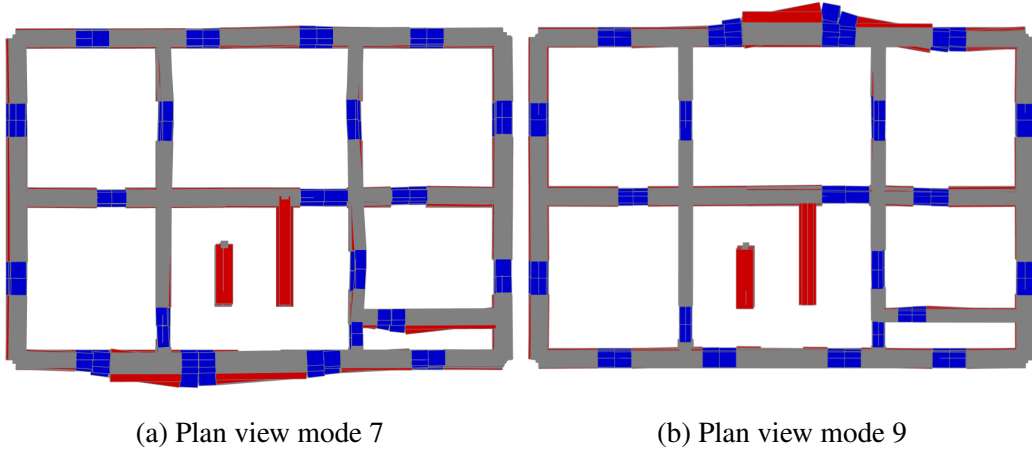


Figure 7.4: Modal shapes of mode 7 and 9

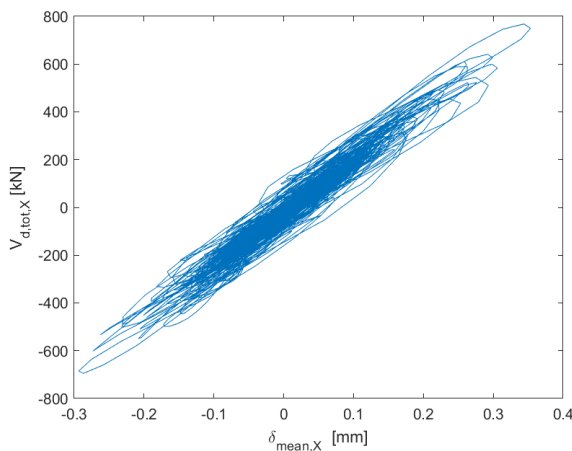
looking at Figure 7.4, it can be seen that two of the ten modes include an OOP movement of the east or the west facade. This validates the hypothesis of Chapters 2.4 and 5.1 and shows that the structure is indeed endangered by local OOP failure mechanisms. Even though the model shows three modes comprising those specific OOP movements, it should be noted that the model does not entirely capture the reality of the failure mechanisms. In practice, the thrust of the interior vaults would increase the OOP movement, making the facades more vulnerable during an earthquake. However, because the vaults are modelled as equivalent orthotropic membranes with elastic stiffnesses, the model does not capture this unique behaviour. This discovery, on the other hand, confirms the decision to model and verify those specific OOP mechanisms separately by the manual calculation shown in Chapter 5.

7.2.2 Response history analysis

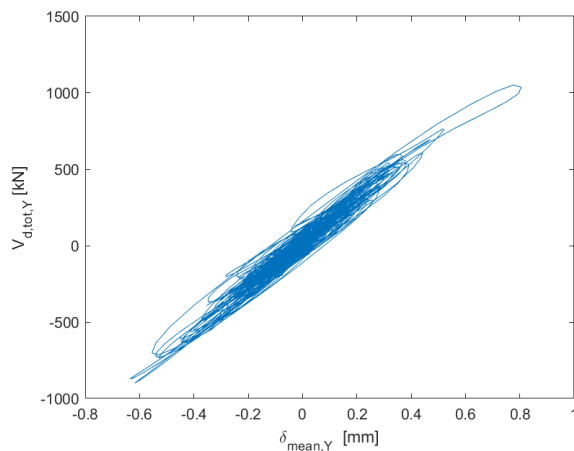
The second type of analysis performed using the OpenSees model is the dynamic non-linear response history analysis (RHA). As previously described the recorded ground acceleration from the 1979 Montenegro earthquake [31] is introduced to model the dynamic behaviour of the structure when being subjected to seismic action. The record of Montenegro 1979 [31] consists of two recorded ground accelerations: one in the north-south direction and one in the east-west direction. To verify the structure four different configurations and three different factors of the acceleration are used. First, to observe the behaviour of the structure when subjected to uni-directional ground acceleration, the north-south record from the Montenegro earthquake is once applied in the longitudinal direction (X-direction) and then in the transversal direction (Y-direction) of the building. The north-south record is chosen for these two cases since its acceleration spectrum fits the Eurocode design spectrum better than the east-west record (see Chapter 4.2.1). After that, two more cases are applied: One where the north-south acceleration record is applied in the longitudinal (north-south) direction of the building, whilst the east-west acceleration record is applied in the transversal (east-west) direction of the building, and a second that consists of switching the ground accelerations to have the east-west record applied to the longitudinal direction while applying the north-south record to the transversal direction. To model the near-collapse (NC) limit state the ground motions are used as they are, whereas to model the damage-limitation (DL) limit state, they need to be multiplied by a factor 0.5 as explained in Chapter 4.2.1. Furthermore, a factor of 2.0 was used to push the structure even farther in the plastification and test what behaviour occurs with larger ground accelerations than the design acceleration. All the results can be found in Appendix J.

Damage limitation

When applying a factor of 0.5 to the ground motion the building mostly behaves elastically. Figure 7.5 shows the total base shear on the vertical axis versus the corresponding mean displacement of the top nodes. Subfigure (a) shows the behaviour in the X-direction for the corresponding uni-directional acceleration and subfigure (b) shows the same for the Y-direction. It's worth noting that ground motion causes more displacement in the east-west direction than in the north-south direction. This can be explained by the lower strength and stiffness of the total piers in the transversal direction compared to the longitudinal direction, also shown in Chapter 7.1. It's also interesting to observe that the mean displacement of the top nodes remains quite small, at less than 0.9 mm. The table below



(a) X-direction for acceleration in X-direction



(b) Y-direction for acceleration in Y-direction

Figure 7.5: Total base shear versus mean roof displacement for uniaxial ground acceleration multiplied by a factor of 0.5

shows the maximum and minimum displacements of all the roof nodes for all the different ground

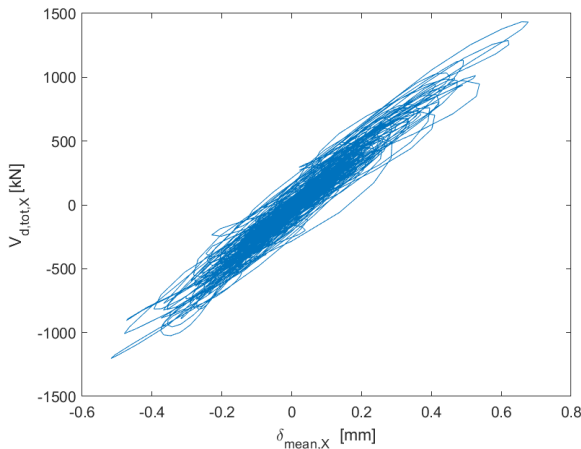
motion combinations:

Ground motion/ Displacement	NS ground motion X-direction	NS ground motion Y-direction	NS in X EW in Y	EW in X NS in X
Maximum in X [mm]	0.5	0.3	0.6	0.5
Maximum in Y [mm]	0.4	1.0	0.7	1.0
Minimum in X [mm]	-0.4	-0.3	-0.5	-0.3
Minimum in Y [mm]	-0.3	-0.9	-0.6	-0.8

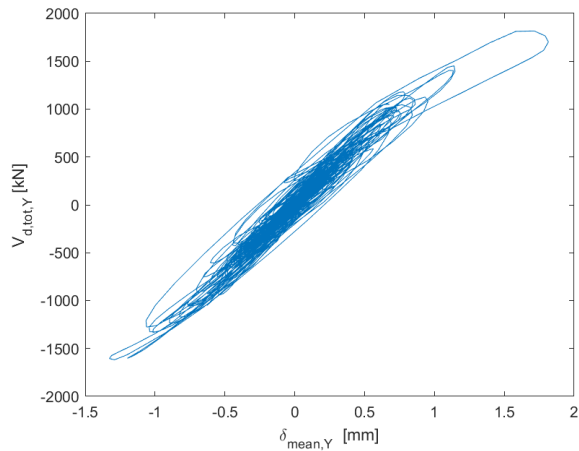
Table 7.3: Minimum and maximum displacements of roof nodes for factor 0.5

Near collapse

To obtain the behaviour of the near-collapse (NC) limit state the ground motions can be applied with a factor of 1.0. The following graphs show the mean displacement of the roof nodes versus the total base shear for an applied ground motion in direction X and direction Y. Looking at Figure 7.6 the



(a) X-direction for acceleration in X-direction



(b) Y-direction for acceleration in Y-direction

Figure 7.6: Total base shear versus mean roof displacement for uniaxial ground acceleration multiplied by a factor of 1.0

following differences can be noted in comparison to the factor 0.5: The mean displacements have nearly doubled for both directions, the total base shear has equally increased and the most important thing to notice is that whilst the behaviour in the X-direction stays mostly elastic, the hysteretic curve in the Y-direction shows first signs of plastification of the structure. Similarly, the minimum and maximum displacements of each ground motion combination can be found in the table below:

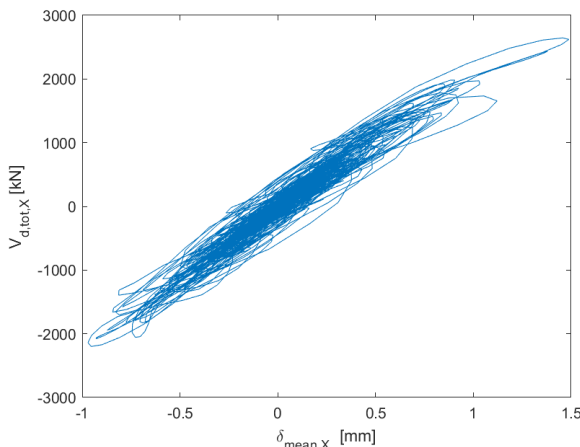
Ground motion/ Displacement	NS ground motion X-direction	NS ground motion Y-direction	NS in X EW in Y	EW in X NS in Y
Maximum in X [mm]	0.9	0.5	1.3	0.9
Maximum in Y [mm]	0.7	2.4	1.6	2.4
Minimum in X [mm]	-0.7	-0.8	-1.0	-0.7
Minimum in Y [mm]	-0.6	-1.8	-1.1	-1.6

Table 7.4: Minimum and maximum displacements for factor 1.0

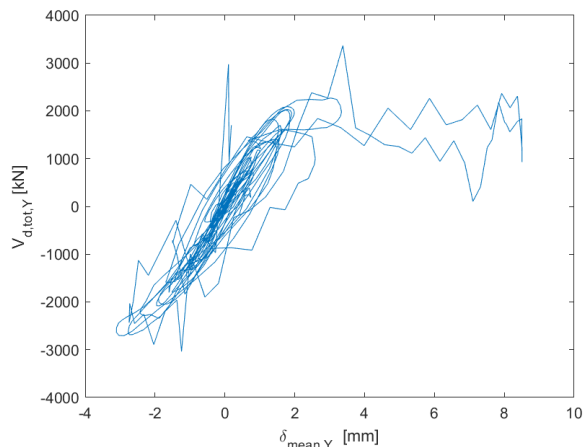
Collapse

For curiosity and to test the limits of the structure, the ground motions are applied with a factor of 2.0. Those results can equally be found in the Appendix J of this report but a few interesting things are pointed out here.

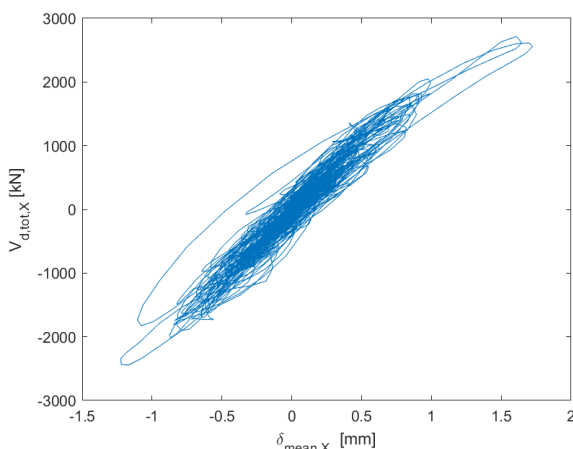
As expected when applying the stronger north-south ground motion either separately in the longitudinal direction to the building or in a combined way with the east-west ground motion in the transverse sense, the building continues to resist but starts to show plastification in the hysteresis. However, when the north-south ground motion is applied to the weaker direction of the building, either separately or combined with the east-west ground motion in the other sense, the building starts to collapse. This can be seen by the non-convergence in the results shown in the two subfigures on the right side of Figure 7.7. There the maximum absolute mean displacement of the roof in the Y direction of the building before collapse can be estimated to be about three millimetres. These results also show that the building is a lot more vulnerable to ground acceleration in the transversal direction compared to the longitudinal direction, which makes sense when looking at the results of the pushover curves. From a qualitative perspective, it is interesting to look at the drifts of the different elements just before



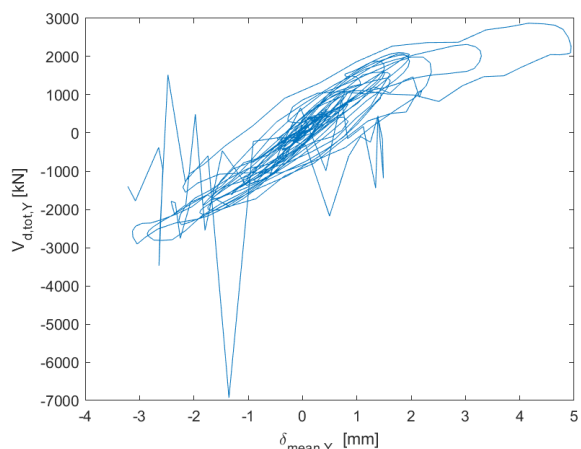
(a) X-direction for acceleration in X-direction



(b) Y-direction for acceleration in Y-direction



(c) X-direction for north-south acceleration in X-direction and east-west acceleration in Y-direction



(d) Y-direction for north-south acceleration in Y-direction and east-west acceleration in X-direction

Figure 7.7: Base shear versus mean roof displacement for a ground acceleration multiplied by 2.0

the collapse of the building. Figure 7.8 shows the shear, as well as the flexural drift of the piers and spandrels just before the collapse. The colour indicates the drift of the element: the darker the colour, the more drift. Comparing those results to the cracks found on the building, the following things can

be found:

1. While the shear drift is mostly concentrated at the south facade, the flexural drift is also elevated in some other walls of the building, even though lower than the drift on the south facade and the south parts of the east and west facades.
2. The building fails due to a concentration of deformation in the south facade, while the drift on the north facade remains rather low. This is not something that can be observed within the crack pattern of the south and north facades (see Figure 2.7).
3. What is observed to be similar is the damage in the spandrels of the south facade: The right (east) spandrels have slightly more drift which corresponds to the bigger/ more concentrated crack patterns found on the damaged building.
4. Contrary to the observed shear cracks of the south and north facades, the deformation observed at collapse is concentrated in the upper piers. This could be due to an overestimation of the loads on the second-floor level.
5. Similarly to the observed behaviour, the damage is mostly situated on the transversal facades and only a few elements of the east and west facades are supposed to have experienced damage.

As can be seen in this quick comparison, the damage pattern of the model does not correspond to the observed damages very well. The fact that a different ground motion was used than the one experienced by the building plays an important role. Therefore, this discrepancy between the observed and the modelled behaviour does not necessarily imply that the model is wrong. To improve the results, it would have been interesting to have an earthquake ground motion record from the Petrinja 2020 earthquake. Thus, the behaviour could have been replicated more precisely by calibrating the model based on the observed results.

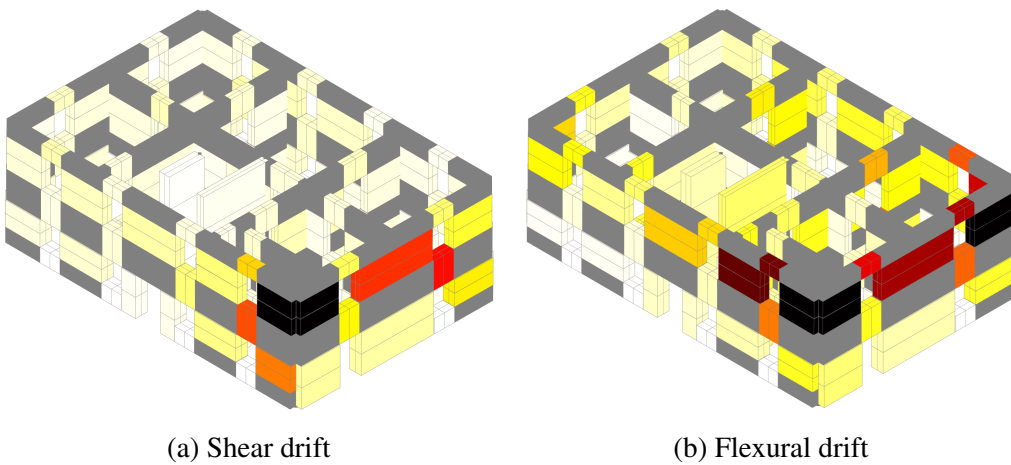


Figure 7.8: Drifts for north-south acceleration in Y direction at collapse

7.3 Verification and discussion

To verify the safety and serviceability of the building against earthquakes in the initial state (undamaged) the maximum absolute displacement amongst all the roof nodes needs to be multiplied by the factor $\gamma_{Sd} = 1.15$ (as defined in Chapter 3.3.1) and then compared to the displacement limit derived in Chapter 7.1.3.

7.3.1 Damage limitation

In the damage-limitation (DL) limit state, the limit displacements are of $d_{Rd, DL, NS} = 1.1 \text{ mm}$ in the longitudinal (north-south) direction, which is approximately the same in the transversal (east-west) direction $d_{Rd, DL, EW} = 1.0 \text{ mm}$. Looking at Table 7.4 the maximum absolute displacement for factor 1.0 is of $d_{Ed, DL, NS} = 1.15 \cdot 0.6 = 0.7 \text{ mm}$ in X direction whereas the maximum absolute displacement in Y direction is of $d_{Ed, DL, EW} = 1.15 \cdot 1.0 = 1.1 \text{ mm}$. The comparison to the limit displacements shows, that the building meets the requirements to verify the DL limit state:

$$d_{Ed, DL, NS} = 0.7 \text{ mm} \leq 1.1 \text{ mm} = d_{Rd, DL, NS} \rightarrow ok \quad (7.6)$$

$$d_{Ed, DL, EW} = 1.1 \text{ mm} \approx 1.0 \text{ mm} = d_{Rd, DL, EW} \approx ok \quad (7.7)$$

It can however be determined that the displacement demand of the DL state is about equal to the limit displacement and it could therefore have been considered to enhance the stiffness of the structure.

7.3.2 Near collapse

The same methodology can be applied to the near-collapse (NC) limit state: First the limit displacements are obtained as in Chapter 7.1.3: $d_{NC, NS} = 13.7 \text{ mm}$ and $d_{NC, EW} = 13.7 \text{ mm}$. Then by comparing them with the maximum absolute displacement obtained in Chapter 7.2.2 the verification results in:

$$d_{Ed, NC, NS} = 1.15 \cdot 1.3 = 1.5 \text{ mm} \leq 13.7 \text{ mm} = d_{Rd, NC, NS} \rightarrow ok \quad (7.8)$$

$$d_{Ed, NC, EW} = 1.15 \cdot 2.4 = 2.8 \text{ mm} \leq 13.7 \text{ mm} = d_{Rd, NC, EW} \rightarrow ok \quad (7.9)$$

This shows that the structure meets its requirements for the global NC limit state. Nevertheless, this does not automatically indicate that the structure is far from collapse and does not need reinforcement: As shown in Chapter 5.7 the structure is prone to fail because of very specific OOP mechanisms that are not captured well by the model. Furthermore, Figure 7.7 shows that when increasing the ground acceleration the structure fails before reaching the before-determined displacement capacities. Indeed, the failure of the structure at this point could be due to a local concentration of forces in specific elements due to the plastic redistribution of the forces in the structure. The pushover curve, however, has been calculated in a more approximate manner. Due to the negligence of plastic redistribution of the forces in the process of yielding of the structure, as well as due to the neglected eccentricities in the structure, the pushover curve in Chapter 7.1 serves more as an upper boundary of the resistance and needs to be handled with care. Even though, the Eurocode approach explained in Chapter 7.1.3 reduces the determined displacement limits by a significant factor (taking only about half of the displacement capacity), the 3D effects present in the structure are only vaguely known and the results should be treated with attention.

8. Proposed retrofitting and behaviour in re-inforced state

The last chapter of this thesis is dedicated to the future utilisation of the building. After the damages due to the earthquake in 2020, the building was classified as not safe to use anymore. Therefore, the community decided to use it as storage space for items not frequently needed, for which they did not need to enter the building frequently. However, before the seismic event, the building had been an important part of the community of St. Lawrence church and home to the church priest. It is therefore important to reestablish the safety of the building by reinforcing the structure so that it can be utilised safely again.

8.1 Methodology

For the development of retrofitting procedures, a systematic approach as presented in the ISCARSAH Guidelines [43] is used. The procedure follows the same steps as modern medicine:

The initial step, **anamnesis**, entails recalling the historical context, past damage, construction history, structural alterations, and the structure's performance in previous events. This phase provides a comprehensive understanding of the structure's evolution and vulnerabilities.

Following anamnesis, the **diagnosis** phase involves assessing the current condition and pinpointing the root of the problem. This is achieved through in-situ inspection, material characterization, and structural analysis. Understanding the current state is crucial for formulating effective retrofitting strategies.

Once the issues are identified, the **therapy** phase comes into play. This step aims to address the root of the problem through the thoughtful design and application of interventions. This may include structural modifications, material reinforcements, or other engineering solutions tailored to the specific challenges revealed during the diagnosis.

Finally, control is an ongoing aspect of retrofitting. **Monitoring** the efficiency of the intervention is essential to ensure the good behaviour of the chosen retrofitting solutions. This involves employing various techniques to track changes in structural behaviour over time, ensuring that the implemented retrofitting measures remain effective and the structure stays resilient to potential risks.

Important criteria

The ISCARSAH Principles [44] provide a set of criteria/rules to apply to ensure compatibility, effectiveness and historical preservation. The following are the most significant conditions that must be met for a retrofitting procedure:

1. Each retrofitting procedure of a historical building is a **multidisciplinary approach**. Engineers, as well as architects, conservators, material scientists etc. are needed to understand every aspect of the structure and to tailor the measures to the project.
2. The retrofitting procedure should aim to **safeguard the cultural and historical significance** of the building as a whole and preserve its authenticity in a cultural context.
3. The **short- and long-term effects** of any intervention should be evaluated before its application. It is a good idea that interventions can be **removed or undone** in case there will be more

appropriate methods in the future.

4. A **scientific methodology**, as proposed above should be applied to get an objective understanding of the problem and apply the right remedies.

8.2 Anamnesis

In the past, the Parish House underwent various challenges, notably during the 20th-century war and the earthquake in 2020. War-induced damage primarily affected the roof and the second-floor slab, as documented in Chapter 2.1. The lightweight roof as well as the second-floor slab acted as a shield during bombings, protecting the main structure from the impacts. Therefore, only those elements were damaged and needed replacement. Reconstruction efforts after the war, finished in 1997, included the addition of a reinforced concrete (RC) ring beam and a FERT slab, to replace the damaged slab and enhance the box behaviour of the building. Furthermore, the entire roof structure was rebuilt using timber beams to create a lightweight solution. It is however assumed that the structural system and behaviour of the building remains unchanged.

The 2020 earthquake caused severe damage to the structural elements, but the main structure remains mostly intact and without collapse. The seismic action caused structural damage, particularly to walls and vaults. Diagonal shear cracks have mainly been observed in the north and south facades and on inside walls with the same orientation. This phenomenon can be explained by the lower stiffness of the building in the east-west direction as established in Chapter 7.1. Some shear cracking can however also be observed in the spandrels of the east facade. In the east and west facades, the main damages, however, come from horizontal cracks due to some global OOP failures as described in Chapter 2.4. All in all, however, the building behaved very robustly and the damage caused does not pose an immediate threat to the integrity of the building.

The FERT slabs, as well as the ring beam, show no signs of decay or damage, meaning they behaved well under the 2020 earthquake. It can be assumed that the FERT slab is well linked to the ring beam and acts as a rather stiff diaphragm holding the top of the walls together. Their addition certainly increased the box behaviour of the building and could have been one of the main reasons for the robust behaviour of the building.

8.3 Diagnosis

As mentioned in the previous chapter, a lot of shear cracks, as well as horizontal cracks, could be observed that alter the rigidity and horizontal resistance of the walls. Those damages are likely to lead to problems during the occurrence of another seismic event: Due to the reduced stiffness and resistance to lateral loads, new in-plane loads will potentially be redistributed to other undamaged parts of the building, possibly damaging those as well. Furthermore, the cracks lead to a separation of the wall into blocks, enabling OOP mechanisms that were previously not compatible. Damaged vaults now only require the reactivation of the already-formed pins during the next earthquake, which needs significantly less energy. Another problem lies in the previously activated OOP facade mechanisms: The cracking pattern shown in Chapter 2.4 shows that the mechanism did to some degree happen and move the walls out of their respective planes. This means that those walls probably have a slight residual OOP displacement, implying that the thrust of the vaults will already be increased. Knowing that this thrust is proportional to the square of the span and inversely proportional to the vault's height (see Chapter 2.2.2), this increased vault span makes the walls more vulnerable to (re-)activation of the OOP mechanisms in the next earthquake.

Looking at the results of the two analyses it can be determined that the building satisfies the ser-

viceability and the ultimate limit state in the undamaged state in the global analysis. The local OOP analyses have however shown, that the safety against the F-mechanisms of the west facade is unsatisfactory.

8.4 Therapy

Based on the observations of the diagnosis, it is of interest to develop a solution to reduce the risk of OOP mechanisms. Furthermore, the building experienced a lot of damage during the last earthquake that needs repairing in order to return to the initial and sufficient global resistance. Therefore the following plan of therapy, i.e. the following measures, are proposed to ensure the safety and serviceability of the building for the next years: In the first step, the cracked walls will be repaired using either the repointing method described in Chapter 8.4.1 or the "scuci-cuci" method explained in Chapter 8.4.2. In addition to the repairing efforts, the vaults receive steel ties that are introduced above them to relieve the thrust experienced by the two opposing support walls. The procedure of this reinforcing measure is described in chapter 8.4.3. Even though only the southwest vault requires steel ties to ensure the stability of the F-mechanism on the west facade, it has been decided to introduce steel ties to all barrel vaults of the building. The main reason is the already experienced damage and deformation of the walls and the vaults, which form a risk. Adding in those steel ties as a preliminary measure ensures the good future behaviour of the vaults and the safety of the building.

8.4.1 Repointing

One method that is frequently used in various types of masonry is deep repointing. This procedure should be used if the deterioration is limited to the mortar. It entails partially replacing the mortar joints with higher-quality mortar in order to improve the mechanical properties of the masonry. It is most effective when applied to both sides of a masonry wall. The masonry resistance to both vertical and horizontal loads can be strengthened by this method, but only by a considerable amount if a significant percentage of the initial weak mortar can be replaced. The best results, however, are shown in terms of rigidity, which increases substantially due to the confinement effect of the joints. The fact that deep repointing's effectiveness is highly dependent on the quality of the on-site application could be a drawback. Since the mechanical properties of the mortar are strongly dependent on the ratio of the mixture, they might vary considerably from batch to batch if the ratio of water to powder differs. Furthermore, it is crucial to replace the entire volume of the ablated mortar to ensure a good connection between the single bricks. [45]

The treatment works especially well on walls that are less than 60 centimetres thick [45]. Although the wall thicknesses of the Parish House are frequently more than 60 centimetres, this does not automatically rule out the technique. In this instance, the technique is applied more to repair than to strengthen the structural element. Particular cases are shown in Figure 8.2 below. It should be applied as a main repair method to cracked walls where the cracks remain within the mortar part of the masonry and did not damage the bricks. In zones where cracks pass through bricks, the method should

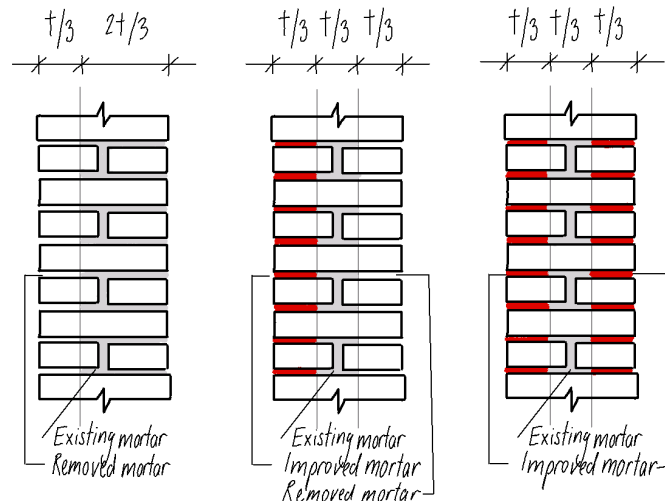


Figure 8.1: Repointing method

be applied in addition around the replaced zone (see Chapter 8.4.2). The stiffening and reinforcing effect of repointing will be neglected in the global analysis of the retrofitted state. It is assumed that its only effect is to reestablish the initial, uncracked state of the walls.



Figure 8.2: Zones where repointing could be efficient

8.4.2 "Scuci-cuci"

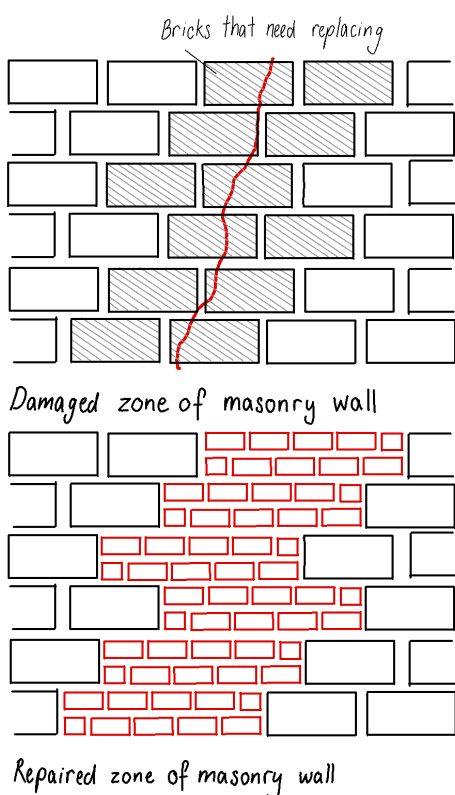


Figure 8.3: "Scuci-cuci" method

The "scuci-cuci" method, i.e. "unstitch-stitch" method, aims to repair damaged walls by replacing the cracked elements with new bricks and mortar. This method is used only locally to recover heavy damages, i.e. cracks that pass through the bricks. The purpose is not to strengthen the masonry and increase its stiffness but to reestablish continuity and connection between them and to restore the wall to its initial state. To be effective and compatible with the rest of the structure, those materials should be similar to the original ones in terms of shape, dimensions, stiffness and strength. The best is to reuse the removed material that remains intact. If this is not possible an extensive analysis of the mechanic, chemical and physical characteristics of the masonry is needed to select compatible substitution materials. In walls where only one leaf is damaged, it is also possible to only replace the damaged leaf. [45]

The procedure consists of the following steps: Before starting the reparation work, it is essential to prop up the structure to redirect the downward movement of the loads and to relieve the area to be replaced. Then, the construction workers will start scraping out the mortar between the bricks that need replacing. Once the bricks are "freed" it is usually possible to pull them out manually. If the thickness of the wall or the loads are more elevated, this step can be done employing hydraulic jacks welded to steel sections. After this step, the new bricks and mortar are introduced from the bottom up, striving for the most penetration possible. Before carefully removing the props, the curing process should be checked: If the mortar is not solid enough this could lead to settlements in the whole structure otherwise. After the phase of settling and adjusting of the wall, the area between the new and old

for the most penetration possible. Before carefully removing the props, the curing process should be checked: If the mortar is not solid enough this could lead to settlements in the whole structure otherwise. After the phase of settling and adjusting of the wall, the area between the new and old

masonry is sealed with more mortar. [45]

Regarding the ISCARSAH Principles mentioned in Chapter 8.1 it would be discouraged to intervene in such an invasive and irreversible manner. However, after considering alternative approaches, it was determined during the research procedure that these interventions would be even less effective at returning the structure to its original state of stiffness and strength while also being much more invasive (see for example jacketing or other methods proposed in [45]).

In the case of the Parish house, most of the cracked zones need to be repaired using this method: Zones pervaded by cracks in multiple directions will need to be replaced entirely (as seen in Figure 8.4), whereas walls that are only damaged by specific isolated cracks can profit of local substitution only in the zone of the crack (for example Figure 8.4).

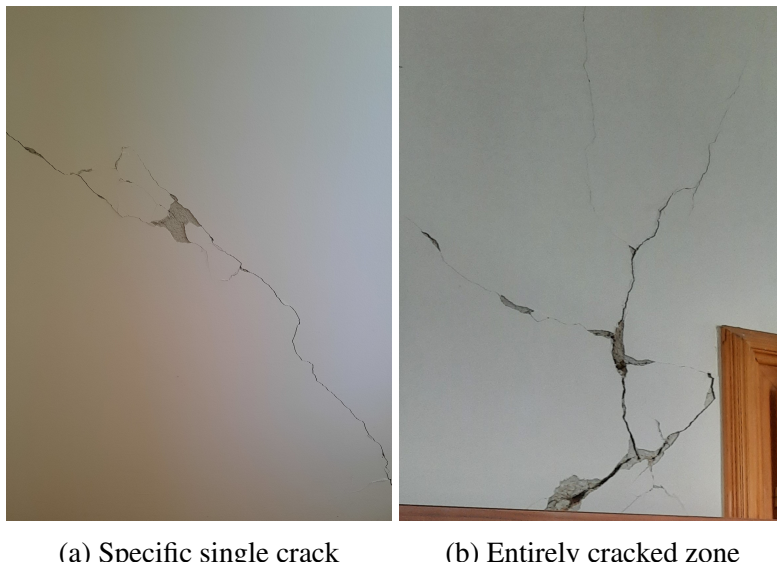


Figure 8.4: Two different zones of cracking

8.4.3 Steel ties against vault thrust

To reduce the horizontal thrust of the vaults acting on the opposing support walls, steel ties will be introduced above the vaults connecting the support walls. Unfortunately, this measure is only possible for those vaults that have enough filling volume above them to find space for the ties. The drawing in Figure 8.5 shows the concept of the ties: In the first step, the timber planks of the floor are removed, as well as part of the filling material, and then the steel ties are introduced. The ties will be anchored to the wall with a steel plate on the other side, introducing the force onto a big enough surface of the wall to avoid local stress concentration. On the facades these plates will need to be embedded into the wall and covered with plastering or mortar to hide them, on the inside walls this is not necessary since the plates will be covered with filling material. When the ties are in place, the infill material and timber boards may be reinstalled.

To define the number of steel ties required for each vault, the thrust of the vault will be calculated as in the OOP calculations before and the required number of ties can be deduced to counter that force. The ties are chosen to have a diameter of 18 millimetres and are made of steel S355, meaning their Young's modulus will be of $E_{ties} = 210 \text{ GPa}$ and their maximum stress can be assumed at $f_y = 355 \text{ MPa}$. The number of ties can be calculated as follows:

$$N_{ties} = \left\lceil \frac{4 \cdot R_{h,vault}}{f_y \cdot d_{tie}^2 \cdot \pi} \right\rceil \quad (8.1)$$

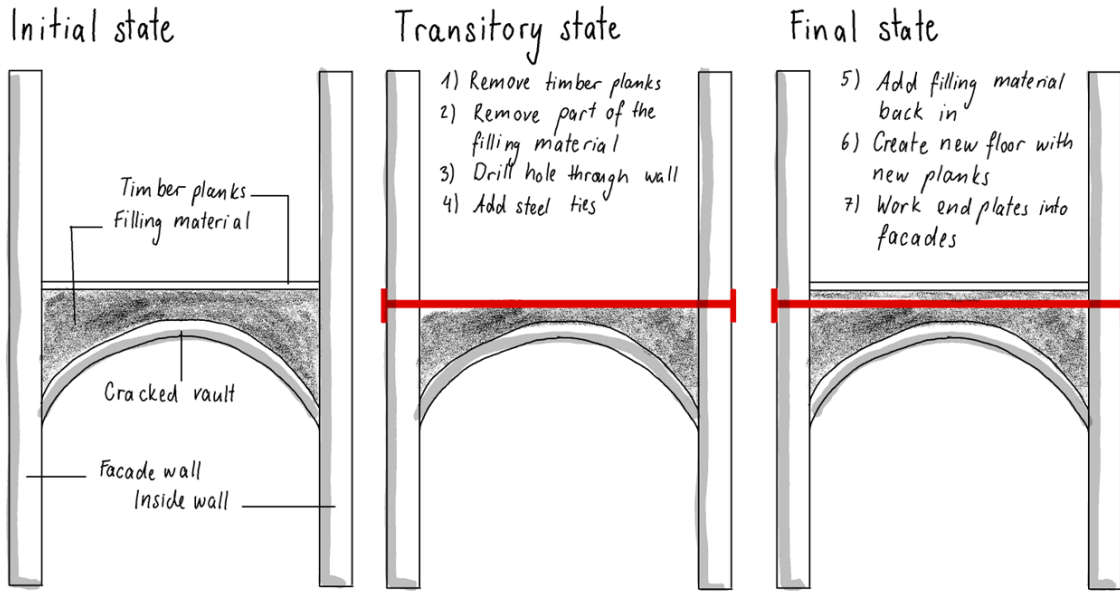


Figure 8.5: Steel ties concept

For the case of the F-mechanisms on the west facade, this number needs to be multiplied by 4 to verify the safety of the OOP mechanism. The calculation for the design of these ties can be found in Appendix H. The ties can only be installed for barrel vaults, thus only the big vault on the east side, the two vaults on the north and south side and the small vault on the southwest side of the building receive this treatment. A schematic plan of the ties is shown in Figure 8.6.

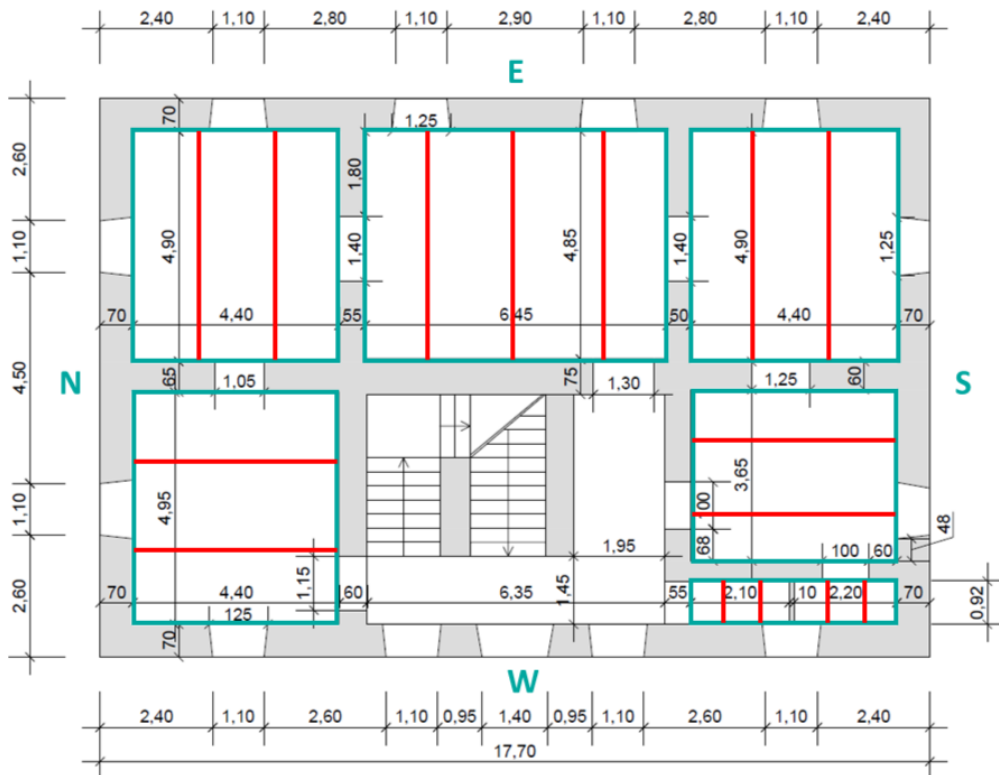


Figure 8.6: Steel ties schema plan

8.5 Behaviour in the retrofitted state

To analyse the behaviour of the Parish House in the retrofitted state and verify the effectiveness of the steel ties, the same analyses as performed on the unretrofitted structure are used. To do so, the steel ties are introduced not only into the OOP calculations as a force holding the wall back, but also in the OpenSees model where they help hold together the opposing walls.

8.5.1 Analysis of the out-of-plane mechanisms

Since the steel ties are applied approximately at the level of the first floor, they do not influence the two G-mechanisms described in Chapter 5.1. This means that the resistance of these two walls against the G-mechanisms stays the same, which is already sufficient. They do however restrain the walls of the F-mechanisms at mid-span, which is the desired behaviour to ensure stability, especially of the west facade. Therefore, only these two mechanisms are treated in this chapter.

Modelling of the steel ties

To model the steel ties in the Jupyter Notebooks (see Appendix H), the only things that need to be introduced are:

- The number of ties used n_{ties}
- The diameter of the steel ties d_{ties}
- The length of the ties L_{ties} is assumed to be the same as the span of the vault.
- The Young's modulus of the used steel $E_{ties} = 210 \text{ GPa}$
- The stress resistance of the steel $f_y = 355 \text{ N/mm}^2$
- The point of application of the ties, which can be assumed to be at the connection of the top and the bottom wall, i.e. at the point where the thickness of the wall changes.

Then the resisting force for a known elongation of the steel ties can be calculated as:

$$R_{ties} = \frac{\delta_{ties} \cdot d_{ties}^2 \cdot \pi \cdot E_{ties}}{4 \cdot L_{ties}} \quad (8.2)$$

This resistance can then be multiplied by the vertical lever arm as done for the other forces. In this specific case the force in the ties is limited by the stress resistance f_y and the elongation is limited by 10% (EN 1993-1-1). After this deformation, the force in the ties drops to zero as they are assumed to have failed. This means the following statements need to be verified as well:

$$R_{ties} \leq \frac{f_y \cdot d_{ties}^2 \cdot \pi}{4} \quad (8.3)$$

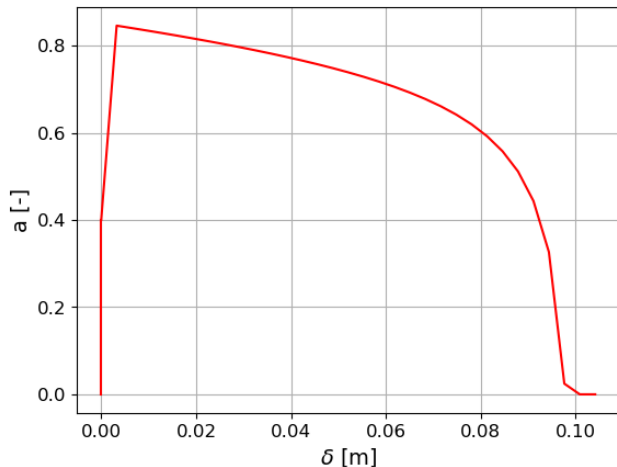
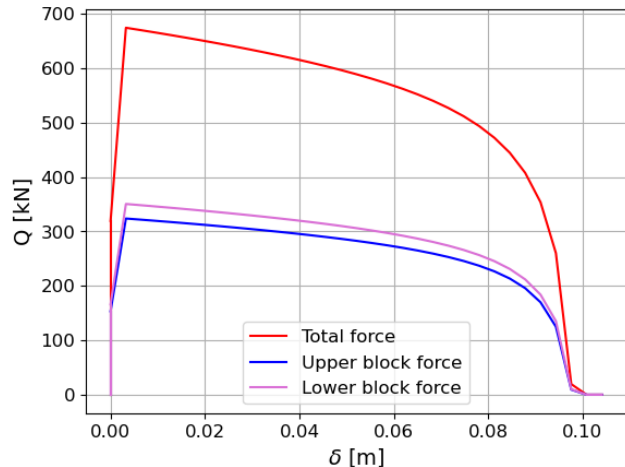
$$\delta_{ties} \leq 0.1 \cdot L_{ties} \quad (8.4)$$

Out-of-plane results

Comparing the results of the pushover curve of the F-mechanism west side after adding the steel ties, the following changes can be noticed:

1. The force to trigger the mechanism stays the same at around 300 kN or at an acceleration of about 3.9 m/s^2 .

2. After the mechanism is triggered, i.e. the displacement starts to increase, the rigidity is still positive and the resisting force continues to increase to approximately double the force required to trigger the mechanism.
3. The displacement capacity, however, remains unchanged. This is explained by the limit displacement in the steel ties that is set at 10% of their length, which means that they fail before the mechanism reaches the point of zero resistance, resulting in the pushover curve going back to its original shape. (This can also be seen by a very small kink in the curve towards the end in Figure 8.7.)

(a) α -Factor describing the seismic load

(b) Force-Displacement curve

Figure 8.7: F-mechanism west side results retrofitted state

Figure 8.8 shows the graph of the N2 verifications of the F-mechanism on the west facade. The limit displacement of the DL, as well as of the NC limit states remain unchanged. The target displacements however change due to the increased rigidity of the mechanism in the beginning. Since the performance point now lies within the plateau of the ADRS curve, the second method is used to determine the target displacement (see Chapter 5.6). The verification is done as follows:

$$d_{DL} = 0.018 \text{ m} \leq d_{u1} = 0.020 \text{ m} \rightarrow \text{ok!} \quad (8.5)$$

$$d_{NC} = 0.010 \text{ m} \leq d_{u2} = 0.030 \text{ m} \rightarrow \text{ok!} \quad (8.6)$$

This shows that the added steel ties enhance the resistance leading to a verification of the limit states compared to the initial state.

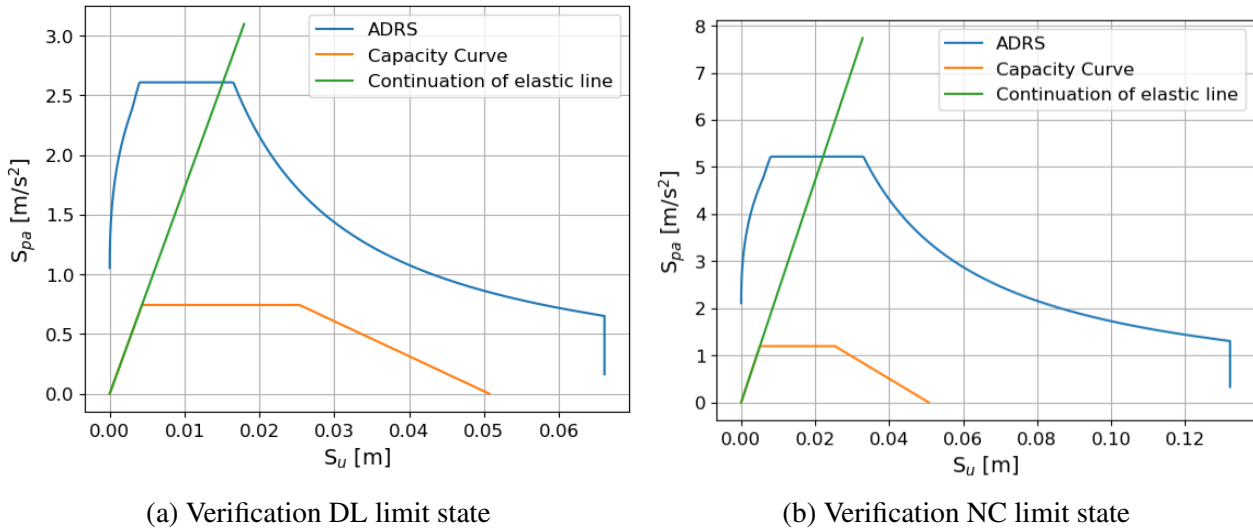


Figure 8.8: Verification of the resistance against the F-mechanism west facade with the N2 method in the retrofitted state

For the F-mechanism on the east facade, approximately the same changes can be noticed as for the west facade. One difference is that, compared to the mechanism on the west facade, the displacement capacity is enhanced because the steel ties do not fail until reaching the point of zero resistance. This increases the displacement capacity by about 40% (from 0.319 m to 0.442 m).

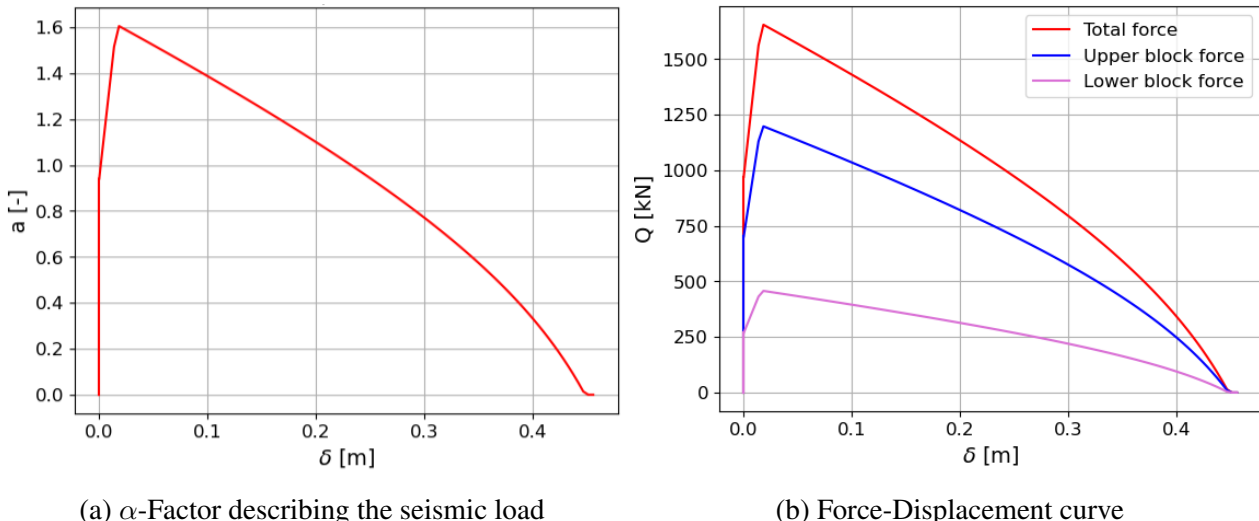


Figure 8.9: F-mechanism east side results retrofitted state

It can also be seen that the retrofitted mechanism verifies the safety conditions for the NC, as well as for the DL limit states. Indeed, it would not have been necessary to reinforce the vaults of the east F-mechanism since they already verified the conditions for safety and serviceability. However, the deformed and already cracked state of the vault bears a risk of reactivation of the mechanism at a lower acceleration in the next earthquake. Therefore, the reinforcements are retained, even though they are not necessary by calculation. The verification is as follows:

$$d_{DL} = 0.028 \text{ m} \leq d_{u1} = 0.093 \text{ m} \rightarrow \text{ok!} \quad (8.7)$$

$$d_{NC} = 0.056 \text{ m} \leq d_{u2} = 0.139 \text{ m} \rightarrow \text{ok!} \quad (8.8)$$

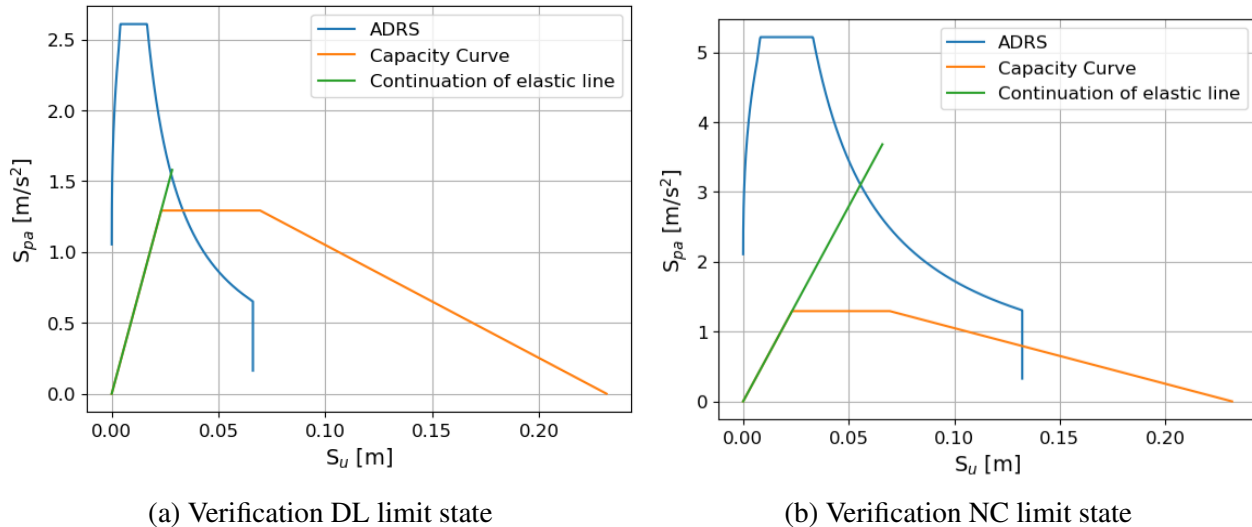


Figure 8.10: Verification of the resistance against the F-mechanism east facade with the N2 method in the retrofitted state

8.5.2 Analysis of the global behaviour

Even though the global behaviour of the building satisfies the standards for safety and serviceability in the near-collapse (NC) and the damage-limitation (DL) limit states as shown in Chapter 7.3, the added steel ties slightly change the structural system of the building. The added resistance could result in an unfavourable redistribution of the loads, creating a local concentration of stresses and potentially increasing the deformation of the structure. Therefore, it is crucial to verify the retrofitted structure to ensure compatibility of the retrofitting method, i.e. the steel ties, with the existing building. The same verification steps, as done before are, hence, also repeated for the retrofitted structure. While the OpenSees model changes with the addition of the steel ties, the pushover curve obtained in chapter 7.1 remains the same as it is a two-dimensional approximation of the real pushover curve. The added steel ties can therefore not be taken into account in this method. Nevertheless, since the ties add resistance and stiffness, the pushover curve remains a conservative approach to the determination of the resistance.

Modelling of the steel ties in OpenSees

Since the OpenSees model consists of a set of nodes between which all the elements span, the only way to introduce the steel ties is to connect them to the existing nodes. In reality, the steel ties are evenly distributed between the two support walls of the vaults. In the model, however, there are no nodes in the centre of the walls (see also plan view of nodes Appendix I). Therefore the total number of steel ties per "vault-slab" is transformed into equivalent steel ties that link the two nodes of the opposing support walls, i.e. the ties of slab 1, representing the vault in the northeast part of the building, would be represented by two equivalent ties between node 89 and 35 and between node 46 and 83. The selected element to represent the tie in the OpenSees model is a truss element, only resisting normal loads, and having a cross-sectional area equivalent to the number of steel ties it represents. The determination of the equivalent steel ties is given in Appendix H.

Results & verification

The same dynamic analyses as described in Chapter 7.2 are also performed on the updated model containing the retrofitting measures. The structure is also verified in a damage-limitation (DL) limit state, as well as a near-collapse (NC) limit state, to ensure the steel ties do not have an unfavourable effect on the structure.

The maximum and minimum displacements for the four analyses of the DL state are the same as shown in Table 7.3. The verification is therefore already given in Chapter 7.3. The same applies to the NC limit state.

8.6 Monitoring

Following the implementation of the previously established retrofitting and restoring techniques, it becomes essential to continue inspecting the structure to verify the materials' compatibility and the efficient operation of the elements. It is intelligent in some buildings to equip the structure with sensors that provide real-time input on structural behaviour. Because these devices are somewhat expensive, it only makes sense to use them in crucial locations where they are necessary. In the case of the Parish House, it is advised that strain gauges be installed on some of the steel ties to monitor their deformation in the event of an earthquake. Because these pieces are tucked away in the infill material and are not accessible during ordinary inspections, it makes sense to monitor their behaviour with sensors. Visual monitoring with routine inspections by an expert is adequate to ensure the safety of the structure's other elements. Especially the repaired zones of masonry need to be checked regularly to ensure the bond between the existing and the new material is still intact. Furthermore, in the event of an earthquake, specific evaluations are required to assure safety.

9. Further investigations

This thesis aimed to investigate the seismic behaviour of the St. Lawrence Parish House in Petrinja. Therefore, the structure was modelled in OpenSees and manual verifications were performed using Jupyter Notebooks developed to calculate the pushover curve of specific mechanisms. Finally, retrofitting procedures have been proposed and the behaviour of the retrofitted structure has been evaluated. Even though this thesis followed a rather complete approach to the seismic evaluation of the Parish House, several interesting subjects could be developed further to gain more comprehension of the structure.

Firstly, the knowledge of the building was very limited in terms of material properties and connection types. Further investigations could be pursued to better define those masonry and mortar properties that are used throughout the whole work of this thesis. In any case, however, the sensitivity of the results to the assumed material characteristics should be evaluated to better understand the influence of the material assumptions.

The second point concerns the modelling of the structure. In the out-of-plane (OOP) analyses, as well as in the OpenSees model the connections between two adjacent walls have been either neglected entirely (OOP analysis) or have been assumed to be monolithic in the horizontal DOFs. In the OOP analysis this approach led to an underestimation of the resistance while it has potentially led to an overestimation of the displacement capacity in the OpenSees model. Therefore, a more detailed modelling approach using for example the frictional model proposed by D'Ayala et al. [12] could give important insight into those fields.

A third point to further investigate is the modelling of the vaults in the OpenSees model. As shown in the calculations of the pushover curves for the OOP mechanisms seen in Chapter 5, the vaults induce a non-negligible thrust to their support walls that destabilize them and push them out of their orthotropic plane. This phenomenon is unfortunately not captured due to the introduction of the vaults as equivalent elastic slabs in the model. The thrust of those vaults could however drastically change the dynamic behaviour of the structure, especially since a lot of mass is situated above the vaults due to the filling material. Likewise, the behaviour after a potential collapse of the vault, i.e. when the displacement between the support walls becomes too big and the vault fails after breaking at mid-span, is not accounted for in the model and could be an interesting subject of further investigation. This is necessary to verify if the structure is resilient and has enough structural redundancy to support a complete failure of a vault.

A smaller, less important topic to further investigate is the modelling approach of the staircase vaults. Due to the important simplification of the model in comparison to the real structure, the dynamic behaviour of the staircase is significantly altered compared to the effective one. Therefore, it could have been interesting to try a more detailed approach to see the difference in behaviour between the simplified and the more detailed model.

Finally, instead of pursuing a simplified method to determine the pushover curve, the OpenSees model could have been calibrated for a pushover analysis to derive a more detailed curve. Indeed, some of the complexity of the structure is lost in the simplified method, especially the 3D effects and the eccentricity of the structural mass to its centre of stiffness are not captured by this approach.

10. Conclusion

To be able to continue safely utilizing the existing unreinforced masonry (URM) building stock, it becomes crucial to reliably assess the buildings and verify their compliance with Eurocode regulations. This work has aimed to perform a complete analysis of the St. Lawrence Parish House of Petrinja, Croatia, in order to propose retrofitting solutions and verify the structure in the strengthened state.

The first step to providing a complete analysis of the building was to document the current state by establishing a complete set of plans and providing a damage inventory that documents the cracks within the masonry.

In the next step, two observed out-of-plane (OOP) mechanisms, as well as two possible mechanisms were analysed using the N2 method proposed by Eurocode 1998-1-1. It was found that one of the two observed mechanisms does not verify the safety conditions and thus needs reinforcing. The other three mechanisms did not constitute a risk.

Next, the structure has been modelled using an equivalent frame model (EFM) approach in the software OpenSees and a dynamic response history analysis (RHA) has been performed, using ground motion records from an earthquake whose spectrum resembles the design spectrum of EN 1998-1-1. The structure has been verified in the damage-limitation (DL), as well as in the near-collapse (NC) limit state to emphasise the safety of the structure.

Finally, three retrofitting methods were proposed that ensure the future reliability of the structural performance. The most important one was the introduction of steel ties above the ground floor vaults to hinder the OOP movement of the supporting walls of the vault and to stabilize already triggered mechanisms in future seismic events. The other two repairing techniques aim to return the structure to its initial state, where safety is assured. To verify the efficiency of the added steel ties, the OOP analyses, as well as the dynamic RHA were repeated for the retrofitted state and it could be shown that the structure satisfies the safety requirements for both analyses.

In conclusion, a rather complete approach to investigating the structure in its initial state has been applied, accompanied by the elaboration of a set of retrofitting techniques to ensure the safe future use of the building. Although there is still room for improvement and more in-depth analysis, this report reflects the work of engineers in the mission of reusing existing, damaged and historical URM structures.

11. Use of AI and data availability

During the writing process, software such as QuillBot AI or ChatGPT was used to improve text quality and provide inspiration for the structure of some text parts; however, the material was derived from the cited sources or is of my own creation. ChatGPT was used to debug certain code snippets and inspire other code snippets for the establishment of the code for the OOP computations in the Jupyter Notebooks and the pre and post-processing of the OpenSees model. However, the code's correct operation has been personally confirmed.

The corresponding data such as the Jupyter Notebooks for the OOP calculations or the Matlab scripts for the dynamic analyses in the OpenSees model are shared on a GitHub repository and can be found here or at this URL: <https://github.com/boenzli/Master-Thesis-2023-24/wiki>

The repository also contains instructions on how to download the necessary software and how to adapt the scripts to work on a different computer.

Bibliography

- [1] Francesco Vanin, Andrea Penna, and Katrin Beyer. A three-dimensional macroelement for modelling the in-plane and out-of-plane response of masonry walls. *Earthquake Engineering & Structural Dynamics*, 49(14):1365–1387, November 2020. ISSN 0098-8847, 1096-9845. doi: 10.1002/eqe.3277. URL <https://onlinelibrary.wiley.com/doi/10.1002/eqe.3277>.
- [2] OpenSees - Open System For Earthquake Engineering Simulation, September 2023.
- [3] Aline Bönzli and Caroline Heitmann. Jupyter Notebook for OOP calculations, June 2023.
- [4] Robbie Andrew. Global CO₂ emissions from cement production, September 2022. URL <https://zenodo.org/record/831454>.
- [5] Zaid Faridi. The Chemistry Behind Concrete. URL <https://www.concretedecor.net/departments/building-with-concrete/>.
- [6] Eduardo Miranda, Svetlana Brzev, Nenad Bijelic, Željko Arbanas, Marko Bartolac, Vojdran Jagodnik, Damir Lazarević, Snježana Mihalić Arbanas, Sonja Zlatović, Andrés Acosta, Jorge Archbold, James Bantis, Jovana Borožan, Ivana Božulić, Nikola Blagojević, Christian Cruz, Héctor Dávalos, Erica Fischer, Selim Gunay, Marijana Hadzima-Nyarko, Pablo Heresi, Dimitrios Lignos, Ting Lin, Marko Marinković, Armando Messina, Sebastian Miranda, Alan Poulos, Giulia Scagliotti, Ingrid Tomac, Igor Tomic, Katerina Ziotopoulou, Željko Žugić, and Ian Robertson. Petrinja, Croatia December 29, 2020, Mw 6.4 Earthquake Joint Reconnaissance Report (JRR). Report, ETH Zurich, January 2021. URL <https://www.research-collection.ethz.ch/handle/20.500.11850/465058>. Accepted: 2021-01-25T06:19:22Z Publication Title: Joint Reconnaissance Report Volume: PRJ-2959.
- [7] Ivan Rizmaul. Obnova sakralnik objekata zupe svetog Lovre u Petrinji 1995 -2015.
- [8] FERT a.s. | Manufacturer of reinforcing steel and prefabricated reinforcement cages, July 2021. URL <https://www.fert.cz/en/>.
- [9] Martina Vujsinović and Hrvoje. Meeting with the engineer working on the project of the parish house in Petrinja, November 2023.
- [10] USGS. M 6.4 - 2 km WSW of Petrinja, Croatia, March 2021. URL <https://earthquake.usgs.gov/earthquakes/eventpage/us6000d3zh/pager>.
- [11] Eurozox. Warehouse spuž | Eurozox. URL <https://www.eurozox.com/en/warehouse-spu%C5%BE/Reinforcing-steel-and-reinforced-mesh/>.
- [12] Dina D’Ayala and Elena Speranza. Definition of Collapse Mechanisms and Seismic Vulnerability of Historic Masonry Buildings. 2003. doi: 10.1193/1.1599896. URL https://www.researchgate.net/publication/249873053_Definition_of_Collapse_Mechanisms_and_Seismic_Vulnerability_of_Historic_Masonry_Buildings.
- [13] European comitee for Standardization (CEN). Eurocode 1990: Basis of structural design, 2002.
- [14] European comitee for Standardization (CEN). Eurocode 1991: Actions on structures - Part 1-1: General actions - Densities, self-weight, imposed loads for buildings, 2002.

- [15] European comitee for Standardization (CEN). Eurocode 1992: Design of concrete structures - Part 1-1: General rules and rules for buildings, 2011.
- [16] European comitee for Standardization (CEN). Eurocode 1993: Design of steel structures - Part 1-1: General rules and rules for buildings, 2009.
- [17] European comitee for Standardization (CEN). Eurocode 1996: Design of masonry structures - Part 1-1: General rules for reinforced and unreinforced masonry structures (Final draft), 2021.
- [18] European comitee for Standardization (CEN). Eurocode 1998: Design of structures for earthquake resistance - Part 1: General rules, seismic actions and rules for buildings, 2022.
- [19] European comitee for Standardization (CEN). Eurocode 1998: Design of structures for earthquake resistance - Part 3: Assessment and retrofitting of buildings and bridges (Draft), 2023.
- [20] Autodesk. Autodesk AutoCAD 2023 - English, September 2022.
- [21] Microsoft Corporation. Microsoft Excel, November 2023.
- [22] Inc The MathWorks. MATLAB, August 2023.
- [23] Pierino Lestuzzi and Marc Badoux. Évaluation parasismique des constructions existantes: bâtiments en maçonnerie et en béton armé. Presses polytechniques et universitaires romandes, Lausanne, 2013. ISBN 978-2-88074-990-3.
- [24] NTC 2008 e Circolare - Norme sismiche per le costruzioni, . URL <https://www.studiopetrillo.com/ntc2018.html>.
- [25] Guido Magenes and Andrea Penna. EXISTING MASONRY BUILDINGS: GENERAL CODE ISSUES AND METHODS OF ANALYSIS AND ASSESSMENT. Eurocode 8 Perspectives from the Italian Standpoint Workshop, pages 185–198, 2009.
- [26] Paulo B. Lourenço and Angelo Gaetani. Finite element analysis for building assessment: advanced use and practical recommendations. Routledge, Abingdon New York, NY, 2022. ISBN 978-0-429-34156-4 978-0-367-35767-2 978-1-03-222839-6.
- [27] SIA 261. SIA 261 Actions sur les structures porteuses, January 2014.
- [28] Francesco Vanin, Dario Zaganelli, Andrea Penna, and Katrin Beyer. Estimates for the stiffness, strength and drift capacity of stone masonry walls based on 123 quasi-static cyclic tests reported in the literature. Bulletin of Earthquake Engineering, 15(12):5435–5479, December 2017. ISSN 1573-1456. doi: 10.1007/s10518-017-0188-5. URL <https://doi.org/10.1007/s10518-017-0188-5>.
- [29] University of Zagreb Department of Geophysics, Faculty of science, Allegretti I, Herak D., Ivancic I., Kuk V., Maric K., Markusic S., and Sovic I. Maps of seismic areas of the Republic of Croatia. URL <http://seizkarta.gfz.hr/hazmap/karta.php>.
- [30] Osnovna geološka karta Republike Hrvatske, 2012.
- [31] Lucia Luzi, Giovanni Lanzano, Chiara Felicetta, Maria Clara D'Amico, Emiliano Russo, Sara Sgobba, Francesca Pacor, and ORFEUS Working Group 5. Engineering Strong Motion Database (ESM), version 2.0. July 2020. doi: 10.13127/ESM.2. URL <https://esm-db.eu>. Publisher: Istituto Nazionale di Geofisica e Vulcanologia (INGV) Version Number: 2.0.
- [32] Bodenbeläge - Parkett | Gebhardt Holz-Zentrum GmbH, . URL <https://www.ghz-cham.de/Bodenbelaege/Parkett/>.

- [33] swisspor. EPS Roof Toiture avec pente intégrée standard. URL <https://www.swisspor.com/ch-fr/eps-roof-toiture-avec-pente-integree-standard>. Publisher: MASSIVE ART WebServices GmbH.
- [34] Dina D' Ayala and Elena Speranza. An Integrated Procedure for the Assessment of Seismic Vulnerability of Historic Buildings. January 2002.
- [35] M. Griffith, Guido Magenes, GIAMMICHELE MELIS, and LUIGINO PICCHI. Evaluation of out-of-plane stability of unreinforced masonry walls subjected to seismic excitation. JOURNAL OF EARTHQUAKE ENGINEERING, 7:141–169, January 2003. doi: 10.1080/13632460309350476.
- [36] EESD EPFL. OpenSees Wiki, October 2023. URL <https://github.com/eesd-epfl/OpenSees/wiki>.
- [37] Igor Tomic. Code and Model parts for OpenSees, 2023.
- [38] Sergio Lagomarsino, Andrea Penna, Alessandro Galasco, and Serena Cattari. TREMURI program: An equivalent frame model for the nonlinear seismic analysis of masonry buildings. Engineering Structures, 56:1787–1799, November 2013. ISSN 01410296. doi: 10.1016/j.engstruct.2013.08.002. URL <https://linkinghub.elsevier.com/retrieve/pii/S0141029613003696>.
- [39] S. Bracchi, M. Rota, A. Penna, and G. Magenes. Consideration of modelling uncertainties in the seismic assessment of masonry buildings by equivalent-frame approach. Bulletin of Earthquake Engineering, 13(11):3423–3448, November 2015. ISSN 1573-1456. doi: 10.1007/s10518-015-9760-z. URL <https://doi.org/10.1007/s10518-015-9760-z>.
- [40] E. Quagliarini, G. Maracchini, and F. Clementi. Uses and limits of the Equivalent Frame Model on existing unreinforced masonry buildings for assessing their seismic risk: A review. Journal of Building Engineering, 10:166–182, March 2017. ISSN 23527102. doi: 10.1016/j.jobe.2017.03.004. URL <https://linkinghub.elsevier.com/retrieve/pii/S235271021630376X>.
- [41] S. Cattari and S. Resemini & S. Lagomarsino. Modelling of vaults as equivalent diaphragms in 3D seismic analysis of masonry buildings. In Structural Analysis of Historic Construction: Preserving Safety and Significance, Two Volume Set. CRC Press, 2008. ISBN 978-0-429-15196-5. Num Pages: 8.
- [42] SIA 2018. SIA 2018 (cahier technique) Vérification de la sécurité parasismique des bâtiments existants, 2004.
- [43] ISCARS AH Guidelines. Technical report, 2005. URL <https://iscarsah.org/documents/>.
- [44] ISCARS AH Principles. Technical report, 2003. URL <https://iscarsah.org/documents/>.
- [45] Deliverable 3.2 - Critical review of retrofitting and reinforcement techniques related to possible failure. WORKPACKAGE 3: Damage based selection of technologies, 2010.
- [46] Beam and block floor slab system, May 2020. URL <https://forums.autodesk.com/t5/revit-structure-forum/beam-and-block-floor-slab-system/td-p/9533987>. Section: Revit Structure Forum.

A. Parish documentation

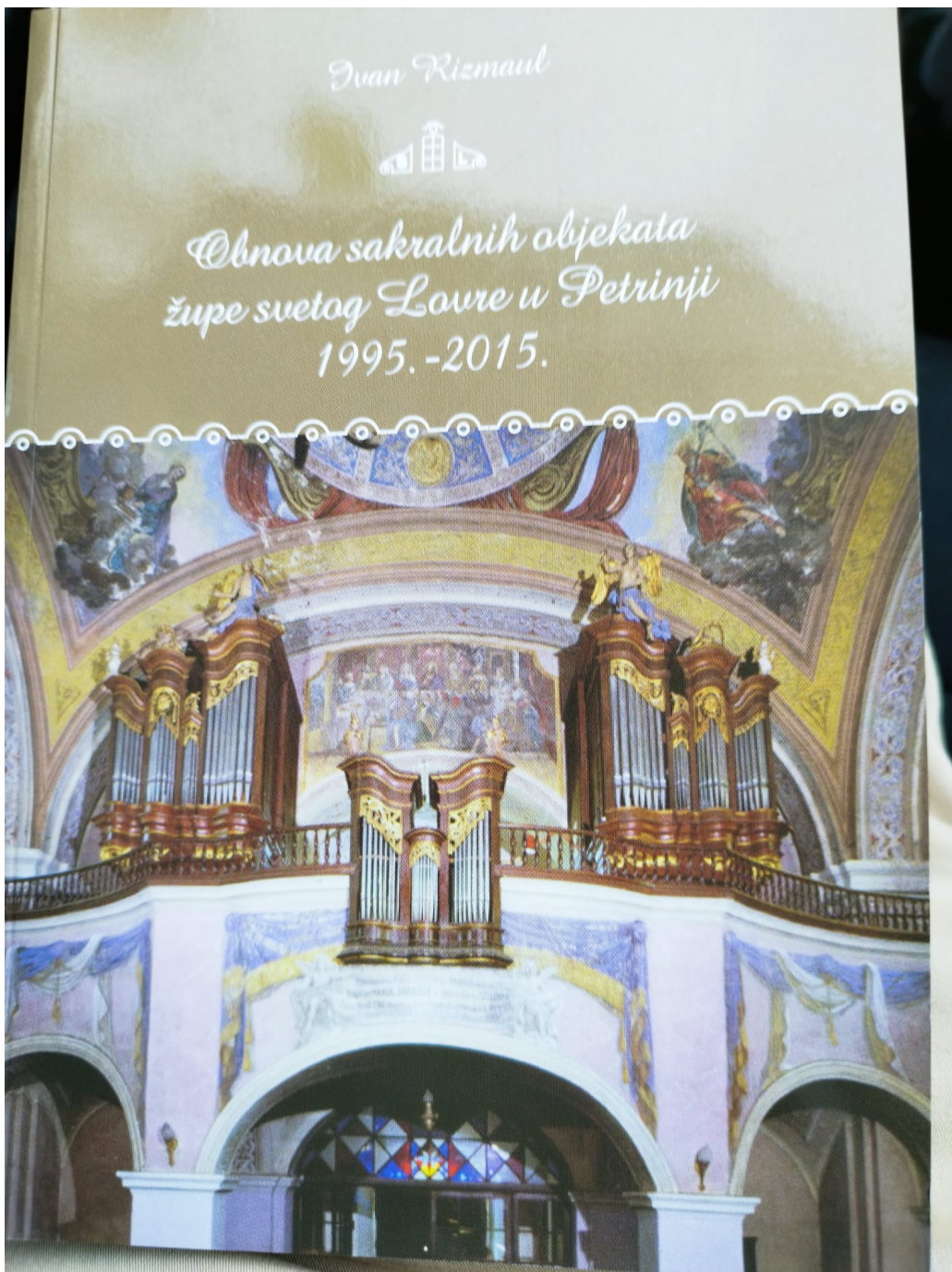


Figure A.1: Title Image



Figure A.2: Page about Parish house

B. Earthquake documentation USGS

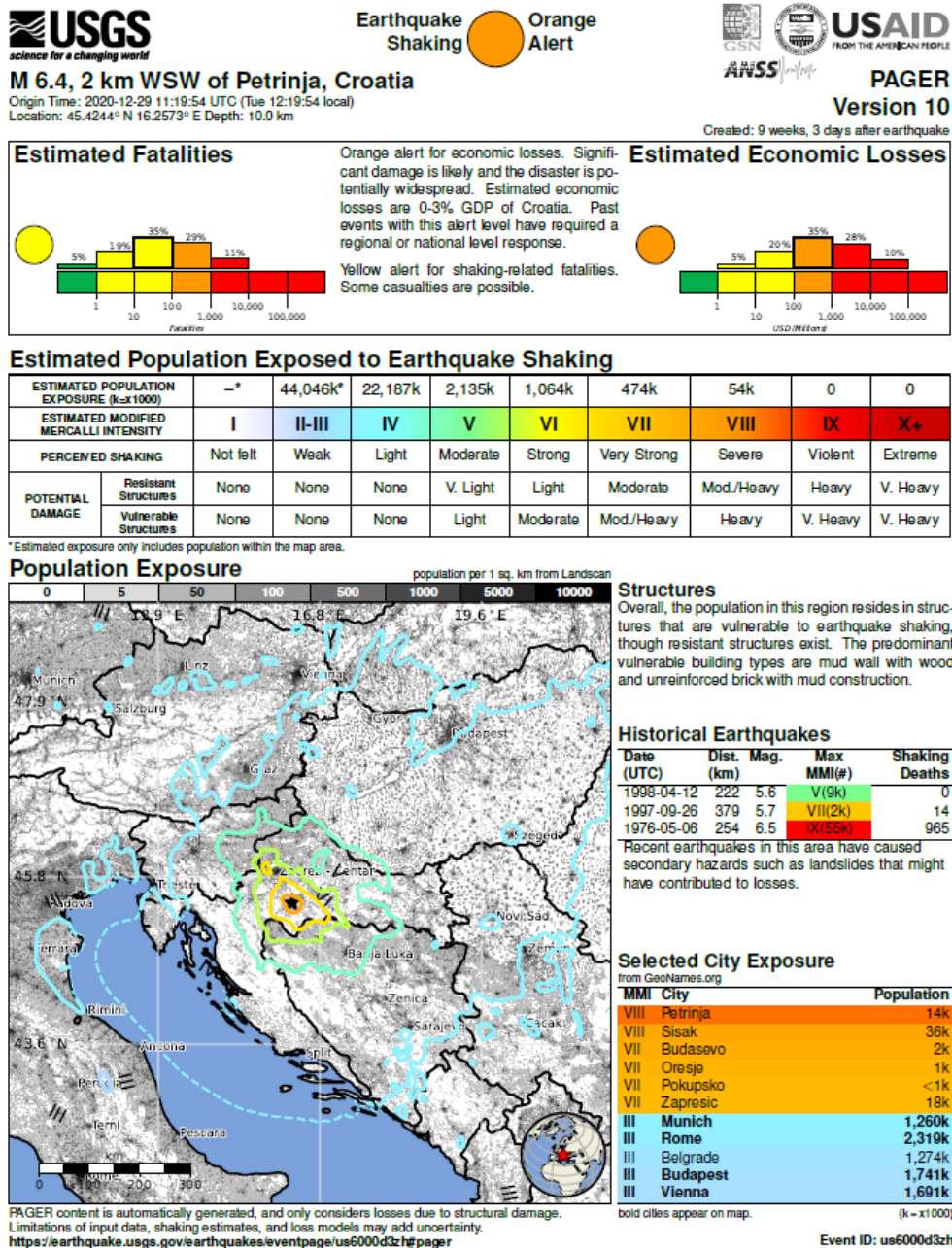
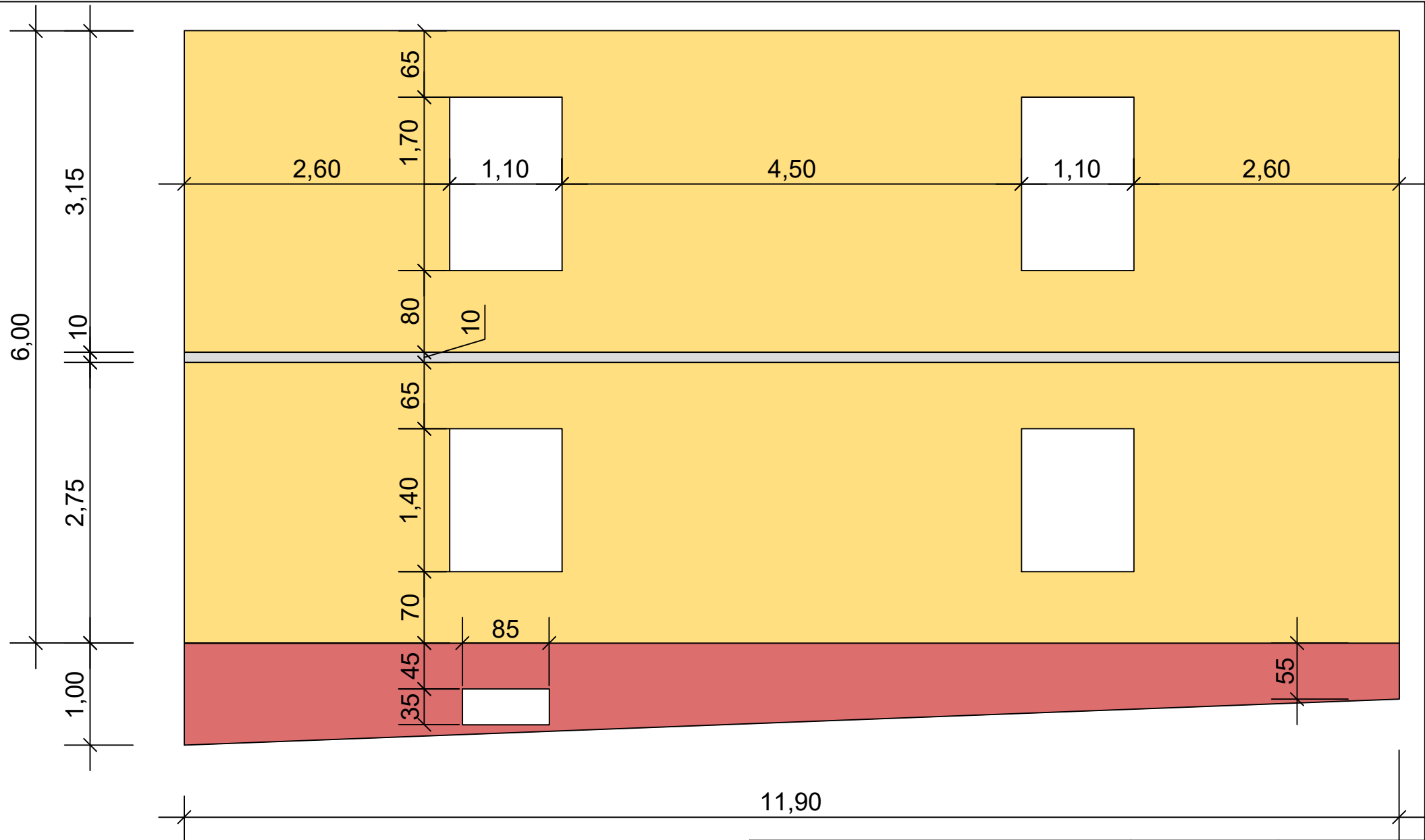


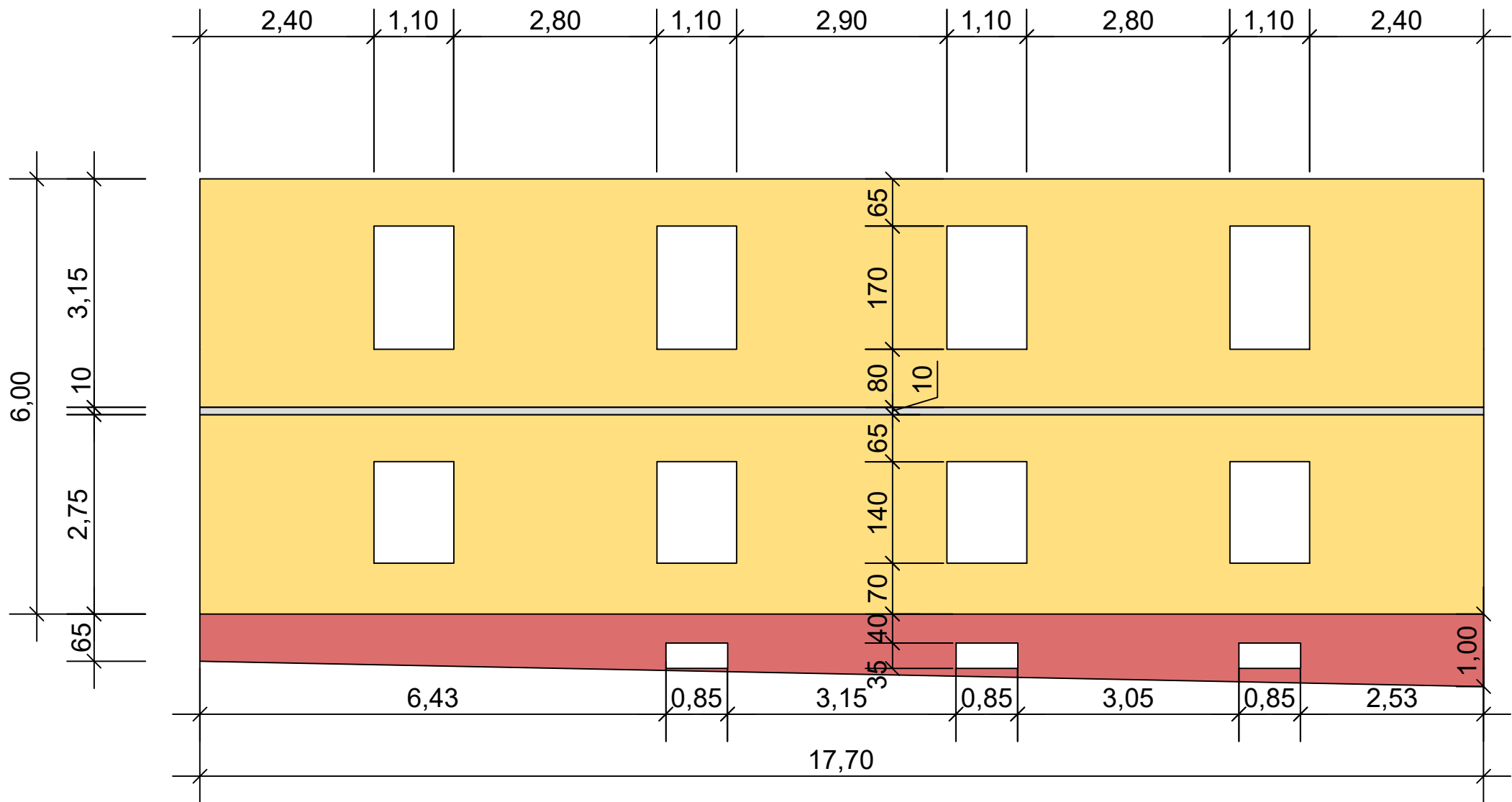
Figure B.1: USGS Earthquake documentation Petrinja 29.12.2020 [10]

C. Plans

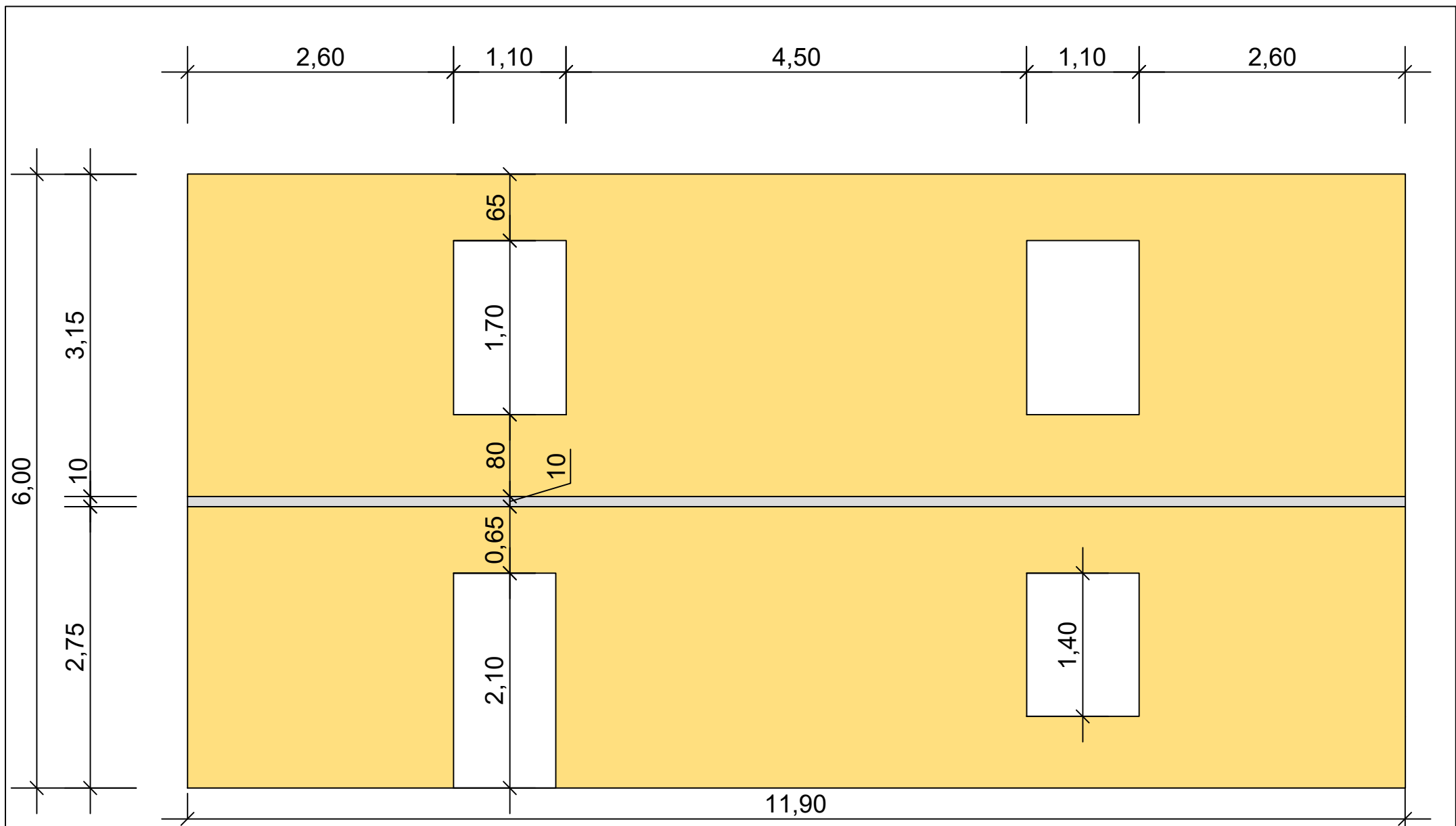
The main task during the site visit in April 2023 was to measure and document the geometry of the building itself. Since those measurements were not done by a professional the plans will therefore have an exactitude of +/- 5 centimeters. This should however be exact enough to give a good indication about the seismic behaviour of the building.



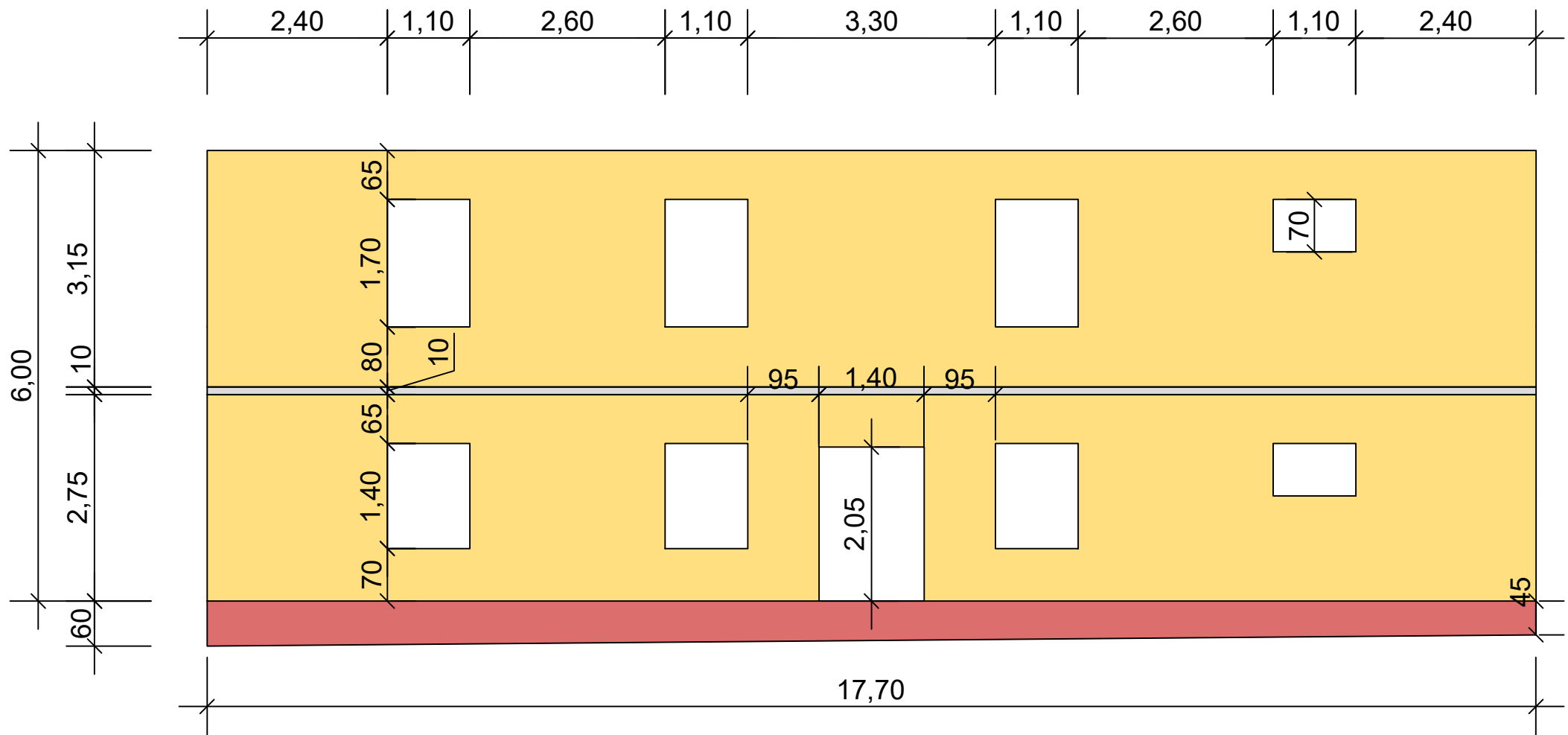
Parish House		Author :	Aline Bönzli
Crkva sv. Lovre		Municipality :	Petrinja
EESD		Country :	Croatia
Norh Facade		Date :	20.05.2023
		Scale :	1:50



Parish House		Author :	Aline Bönzli
Crkva sv. Lovre		Municipality :	Petrinja
EESD		Country :	Croatia
East Facade		Date :	20.05.2023
		Scale :	1:75

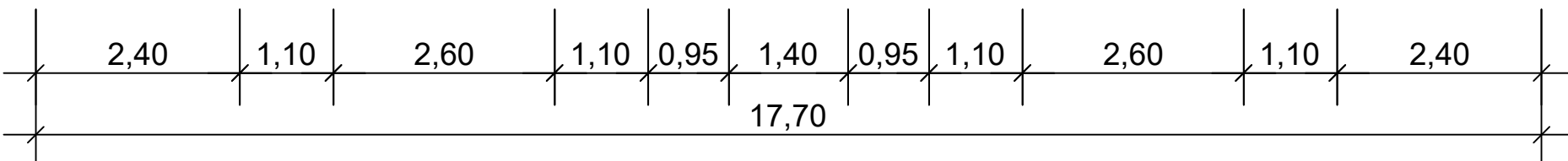
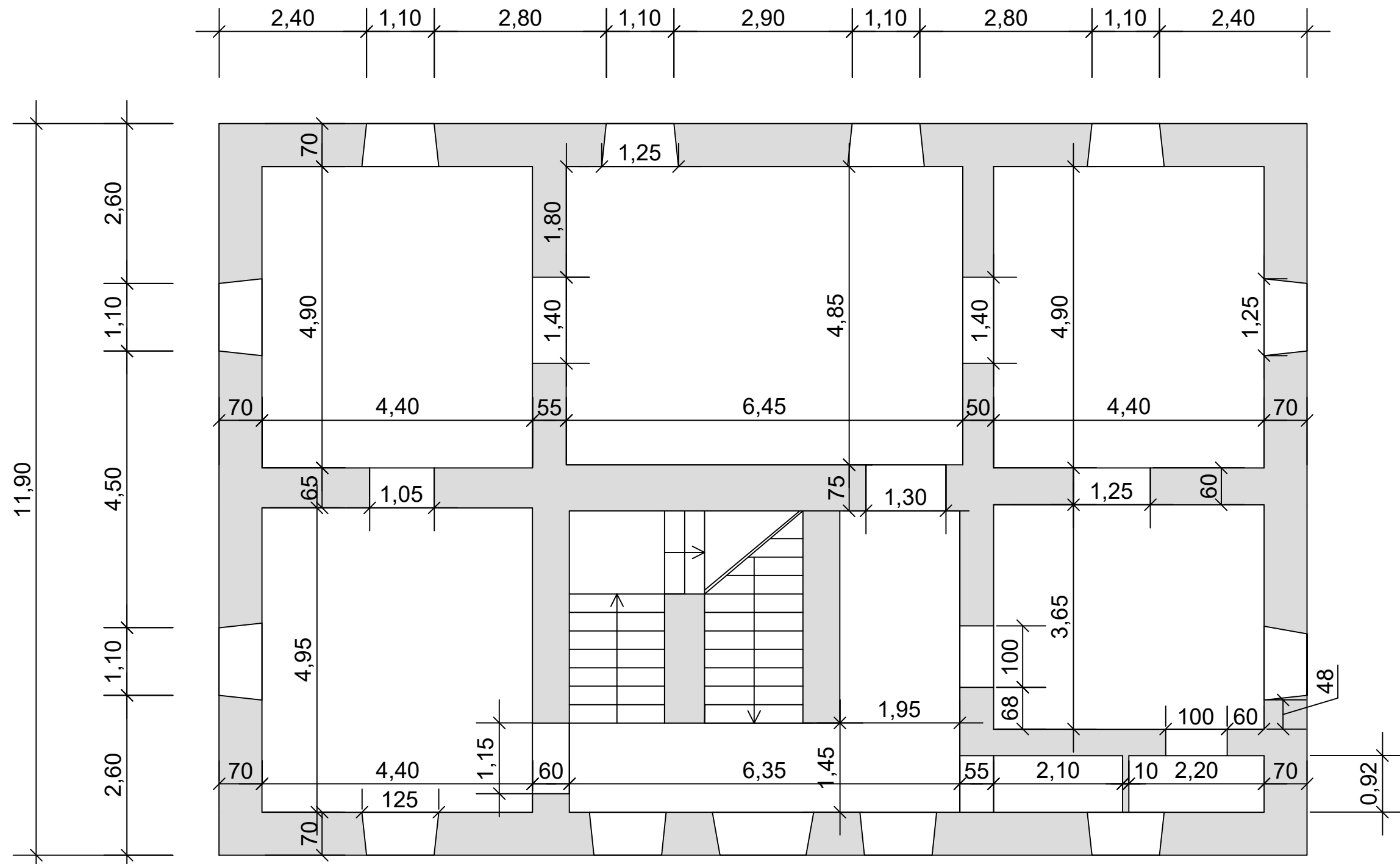
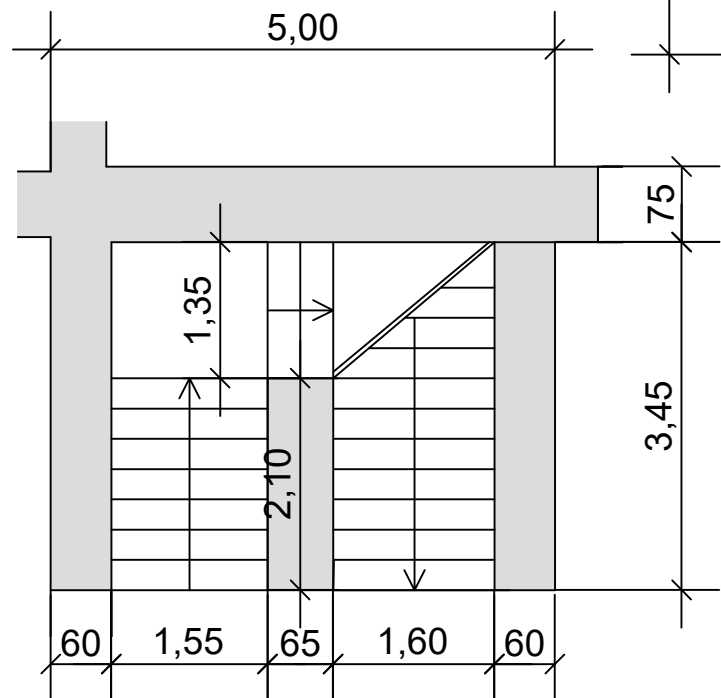


Parish House		Author :	Aline Bönzli
Crkva sv. Lovre		Municipality :	Petrinja
EESD		Country :	Croatia
South Facade		Date :	20.05.2023
		Scale :	1:50



Parish House	Author :	Aline Bönzli
Crkva sv. Lovre	Municipality :	Petrinja
EESD	Country :	Croatia
West Facade	Date :	20.05.2023
	Scale :	1:75

Stair case detail (S 1:75)

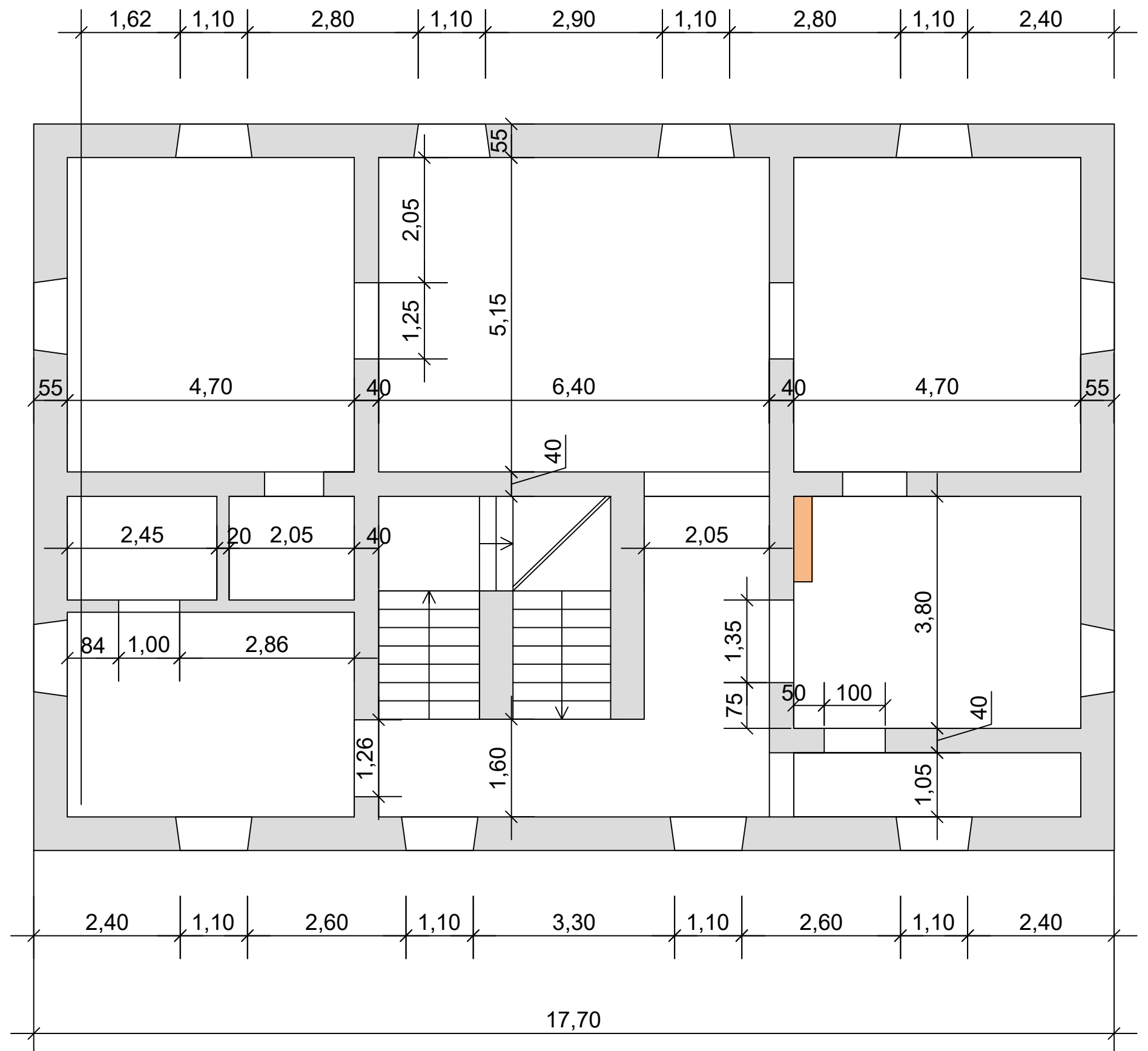
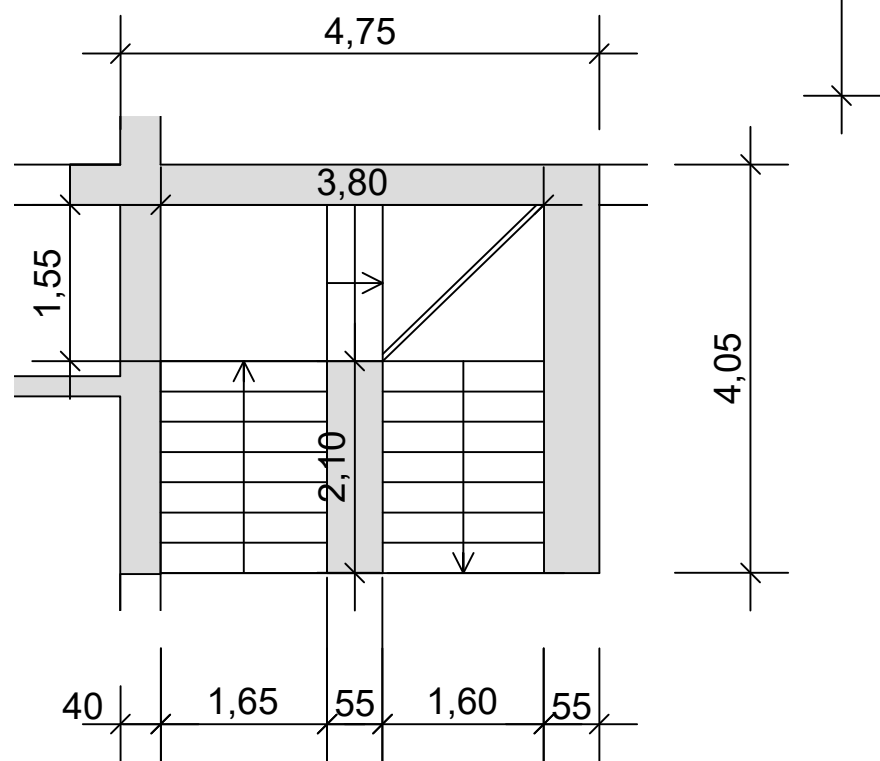


Parish House



<h1>Parish House</h1>	Author :	Aline Bönzli
	Municipality :	Petrinja
Crkva sv. Lovre	Country :	Croatia
Ground Floor, Plan view	Date :	25.05.2023
EESD	Scale :	1 : 75

Stair case detail (S 1:75)

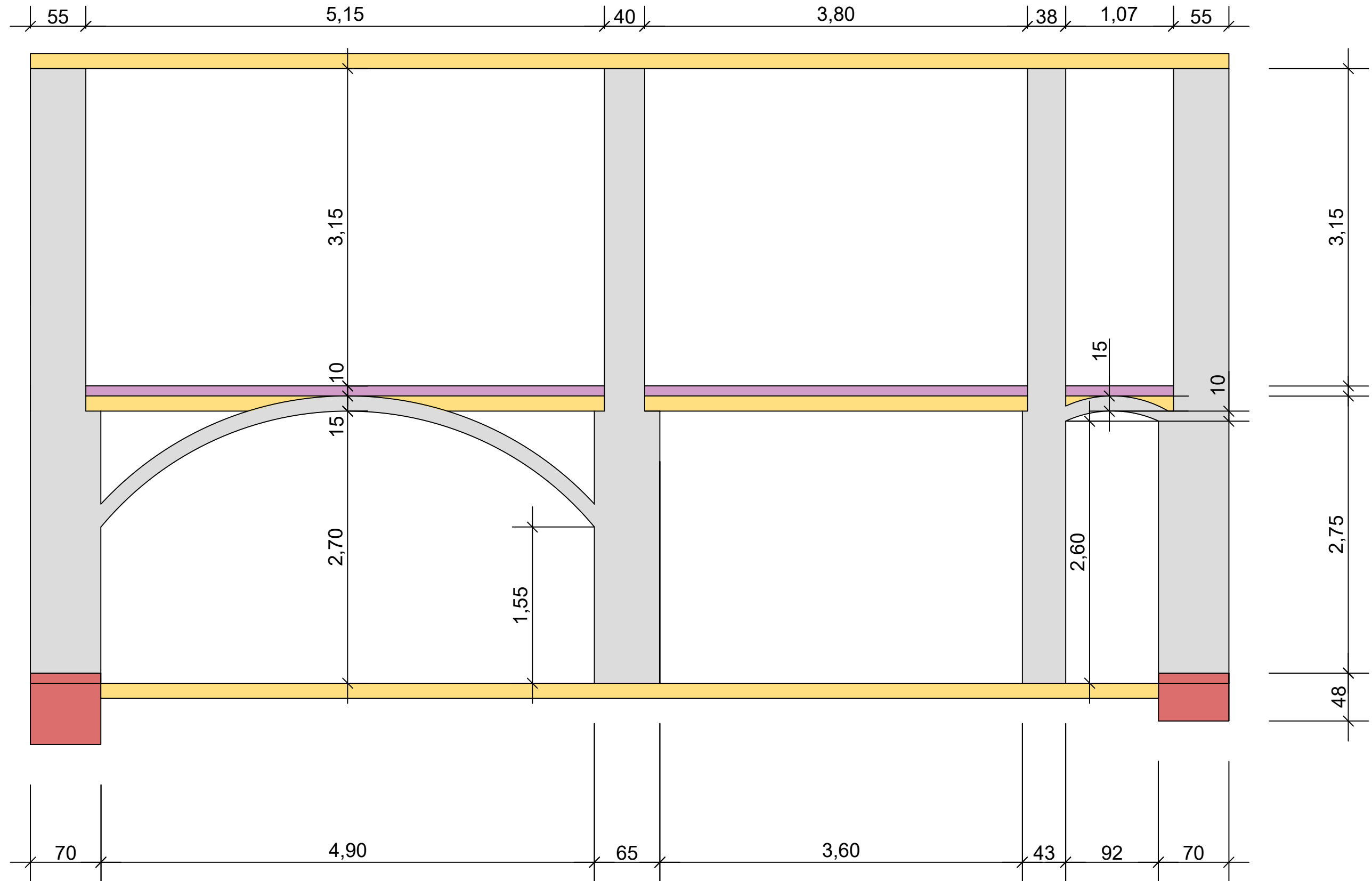


Parish House



Crkva sv. Lovre
First Floor, Plan
view

Author :	Aline Bönzli
Municipality :	Petrinja
Country :	Croatia
Date :	28.09.2023
Scale :	1:75



Parish House		Author :	Aline Bönzli
Municipality :		Petrinja	
Crkva sv. Lovre		Country :	Croatia
E-W (South), Cross-section		Date :	01.06.2023
EESD		Scale :	1:40

D. Crack inventory

During the site visit in April 2023, the building was thoroughly documented through photos and scans (using the MatterPort system on a smartphone and a tripod). Using these images, the phases of the crack documentation were the following:

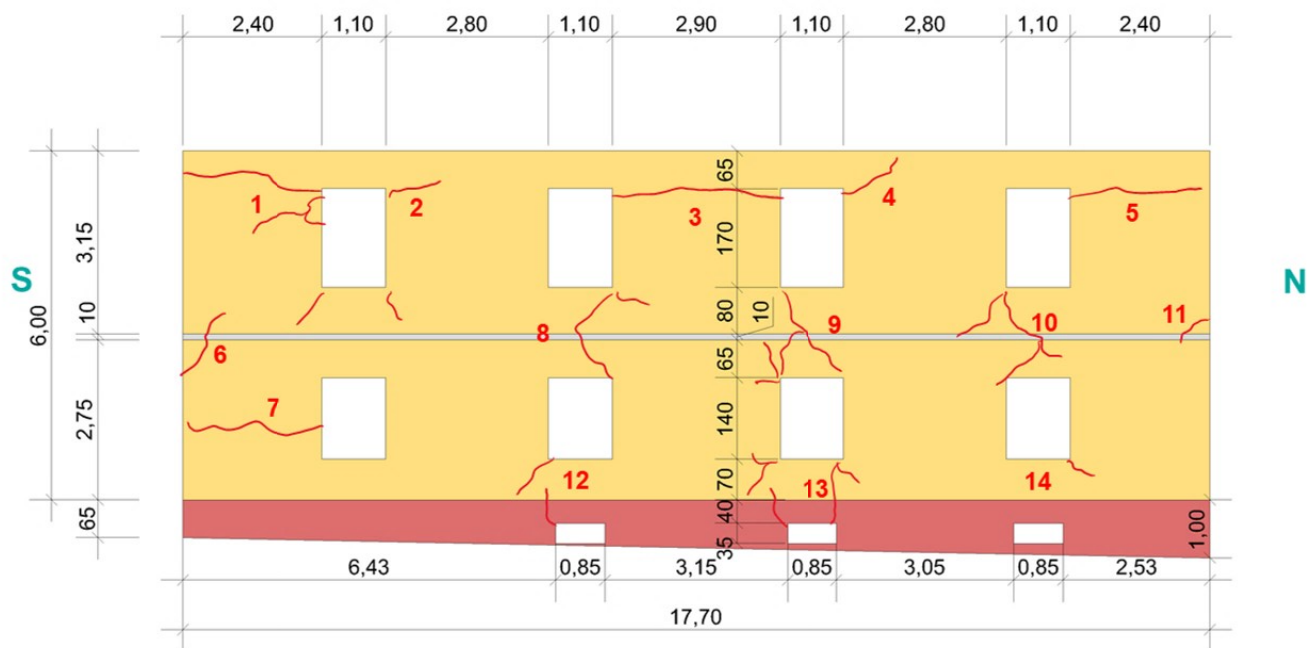
1. Draw all visible cracks of the facade or interior wall on a picture.
2. Transfer the cracks to AutoCAD plans and elevations.
3. Number the cracks.
4. Describe the cracks and location and their associated mechanism in an Excel sheet.
5. Give the crack a distinct label (add an acronym before the number to distinguish between different facades and floors, e.g. GF = ground floor, FF = first floor etc.).
6. Highlight the mechanisms by connecting the cracks that are the result of the same failure.

Visual documentation

East Facade



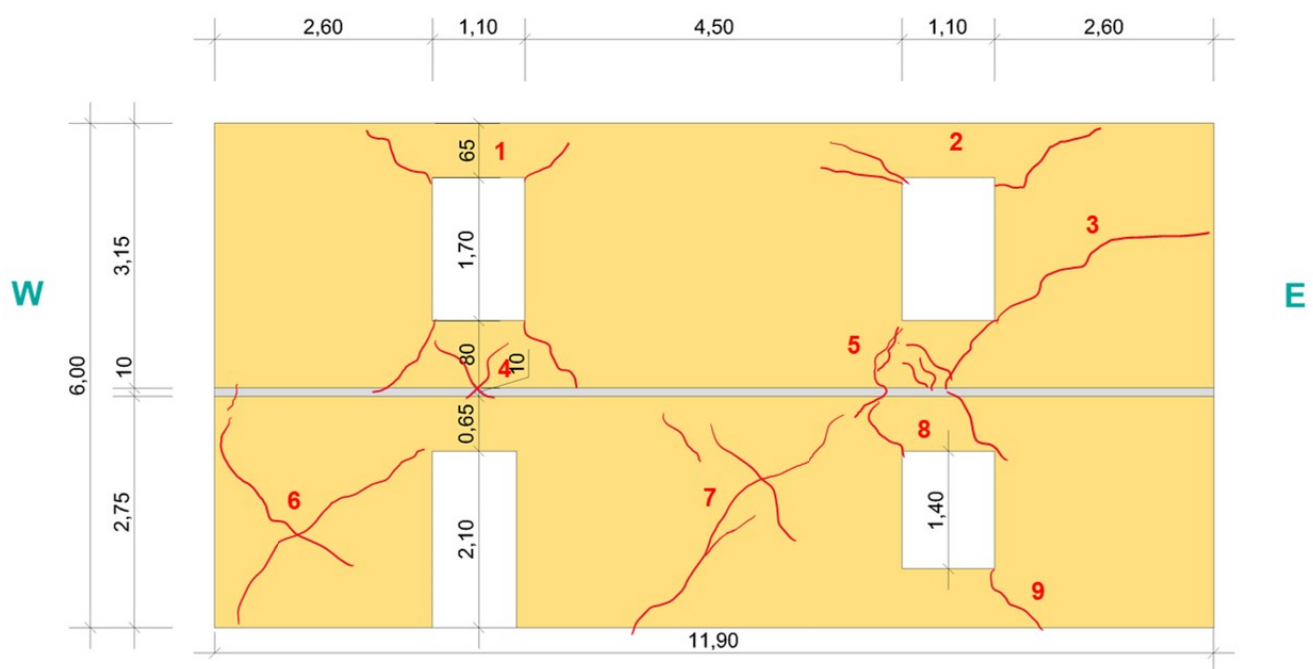
East Facade



South Facade



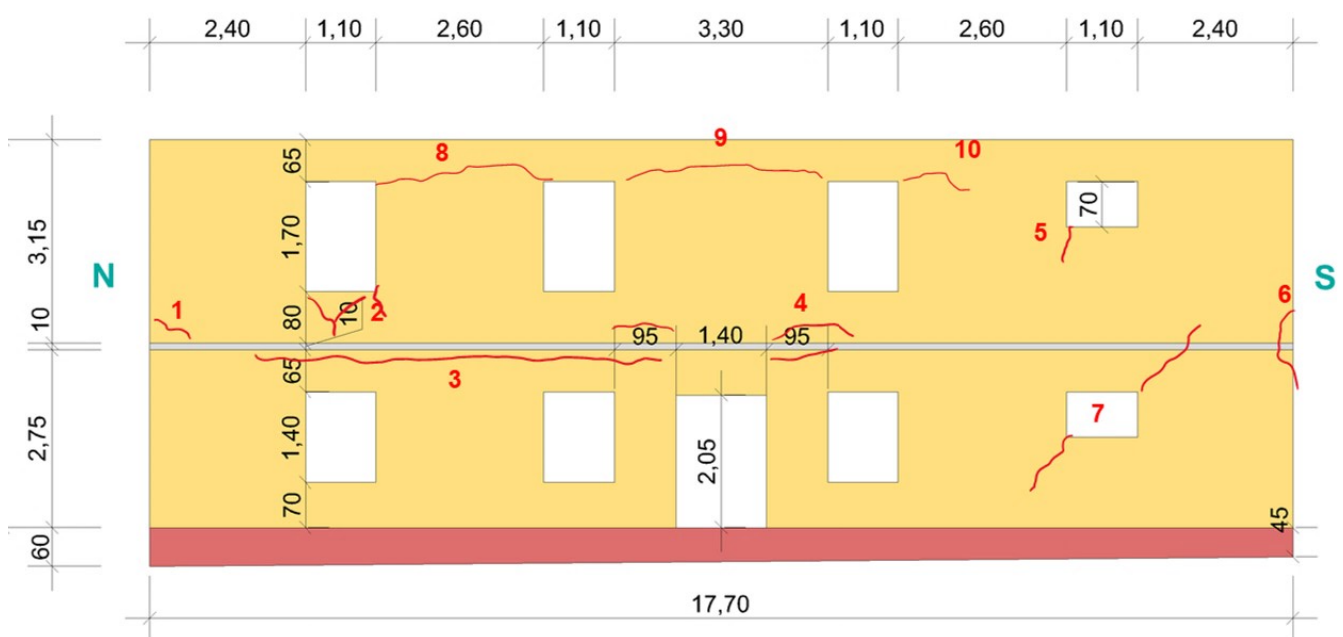
South Facade

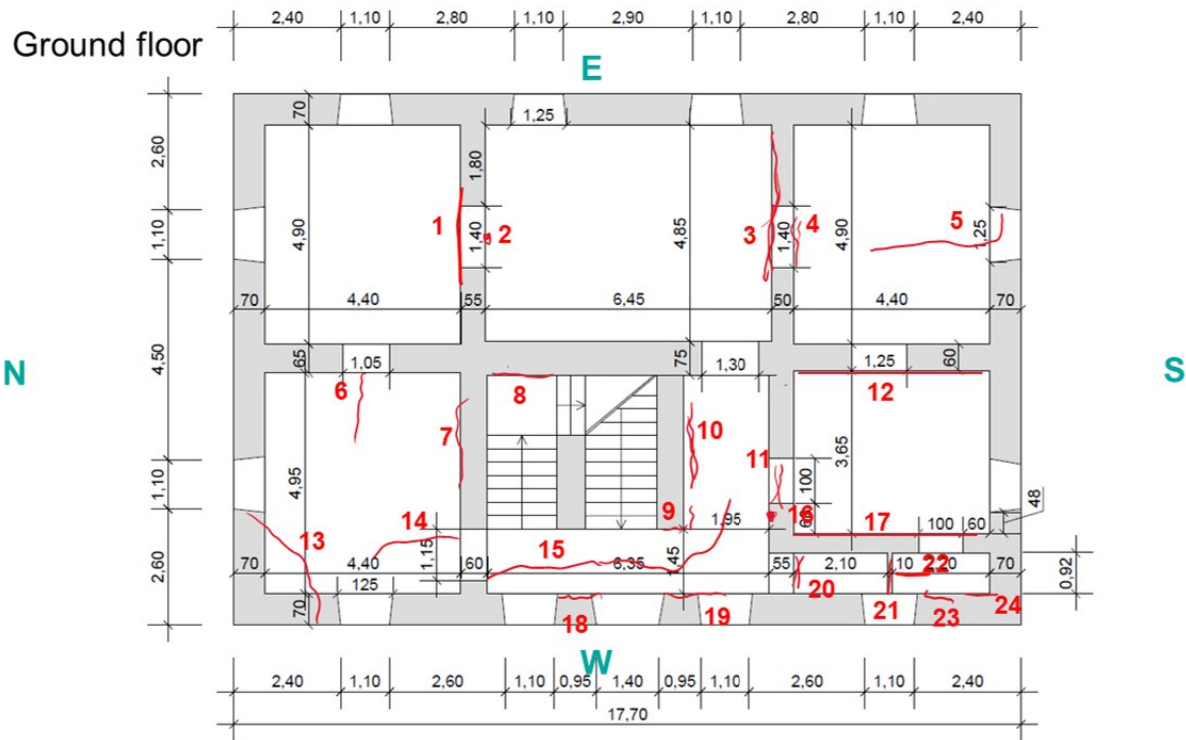


West Facade



West Facade





N° 1



N° 2



N° 3



N° 4



N° 5



N° 6



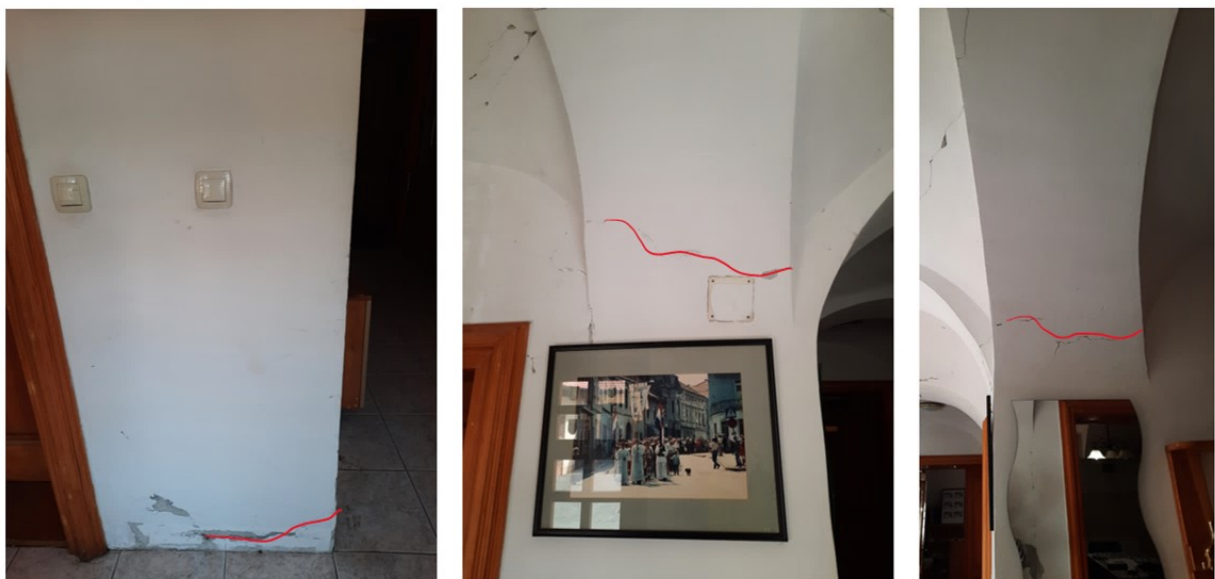
N° 7



N° 8



N° 9



N° 10



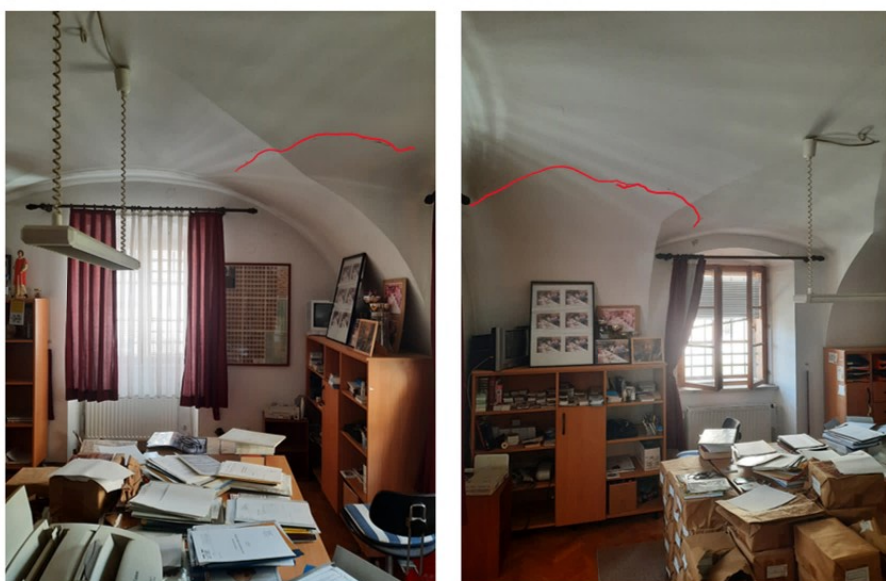
N° 11



N° 12



N° 13



N° 14



N° 15



N° 16



N° 17



N° 18



N° 19 Top



N° 19
Bottom



N° 20



N° 21



N° 22

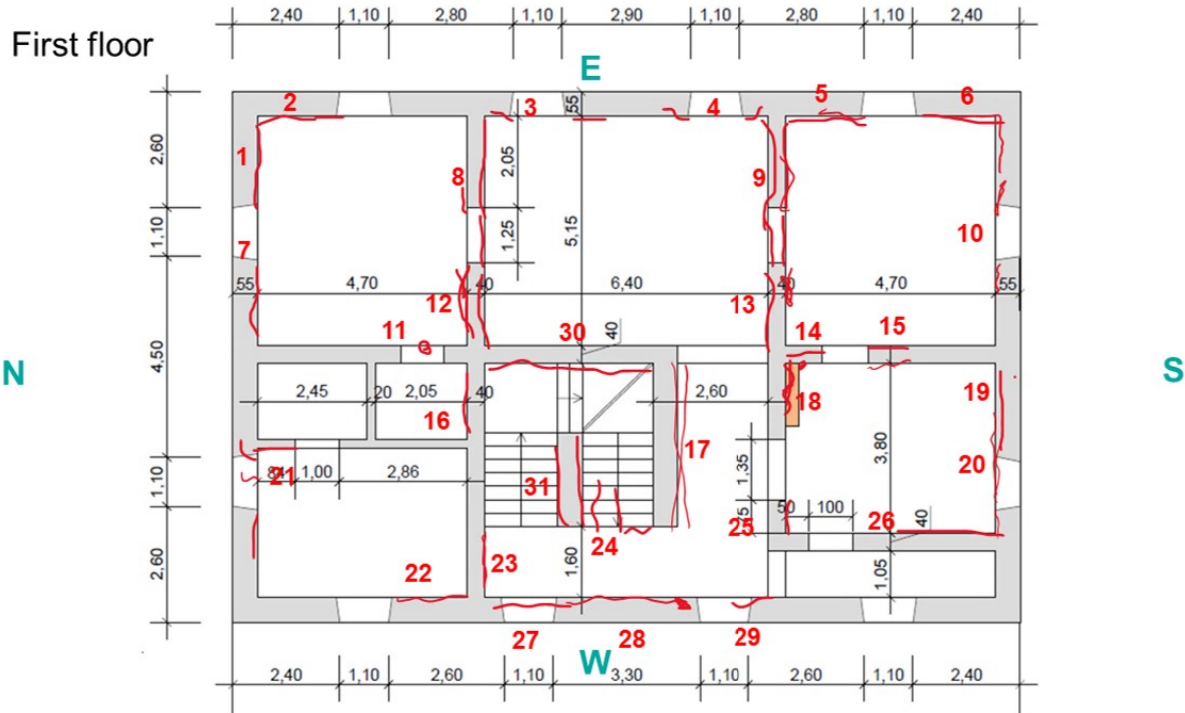


N° 23



N° 24





N° 1



N° 2



N° 3



N° 4



N° 5



N° 6



N° 7



N° 8



North side



South side

N° 9



North side



South side

N° 10



N° 11



N° 12



North side

N° 13

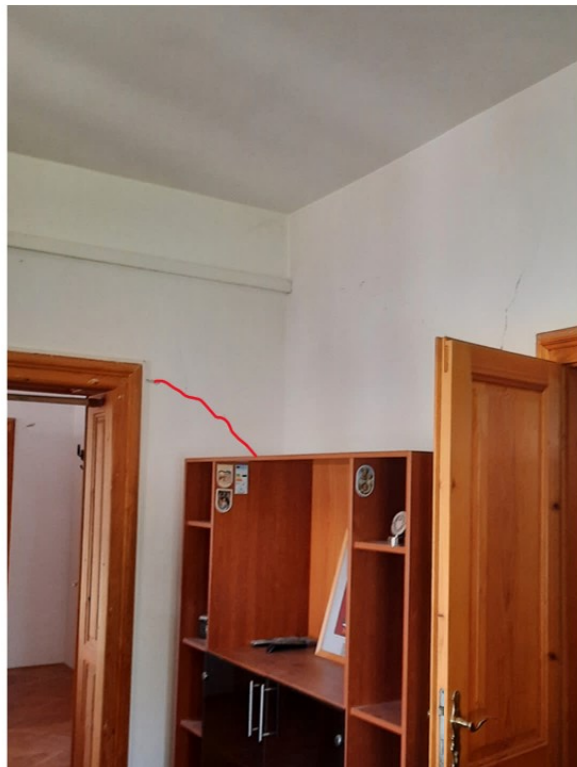


North side



South side

N° 14



N° 15



East side



West side

N° 16



North side



Sourth side

N° 17



N° 18



N° 19



N° 20



N° 21



N° 22



N° 23



N° 24



N° 25



N° 26



N° 27



N° 28



N° 29



N° 30



N° 31



North Facade



North Facade

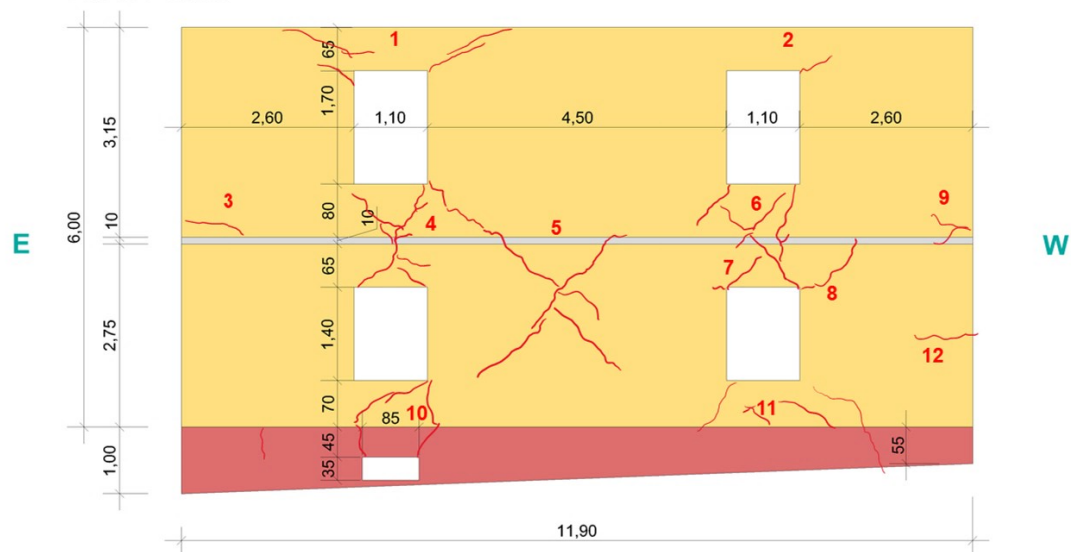


Table crack documentation

Damage inventory:

Author: Aline F.Bönzli
Date: 06.06.2023
Item: North Facade

Number	Description	Localization	Associated mechanism	Label	Connected cracks
1	Diagonal cracks	Starting from either top corner of the top east window	Cracking due to flexural mechanism with lifting off of the roof	NF1	FF7
2	Diagonal crack	Starting from the top west corner of the west top window and bottom east corner of top west window	Flexural crack due to force from south	NF2	FF21
3	Horizontal crack	Starting at the east extremity of the facade, at mid-height	Flexural crack from a global mechanism bending the whole facade or shear crack from a stress concentration in the corner of the building together with crack n° 11 on east facade	NF3	EF11
4	Diagonal spandrel cracks	Between the east side windows	Shear cracks / spandrel cracks	NF4	NF5 / NF6 / NF7
5	Diagonal cracks through the	Center of the facade	Shear crack in between the pier and node zone -> might be difficult to achieve in simulations?	NF5	NF4 / NF6 / NF7
6	Vertical/Diagonal cracks	Starting from the bottom corners of the top west window	Cracking due to a possible OOP mechanism in the spandrel below the top window. Due to the lower vertical load and no restraining slab on top this part of the wall is sensible to OOP bending.	NF6	NF4 / NF5 / NF7
7	Diagonal cracks	Above bottom west window	Shear crack in spandrel	NF7	NF4 / NF5 / NF6
8	Diagonal crack	Starting from the top west and bottom east corner of bottom west window	Flexural or shear crack due to seismic excitation towards the the east	NF8	
9	Horizontal crack	Starting at the west extremity of the facade, at mid-height	Flexural crack from a global mechanism bending the whole facade or shear crack from a stress concentration in the corner of the building together with crack n° 1 on west facade	NF9	WF1
10	Diagonal cracks	Between the corners of the bottom east window and the cellar window	Spandrel failure in shear	NF10	
11	Diagonal cracks	Starting from the bottom corners of the bottom west window	Shear cracks in spandrel	NF11	
12	Horizontal crack	Starting at the west extremity of the facade, at quarter-height (middle of bottom storey wall)	Corner stress concentration, might be in relation with ground floor crack 13 to cope with the out of plane failures GF14, GF15, GF18, GF19	NF12	GF14 / GF15 / GF18 / GF19 / WF3 / WF4

Damage inventory:

Author: Aline F.Bönzli
 Date: 06.06.2023
 Item: East Facade

Number	Description	Localization	Associated mechanism	Label	Connected cracks
1	Horizontal/Diagonal crack	Starting from top south corner of top south window	Flexural crack- in relation with n° 3 south facade	EF1	SF3
2	Diagonal cracks	Starting from all corners of the top most south window	Shear crack of seismic excitation in both directions	EF2	
3	Horizontal crack	Connecting the inner corners of the top middle windows	Crack from possible OOP failure or lift off of roof together with cracks 1,2,4,5?	EF3	EF1 / EF2 / EF4 / EF5
4	Diagonal crack	Starting from the top north corner of the top middle north window	Shear crack from seismic excitation from south (north)	EF4	
5	Horizontal crack	Starting at the north extremity of the facade, at the level of the top corner of the top window	Flexural crack from a global bending of the wall in relation with crack n° 1 on north facade??	EF5	NF1 / FF2 / FF1
6	Diagonal crack	Starting at the south extremity of the facade, at mid height	Stress concentration in corner?	EF6	??
7	Horizontal crack	Starting at the south extremity of the facade, at mid height of the bottom window	Corresponding to the outer hinge of the vault mechanism associated with crack n°5 in the ground floor vault	EF7	GF5
8	Diagonal crack	Between the middle south windows, starting at bottom north corner of top window and top north corner of bottom window	Shear crack in spandril between the windows	EF8	EF9 / EF10
9	Diagonal crack	Between the middle north windows, starting from top corners of bottom windows and bottom south corner of top window	Shear crack in spandril between the windows	EF9	EF8 / EF10
10	Diagonal crack	Between the north windows, starting from top south corner of bottom windows and bottom south corner of top window	Shear crack in spandril between the windows	EF10	EF8 / EF9
11	Horizontal crack	Starting at the north extremity of the facade, at mid-height	Flexural crack from a global mechanism bending the whole facade or shear crack from a stress concentration in the corner of the building together with crack n° 3 on east north	EF11	NF3
12	Vertical/Diagonal crack	Middle south window at bottom south corner and cellar window beneath it	Cracking due to combination of spandril shear crack and a possible OOP mechanism in the spandril below the bottom window. Due to the lower vertical load and no restraining slab on top this part of the wall is sensible to OOP bending.	EF12	
13	Vertical/Diagonal crack	Middle north bottom window, between bottom corners and top corners of cellar window beneath it	Cracking due to combination of spandril shear crack and a possible OOP mechanism in the spandril below the bottom window. Due to the lower vertical load and no restraining slab on top this part of the wall is sensible to OOP bending.	EF13	
14	Diagonal crack	Bottom north corner of bottom north window	Flexural crack from seismic excitation from north (south)	EF14	

Damage inventory:

Author: Aline F.Bönzli

Date: 06.06.2023

Item: South Facade

Number	Description	Localization	Associated mechanism	Label	Connected cracks
1	Diagonal cracks	Top and bottom corners of top west window	Flexural crack from seismic excitation in both directions, maybe in relation with global lift off mechanism of roof	SF1	SF1/2 / FF10/19/20
2	Diagonal cracks	Top corners of top east window	Flexural crack from seismic excitation in both directions, maybe in relation with global lift off mechanism of roof	SF2	SF1/2 / FF10/19/20
3	Horizontal /Diagonal crack	east (east) extremity of the facade ad mid height of the top storey connecting to the bottom east corner of the top east window	Flexural crack coming from global mechanism, in relation with crack n°1 on east facade	SF3	
4	Diagonal cracks	Spandrel cracks below top west window	Shear crack in spandril from seismic excitation in both directions, possibly in combination of OOP failure below the window.	SF4	
5	Diagonal cracks	Spandrel cracks below top east window	Shear crack in spandril/OOP failure mode below window -> in combination with crack n°8	SF5	SF8
6	Diagonal cracks	Crossed shear cracks in bottom west pier	Shear crack in pier from seismic excitation in both directions	SF6	
7	Diagonal cracks	Crossed shear cracks in bottom center pier	Shear crack in pier and node from seismic excitation in both directions -> could be difficult to reproduce in model	SF7	
8	Diagonal cracks	Spandrel cracks above bottom east window	Shear crack /maybe in relation with an OOP mechanism related to crack n° 5?	SF8	SF5
9	Diagonal cracks	Starting from bottom east corner of bottom east window	Flexural/shear crack due to seismic excitation to the east (west)	SF9	

Damage inventory:

Author: Aline F.Bönzli

Date: 06.06.2023

Item: West Facade

Number	Description	Localization	Associated mechanism	Label	Connected cracks
1	Horizontal crack	Starting at the north extremity of the facade, at mid-height	Flexural crack of a global bending of the facade and/or a stress concentration in the corner, causin sliding between the bricks ->in relation with n°8 of the north facade	WF1	NF3
2	Diagonal crack	Spandrel crack between the bottom of the north most top window and the top of the north most bottom windwow	Shear crack in spandril zone in combination with eventual OOP failure of wall below window moving out of its plane due to lower vertical load and absence od restraining force	WF2	
3	Horizontal crack	Ad midheight of the facade above the bottom south two windows	OOP Failure from the vault pushing outside	WF3	WF 4, WF 8, WF 9, WF 10, GF 9, GF 13, GF 14, GF 15, GF 17, GF 22
4	Horizontal crack	At mid height of the facade in the middle above the door and the bottom window next to it	OOP Failure from the vault pushing outside -> continuation of crack n°3	WF4	WF 3, WF 8, WF 9, WF 10, GF 9, GF 13, GF 14, GF 15, GF 17, GF 22
5	Vertical crack	Starting at bottom north corner of top south most window	???	WF5	
6	Vertical / Diagonal crack	Starting at the south extremity of the facade, at mid-height	???	WF6	
7	Diagonal crack	Starting at the top south corner and at the bottom north corner of the bottom south most window	Shear crack from a seismic excitation to the north (norht)	WF7	
8	Horizontal crack	Connecting the tom corners of the two top north windows	Flexural crack from a global lift off mechanism of the roof? Mayve also from and OOP failure of the west facade turning about its middle axis being pushed out by the vaulting system in the ground floor	WF8	WF 3, WF 4, WF 9, WF 10, GF 9, GF 13, GF 14, GF 15, GF 17, GF 22
9	Horizontal crack	Connecting the tom corners of the two middle top windows	Flexural crack from a global lift off mechanism of the roof? Mayve also from and OOP failure of the west facade turning about its middle axis being pushed out by the vaulting system in the ground floor	WF9	WF 3, WF 4, WF 8, WF 10, GF 9, GF 13, GF 14, GF 15, GF 17, GF 22
10	Horizontal crack	On the top south corner of the top middle south window	Flexural crack from a global lift off mechanism of the roof? Mayve also from and OOP failure of the west facade turning about its middle axis being pushed out by the vaulting system in the ground floor	WF10	WF 3, WF 4, WF 8, WF 9, GF 9, GF 13, GF 14, GF 15, GF 17, GF 22

Damage inventory:

Author: Aline F.Bönzli
Date: 06.06.2023
Item: Ground floor

Number	Description	Localization	Associated mechanism	Label	Connected cracks
1	Vertical and diagonal cracks	Above north-east door connecting the eastern smaller room to the big room in the east	Shear cracks, maybe OOP failure of the wall beneath the vault	GF1	GF1/2/3/4/5/12, EF3/4/7, FF3/4
2	Vertical crack	Above north-east door connecting the big room in the east to the eastern smaller room, on the other side of the wall as crack n°1	Another vault mechanism that is not visible forming in the vault of the big east room	GF2	GF1/2/3/4/5/12, EF3/4/7, FF3/4
3	Diagonal crack crossing the	On the wall between the big eastern room and the smaller south eastern room. Starting at the bottom left corner and ending in the middle above the door.	Shear failure of the wall stabilizing the vault in the big room in the east.	GF3	GF1/2/3/4/5/12, EF3/4/7, FF3/4
4	Diagonal crack (partly vertical)	On the wall between the smaller south-eastern room and the big eastern room, above the door on the other side of wall as crack n°3	Shear failure of the wall stabilizing the vault in the big room in the east. Maybe connected to an OOP failure of the wall above the door.	GF4	GF1/2/3/4/5/12, EF3/4/7, FF3/4
5	Longitudinal vault crack	Starting from the south window of the sout-eastern room and continuing in the longitudinal direction of the vault	OOP failure of the walls connected to the vault creating the first hinge in the middle of the vault. Due to seismic excitation in the east-west direction. Outer hinge crack can be associated to n°7 on east facade?	GF5	GF1/2/3/4/5/12, EF3/4/7, FF3/4
6	Longitudinal vault crack	Starting above the east door connecting the norht-west room to the north-east room	OOP failure of the walls connected to the vault creating the first hinge in the middle of the vault. Due to seismic excitation in the north-south direction. Outside hinge forming on the wall to the kitchen associated to crack n°12	GF6	GF13
7	Vertical /diagonal crack	On the south wall of the north-west room (between room and staircase).	Shear cracks taking seismic excitation in the east west direction	GF7	GF10
8	Diagonal crack	On the back wall of the staircase	Shear cracks taking seismic excitation in the north-south direction	GF8	
9	Horizontal cracks	Around the top and bottom of inside column/pier in the corner of the staircase leading down.	Cracks can be associated to the vault cracks n°15, constituting the hinges of the OOP movement of the support of the vaults. Seismic excitation in all directions	GF9	WF 3/4/8/ 9/10, GF 9/13/14/15/17/18/19/ 22, FF22/27/28/29
10	Diagonal cracks	On the south wall between staircase and hallway	Mirrored cracks, symmetric to n°7 coming from seismic excitation in the east-west direction. Cracks going through the entire wall, visible from the stairs as well as from the hall way.	GF10	
11	Diagonal cracks	Above door leading to the kitchen.	Spandril cracking from east-west seismic excitation	GF11	
12	Horizontal cracks	On the interface of east wall of the kitchen and the vaulted ceiling	Cracking coming from vault failure associated to crack n°5 forming the outside hinge or coming from differential movement between wall and vault	GF12	GF1/2/3/4/5/12, EF3/4/7, FF3/4
13	Horizontal crack	Around vault corner in north west corner of the north-west room	Could be associated to crack n°12 on north facade->out of compatibility of the global OOP failure of the West facade	GF13	WF 3/4/8/ 9/10, GF 9/13/14/15/17/18/19/ 22, FF22/27/28/29
14	Longitudinal vault crack	Crack at middle of local door vault of the sout entrance to the north-west room	Continuation of crack n° 15 corresponding to a vault failure leading to and OOP mechanism of the west facade, associated with crack n°3 on the west facade forming the outside hinge	GF14	WF 3/4/8/ 9/10, GF 9/13/14/15/17/18/19/ 22, FF22/27/28/29
15	Longitudinal vault crack	Crack at mid span of vault in the entrance in the north-south direction of the building	Continuation of crack n° 14 corresponding to a vault failure leading to and OOP mechanism of the west facade, associated with crack n°3 on the west facade forming the outside hinge	GF15	WF 3/4/8/ 9/10, GF 9/13/14/15/17/18/19/ 22, FF22/27/28/29
16	Vertical crack	Crack on the right side of the north entry to the kitchen	Differential movement of the walls?	GF16	
17	Horizontal crack	On the interface of west wall of the kitchen and the vaulted ceiling	Cracking coming from vault failure associated to crack n°22 forming the outside hinge or coming from differential movement between wall and vault	GF17	WF 3/4/8/ 9/10, GF 9/13/14/15/17/18/19/ 22, FF22/27/28/29
18	Horizontal crack	On the north side of the main entrance, below the end of an arch stabilizing the vaulted system in the hallway	Could be associated to crack n°15 from crushing on the inside of the low hinge of the vault mechanism, similar as crack n°19	GF18	WF 3/4/8/ 9/10, GF 9/13/14/15/17/18/19/ 22, FF22/27/28/29
19 top	Horizontal crack	On the south side of the main entrance, below the end of an arch stabilizing the vaulted system in the hallway	Could be associated to crack n°15 from crushing on the inside of the low hinge of the vault mechanism, similar as crack n°18	GF19	WF 3/4/8/ 9/10, GF 9/13/14/15/17/18/19/ 22, FF22/27/28/29
19 bottom	Horizontal & diagonal cracks	On the pier on the south side of the main entrance	1. Horizontal crack at the bottom of the pier corresponding from a felxural/OOP failure in relation with the vault mechanism n°15 pushing the top of the wall out creating a hinge at the inside of the pier base 2. Crossed diagonal crack corresponding to a shear failure of the pier in the middle	GF20	
20	Diagonal cracks	Above door leading to the toilet.	Spandril cracking from east-west seismic excitation	GF21	
21	Horizontal crack	At mid height on the wall separating the toilet from the storage room	Shear mechanism creating sliding between the upper and the lower wall parts?	GF22	WF 3/4/8/ 9/10, GF 9/13/14/15/17/18/19/ 22, FF22/27/28/29
22	Longitudinal vault crack	On the vault of the storage room starting at the wall against the toilet	Vault mechanism connected to crack n°17 in the kitchen forming the outside hinge.	GF23	
23	Diagonal crack	Starting from the south corner of the window in the storage room.	Associated to shear crack around the window in n° 7 of the west facade cracks	GF24	
24	Horizontal crack	In the south-west corner of the storage space ->associated to local vault failure n°22	??	GF25	

Damage inventory:

Author: Aline F.Bönzli
Date: 06.06.2023
Item: First Floor

Number	Description	Localization	Associated mechanism	Label	Connected cracks
1	Horizontal crack	Starting at the east upper corner of the east window on the north facade/ crack 1 on north facade	Flexural cracking from a seismic excitation in the east-west direction, or uplifting roof from a seismic excitation in the north-south direction. Or maybe even outward pushing of the purlin roof beams.	FF1	NF1
2	Horizontal crack	Starting at north corner of north window on east facade / crack 5 on east facade	Flexural cracking from a seismic excitation in the north-south direction, or uplifting roof from a seismic excitation in the east-west direction. Possible hinge for global OOP failure starting with the outpush of the vault in the ground-floor. Or maybe even outward pushing of the purlin roof beams.	FF2	EF5
3	Horizontal cracks	Starting on either top corner of the middle-north window on the east facade / cracks 3 and 4 of east facade	Uplifting of the rigid roof structure due to a seismic excitation in the east west direction or pushing outwards of the purlin roof beams. Possible hinge for global OOP failure starting with the outpush of the vault in the ground-floor.	FF3	GF1/2/3/4/5/12, EF3/4/7, FF3/4
4	Horizontal cracks	Starting on either top corner of the middle-south window on the east facade / crack 3 east facade	Uplifting of the rigid roof structure due to a seismic excitation in the east west direction or pushing outwards of the purlin roof beams. Possible hinge for global OOP failure starting with the outpush of the vault in the ground-floor.	FF4	GF1/2/3/4/5/12, EF3/4/7, FF3/4
5	Horizontal crack	Starting from top north corner of south window on east facade/related to crack 2 on east facade	Uplifting of the rigid roof structure due to a seismic excitation in the east west direction or pushing outwards of the purlin roof beams. Possible hinge for global OOP failure starting with the outpush of the vault in the ground-floor.	FF5	EF2
6	Horizontal crack	Starting from top south corner of south window on east facade and continuing to the sout facade/related to crack 1 on east facade and 3 on south facade	Shear crack from east-west excitation?	FF6	EF1 / SF3
7	Horizontal crack	Starting at the upper corners of the east window on the north facade/ crack 1 on north facade	Flexural cracking from a seismic excitation in the east-west direction, or uplifting roof from a seismic excitation in the north-south direction. Or maybe even outward pushing of the purlin roof beams.	FF7	NF1
8	Diagonal cracks	On the east side of the door connecting the big central eastern room to the north east room	Shear and flexural cracks from a seismic excitation in the east-west direction, similar to crack 9,12 and 13	FF8	FF8/9/12/13
9	Diagonal cracks	On the east side of the door connecting the big central eastern room to the south east room	Shear and flexural cracks from a seismic excitation in the east-west direction, similar to crack 8, 12 and 13	FF9	FF8/9/12/13
10	Diagonal/horizontal cracks	On either side of the window on the south facade of the room in the south east/ crack 2 south facade	Flexural cracking from a seismic excitation in the east-west direction, or uplifting roof from a seismic excitation in the north-south direction. Or maybe even outward pushing of the purlin roof beams.	FF10	SF1/2 / FF10/19/20
11	Vertical crack	On the north upper corner of the door to the bathroom of the north east room	??	FF11	
12	Diagonal cracks	On the west side of the door connecting the big central eastern room to the north east room	Shear and flexural cracks from a seismic excitation in the east-west direction, similar to crack 8, 9 and 13	FF12	FF8/9/12/13
13	Diagonal/horizontal cracks	On the west side of the door connecting the big central eastern room to the south east room	Shear and flexural cracks from a seismic excitation in the east-west direction, similar to crack 8, 9 and 12	FF13	FF8/9/12/13
14	Diagonal cracks	On the north side of the door connecting the south east to the south west room	Shear crack from east-west excitation?	FF14	FF15
15	Diagonal cracks	On the south side of the door connecting the south east to the south west room	Shear crack from east-west excitation?	FF15	FF14
16	Diagonal cracks	On the north wall of the staircase	Shear cracks due to a seismic excitation in the east-west direction, together with cracks 17	FF16	FF17
17	Diagonal cracks	On the south wall of the staircase	Shear cracks due to a seismic excitation in the east-west direction, together with cracks 16	FF17	FF16
18	Diagonal/vertical cracks	On the east side of the north access door of the south-west room	??	FF18	
19	Horizontal crack	On the east side of the window of the sout west room (south facade)/crack 1 south facade?	Flexural cracking from a seismic excitation in the east-west direction, or uplifting roof from a seismic excitation in the north-south direction. Or maybe even outward pushing of the purlin roof beams.	FF19	SF1/2 / FF10/19/20
20	Horizontal crack	On either side of the window on the south facade of the room in the south west/ crack 1 south facade	Flexural cracking from a seismic excitation in the east-west direction, or uplifting roof from a seismic excitation in the north-south direction. Or maybe even outward pushing of the purlin roof beams.	FF20	SF1/2 / FF10/19/20
21	Diagonal/vertical cracks	around window of the north west room on the north facade/ crack 2 north facade	Flexural cracking from a seismic excitation in the east-west direction, or uplifting roof from a seismic excitation in the north-south direction.	FF21	
22	Horizontal crack	Starting from south corner of west window of north west room	Uplifting of the rigid roof structure due to a seismic excitation in the east west direction or pushing outwards of the purlin roof beams. Possible hinge for global OOP failure starting with the outpush of the vault in the ground-floor.	FF22	FF22/27/28/29
23	Horizontal crack	Above door to north west room	Flexural cracking to accomodate movements: uplift of of roof structure or OOP failure of west facade starting from out push of the vaults in the ground floor	FF23	
24	Horizontal crack	At middle of vault of the stars coming up to the first floor	Local failure from staircase vault pushing outward and creating the first hinge in the middle	FF24	
25	Diagonal/vertical crack	On the west side of the north door to the south-west room	Maybe shear cracking due to seismic excitation in the east-west direction	FF25	
26	Horizontal/diagonal crack	on west wall of south west room starting on east corner of the door to the bathroom	Flexural cracking from a seismic excitation in the north-south direction, or uplifting roof from a seismic excitation in the east-west direction.	FF26	
27	Horizontal cracks	On either side of the middle-north window on the west facade	Uplifting of the rigid roof structure due to a seismic excitation in the east west direction or pushing outwards of the purlin roof beams. Possible hinge for global OOP failure starting with the outpush of the vault in the ground-floor.	FF27	FF22 / FF28 / FF29 / WF8 / WF9 / WF10
28	Horizontal crack	Connecting cracks 27 and 29	Uplifting of the rigid roof structure due to a seismic excitation in the east west direction or pushing outwards of the purlin roof beams. Possible hinge for global OOP failure starting with the outpush of the vault in the ground-floor.	FF28	FF22 / FF27 / FF29 / WF8 / WF9 / WF10
29	Horizontal crack	On either side of the middle-south window on the west facade	Uplifting of the rigid roof structure due to a seismic excitation in the east west direction or pushing outwards of the purlin roof beams. Possible hinge for global OOP failure starting with the outpush of the vault in the ground-floor.	FF29	FF22 / FF27 / FF28 / WF8 / WF9 / WF10
30	Horizontal crack	On the east wall of the staircase	Flexural crack or uplifting of the roof, but both seem improbable...	FF30	
31	Horizontal/diagonal crack	On the middle wall of the staircase	Shear/flexural cracking due to seismic excitation in the east-west direction	FF31	

E. Meeting with the project engineers

This is a transcript of a meeting with the two project engineers who are currently working on the retrofitting of the Parish House. **Name:** Hrvoje & Martina Vujasinović, INTRADOS-PROJEKT d.o.o., Zagreb, Croatia [9]

The interview was led by Aline Bönzli in English with translations to Croatian by Dr Igor Tomić, a post-doctoral researcher at the EESD Laboratory of EPFL.

Question: Do you have any knowledge of the materials used for construction? Did you perform tests to get some material characteristics?

Answer: No material tests were performed on the material of the Parish house. However, by opening parts of the façade, it could be confirmed that the whole walls are made out of brick masonry. Question: What do you know about the vaults that form the support system for the slab above the ground floor?

Answer: The vaults are formed by one layer of bricks, meaning they have a thickness of 15 cm. The volume between the curved outer surface of the vaults, the walls and the slab supporting the living surface of the above floor has been filled with some sort of gravel/sand with a density of 14 kN per m³. The top surface is formed by timber planks supporting the parquet flooring.

Question: The slab above the first floor had been exposed after the damages of the homeland war in the late 20th century. There have been some renovation and remodelling works on that floor and the roof of the building. What do you know about the structural system and materials used?

Answer: Floor above first floor: The structural system of the slab above the first floor is a Fert system. The slab is made out of concrete beams with clay bricks in between (see figure below).

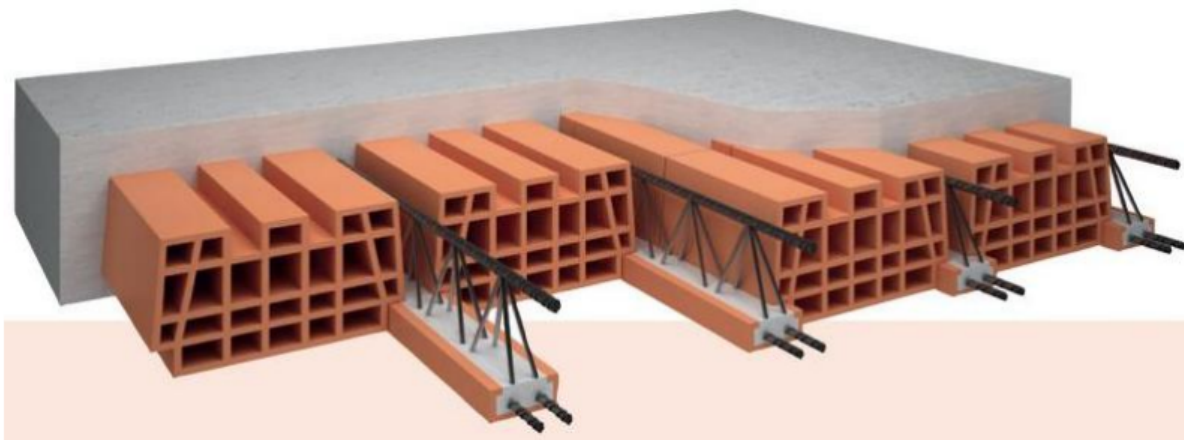


Figure E.1: Fert slab [46]

Those slabs support the load between two parallel walls and can be modelled by an equivalent concrete slab of thickness 10-12 cm. It has also been found that a reinforced concrete ring beam was added to the building during the remodelling process. The ring beam goes around the whole building and is well connected to the concrete beams of the Fert slab. This system adds stiffness to the whole building. Roof: The roof was completely reconstructed with timber elements. The roof structure is supported by the ring beam as well as by two columns bringing the load down to the walls of the first floor.

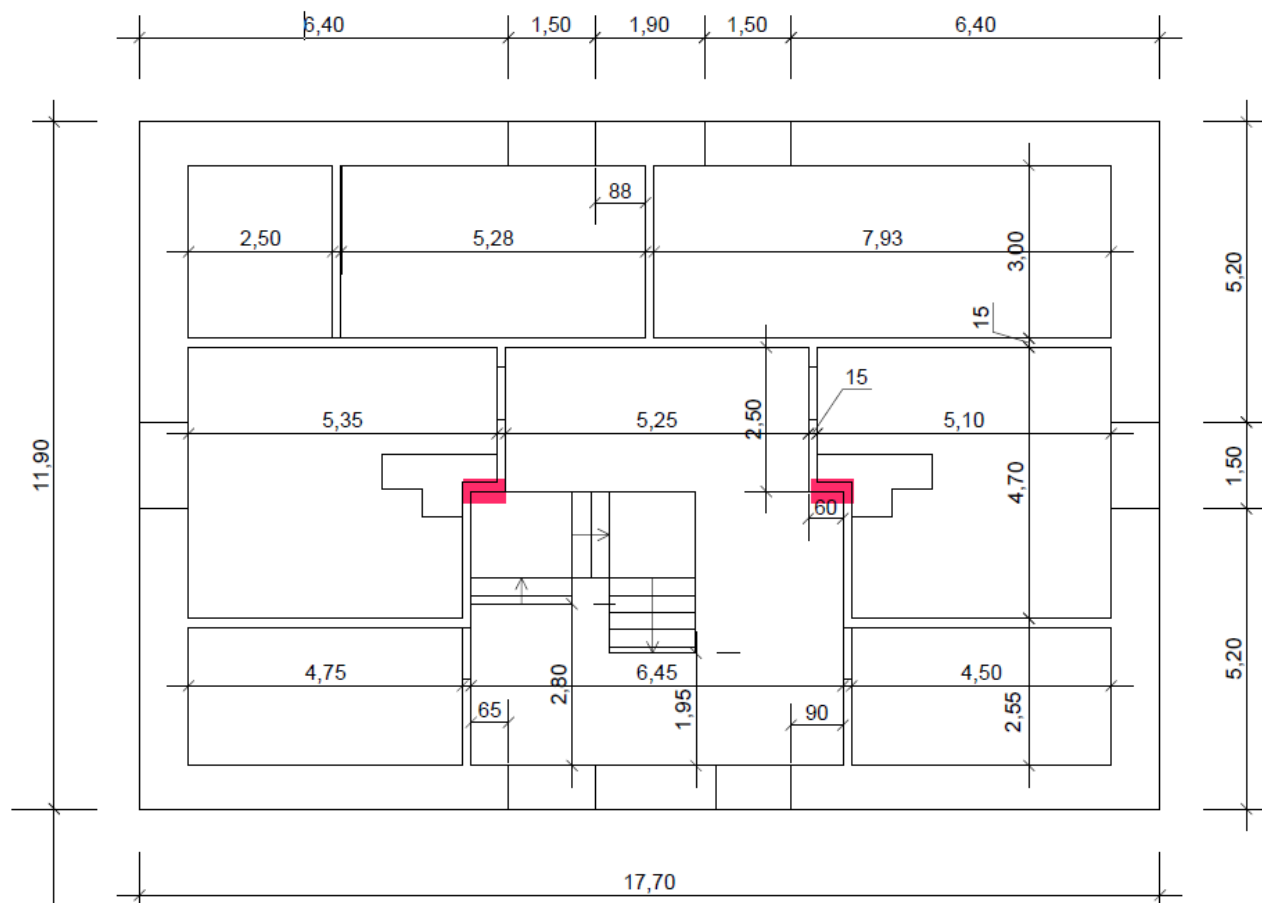
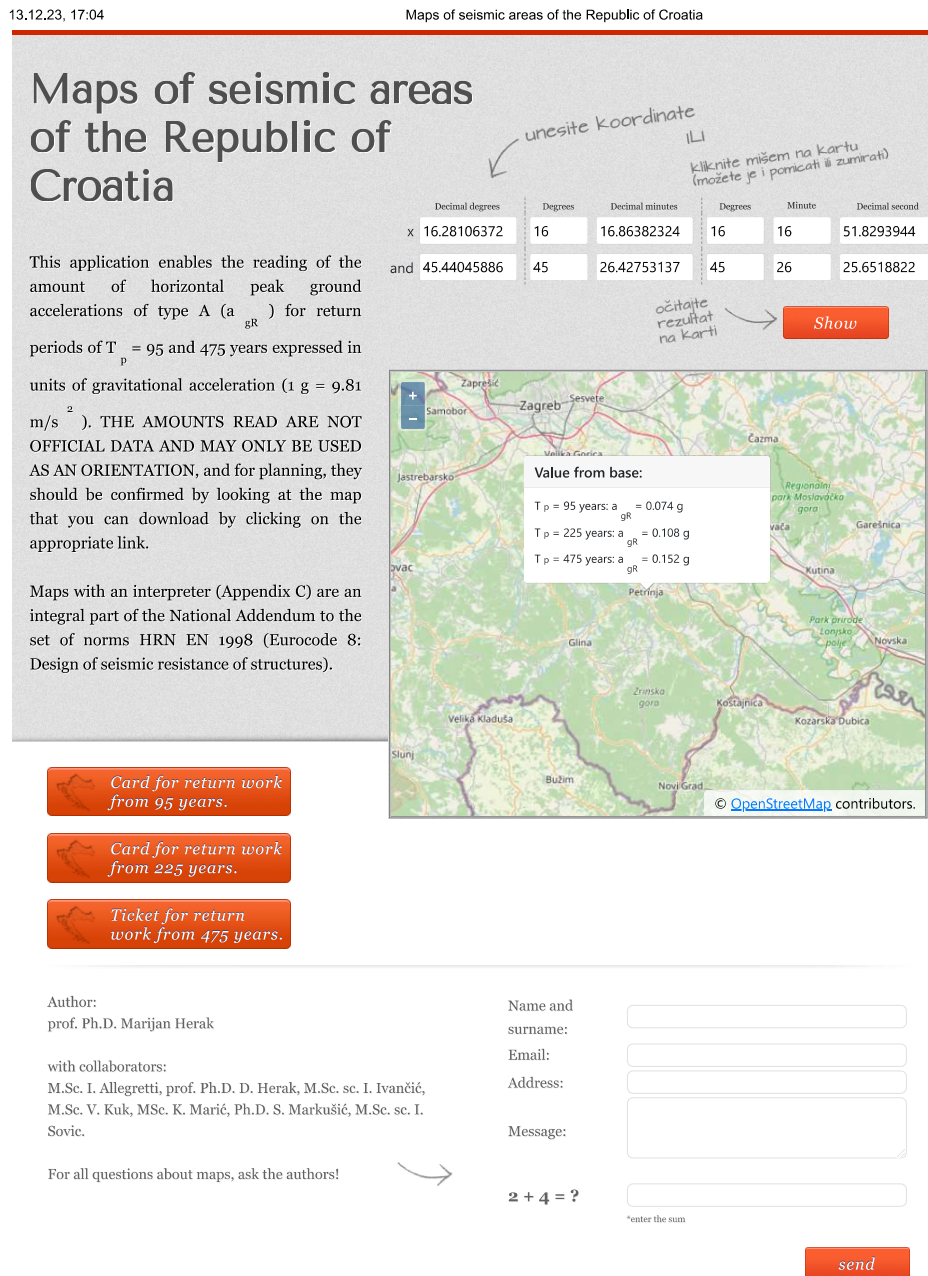


Figure E.2: Plan of the second floor with columns supporting the Roof structure

F. Reference peak ground acceleration Petrinja



seizkarta.gfz.hr/hazmap/karta.php

1/2

Figure F.1: Reference peak ground acceleration (PGA) of Petrinja [29]

G. Geological map Sisak region, Croatia

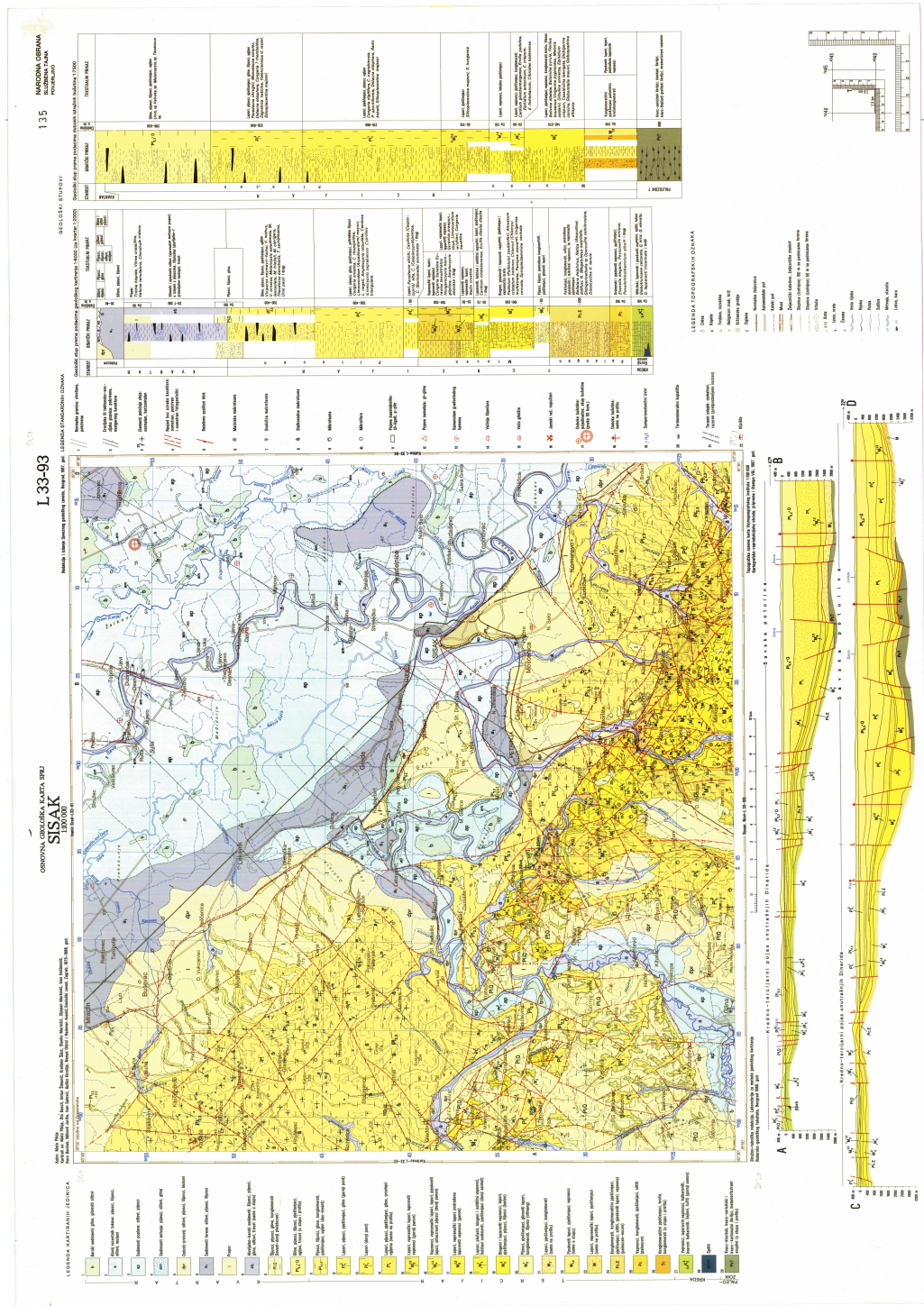


Figure G.1: Geological map Sisak [30]

H. Calculations, codes and excel files

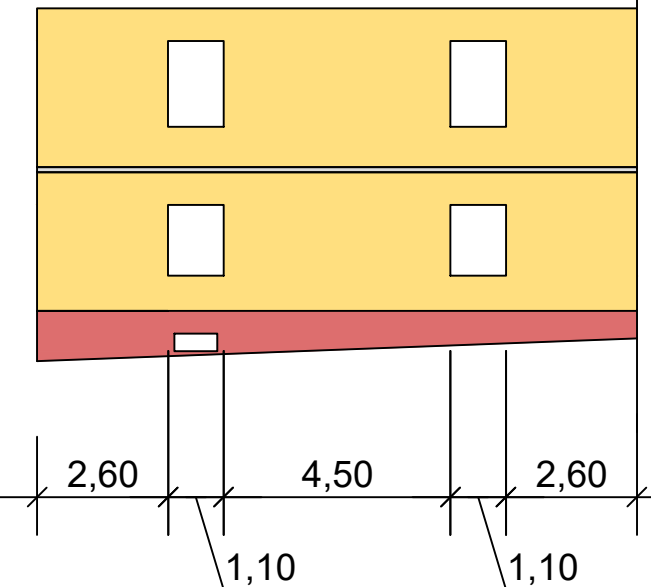
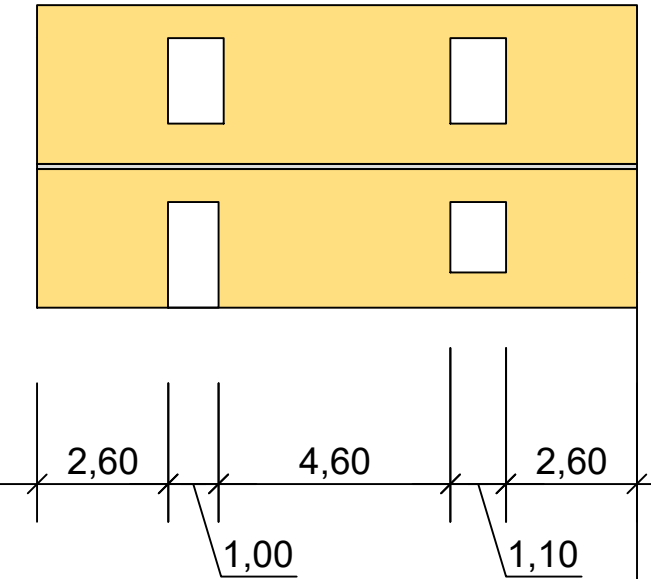
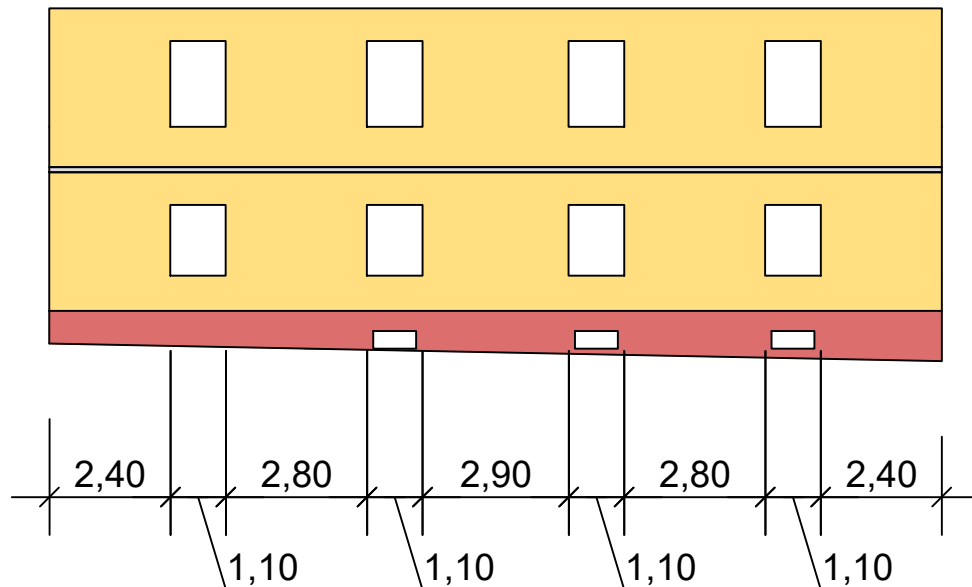
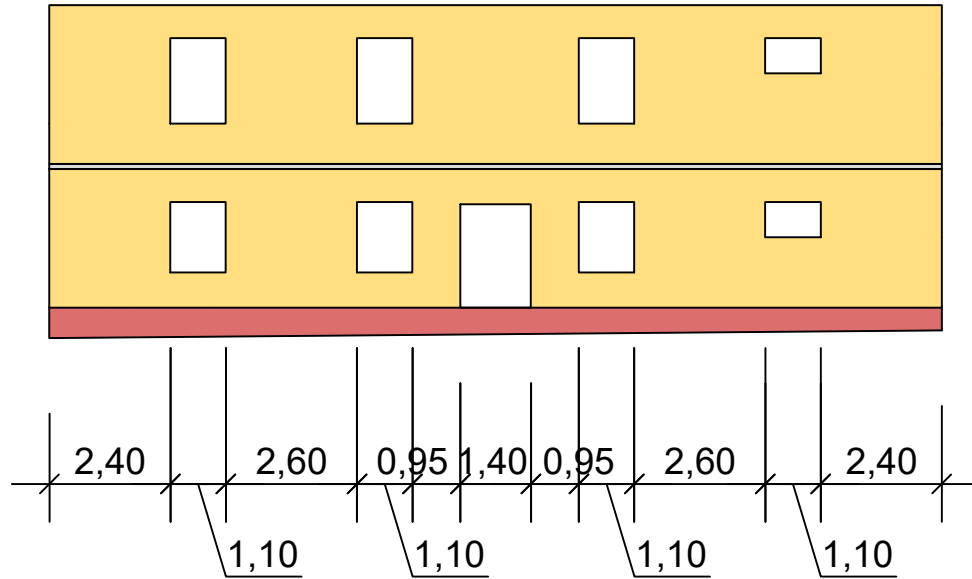
The content of this appendix can be found on the dedicated GitHub repository under the following link:

<https://github.com/boenzli/Master-Thesis-2023-24/wiki>

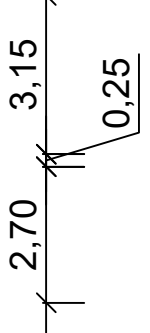
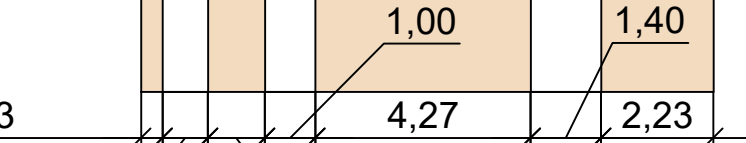
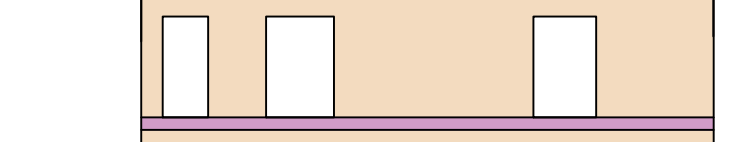
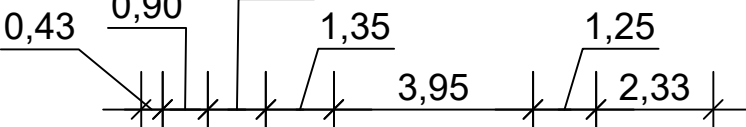
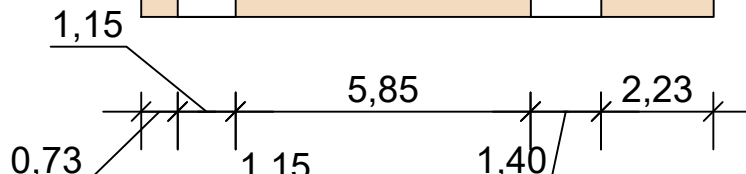
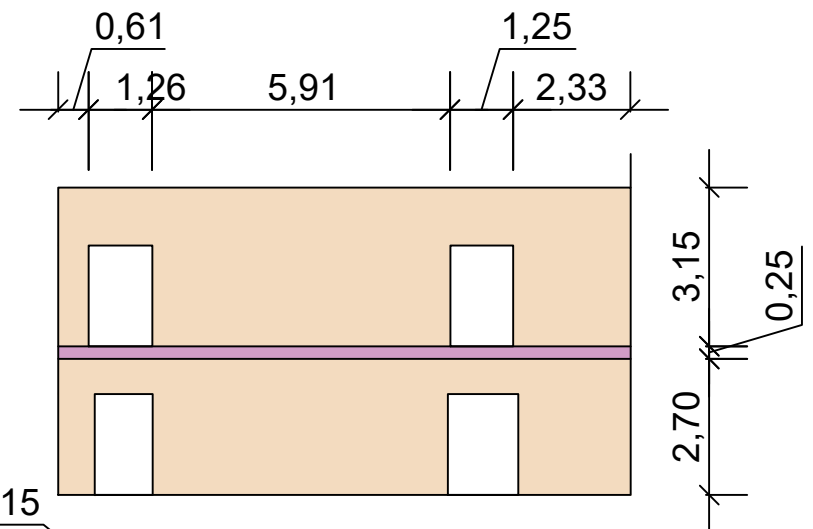
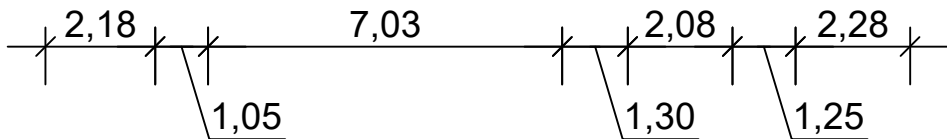
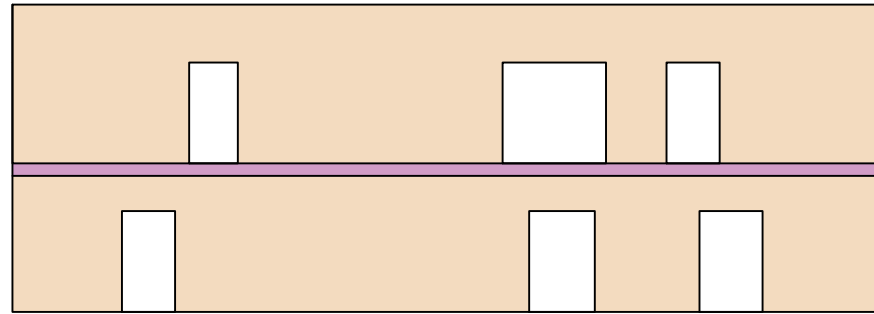
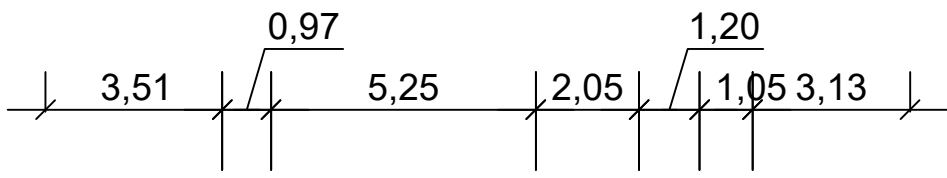
The content of the GitHub contains the following elements:

- Jupyter Notebooks/scripts for the out-of-plane calculations in the initial state
- All calculations related to the pushover curve
- Derivation of modelling parameters for the OpenSees model in the initial and the retrofitted state
- The necessary files to run the OpenSees model of the initial state
- Design of the steel ties
- Jupyter Notebooks/scripts for the out-of-plane calculations in the retrofitted state
- The necessary files to run the OpenSees model of the retrofitted state

I. Modelling



Facade geometry	Author :	Aline Bönzli
EESD All Facades	Date :	10.10.2023
	Scale :	1:150



Inside geometry

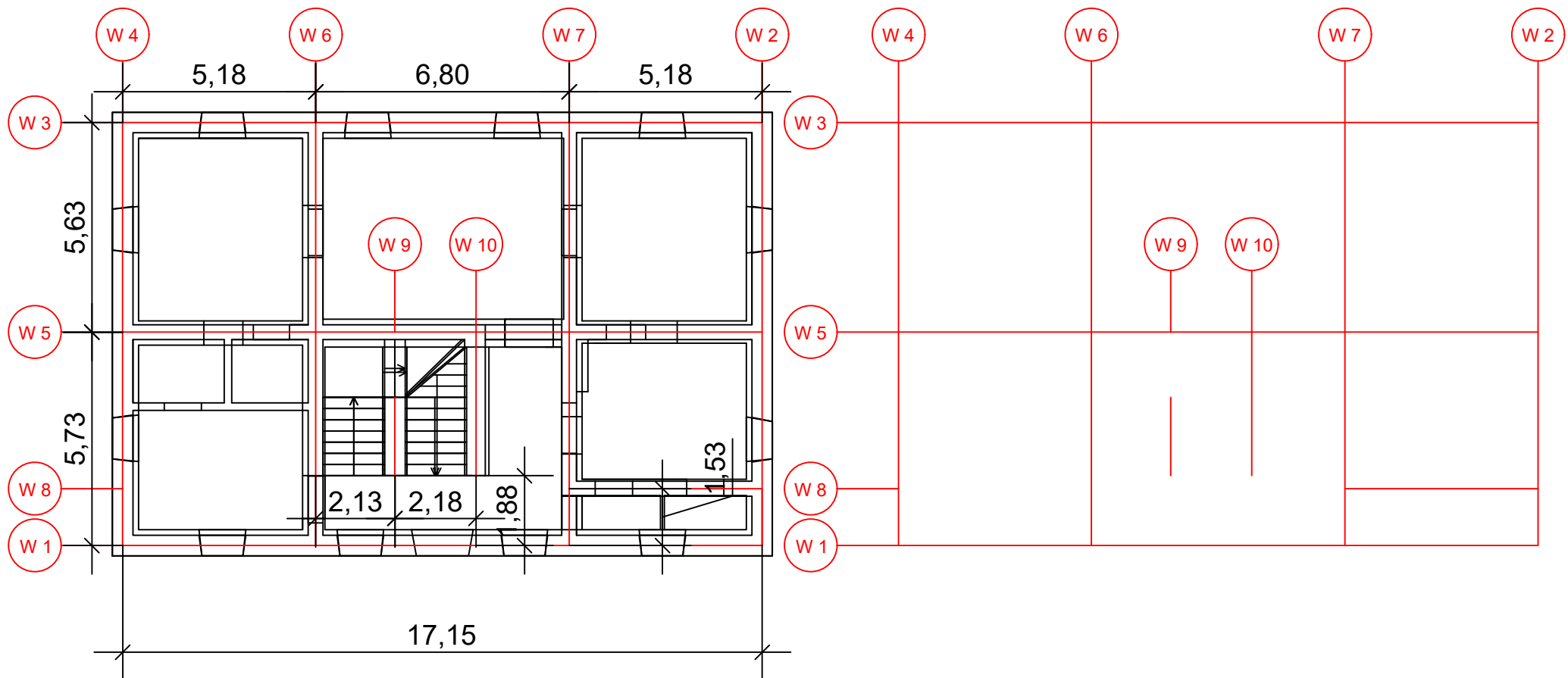
Author : Aline Bönzli

EESD

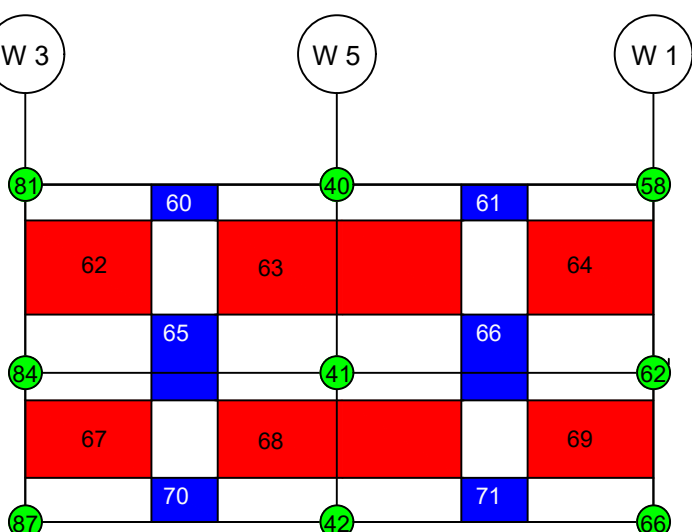
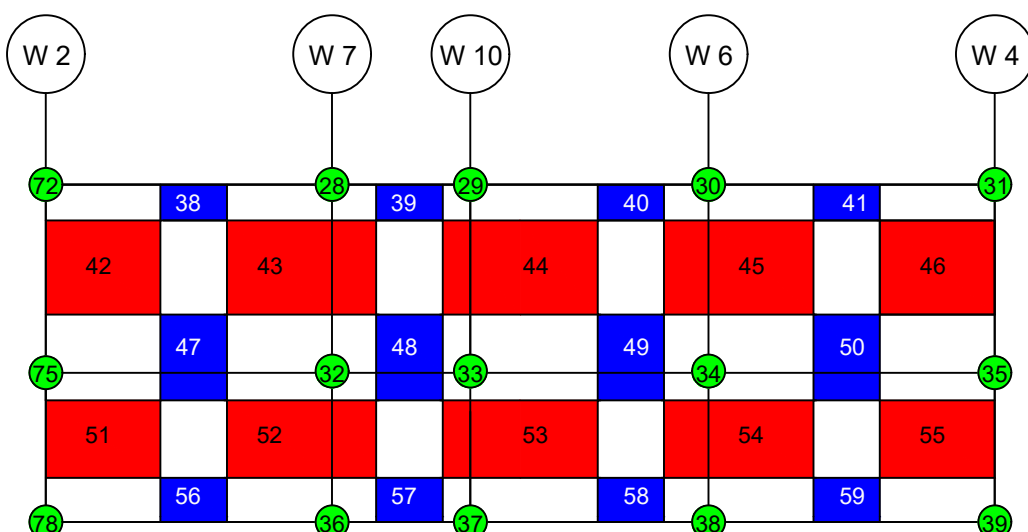
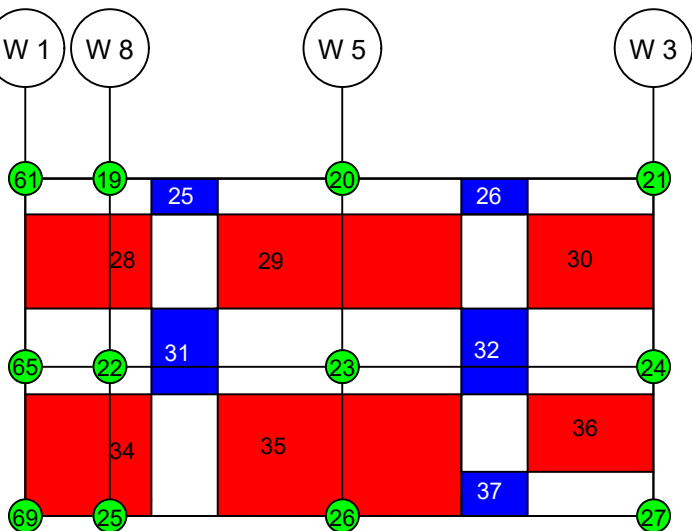
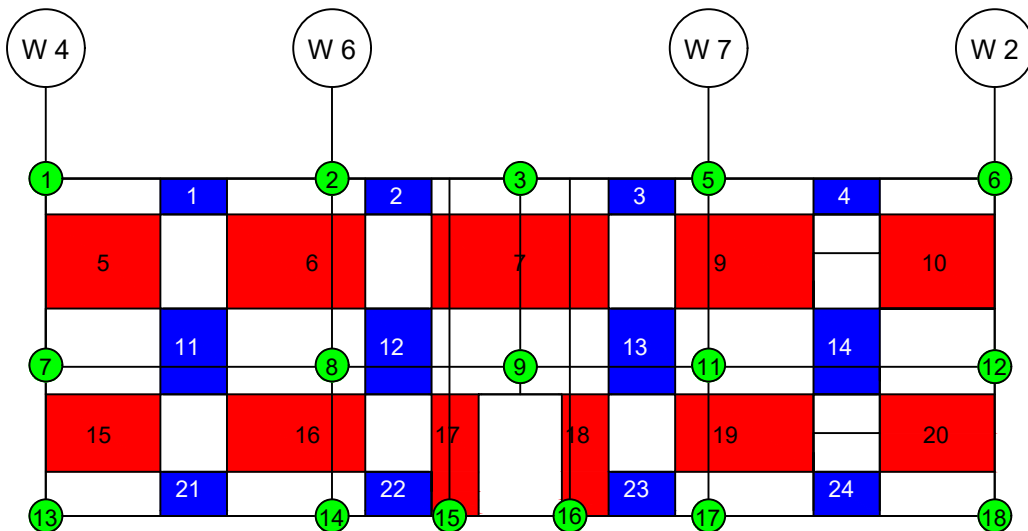
Walls with
openings

Date : 10.10.2023

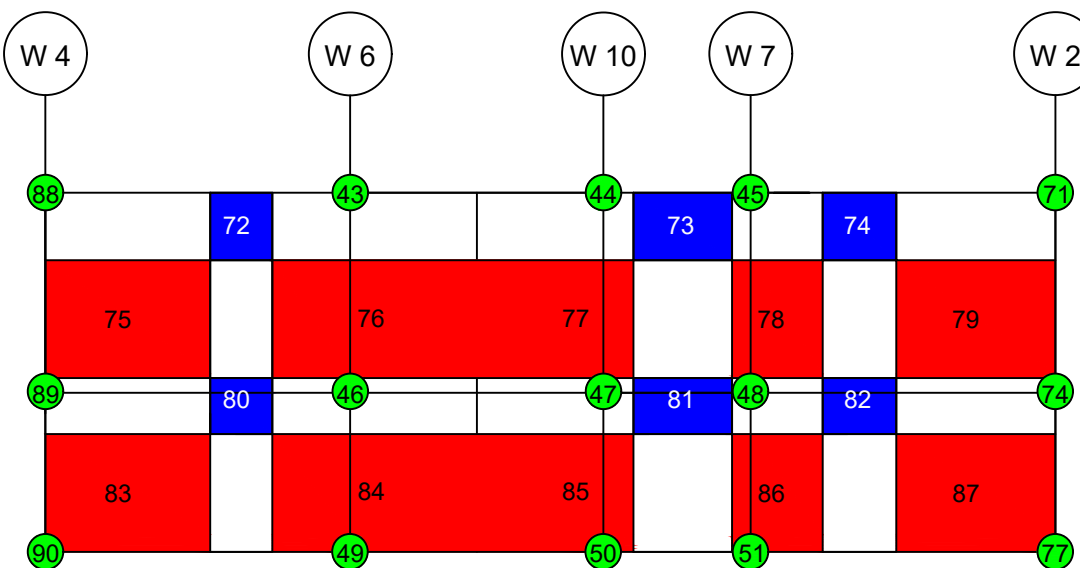
Scale : 1:150



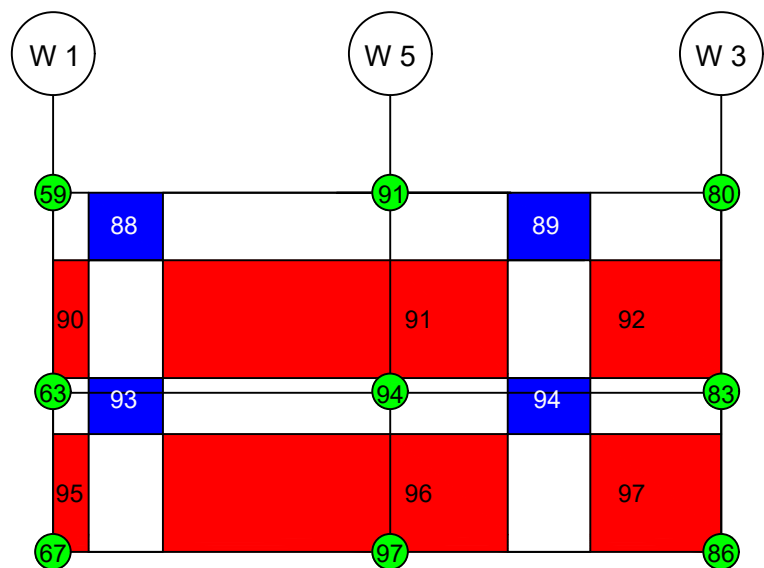
Makro elements EFM	Author :	Aline Bönzli
EESD Plan view walls OpenSees	Date :	21.11.2023
	Scale :	-



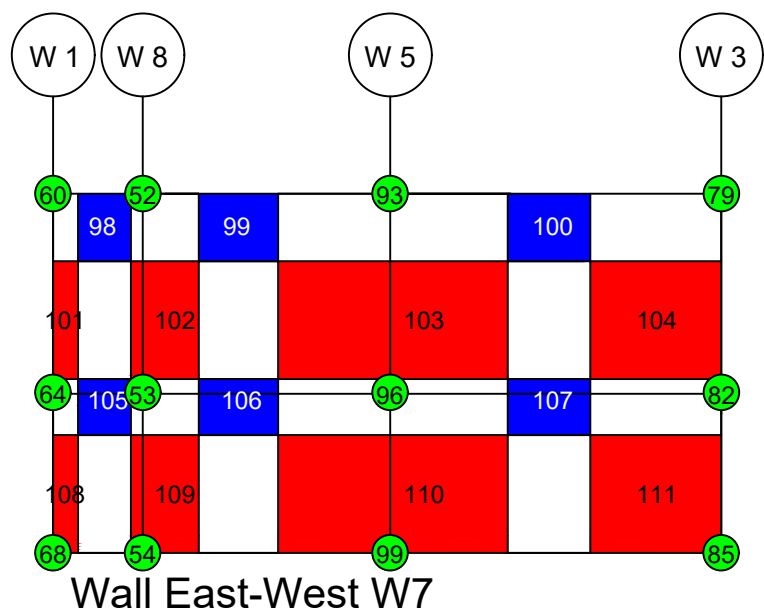
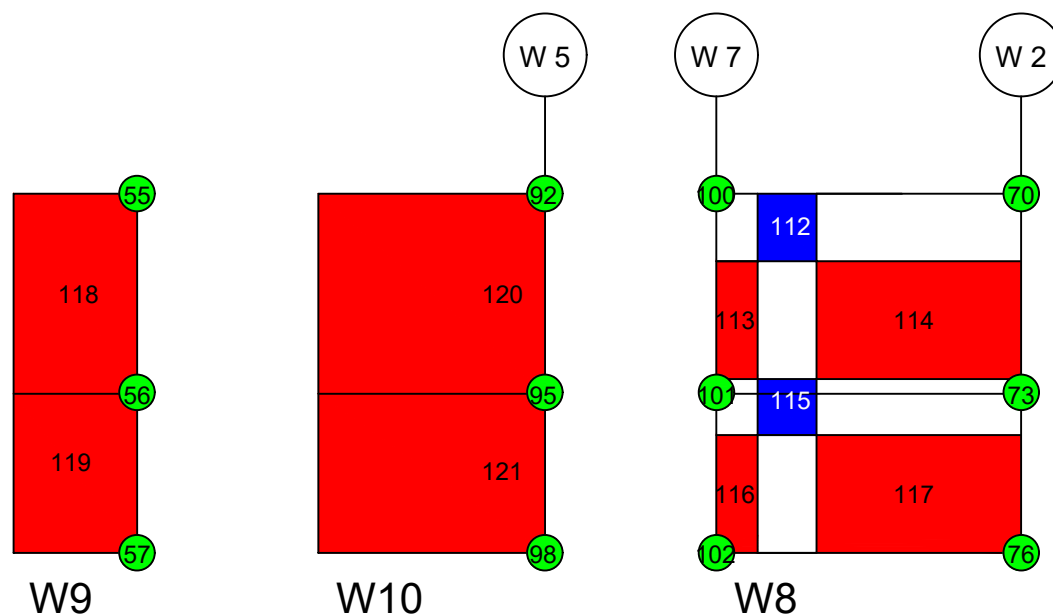
Macro elements EFM	Author :	Aline Bönzli
EESD All Facades OpenSees	Date :	21.11.2023
	Scale :	-



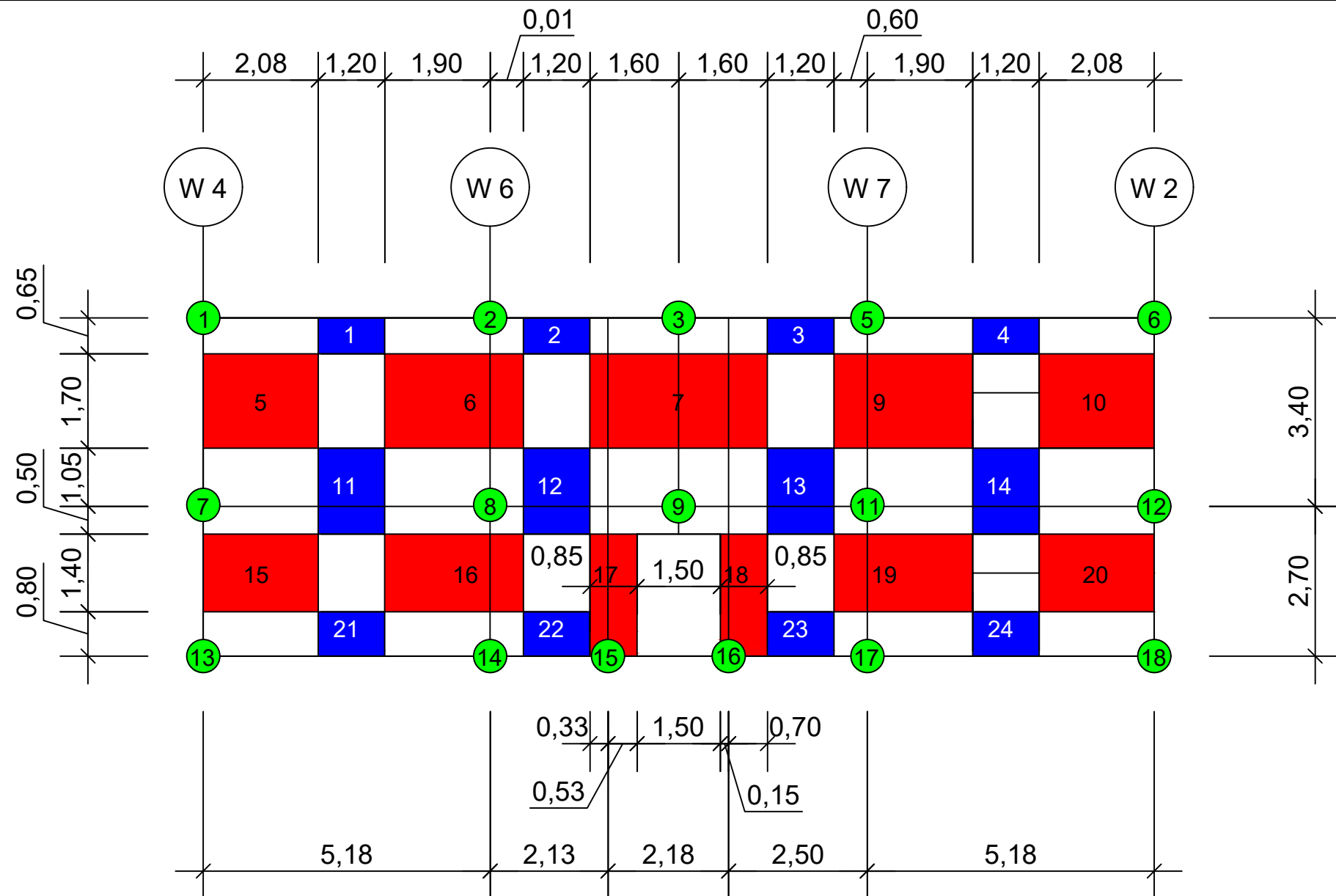
Wall North-South W5



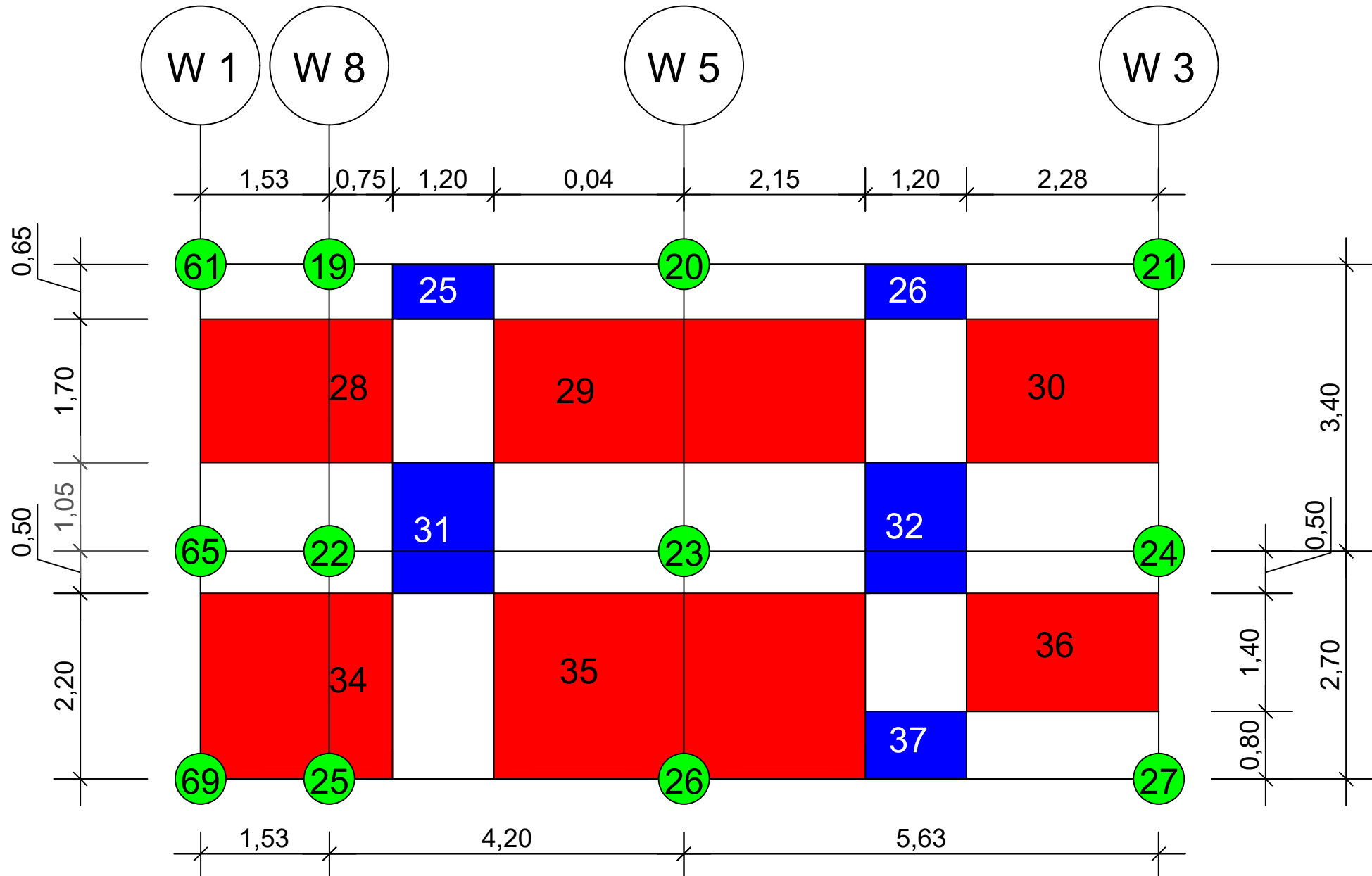
Wall East-West W6



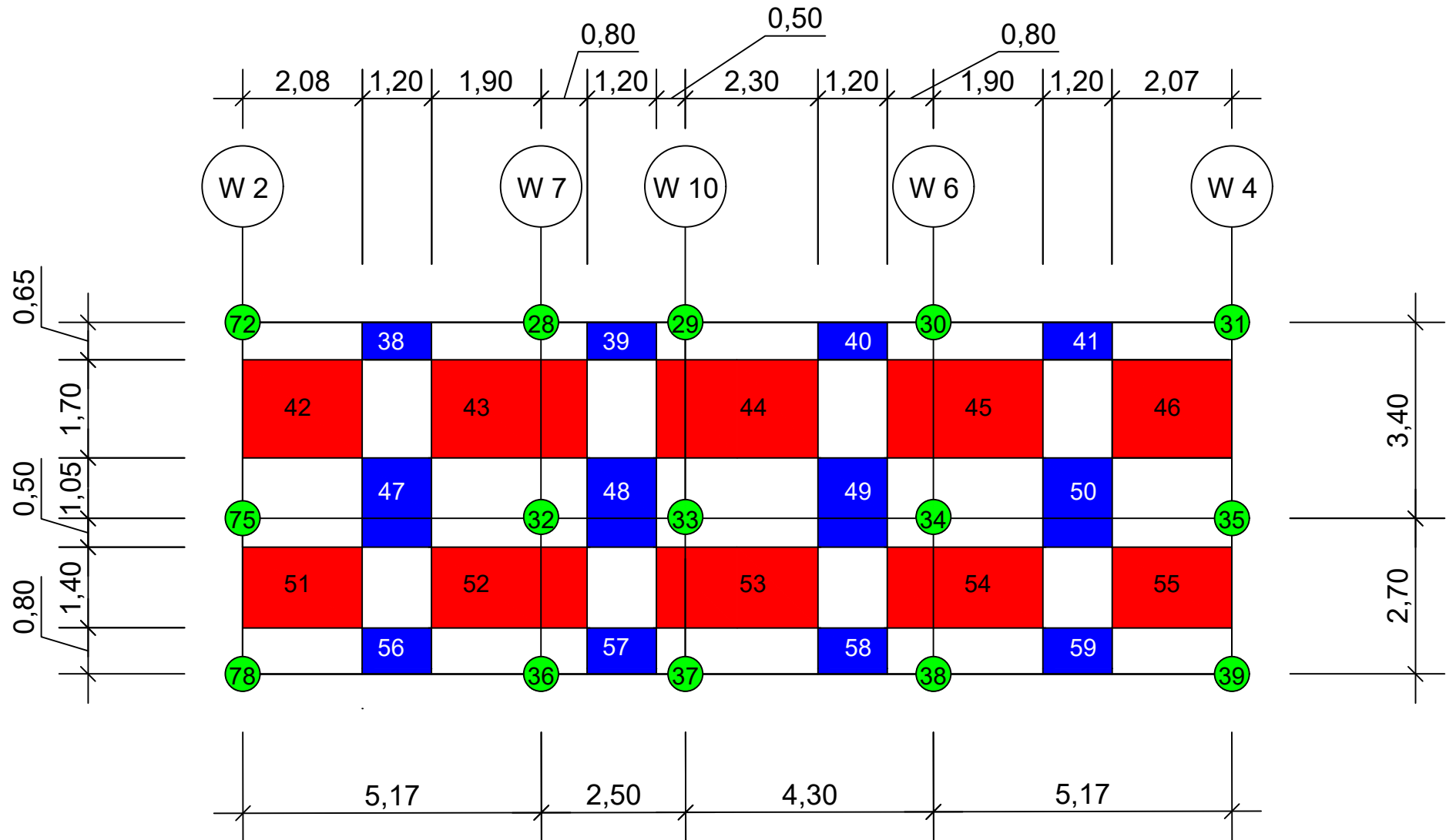
Macro elements EFM	Author :	Aline Bönzli
EESD OpenSees	Inside Walls	Date : 21.11.2023
	Scale :	-

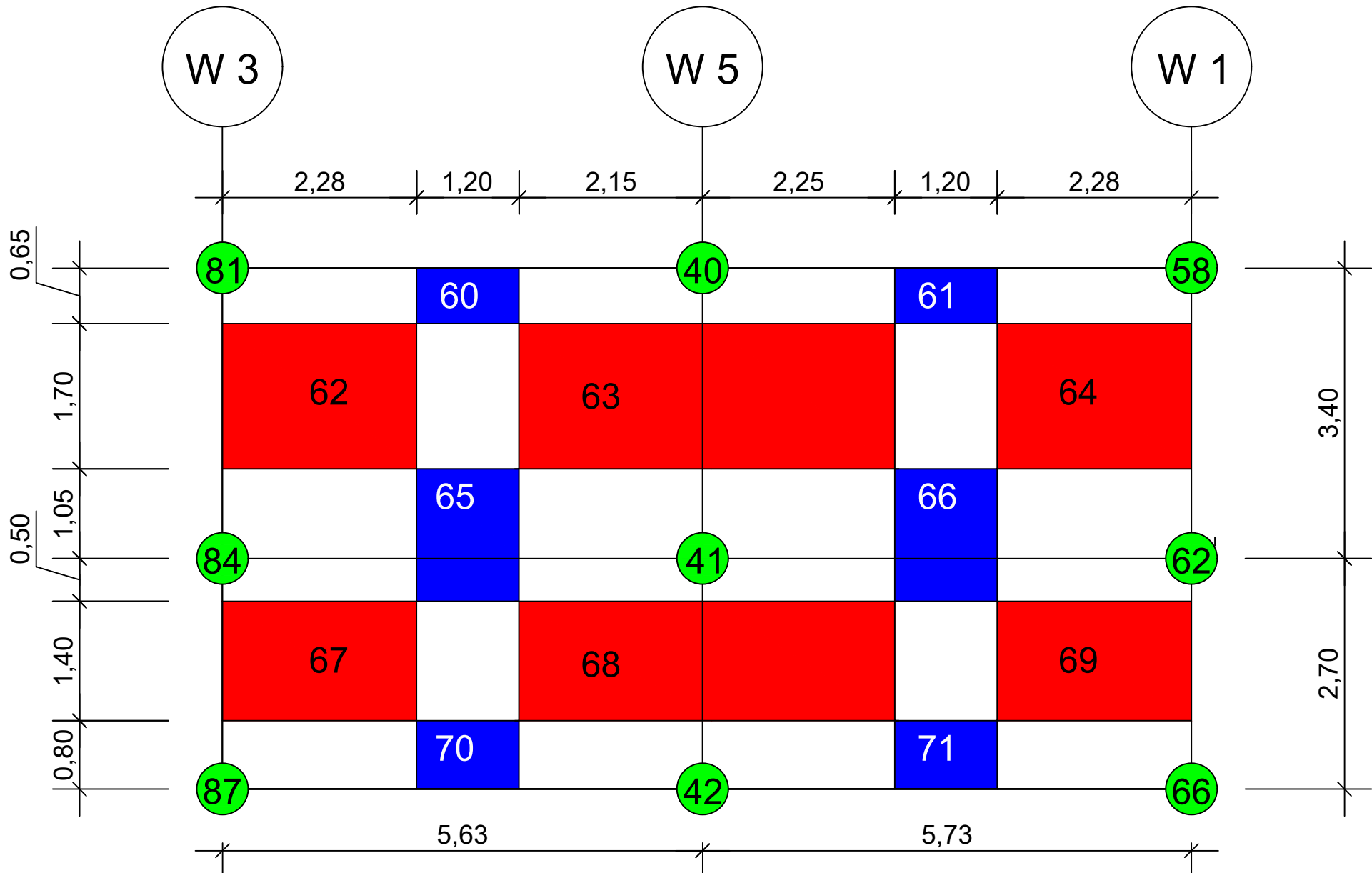


Macro elements EFM	Author :	Aline Bönzli
EESD OS W1 (West)	Date :	20.11.2023
	Scale :	-

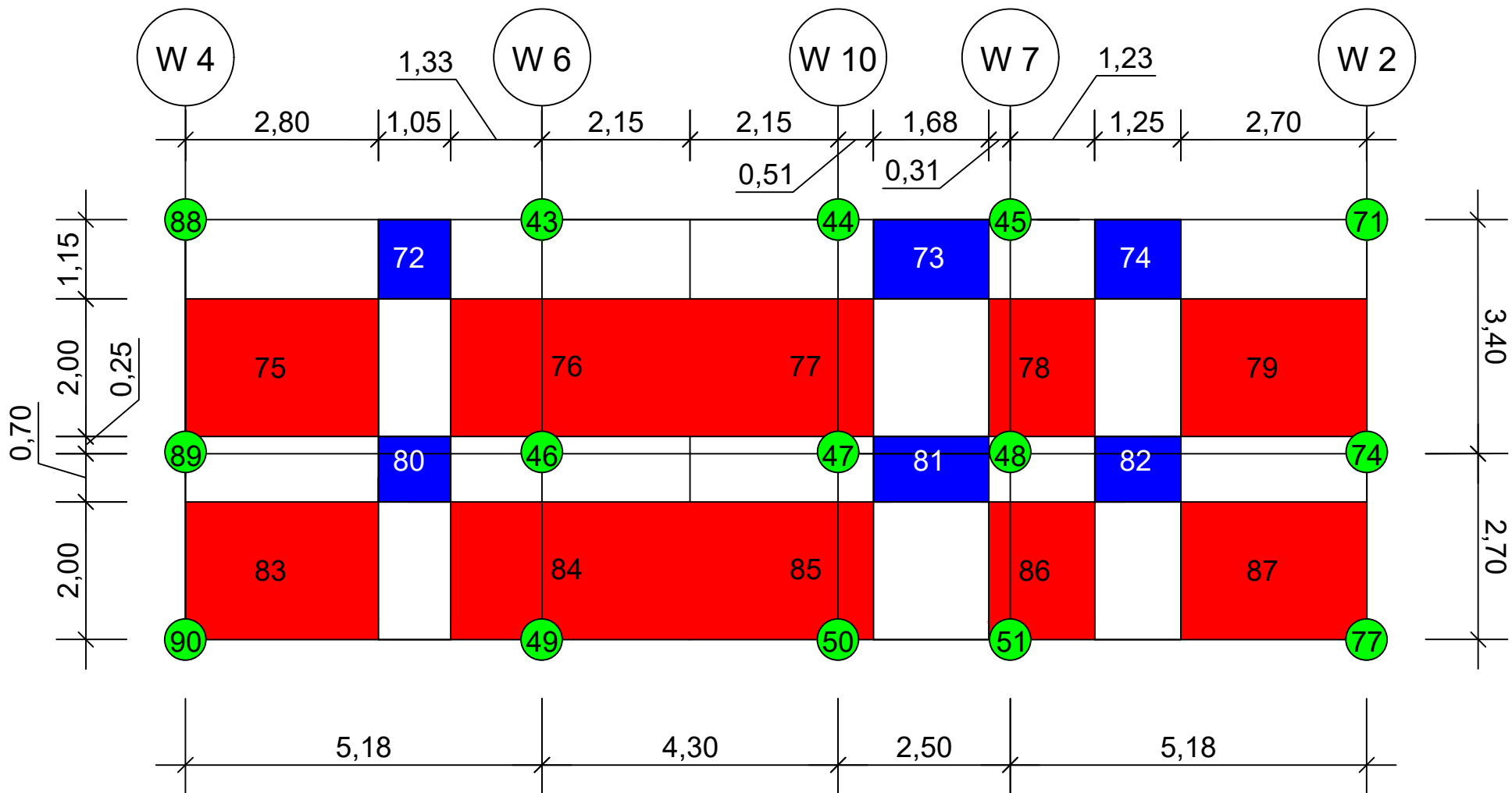


Macro elements EFM	Author :	Aline Bönzli
EESD OS W2 (South)	Date :	20.11.2023
	Scale :	-

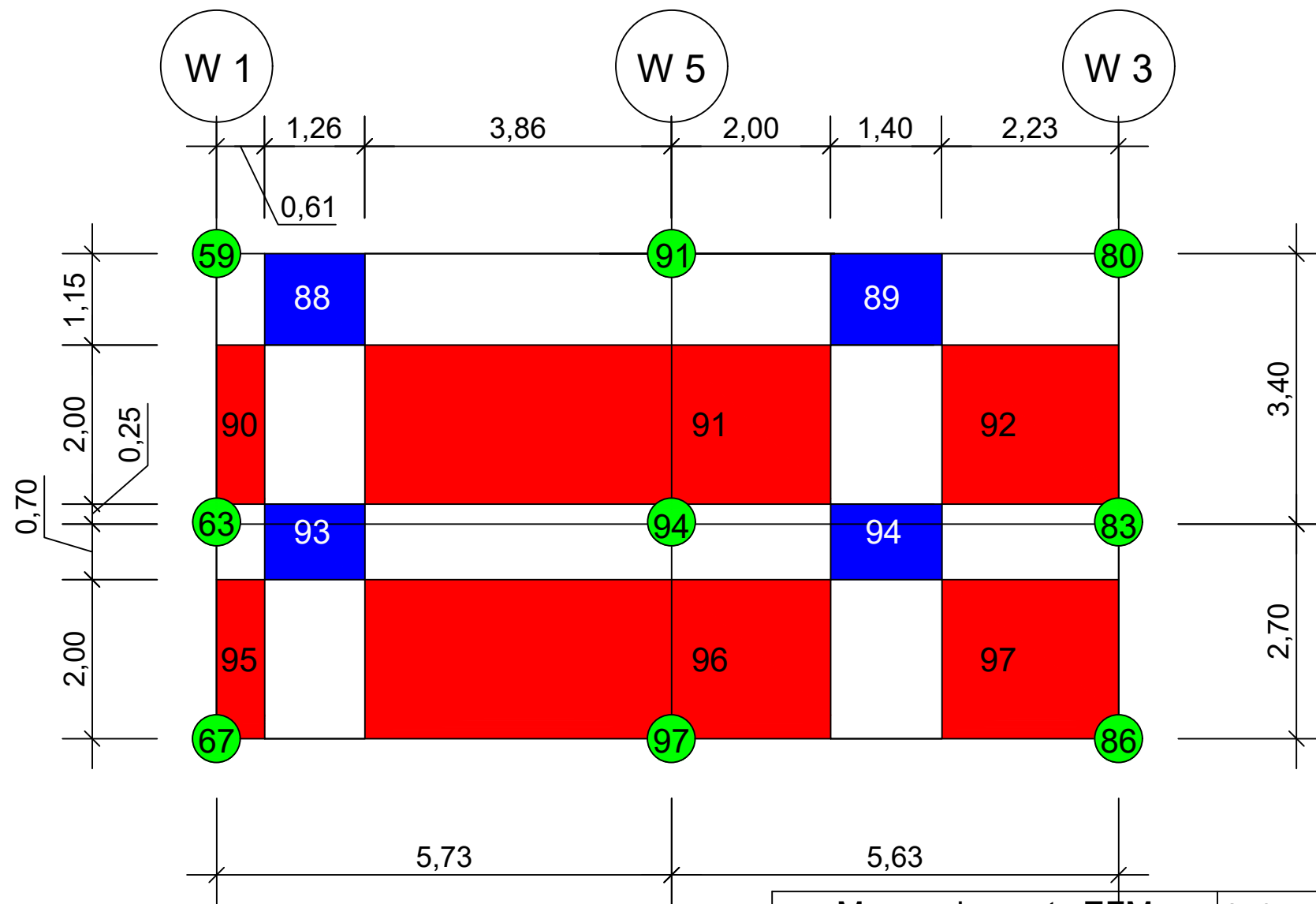




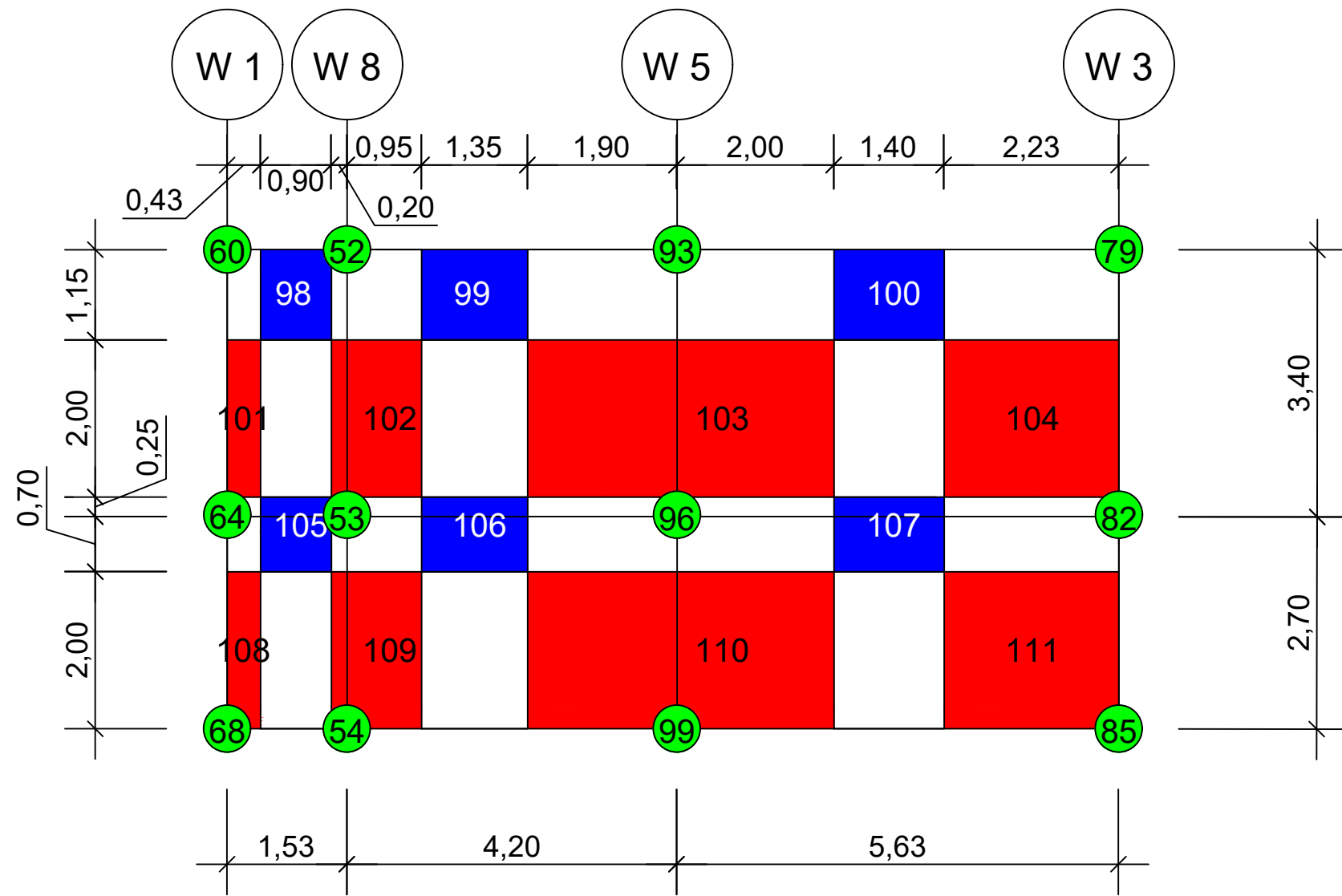
Macro elements EFM	Author :	Aline Bönzli
EESD OS W4 (North)	Date :	21.11.2023
	Scale :	-



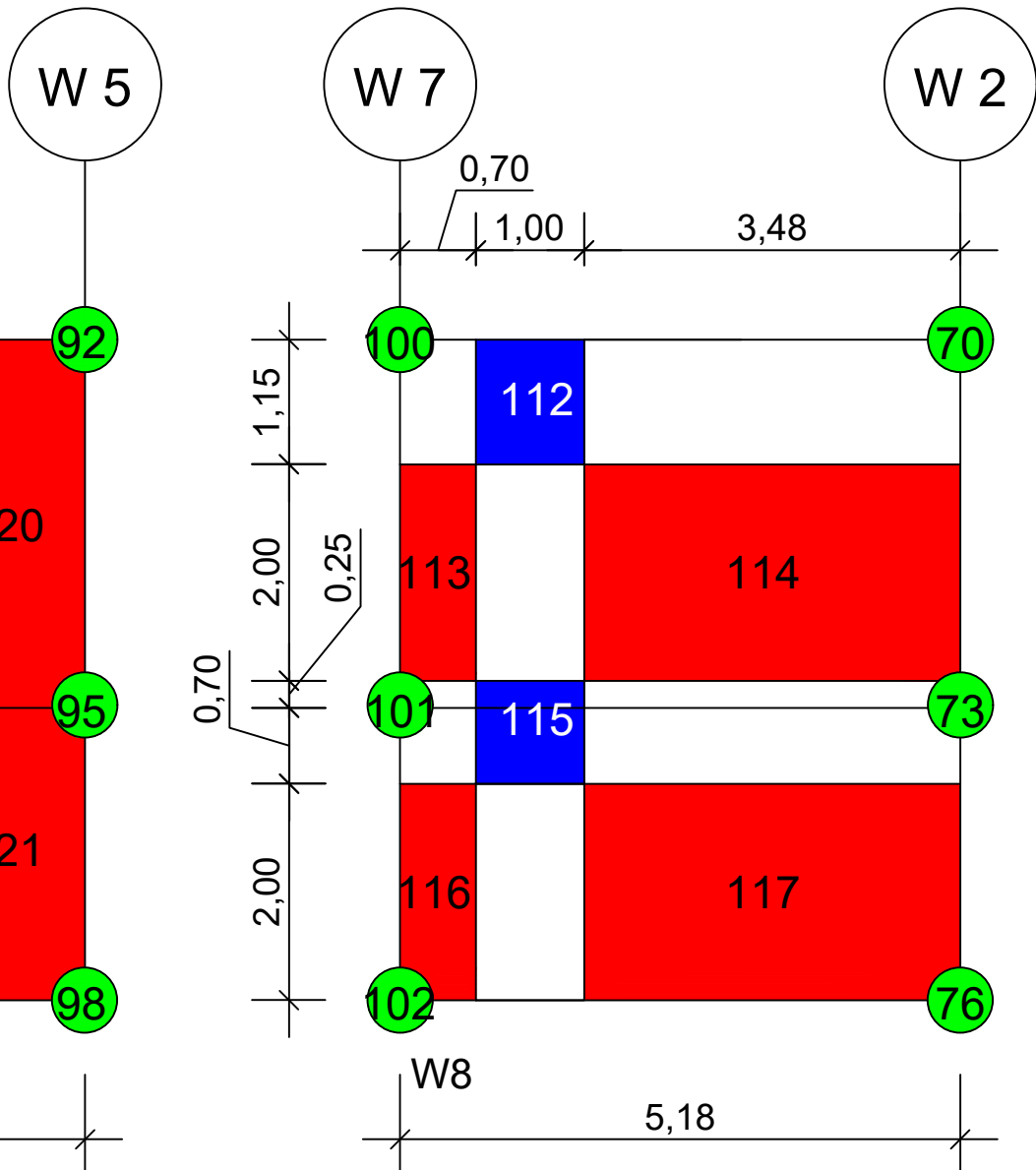
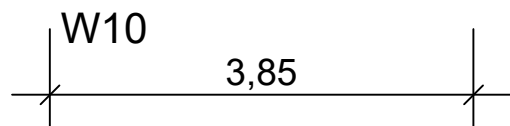
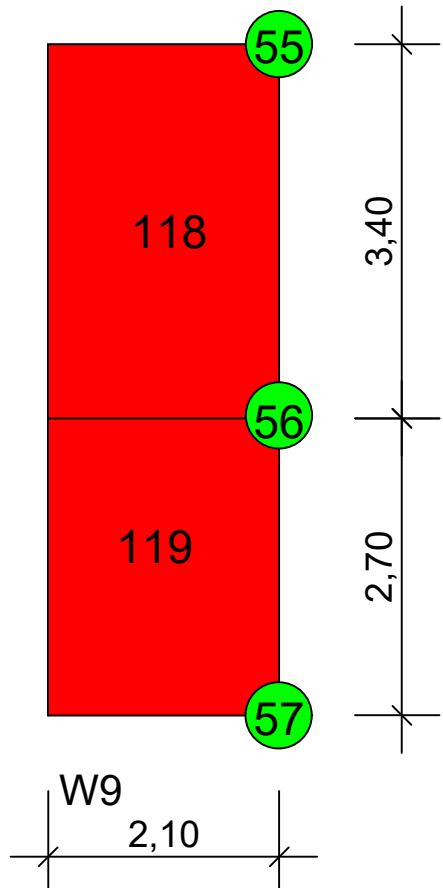
Macro elements EFM		Author :	Aline Bönzli
EESD OS W5		Date :	23.11.2023
		Scale :	-



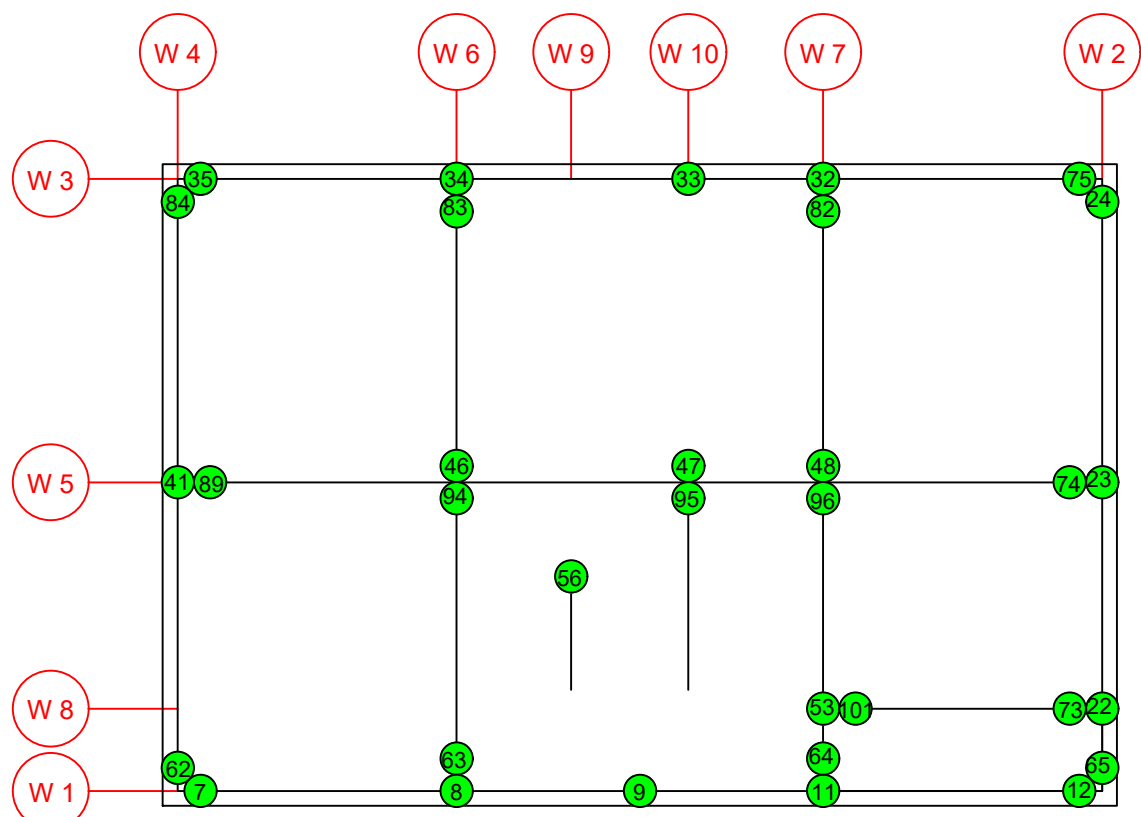
Macro elements EFM		Author :	Aline Bönzli
EESD	OS W6	Date :	21.11.2023
		Scale :	-



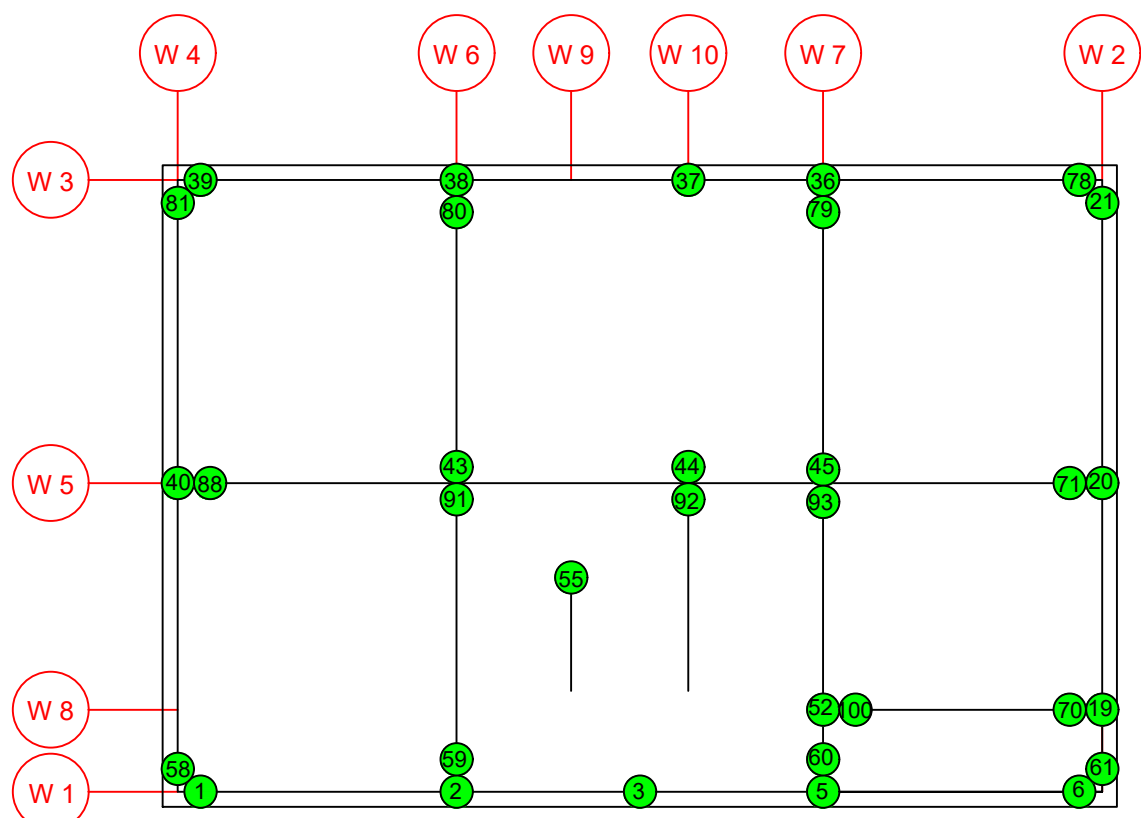
Macro elements EFM		Author :	Aline Bönzli
EESD OS W7		Date :	21.11.2023
		Scale :	-



Macro elements EFM	Author :	Aline Bönzli
EESD OS W8-10	Date :	21.11.2023
	Scale :	-

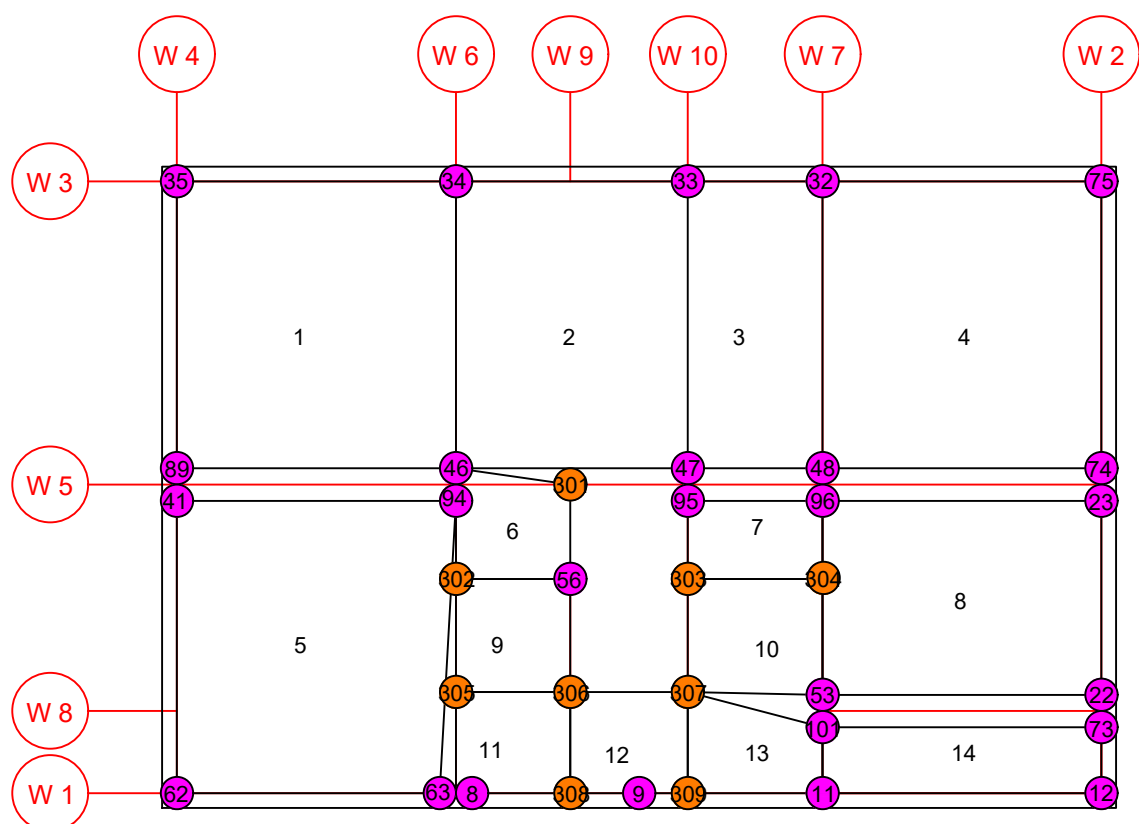


First floor slab

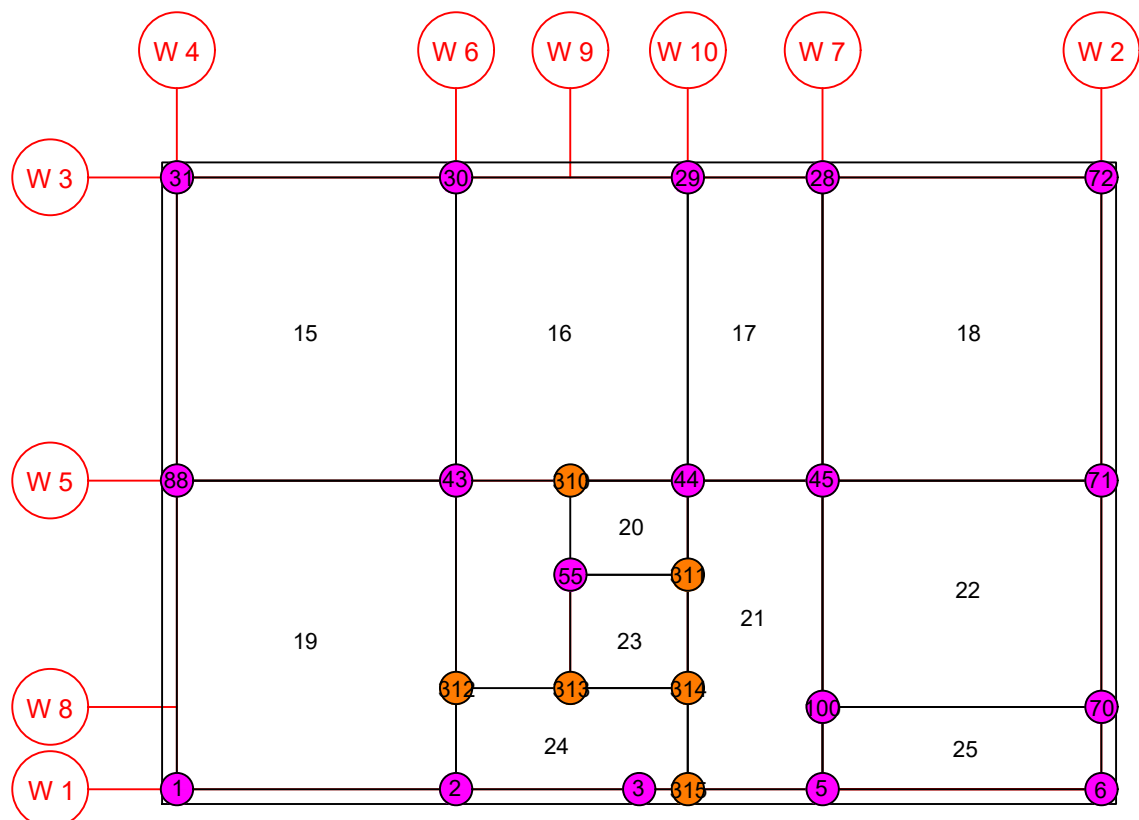


Second floor slab

OpenSEES	Author :	Aline Bönzli
EESD Plan view nodes	Date :	16.11.2023
	Scale :	-



First floor slab

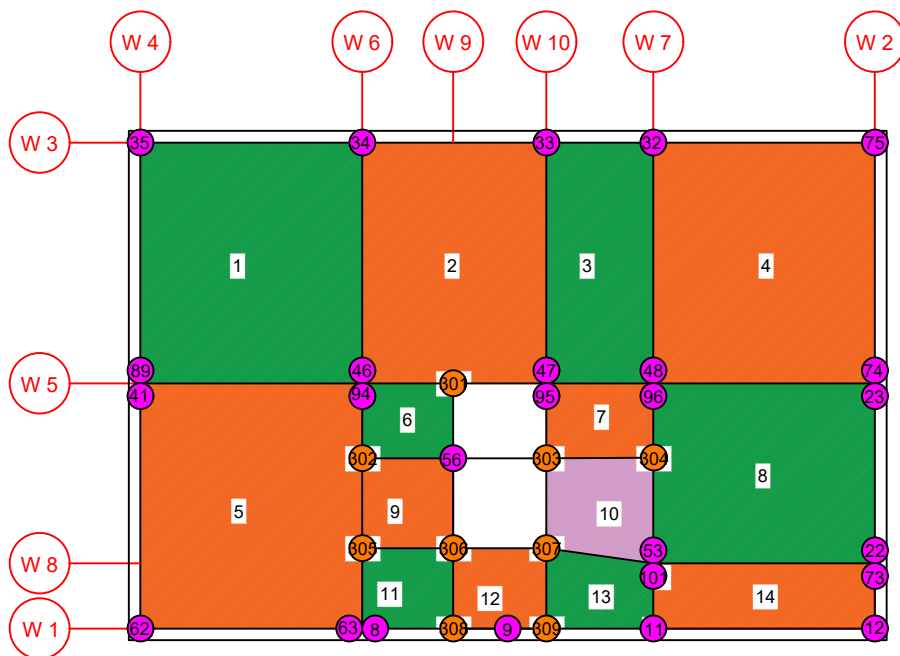


Second floor slab

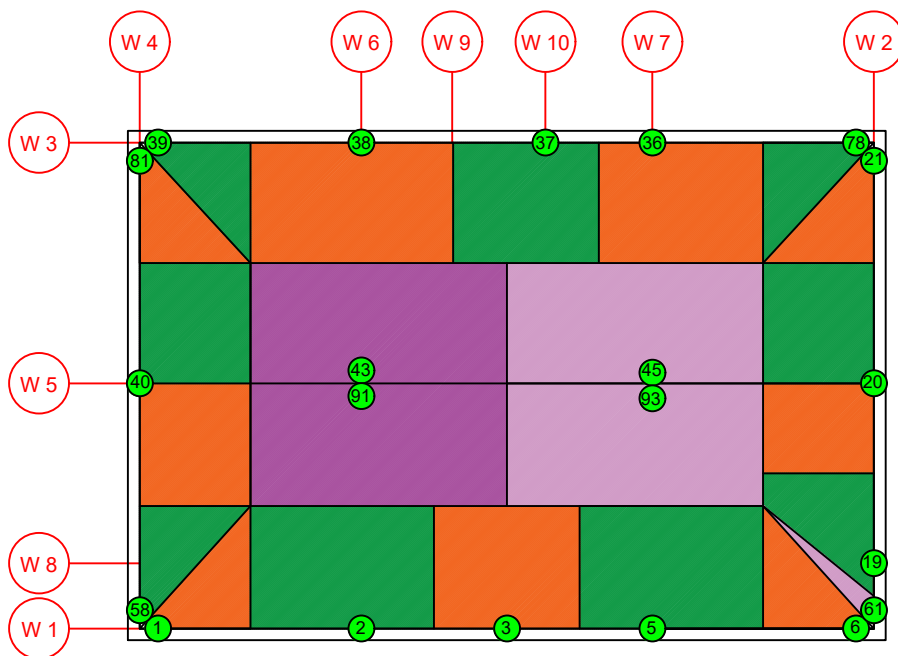
OpenSEES		Author :	Aline Bönzli
EESD	Plan view slab nodes	Date :	08.12.2023

Scale :

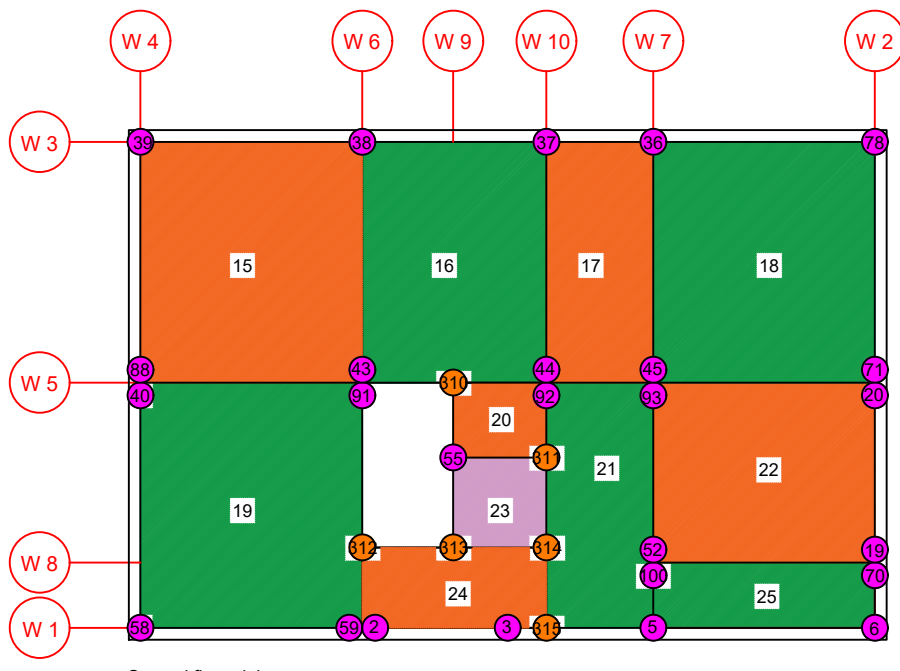
-



First floor slab

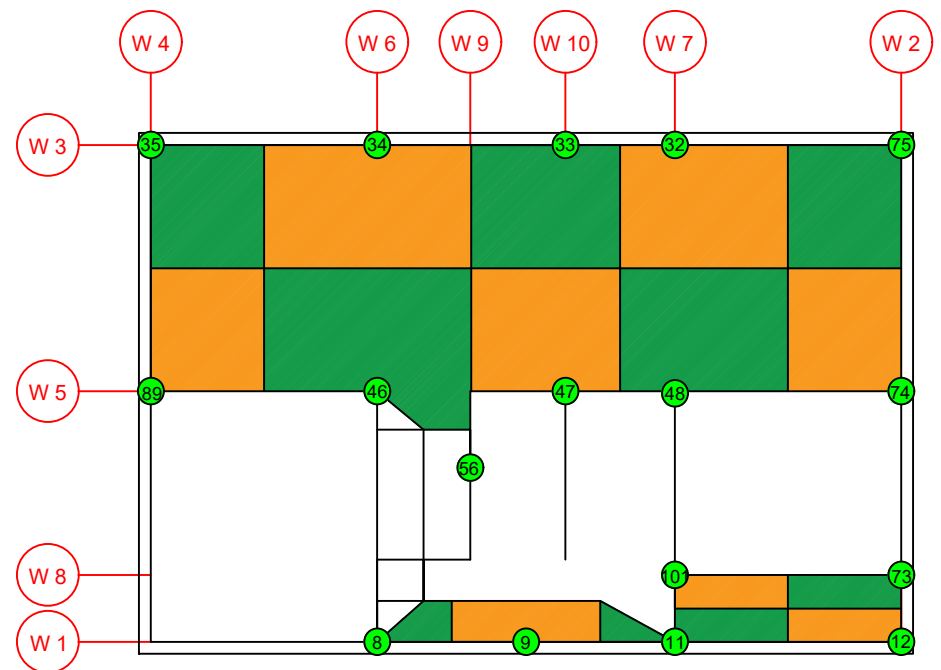


Second floor slab

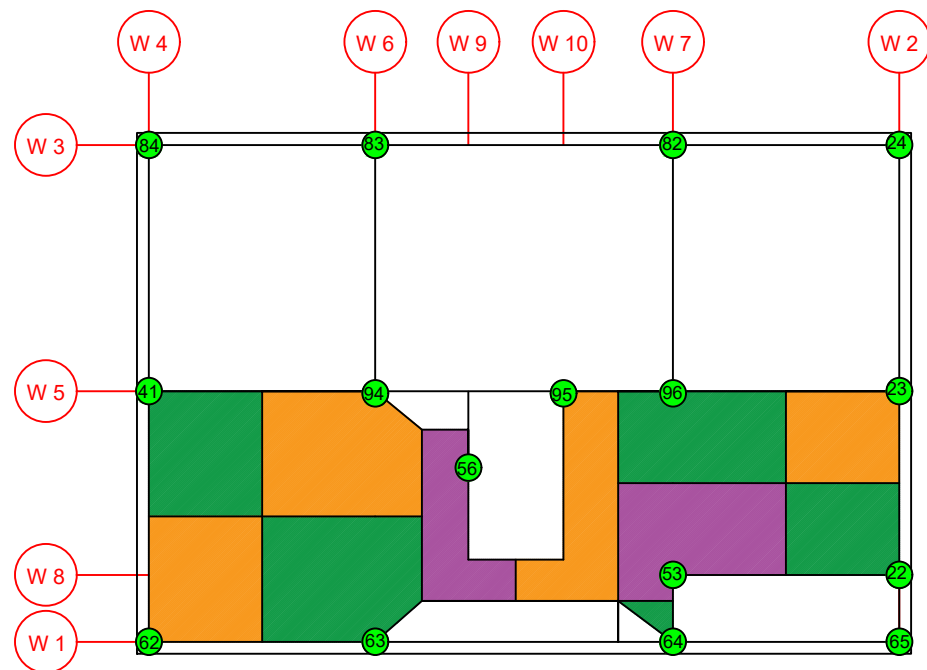


Second floor slab

Macro elements EFM		Author :	Aline Bönzli
EESD Mass distribution slabs		Date :	04.12.2023
		Scale :	-

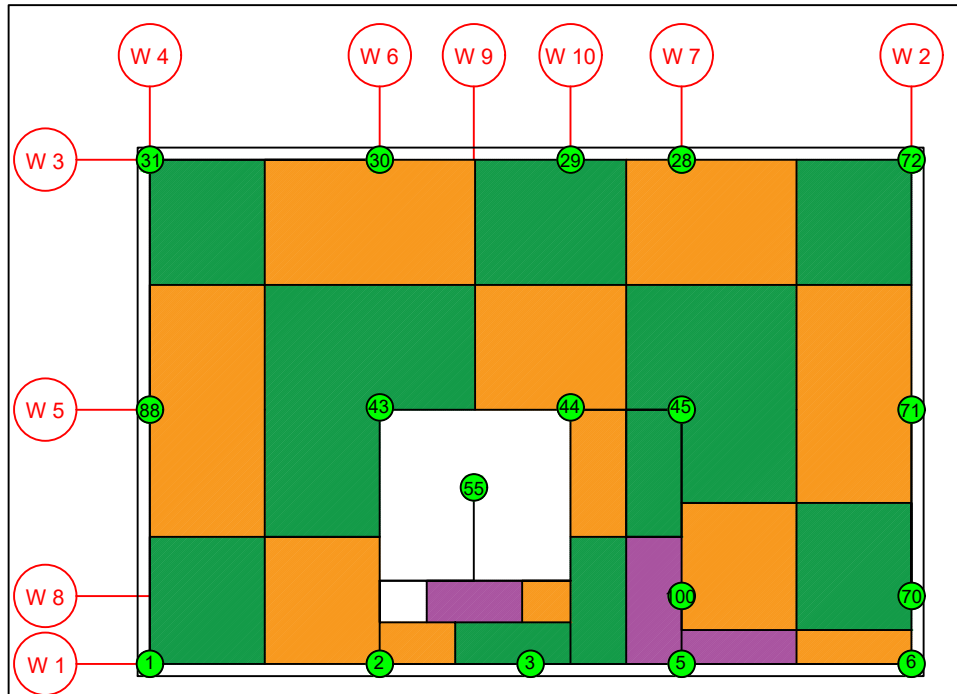


First floor slab, east-west support direction

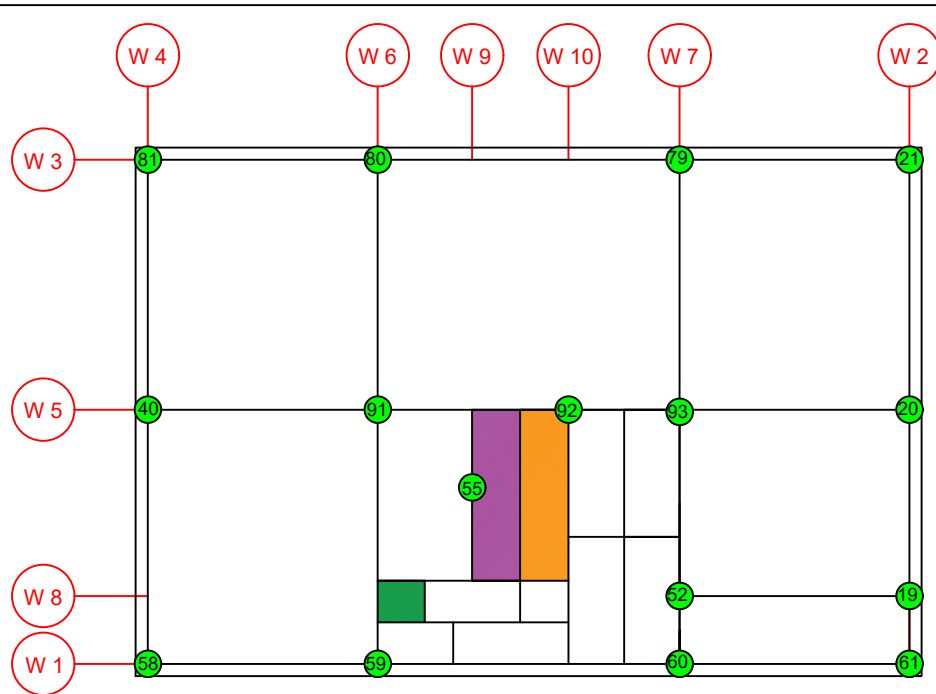


First floor slab, north-south support direction

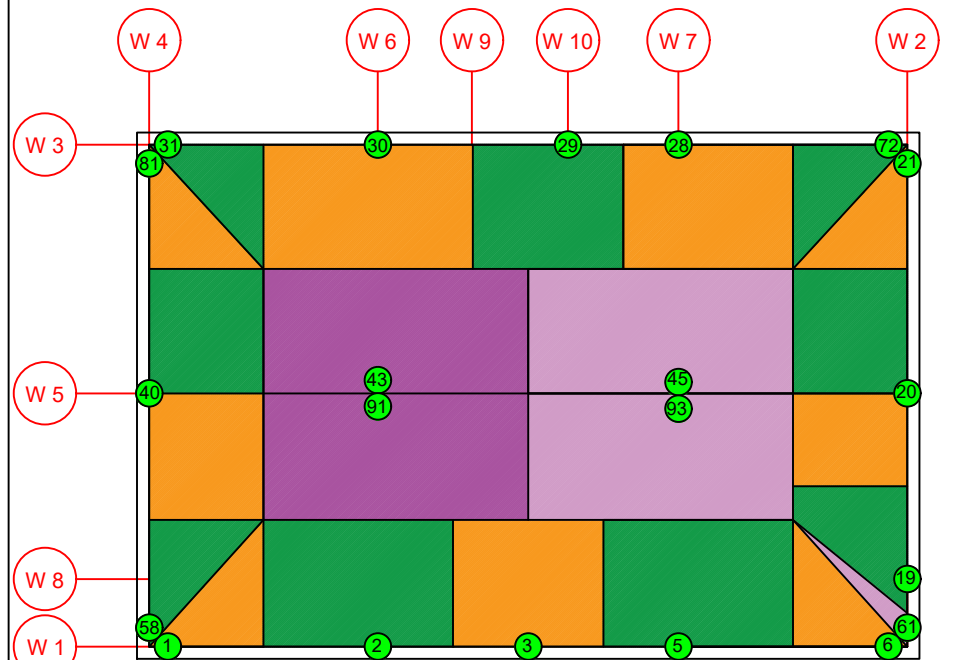
Macro elements EFM		Author :	Aline Bönzli
EESD	Load distribution slabs, 1.FL	Date :	08.12.2023
		Scale :	-



Second floor slab, east-west support direction



Second floor slab, north-south support direction

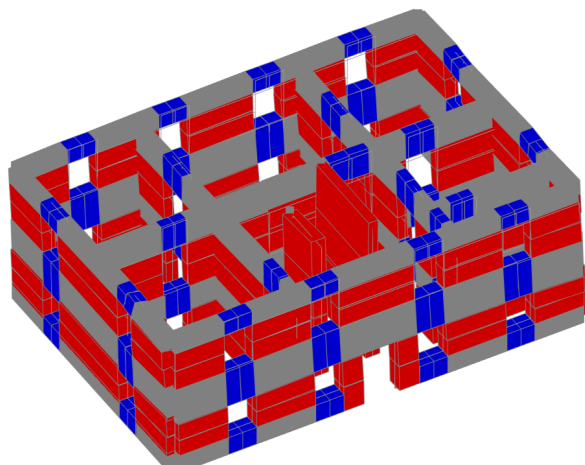


Roof load distribution

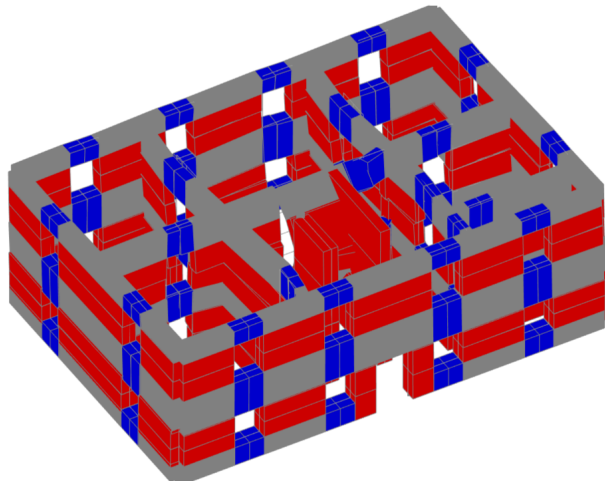
Macro elements EFM		Author :	Aline Bönzli
EESD Load distribution slabs, 2.FL		Date :	04.12.2023
		Scale :	-

J. Global results in the initial state

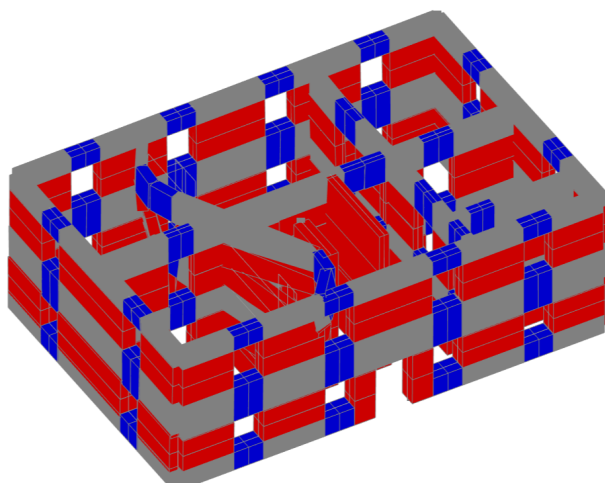
Modal shapes of dynamic analysis in unretrofitted state



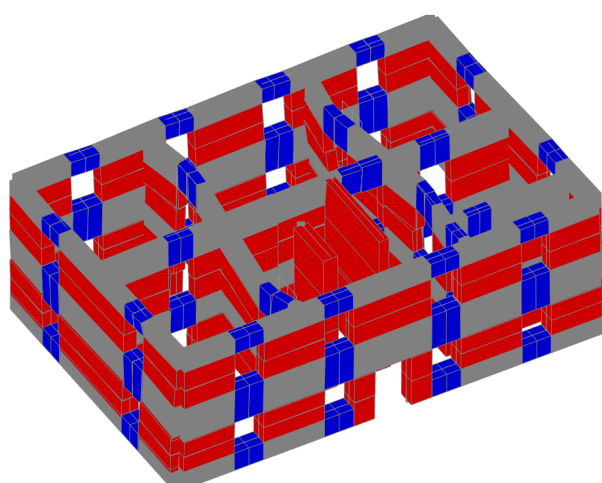
(a) Mode 1 overview



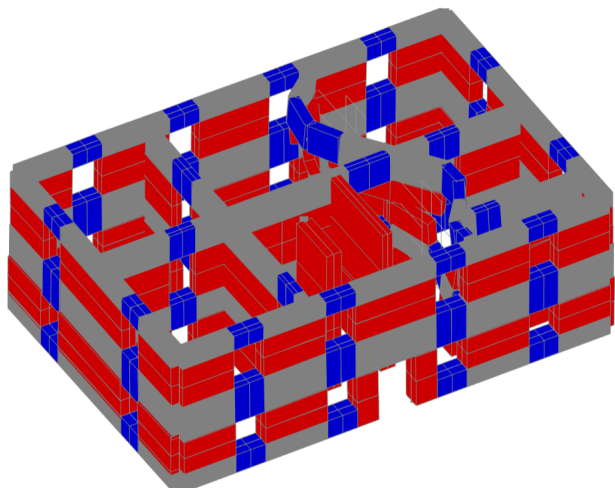
(b) Mode 2 overview



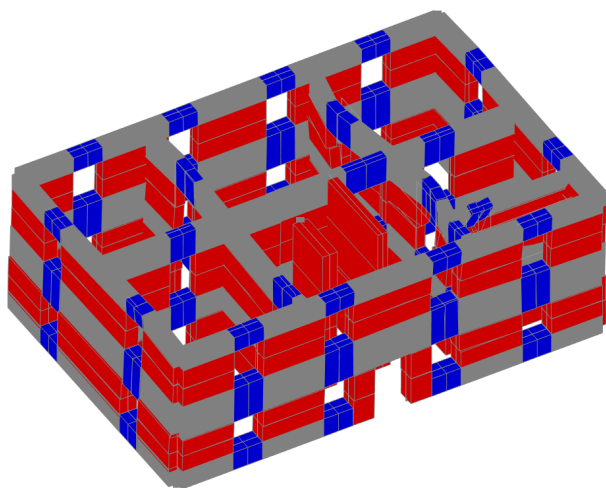
(a) Mode 3 overview



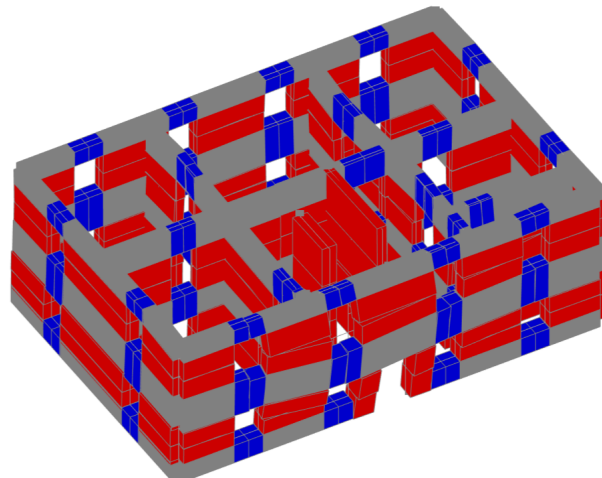
(b) Mode 4 overview



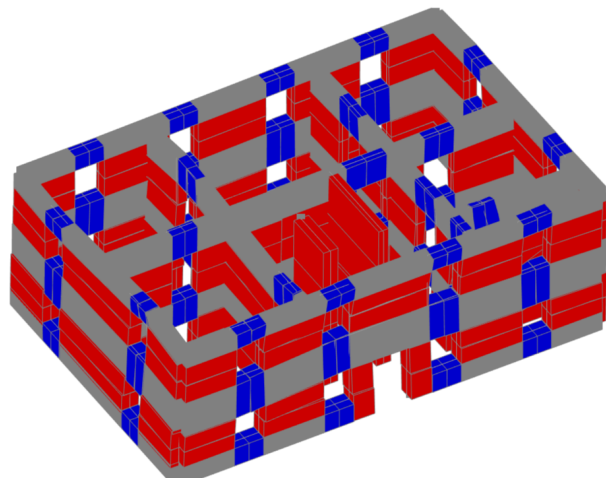
(a) Mode 5 overview



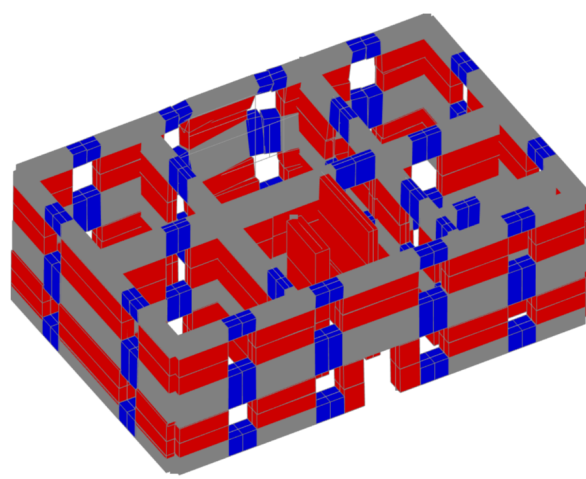
(b) Mode 6 overview



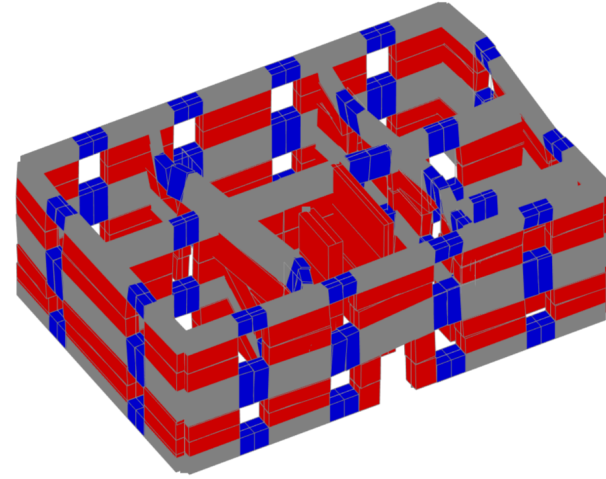
(a) Mode 7 overview



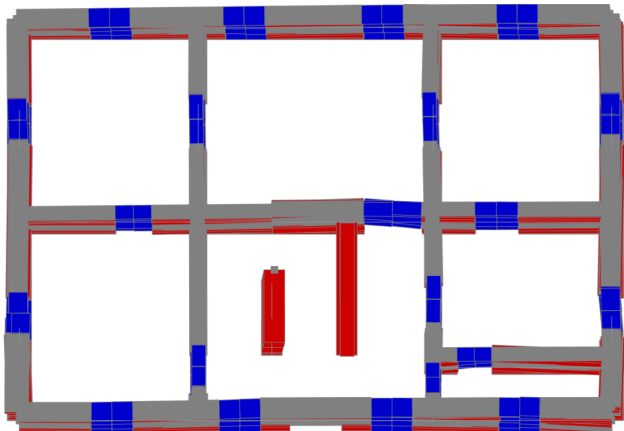
(b) Mode 8 overview



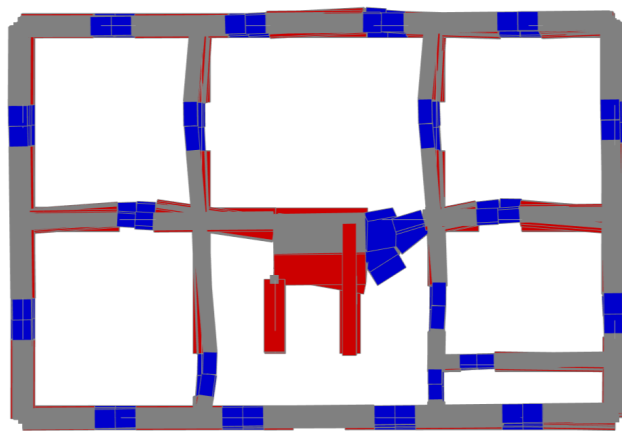
(a) Mode 9 overview



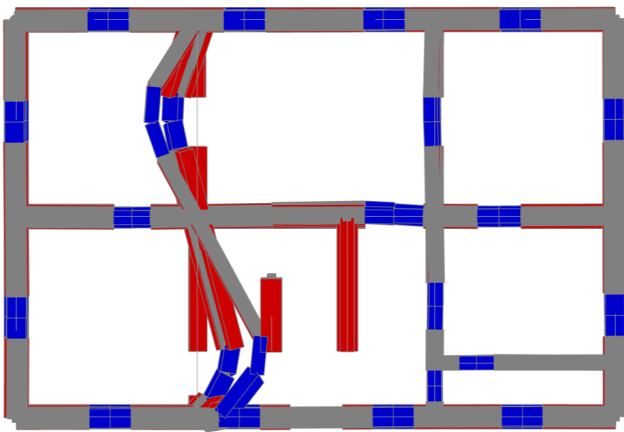
(b) Mode 10 overview



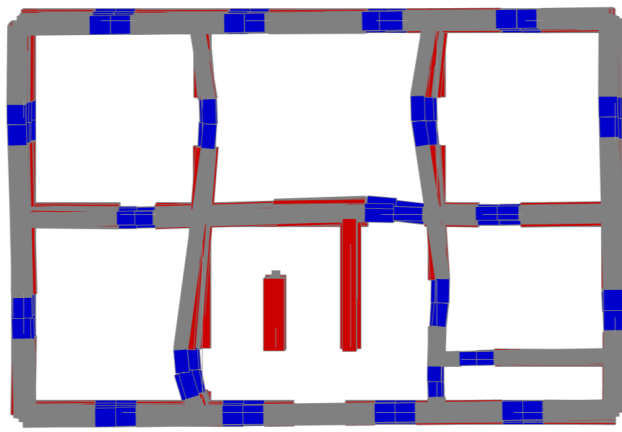
(a) Mode 1 plan view



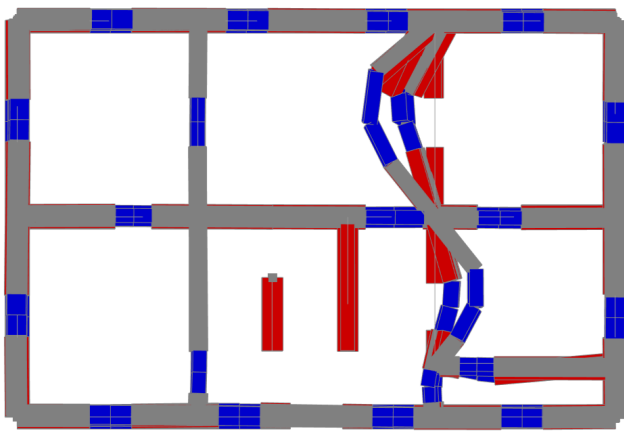
(b) Mode 2 plan view



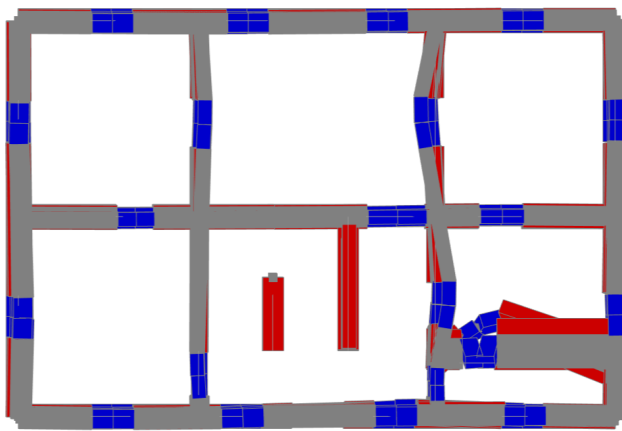
(a) Mode 3 plan view



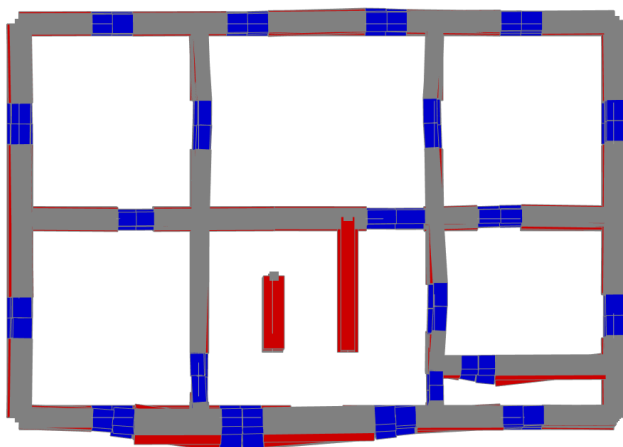
(b) Mode 4 plan view



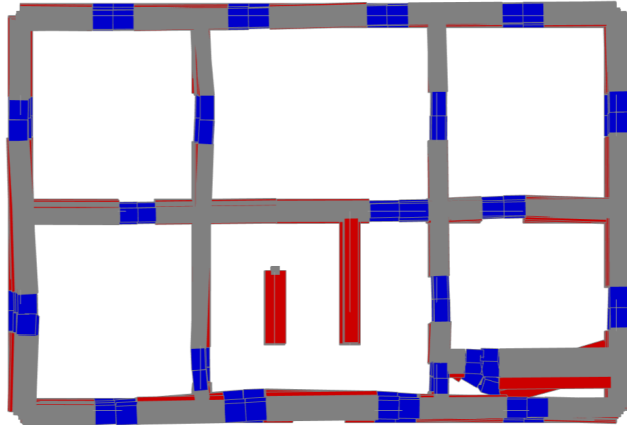
(a) Mode 5 plan view



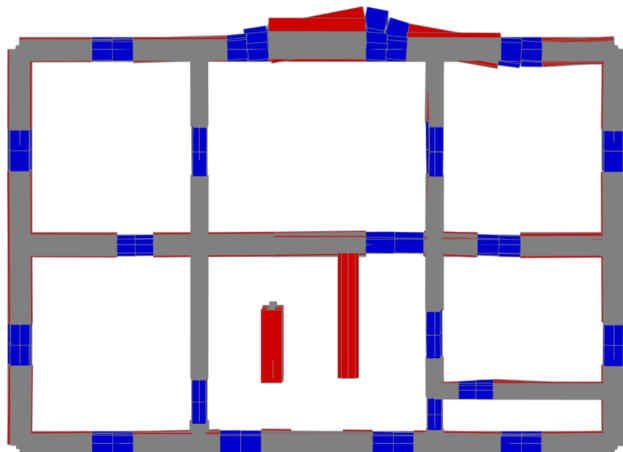
(b) Mode 6 plan view



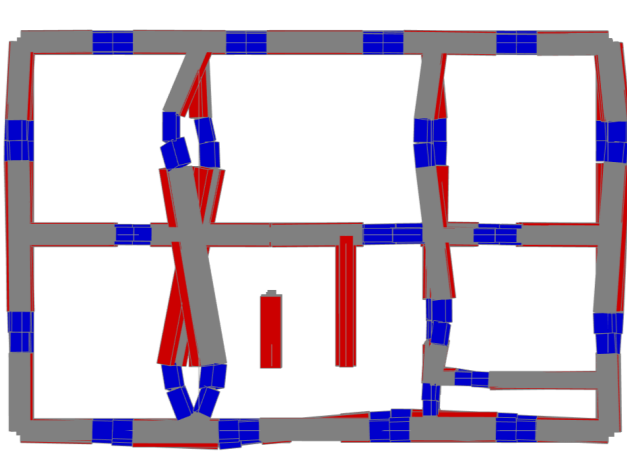
(a) Mode 7 plan view



(b) Mode 8 plan view



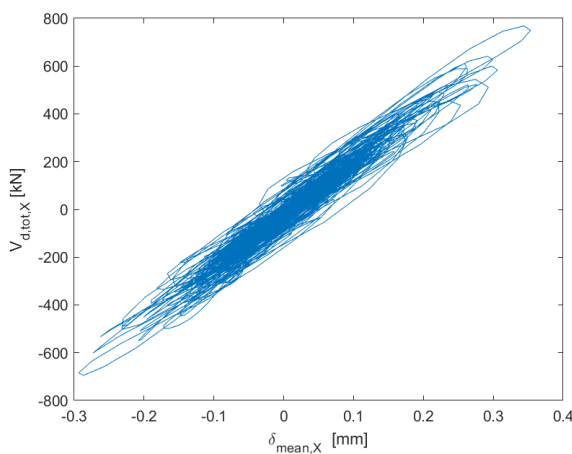
(a) Mode 9 plan view



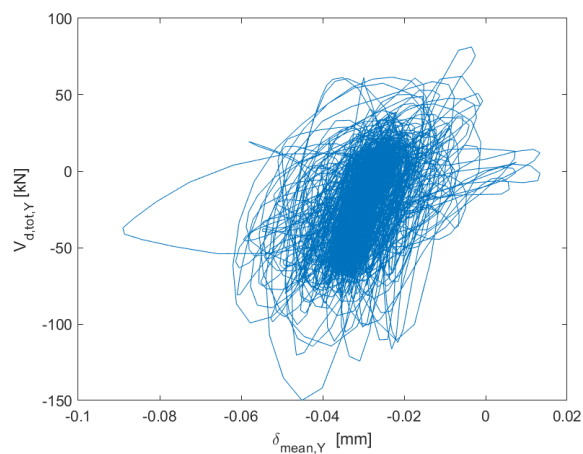
(b) Mode 10 plan view

Dynamic results

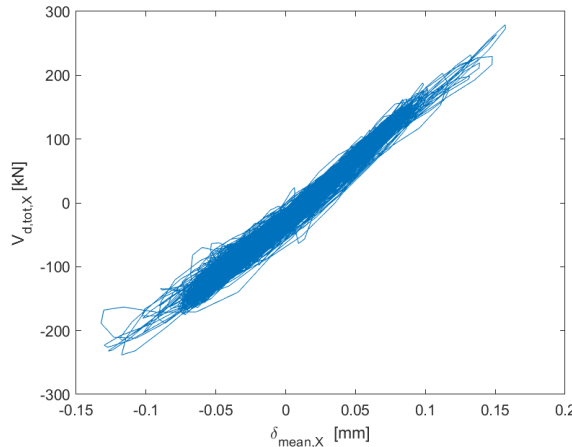
NS acceleration in X-direction, factor 0.5



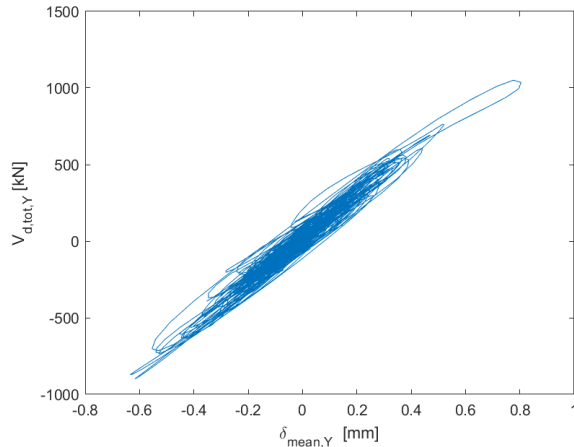
(a) Total base shear versus average roof displacement direction X



NS acceleration in Y-direction, factor 0.5

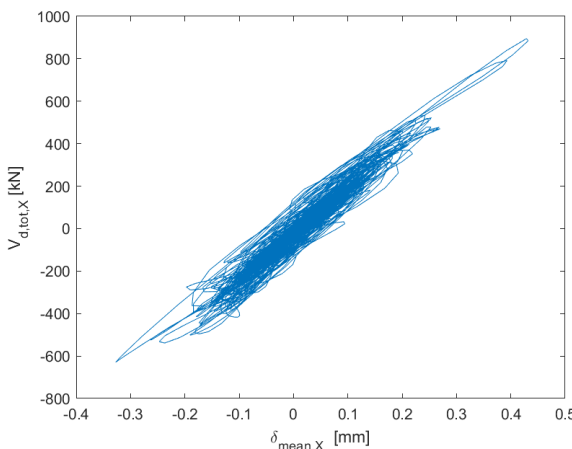


(a) Total base shear versus average roof displacement direction X

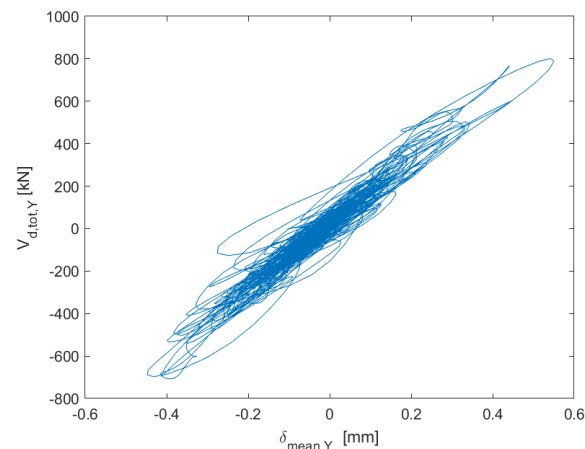


(b) Total base shear versus average roof displacement direction Y

NS acceleration in X-direction, EW acceleration in Y-direction, factor 0.5

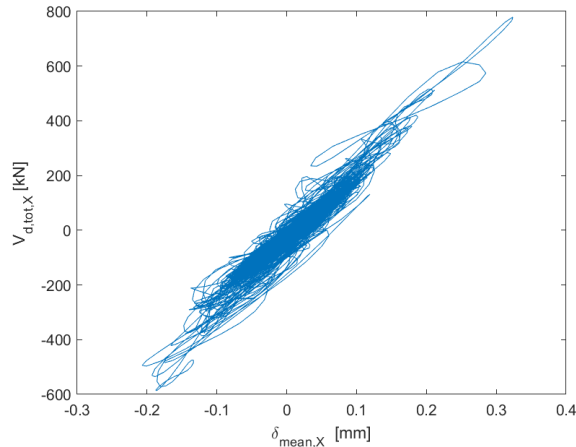


(a) Total base shear versus average roof displacement direction X

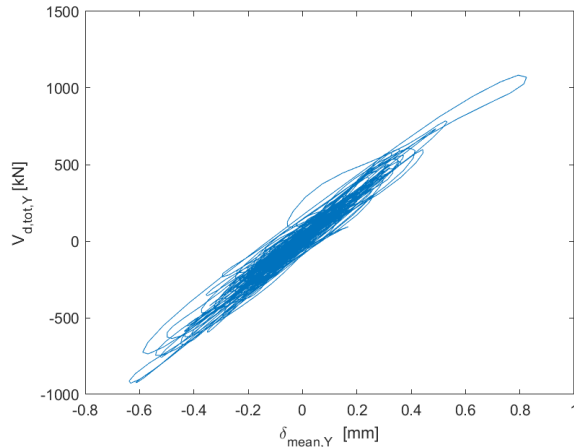


(b) Total base shear versus average roof displacement direction Y

NS acceleration in Y-direction, EW acceleration in X-direction, factor 0.5

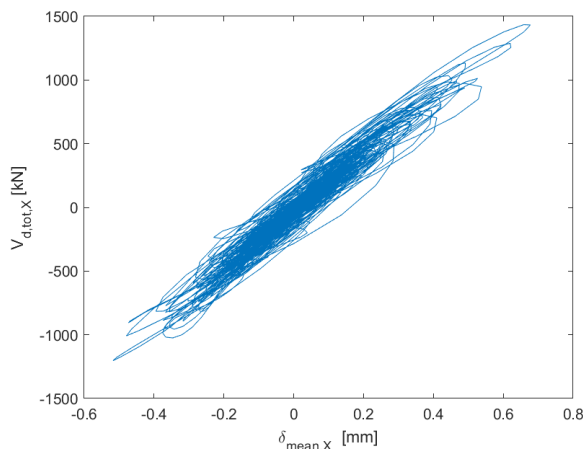


(a) Total base shear versus average roof displacement direction X

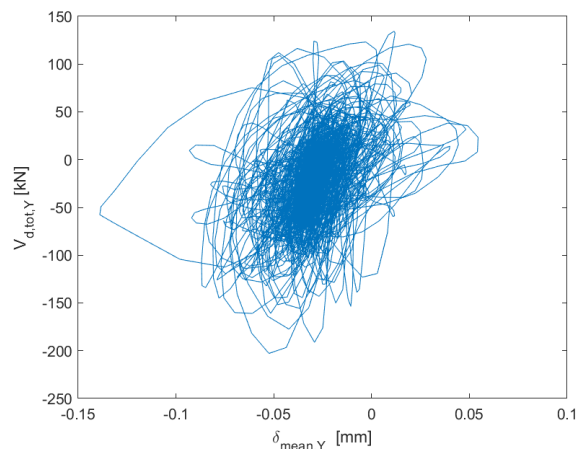


(b) Total base shear versus average roof displacement direction Y

NS acceleration in X-direction, factor 1

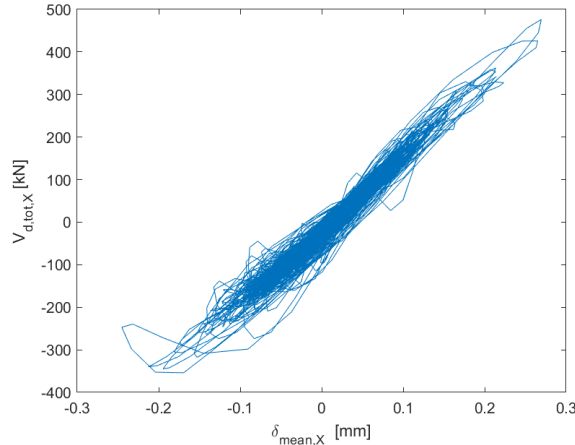


(a) Total base shear versus average roof displacement direction X

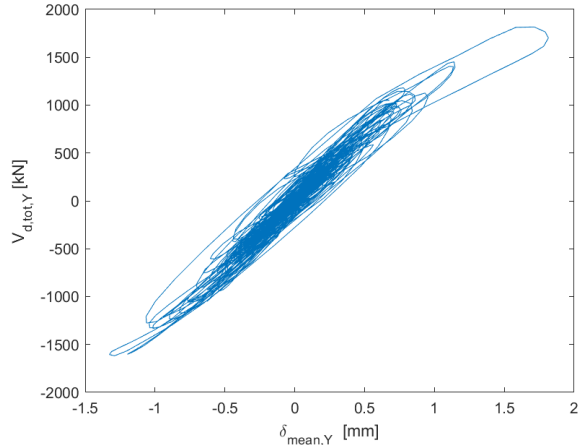


(b) Total base shear versus average roof displacement direction Y

NS acceleration in Y-direction, factor 1

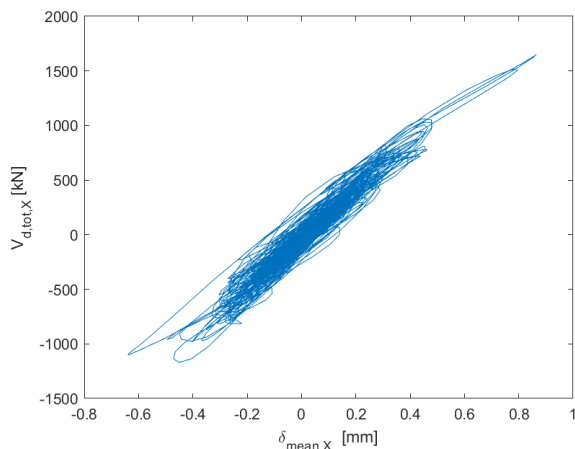


(a) Total base shear versus average roof displacement direction X

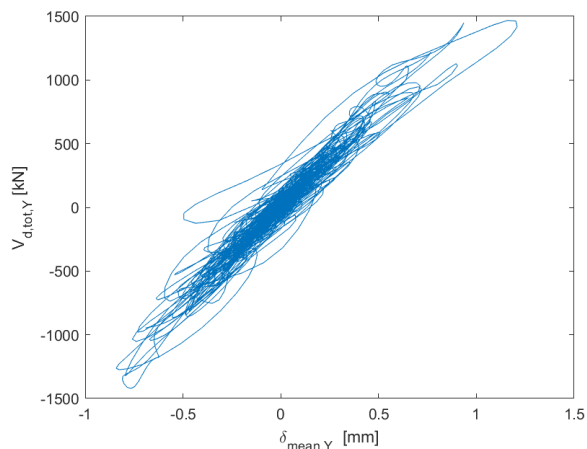


(b) Total base shear versus average roof displacement direction Y

NS acceleration in X-direction, EW acceleration in Y-direction, factor 1

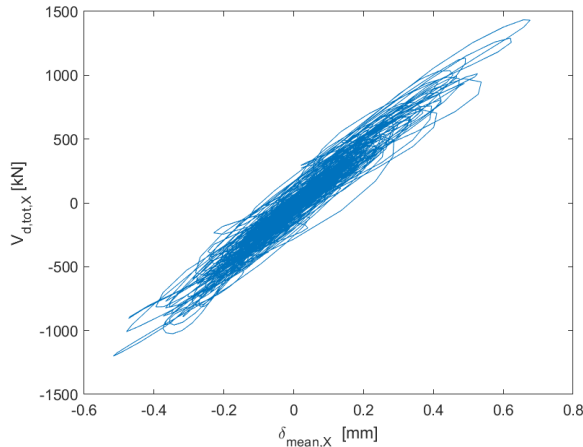


(a) Total base shear versus average roof displacement direction X

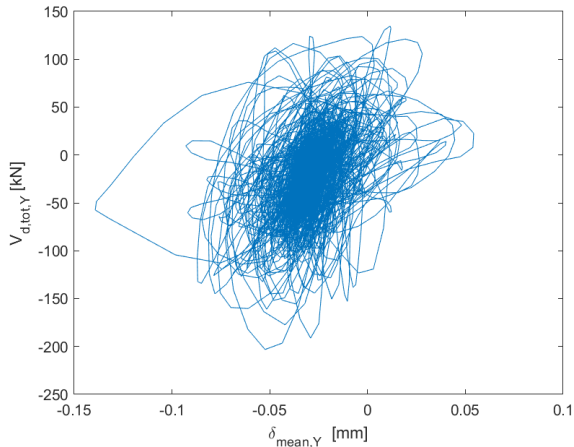


(b) Total base shear versus average roof displacement direction Y

NS acceleration in Y-direction, EW acceleration in X-direction, factor 1

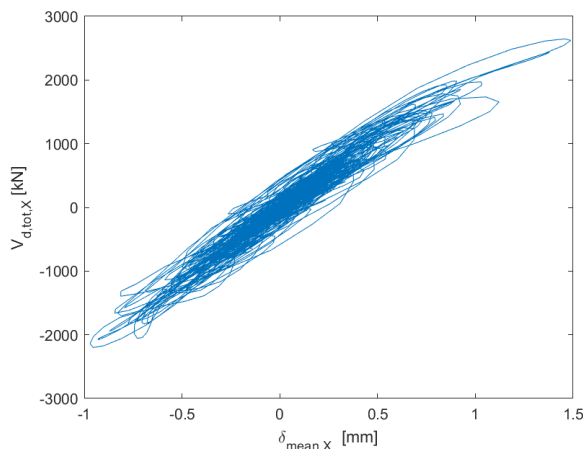


(a) Total base shear versus average roof displacement direction X

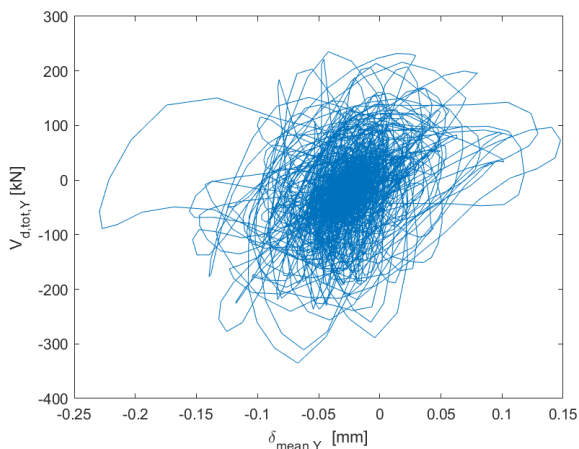


(b) Total base shear versus average roof displacement direction Y

NS acceleration in X-direction, factor 2

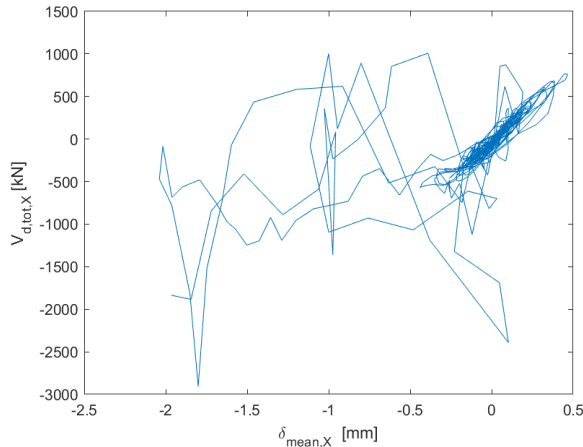


(a) Total base shear versus average roof displacement direction X

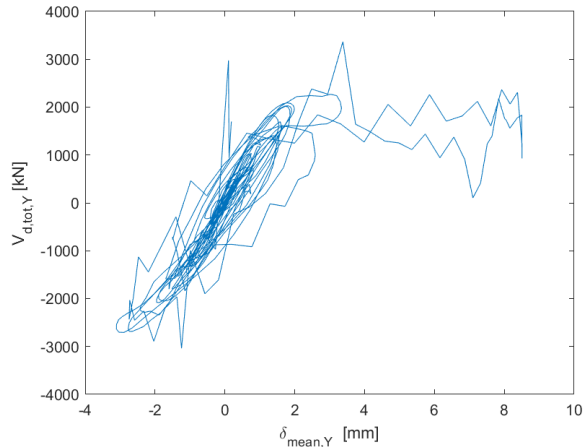


(b) Total base shear versus average roof displacement direction Y

NS acceleration in Y-direction, factor 2

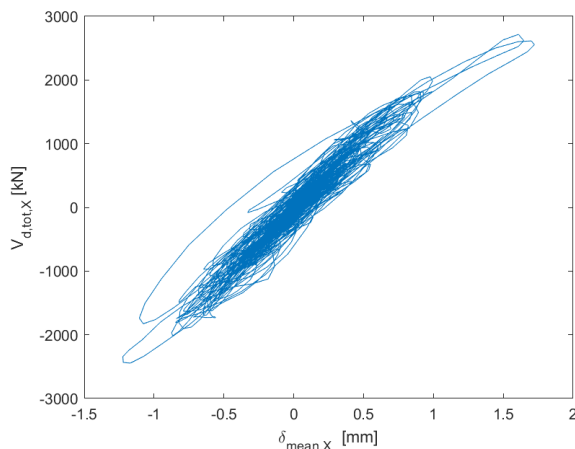


(a) Total base shear versus average roof displacement direction X

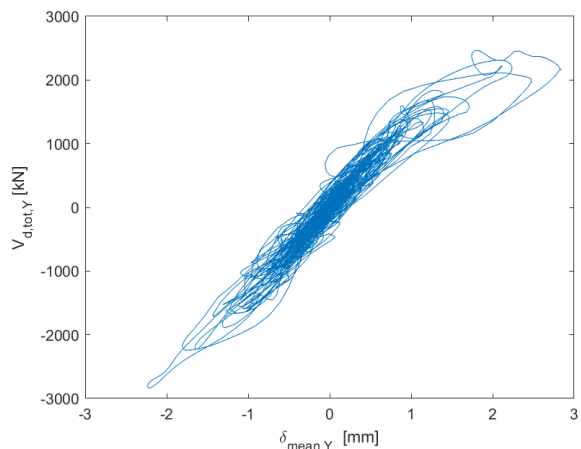


(b) Total base shear versus average roof displacement direction Y

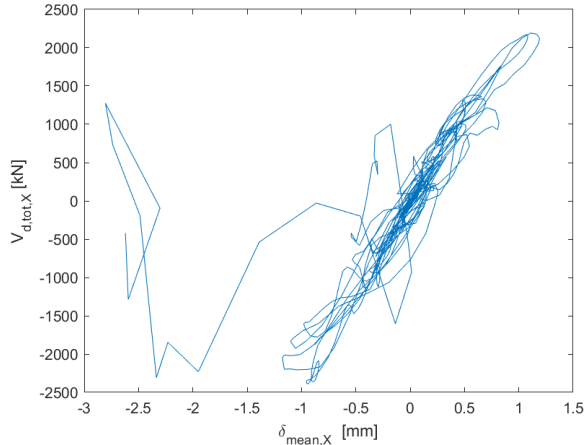
NS acceleration in X-direction, EW acceleration in Y-direction, factor 2



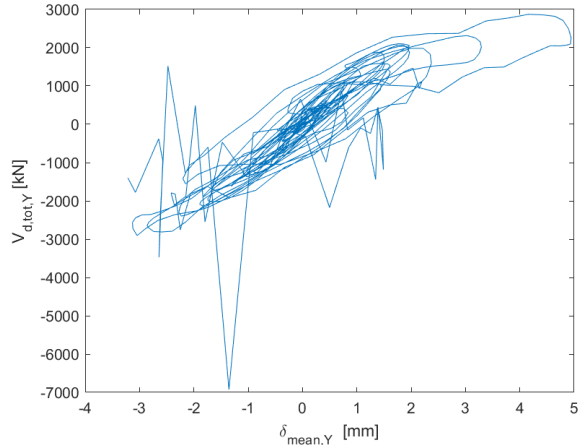
(a) Total base shear versus average roof displacement direction X



(b) Total base shear versus average roof displacement direction Y

NS acceleration in Y-direction, EW acceleration in X-direction, factor 2

(a) Total base shear versus average roof displacement direction X



(b) Total base shear versus average roof displacement direction Y